Functional and structural characterisation of the Malignant Hyperthermia associated *RYR1* mutation R2452W

A thesis presented to Massey University in partial fulfillment of the requirements for the degree of Doctor of Philosophy in Biochemistry

Cornelia Roesl

2013

ACKNOWLEDGEMENTS

First of all, I would like to thank my supervisor, Associate Professor Kathryn Stowell, who gave me the opportunity to come to New Zealand and to work in her lab. Thank you for your support, help and advice throughout the last four years and for teaching me how to become an independent researcher.

Thanks to my second supervisor Andrew Sutherland-Smith, for always having time and helping me exploring a new field. Thank you Greg, Jan and Trevor for your help with protein purification and trouble shooting of various issues I faced. Without you this work could have never been done. Special thanks to Trevor for analysing my Mass Spec data. You are awesome!

Thanks to Susan Treves for your never ending help, feedback and patience.

Thanks to Sarah for taking images of my immunostaining at the confocal microscope. You are just the best! Many thanks to Doug Hopcroft for helping me solving any microscopy issues and always having a good chat. I will miss you!

Also thanks to Neil Pollock (Palmerston North hospital) for supplying blood samples for lymphocyte extraction.

I would like to thank every former and current member in the Twilite Zone and Park Lands for having a great time which never became boring. Tilly and Kerry, thanks for the awesome year we had together, I still miss you! Kei, I would not know what I had done without you. Over the years you have become a very good friend to me, even though I am not the most reliable person in emailing. Thank you for your help and encouragement as well as understanding. Robyn, thanks for the conversations and the fun we had in the lab and all the good weekend activities you suggested. Lili, I am so glad you returned to the lab. Thanks for your help with sequencing and the awesome chats. Bex, thanks for having a good time with lots of laughing and Tian for never ending conversations and fun. Most of all, thanks to Anja for all the help, advice and discussions we had. Without you my PhD would not

have been that interesting. It was also nice to have good conversations in German even though we mixed up German and English quite a bit.

I am grateful to IMBS for providing me with a bursary to start my PhD as well as to Massey University for awarding me a Massey University Scholarship. Special thanks to Barry Scott, without your ongoing support I would not have been able to achieve any of this. Thank you!

Finally I would like to thank my family for their love and understanding even though I moved to the other side of the world. The person to whom I am most grateful is my partner Wolf. Without you I would not have been able to do this. Thanks for your love, support, understanding and encouragement as well as keeping stuff off my back when I was busy writing. I hope I will always be as supportive to you as you have been to me!

Abstract

Malignant hyperthermia (MH) is an autosomal dominant pharmacogenetic disorder of skeletal muscle triggered by volatile halogenated anaesthetics. Susceptible individuals can exhibit symptoms including tachycardia, high temperature, hypoxia, hypermetabolism and skeletal muscle rigidity. There are usually no symptoms of MH in normal day to day life although “awake” episodes have been reported as a result of extreme exercise in MH-susceptible subjects. Genetic variants have been associated with the skeletal muscle ryanodine receptor gene (*RYR1*) in 50-70 % of susceptible patients. At the molecular level susceptible patients are thought to have an increased sensitivity to RYR1 agonists in skeletal muscle compared to non-affected patients that results in disregulated skeletal muscle Ca^{2+} homeostasis. In 2000 a novel *RYR1*-mutation, c.G7354T (p.R2452W), associated with MH, was identified in a New Zealand (NZ) family. Subsequently the same mutation was identified in a separate NZ family and has also been reported in the United Kingdom. To date this mutation had not been shown to be causative of MH. Therefore, the aim of this study was to carry out functional analyses to test whether the R2452W mutant receptor alters Ca^{2+} release compared to wildtype. For this study Ca^{2+} release assays were carried out in three different cell types: B-lymphoblastoid cells, myotubes and HEK293 cells transfected with full-length human *RYR1* cDNA. Cells were exposed to the RYR1-specific agonist 4-chloro-*m*-cresol, which stimulates Ca^{2+} release through the receptor while the increase in cytosolic Ca^{2+} was detected using a membrane-permeable fluorophore. Cells expressing R2452W mutant RYR1 showed altered Ca^{2+} release from the sarco(endo)plasmic reticulum suggesting a hypersensitive channel. In order to study structure/function relationships of the R2452W mutation within the RYR1 protein, as well as the 3D structure of a central RYR1 domain (amino acid 2144-2489), a region encompassing this substitution was cloned for bacterial expression and subsequently purified. Wildtype and mutant proteins were compared to determine any effects the mutation may have upon the stability of the protein. Wildtype and R2452W RYR1 protein showed no obvious differences in stability but both proteins appeared to oligomerise suggesting this region might be involved in RYR1-RYR1 domain interactions.

Abbreviations

A_{280}	Absorbance at 280 nm
aa	Amino acid
ACN	Acetonitrile
ADP	Adenosine diphosphate
APS	Ammonium peroxodisulfate
ATP	Adenosine triphosphate
bp	Base pair
BSA	Bovine serum albumin
C	coil
CaM	Calmodulin
CCD	Central core disease
CD	Circular dichroism
CHCT	Caffeine-halothane contracture test
CICR	Ca^{2+} induced Ca^{2+} release
4CmC	4-chloro-*m*-cresol
Cp values	PCR crossing point
CY	Cytosolic domain
Cy	Cytosol
DAG	Diacylglycerol
DAPI	4',6-diamidino-2-phenylindole
DHPR	Dihydropyridine receptor
DMSO	Dimethyl sulfoxide
DP4	Domain peptide 4
DTT	Dithiothreitol
E	β-sheet
EC_{50}	Half maximal effective concentration
ECCE	Excitation-coupled Ca^{2+} entry
EC-coupling	Excitation-contraction coupling
EGTA	Ethylene glycol tetraacetic acid
EM	Electron microscopy
EMHG	European Malignant Hyperthermia Group
ER	Endoplasmic reticulum
FA	Formic acid

FCS	Fetal calf serum
FITC	Fluorescein isothiocyanate
FK506	Tacrolimus, a immunosuppressive drug
FKBP12	12-kDa FK506-binding protein
FPLC	Fast protein liquid chromatography
G418	Geneticin
H	α-helix
HEK293	Human embryonic kidney cells
HEPES	4-(2-hydroxyethyl)-1-piperazineethanesulfonic acid
HPLC	High-performance liquid chromatography
HRM	High resolution melting
HS	Horse serum
IP3R	Inositol 1,4,5 trisphosphate receptor
IPTG	Isopropyl β-D-1-thiogalactopyranoside
IVCT	*In vitro* contracture test
kDa	kilo Dalton
LB	Luria-Bertoni
LC	Light cycler
MEM	Modified Eagle Medium
MH	Malignant hyperthermia
MHE	Malignant hyperthermia equivocal
MHN	Malignant hyperthermia negative
MHS	Malignant hyperthermia susceptible
MIR domain	Mannosyltransferase and IP3R homology domain
MS	Mass spectrometry
NAMHG	North American Malignant Hyperthermia Group
NC	Negative control
nt	not tested
PBS	Phosphate buffered saline
PC	Positive control
PIP2	Phosphatidylinositol 4,5-bisphosphate
RIH domain	RYR and IP3R homology domain

PDI	Protein Disulphide-Isomerase
PLC	Phospholipase C
RYR	Ryanodine receptor
RT-qPCR	Reverse transcription quantitative polymerase chain reaction
SDS-PAGE	Sodium dodecyl sulfate-polyacrylamide gel electrophoresis
SEM	Standard error of the mean
SERCA	Sarco- and endoplasmic reticulum ATPase
SNP	Single nucleotide polymorphism
SOCE	Store-operated Ca^{2+} entry
SR	Sarcoplasmic reticulum
STIM1	Stromal interaction molecule 1
T	turn
TAE	Tris acetate EDTA buffer
TBST	Tris buffered saline Tween 20
TEMED	Tetramethylethylenediamine
Tm	Melting temperature
TM	Transmembrane domain
TRITC	Tetramethyl Rhodamine Isothiocyanate
Tris	Trisaminomethane
T-tubule	Transverse tubule
Trx	Thioredoxin
UV	Ultraviolet light
WT	Wildtype

List of Figures

Figure 1.1 Threshold concentration of caffeine and halothane in IVCT in 73 control biopsies. 2
Figure 1.2 Interaction between RYR1 and the DHPRα_{1a} II-III loop in EC coupling. 4
Figure 1.3 Schematic drawing of the upstream and downstream regulation factors controlling Ca^{2+} homeostasis in skeletal muscle. 5
Figure 1.4 Schematic drawing of MH hotspot regions. 7
Figure 1.5 A 9.6-Å resolution cryo-EM density map of RYR1 in the closed state. 9
Figure 1.6 Three-dimensional map of the ryanodine receptor 1 assembly. 11
Figure 1.7 3D structure of IP3R and RYR viewed from the ER lumen and membrane. 13
Figure 1.8 Positioning of RYR1 and IP3R homology domains within the ryanodine receptor 1. 14
Figure 1.9 Interaction between N- and C-terminal domains in RYR1. 15
Figure 1.10 NMR structural model of DP4 16
Figure 1.11 Schematic model of abnormal Ca^{2+} release mechanism in RYR1. 28
Figure 3.1 Pedigree of family B. 60
Figure 3.2 HRM and hybridisation probe assays to detect R2452W and H4833Y mutations in B-lymphoblastoid cells. 62
Figure 3.3 Immunoblotting for RYR1 using immortalised B-lymphocyte microsomes extracts. 64
Figure 3.4 Immunostaining of B-lymphoblastoid cells. 65
Figure 3.5 Immunostaining of myoblasts using α-desmin antibody. 66
Figure 3.6 Co-localisation studies using PDI and RYR1 antibody in myotubes. 66
Figure 3.7 Raw data of the 340/380 nm ratio change after the addition of 4CmC. 68
Figure 3.8 Ca^{2+} release assays for the MHN patient C1 in buffers containing different Ca^{2+} and EGTA concentrations in response to 4CmC. 70
Figure 3.9 Concentration-response curve using B-lymphoblastoid upon 4CmC stimulation. 73
Figure 3.10 Concentration-response curve of B-lymphoblastoid cells from MHE patients upon 4CmC stimulation. 75

Figure 3.11 Ca^{2+} release data and concentration-response curve for myotubes upon 4CmC stimulation. 77
Figure 3.12 Concentration-response curve using myotubes of MHE patients after 4CmC stimulation. 79
Figure 4.1 Restriction endonuclease digest of the pc*RYR1*-R2452W plasmid. 89
Figure 4.2 Sequencing result of pc*RYR1*-R2452W to confirm the presence of R2452W. 90
Figure 4.3 Western blotting for transfected HEK293 cells using different ratios of pc*RYR1*-R2452W cDNA and FugeneHD. 92
Figure 4.4 Western blotting for detection of transiently expressed RYR1 protein in HEK293 cells 93
Figure 4.5 Immunofluorescence of transient transfected WT and R2452W mutant RYR1. 95
Figure 4.6 Primer design for RT-qPCR using two different primer pairs. 96
Figure 4.7 mRNA *RYR1* expression levels in transient transfected HEK293 cells. 98
Figure 4.8 Concentration-response curve of H4833Y transient transfected HEK293 cells in different imaging buffers upon 4CmC stimulation. 100
Figure 4.9 Concentration-response curve for *RYR1* transient transfected HEK293 cells upon 4CmC stimulation. 102
Figure 4.10 Immunostaining of stably transfected and untransfected HEK293 cells. 105
Figure 4.11 Western blotting showing RYR1 protein in stable transfected HEK293 cells. 107
Figure 4.12 mRNA expression levels of *RYR1* in stable transfected HEK293 cells. 108
Figure 4.13 Binding sites of LC primer pair 1 in *RYR1* gDNA. 109
Figure 4.14 PCR products for gDNA and cDNA of stable transfected R2452W *RYR1*. 109
Figure 4.15 Sequencing results for cDNA of HEK293 cells stably transfected expressing R2452W and WT RYR1 110
Figure 4.16 IP3R Ca^{2+} release pathway inhibited by G418. 111
Figure 4.17 Concentration-response curve for stably transfected HEK293 cells upon 4CmC stimulation. 112

Figure 5.1 Secondary protein structure prediction for WT (A) and R2452W mutant (B) RYR1 central domain using Mobyle portal. 125
Figure 5.2 Sequence alignment of RYR1 domain (amino acid 2144-2284) and IP3R. 127
Figure 5.3 Schematic diagram showing the cloning strategy using vector pET32a(+). 130
Figure 5.4 PCR amplification of pc*RYR1*-R2452W mutant plasmid and colony PCR for pProEXHtb. 131
Figure 5.5 PCR amplification of pcRYR1-R2452W and colony PCR for pET32a(+). 132
Figure 5.6 Expression tests for recombinant pET32a(+) and pProExHtb..... 134
Figure 5.7 Expression of construct 3 in pET32a(+) for WT and R2452W mutant. 136
Figure 5.8 Elution chromatogram of WT RYR1 protein from Ni^{2+} NTA column. 139
Figure 5.9 Chromatogram for the second elution from the His_6trap column using a step gradient. 140
Figure 5.10 S200 size exclusion results of WT and R2452W mutant RYR1 fusion protein. 141
Figure 5.11 CD spectra for RYR1 fusion and N-terminal tag proteins (A) and thermal denaturation of R2452W mutant fusion (B) and N-terminal tag protein (C). 144
Figure 5.12 Plot of normalised CD data under thermal denaturation at 209 nm (A) and 217 nm (B). 146
Figure 5.13 Protein cleavage experiments using enterokinase and thrombin. 149
Figure 5.14 Time course experiment for enterokinase digest of RYR1 fusion protein. 151
Figure 5.15 Size exclusion chromatogram using Triton X-100 in purification procedure 152
Figure 5.16 Spontaneously cleaved R2452W mutant RYR1 domain. 154
Figure 5.17 MS-MS results for gel purified RYR1 protein sample 155
Figure 5.18 HPLC separation of spontaneously cleaved RYR1 protein 156
Figure 5.19 Coverage obtained from liquid digestion of R2452W mutant RYR1 cleaved protein 158

Figure 5.20 Sequence alignment of the N-terminal region of rabbit and three human RYR isoforms. 161
Figure 5.21 Localisation of specific residues in the 3D structure of the RYR1 oligomer. 164

List of Tables

Table 2.1 Reaction components for RT-qPCR. 34
Table 2.2 Reaction component for standard PCR. 35
Table 2.3 Cycle parameters for standard PCR with varying annealing temperatures. 35
Table 2.4 Standard HRM protocol for primers detecting the R2452W mutation in DNA. 36
Table 2.5 PCR protocol for HRM assays showing standard parameters. 37
Table 2.6 Protocol for restriction endonuclease digest using two enzymes. 38
Table 2.7 Standard protocol for antarctic phosphatase treatment of digested vector. 38
Table 2.8 Ligation protocol. 39
Table 2.9 Mutagenesis PCR protocol. 39
Table 2.10 Standard protocol used for mutagenesis PCR. 40
Table 2.11 List of components for either 7.5 or 12.5 % SDS-PAGE gels. 43
Table 2.12 Media and CO_2 concentrations used to cultivate different cell lines. 49
Table 3.1 Patient-derived samples used in Ca^{2+} release assays. 59
Table 3.2 Influence of different Ca^{2+} concentrations in buffer on Ca^{2+} release in B-lymphoblastoid cells in response to 4CmC. 68
Table 3.3 EC_{50} values for 4CmC stimulation obtained in different buffer conditions. 71
Table 3.4 EC_{50} values for B-lymphoblastoid cell lines upon 4CmC stimulation. 74
Table 3.5 EC_{50} values for 4CmC stimulation in B-lymphoblastoid cells of MHE patients showing a positive reaction to halothane (h). 76
Table 3.6 EC_{50} values for 4CmC stimulation calculated from concentration-response curves using myotubes. 78
Table 3.7 EC_{50} values for myotubes of MHE patients upon 4CmC stimulation. 80
Table 4.1 List of synonymous polymorphisms found in the pc*RYR1*-R2452W plasmid. 91
Table 4.2 PCR efficiencies for three primer pairs calculated by the REST 2009 software. 97
Table 4.3 Cp values obtained for three samples used in one real-time PCR experiment. 97

Table 4.4 EC_{50} values of transient transfected H4833Y mutant RYR1 in different buffers upon 4CmC stimulation. 101
Table 4.5 EC_{50} values for 4CmC stimulation of *RYR1* transient transfected HEK293 cells. 103
Table 4.6 EC_{50} values for 4CmC activation of WT and R2452W mutant RYR1 stable transfected HEK293 cells. 113
Table 4.7 Summary of EC_{50} values for 4CmC activation obtained from concentration-response curves of either B-lymphoblastoid cells, myotubes or transfected HEK293 cells. 120
Table 5.1 Predicted secondary structure motifs for WT and R2452W mutant RYR1 domain 125
Table 5.2 Table of RYR1 inserts cloned into either the pProExHtb or pET32a(+) vector. 129
Table 5.3 Expression summary of RYR1 constructs in pProExHtb and pET32a(+). 135
Table 5.4 Physical properties of overexpressed RYR1 fusion, cleaved and N-terminal tag proteins. 137
Table 5.5 Deconvolution results determining percentage of secondary structures. 145

Table of Contents

Chapter 1 Introduction 1
1.1 Malignant Hyperthermia 1
1.2 EC (excitation-contraction) coupling in skeletal muscle 3
1.3 RYR1 gene and mutations 6
1.4 Ryanodine receptor and protein interaction 7
1.5 Other Ca^{2+} release channels 12
1.6 DP4 domain 14
1.7 Pharmacology 17
1.7.1 Dantrolene 17
1.7.2 Caffeine and halothane 17
1.7.3 4-chloro-*m*-cresol (4CmC) 19
1.7.4 Other agonists 19
1.8 RYR1 associated disorder central core disease (CCD) 22
1.9 Methodology of functional assays 23
1.10 Functional disorganisation of the RYR1 receptor 26
1.10.1 Hypersensitive RYR1 26
1.10.2 Leaky Ca^{2+} channels 26
1.10.3 EC uncoupling 27
1.11 Reduced RYR1 expression 29
1.12 Other MH-associated loci 29
1.13 Project outline 30
Chapter 2 Materials and Methods 32
2.1 Materials 32
2.2 General Methods 33
2.2.1 Isolation of genomic DNA from different cell lines 33
2.2.2 RNA isolation from different cell lines 34
2.2.3 Reverse Transcriptase PCR 34
2.2.4 Polymerase chain reaction (PCR) 35
2.2.5 PCR product purification 36
2.2.6 DNA sequencing 36
2.2.7 High resolution melting (HRM) analysis of genomic DNA 36
2.2.8 Restriction endonuclease digest 37
2.2.9 Antarctic phosphatase treatment of digested vectors 38

2.2.10 Ligation 38
2.2.11 Site-directed mutagenesis....39
2.2.12 Competent *E. coli* cells....40
2.2.13 *E. coli* transformation 41
2.2.14 Glycerol stocks of transformed DH5α cells 41
2.2.15 Rapid boil plasmid isolation....41
2.2.16 Isolation of plasmid DNA: small scale 42
2.2.17 Isolation of plasmid DNA: medium scale....42
2.2.18 Protein isolation from mammalian cell lines 42
2.2.19 Sodium dodecyl sulfate polyacrylamide gel electrophoresis (SDS-PAGE) 43
2.2.20 Western blotting....44
2.2.21 Coating of tissue culture plastic 45
2.2.22 Immunofluorescence staining 45
2.2.23 Establishment of primary lymphocyte cultures from blood 46
2.2.24 Isolation of muscle cells from fresh muscle....47
2.2.25 Reviving frozen cell stocks....48
2.2.26 Passage of cells....49
2.2.27 Freezing cells....50
2.2.28 Transfections 50
2.2.29 Ca^{2+} release assays....51
2.3 Protein purification methods 52
2.3.1 Induction of transformed *E. coli*....52
2.3.2 Protein extraction from induced *E. coli*....52
2.3.3 His_6-tag purification via Ni^{2+}-NTA affinity column 52
2.3.4 Size exclusion purification for RYR1 central domain....53
2.3.5 Cleavage of affinity tag using enterokinase....53
2.3.6 Circular dichroism spectroscopy....53
2.3.7 Mass spectrometry 54
Chapter 3 Functional characterisation of the RYR1 R2452W mutation using patient-derived cells 56
3.1 Introduction....56
3.1.1 B-Lymphoblastoid cells 57
3.1.2 Myoblasts....57
3.2 Patient samples 58

3.3 Results 61
3.3.1 Confirmation of the presence of R2452W mutation in assayed samples 61
3.3.2 Optimisation of myoblast extraction 62
3.3.3 RYR1 detection in different cell types 63
3.3.4 Optimisation of Ca^{2+} release assays 67
3.3.5 Results for Ca^{2+} release assays in lymphoblastoid cell lines 72
3.3.6 Ca^{2+} release assays using myotubes 76
3.4 Discussion 80
3.4.1 B-lymphoblastoid cells 80
3.4.2 Myotubes 84
Chapter 4 Functional characterisation of the R2452W mutation using a recombinant system 88
4.1 Introduction 88
4.2 Results 88
4.2.1 Full-length R2452W mutant *RYR1* cDNA 88
4.2.2 Transient transfected HEK293 cells 92
4.2.3 Stable transfected HEK293 cells 103
4.3 Discussion 113
4.3.1 Cloning 113
4.3.2 RYR1 Expression 113
4.3.3 Ca^{2+} release assays 117
Chapter 5 Overexpression and purification of the ryanodine receptor 1 central domain 122
5.1 Introduction 122
5.2 Bioinformatics 123
5.2.1 Mobyle portal 123
5.2.2 SMART database 125
5.2.3 $Phyre^2$ 126
5.3 Results 128
5.3.1 Cloning strategy 128
5.3.2 PCR amplification and cloning 130
5.3.3 Initial expression tests 133
5.3.4 Optimisation of expression 134
5.3.5 Mutagenesis PCR 137

5.3.6 Physical properties of RYR1 central domain construct 3 137
5.3.7 Purification of RYR1 central domain 138
5.3.8 Circular dichroism (CD) 142
5.3.9 Protease digestion 148
5.3.10 Mass spectrometry 153
5.4 Discussion 159
5.4.1 Bioinformatics 160
5.4.2 Cloning and expression tests for the RYR1 central domain 161
5.4.3 Purification of overexpressed RYR1 protein 162
5.4.4 Stability assays using CD spectra and thermal melting 166
5.4.5 Spontaneously cleaved fusion protein 167
5.4.6 Crystallisation 169
Chapter 6 Summary and future directions 171
6.1 Functional assays 171
6.2 Structural characterisation of the RYR1 central domain 175
Chapter 7 References 179
Chapter 8 Appendices 7-A1

Chapter 1 Introduction

1.1 Malignant Hyperthermia

Malignant hyperthermia (MH; OMIM# 145600) is an autosomal dominant pharmacogenetic disorder of skeletal muscle triggered by volatile halogenated anaesthetics [1]. Susceptible individuals can exhibit symptoms including tachycardia, high temperature, hypoxia, hypermetabolism and skeletal muscle rigidity in response to depolarising agents like succinylcholine or volatile halogenated anaesthetics which have lead to death in several families [2]. The frequency of MH episodes has been estimated to be one in 15,000 anaesthetics in children and one in 40,000 anaesthetics in adults [3]. As only a few people are screened for MH this number is likely to be an underestimation and Monnier et al. (2002) suggested that mutations causing this disorder may occur with an incidence of 1 in 2000-3000 in the French population [4]. A similar estimate has been predicted for Japan [5]. The population residing in the lower part of the North Island of New Zealand has a relatively high incidence of MH. Fifty-three families throughout New Zealand have been identified as MH susceptible (MHS), at least 5 of which are Maori [6, 7] (and personal communication with Neil Pollock, Palmerston North Hospital).

More than 300 MH-associated point mutations or deletions have been found in the ryanodine receptor isoform 1 (*RYR1*) gene located on chromosome 19q13.1, which encodes the Ca^{2+} release channel of the sarcoplasmic reticulum (SR) in skeletal muscle [3, 8] but only 31 have been shown to be causative ([9], accessed in December 2012). At least 50 % of MH families show mutations in the *RYR1* gene but five other loci have been reported [10, 11]. In order to classify a mutation as MH causative the mutation has to segregate with MH in at least two different pedigrees and functional assays showing abnormal Ca^{2+} release from different RYR1 expressing cell types carrying a patients mutation, have to be performed. It is now accepted that most MHS patients have an increased sensitivity to Ca^{2+} activation compared to non-affected patients (MHN) [12]. The initial high mortality rate (70 %), caused by a rapid rise in myoplasmic Ca^{2+} released from the sarcoplasmic

reticulum (SR), has been reduced to below 5 % with the introduction of dantrolene, a Ca^{2+} channel blocking agent [13, 14].

MH symptoms cannot be detected in normal day-to-day life, therefore patients suspected to be MHS must be diagnosed using an *in vitro* muscle contracture test (IVCT) which is used as the ”gold” standard diagnostic test. This *in vitro* test simulates the reaction of muscle to anaesthetic agents. A biopsy is taken from the patient’s quadriceps muscle and, after dissection into bundles of fibres, it is exposed to triggering agents while measuring the associated response in muscle tension. An abnormal reaction represented by a high muscle contraction to the drugs halothane and caffeine diagnoses MH susceptibly (MHS) [15]. The IVCT has a sensitivity of 99 % with 93.6 % specificity [16] and does not always give a definite positive or negative result (figure 1.1). An equivocal result (MHE) is returned with an abnormal response to either halothane (MHE_h) or caffeine (MHE_c). It is more likely that patients will have a stronger response to caffeine since caffeine also stimulates unspecific Ca^{2+} release [16].

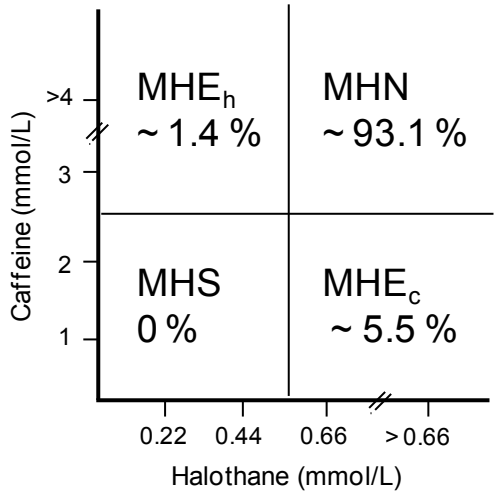

Figure 1.1 Threshold concentration of caffeine and halothane in IVCT in 73 control biopsies. The European MH Group obtained data from 73 control biopsies and calculated the percentage of MHS= MH susceptible, MHN= MH negative and MHE= equivocal results by either halothane (h) or caffeine (c). Figure adapted from Ørding et al. [17].

The caffeine–halothane contracture test (CHCT) is widely used throughout North America with minor differences in protocols such as the specific caffeine concentration and the exposure time of the muscle. Major

differences between the protocols include the threshold for positive reactions to caffeine (0.2 or 0.3 g for the EMHG or NAMHG, respectively) [18]. Furthermore MHS patients have been shown to have an increased cytosolic Ca^{2+} concentration when cells are exposed to triggering agents like halothane using the IVCT. These data were obtained by measuring cytosolic Ca^{2+} concentrations using an intracellular Ca^{2+} indicator. This affect was absent with *in vivo* stimulation using alternative RYR1 specific agonists [19, 20]. MH does not only occur in humans, it is also known to affect pigs, horses, dogs and cats [21-23]. MH in pigs occurs in a similar way as in humans and is triggered by stress and high temperature. MHS in pigs is autosomal recessive and they have a tendency to grow increased muscle mass which is an advantage for pig breeders [24]. The first mutation R615C, associated with MH, was found in pigs [25] and is the only MH-associated mutation to be identified in pigs.

1.2 EC (excitation-contraction) coupling in skeletal muscle

EC (excitation-contraction) coupling depends upon a gradient between extracellular and intracellular Ca^{2+} concentrations. The intracellular Ca^{2+} concentration in resting cells is ~100 nM and is increased rapidly to a tenfold higher concentration when an action potential activates the surface membrane of a muscle cell (reviewed in [26]). This surface membrane has a tubular infolding (t-tubule) and is in close contact with the sarcoplasmic reticulum (SR), the main Ca^{2+} storage compartment in the muscle (figure 1.2). The dihydropyridine receptor (DHPR) is situated in the t-tubule membrane and is an L-type voltage-dependent Ca^{2+} channel, which interacts directly with the ryanodine receptor 1 and transmits the signal from the t-tubule to RYR1 (reviewed in [27]). EC coupling in skeletal muscle depends upon a physical interaction of the α_{1s} subunit of the skeletal muscle DHPR with RYR1, where the II-III loop (the putative cytoplasmic region between repeats II and III of the DHPR) plays an essential role [27] (figure 1.2).

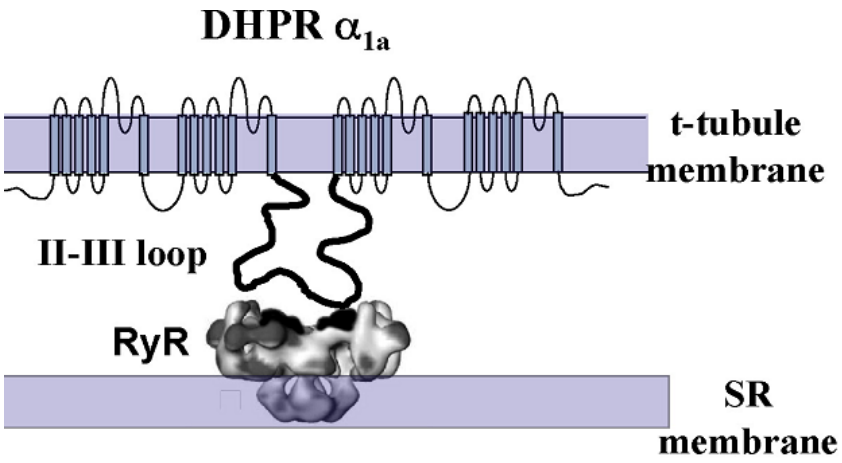

Figure 1.2 Interaction between RYR1 and the DHPRα_{1a} II-III loop in EC coupling.
RYR1 is located at the sarcoplasmic reticulum membrane and interacts via the II-III loop with DHPRα_{1a} in the t-tubule membrane [28] (permission for publishing figure was obtained through RightsLink).

DHPR activates RYR1, inducing conformational changes in RYR1 and release of Ca^{2+} from the SR into the cytosol. The increased Ca^{2+} concentration in the SR triggers muscle contraction by the binding of Ca^{2+} to troponin which undergoes a conformational change allowing the actin-myosin-filaments to interact and the metabolism of ATP hydrolysis (figure 1.3). The metabolic effects of increased cytosolic Ca^{2+} explain the symptoms in an MH episode including a rise in body temperature and muscle rigidity. The free cytosolic Ca^{2+} is transported back into the SR by the sarco- and endoplasmic reticulum ATP-ase (SERCA). This channel hydrolyses ATP to transport Ca^{2+} against its concentration gradient back into the SR. SERCA is essential for EC coupling as without it the SR Ca^{2+} would become depleted and no muscle contraction would occur [27].

When SERCA is specifically inhibited by thapsigargin, a plant-derived sesquiterpene lactone, the concentration of Ca^{2+} in the cytosol increases while thapsigargin forms a dead end complex with the ATPase making it unable to pump Ca^{2+} back into the SR [29].

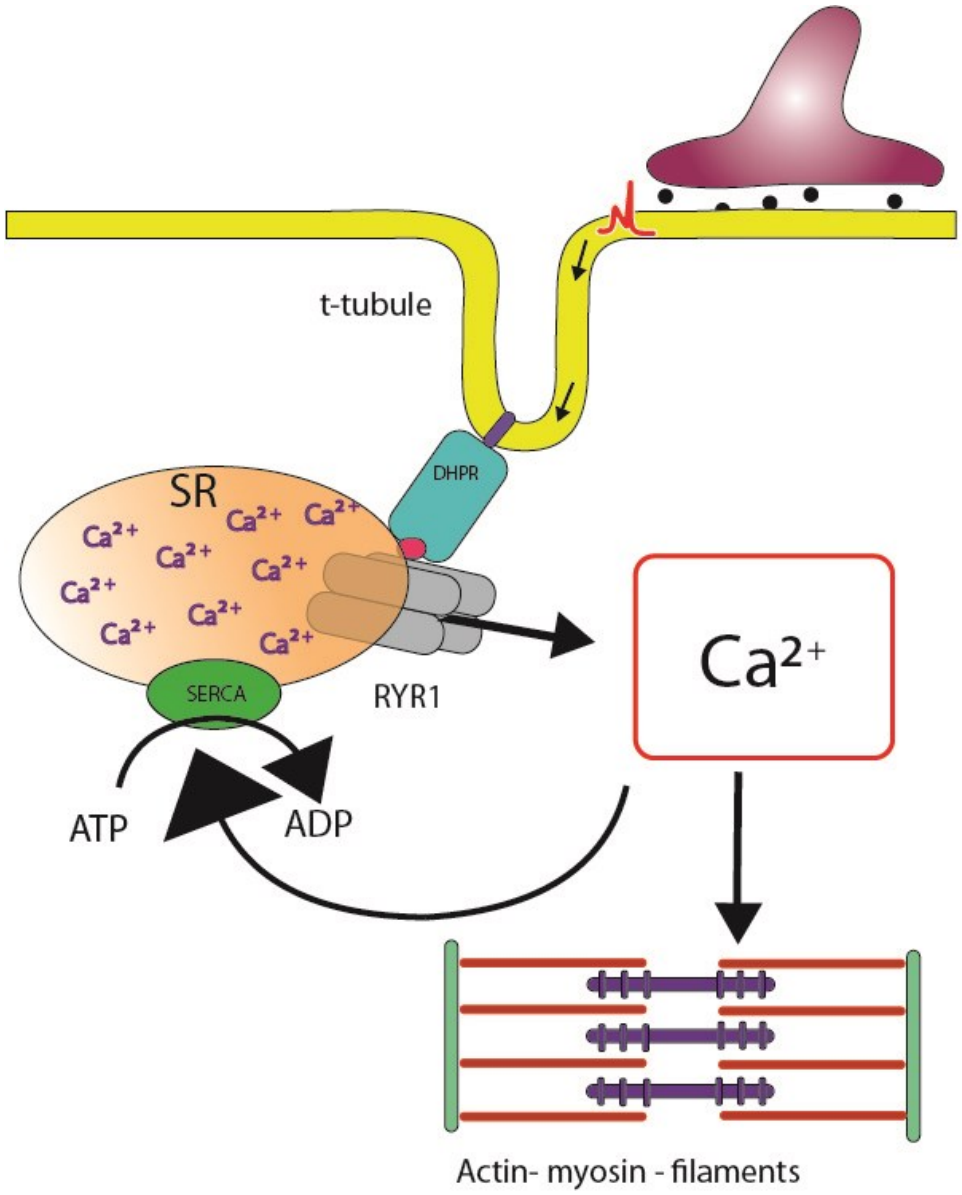

Figure 1.3 Schematic drawing of the upstream and downstream regulation factors controlling Ca^{2+} homeostasis in skeletal muscle.

An action potential arrives at a muscle cell (top synapse in purple) and is transmitted along the t-tubule (yellow) to the dihydropyridine receptor (DHPR, rectangle blue). DHPR activates the ryanodine receptor (RYR1 in grey) which releases Ca^{2+} from the sarcoplasmic reticulum (SR) into the cytosol. Ca^{2+} released from the SR leads to muscle contraction involving Ca^{2+} binding to troponin leading to the induction of muscle contraction by the actin-myosin-filaments. Ca^{2+} can be transported back into the SR via SERCA (Ca^{2+}-ATPase, green in SR membrane), powered by ATP hydrolysis (adapted from Anetseder and Roewer, Maligne Hyperthermie; in: Die Anästhesiologie, Springer Verlag, Heidelberg).

FK506-binding protein (FKBP-12.0), another RYR1 binding protein, binds RYR1 around amino acid position 2461 and regulates the gating function of RYR1 [30]. One FKBP-12.0 binds to one RYR1 subunit and stabilises the

channel gating between the four subunits. If this interaction is disrupted, for example by mutations in either RYR1 or FKBP-12.0, it leads to a failure of EC coupling [31]. Depletion of the SR Ca^{2+} stores during muscle contraction induces Ca^{2+} entry from the extracellular medium by opening of plasma membrane channels. This is called store-operated Ca^{2+} entry (SOCE). Several proteins are involved in this mechanism including the transmembrane-spanning stromal interaction molecule 1 (STIM1) which senses the SR Ca^{2+} concentration (Ca^{2+}_{SR}). When Ca^{2+}_{SR} decreases, the store-operated Ca^{2+} channels become activated and extracellular Ca^{2+} enters the cell. The plasma membrane pore-forming protein Orai1 interacts with STIM1 and activates SOCE. SOCE is important in many physiological processes and may influence Ca^{2+} homeostasis if these proteins have altered function (reviewed in [32]). Myotubes carrying the R615C mutation showed an enhanced excitation-coupled Ca^{2+} entry (ECCE) which could be restored by the addition of dantrolene. ECCE is activated by membrane depolarisation and is independent of the sarcoplasmic reticulum Ca^{2+} content. It is altered in MH susceptible patients and may contribute to enhanced Ca^{2+} release from the SR [33, 34]. Micromolar free Ca^{2+} can also trigger Ca^{2+} release (Ca^{2+} induced Ca^{2+} release, CICR) from the SR due to an increased Ca^{2+} concentration in the cytosol while millimolar Ca^{2+} concentrations inhibit the ryanodine receptor [35]. CICR does not play a major role in physiological Ca^{2+} release but seems to play a major role in agonist induced Ca^{2+} release ([35], see 1.7.2 for further details). Both CICR and ECCE are regulated by a negative feedback mechanism which prevents Ca^{2+} release (ECCE is inhibited by dandrolene binding to RYR1 [33] while in CICR the DHPR subunit α1s bound to RYR1 inhibits Ca^{2+} release [36]). When a mutation occurs in either of these binding regions, the negative feedback is no longer intact and can cause MH.

1.3 RYR1 gene and mutations

The *RYR1* gene on chromosome 19q13.1 was linked to MH by positional cloning in 1990 [37]. It is comprised of 106 exons and represents a cDNA length of over 15,000 bp. Exons range in size from 15 to 813 bp while the

introns range from 85 to ~16,000 bp. The gene is ~160,000 bp in total [38]. Over 300 MH-associated mutations have been reported to date (source Human Gene Mutation Database). Most mutations are clustered in three "hot spot" regions (figure 1.4): domain 1 including exons 1-17 (N-terminal domain, MH1), domain 2 within exons 39-45 (central domain, MH2) and domain 3 consisting of exons 90-104 (C-terminal domain, MH3, figure 1.4) [39, 40] but increasingly mutations are being found outside these regions [41].

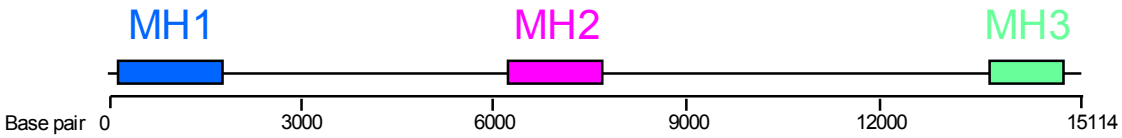

Figure 1.4 Schematic drawing of MH hotspot regions.
The three *RYR1* hot spot domains MH1 (blue), MH2 (pink) and MH3 (green) with the associated cDNA nucleotides are shown. (The drawing is a schematic diagram and not to scale, adapted from [1, 42]).

Point mutations in the *RYR1* gene have been found in over 50 % of affected patients, with most MH-associated mutations in humans being heterozygous and inherited in an autosomal dominant fashion [43, 44]. The first MH-associated mutation in humans was found in 1992 by Hogan et al. and was a thymine to cytosine substitution at position 1840 of the *RYR1* mRNA transcript leading to the amino acid change R614C [45]. This is synonymous with the porcine R615C mutation.

1.4 Ryanodine receptor and protein interaction

The ryanodine receptor (RYR) is the largest known ion channel with a molecular mass of 2.3 MDa. It has three different isoforms: type 1 (*RYR1*) which is expressed at high levels in skeletal muscle cells; type 2 (*RYR2*) expressed in cardiac muscle and in the brain and type 3 (*RYR3*) is expressed in a wide variety of cell types. All isoforms show an amino acid identity of around 65 % but only isoform 1 is associated with MH while RYR2 is associated with cardiovascular disease (reviewed in [46]).

RYR1 is comprised of four identical subunits, approximately 5000 amino acid (aa) long, where each subunit has a molecular mass of ~565 kDa [38]. The

ryanodine receptor, located in the membrane of the sarcoplasmic reticulum, functions as a Ca^{2+} release channel to release Ca^{2+} from the lumen of the SR into the cytosol. The C-terminal part of the protein is situated in the transmembrane domain and comprises 1/5 of the mass of the protein. The main part of the channel extends into the cytoplasm and includes the N-terminal and central domains making up 4/5 of the receptor mass [47]. The three hot spot domains are located at amino acid positions 35 to 614 (MH1), 2163 to 2458 (MH2) and 4637 to 4906 (MH3) [40]. Hotspot region 3 is located in the transmembrane domain. The exact 3D structure of the receptor is unknown but different models have been suggested predicting between 4 and 10 transmembrane domains [48-51]. Due to the large size of the ryanodine receptor there are few three dimensional structures currently available. Cryo-EM (electron microscopy) studies have been undertaken and used to create a 3D model dividing RYR1 into different domains and suggest an overall mushroom-shaped receptor. Subdomains have been labelled as “clamp” shaped and are located at the corners of the cytosolic domains and are connected by a “handle” shaped region (figure 1.5) [52].

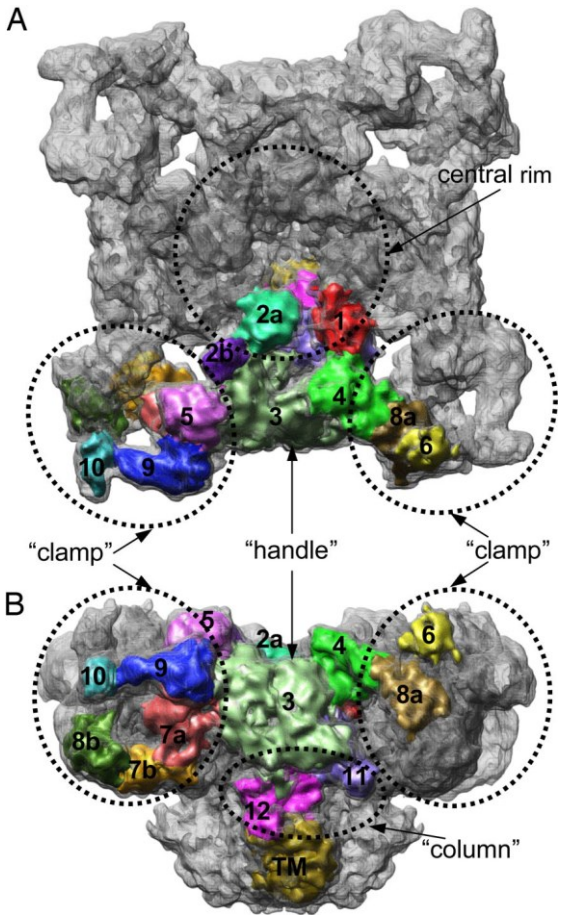

Figure 1.5 A 9.6-Å resolution cryo-EM density map of RYR1 in the closed state.
This figure indicates the different subregions of RYR1. Each colour represents a different region within one subunit. The 3D structure can be divided into a "clamp", a "handle" and a "column". A) View from the cytoplasm. B) View from the side. TM indicates the transmembrane region of RYR1 (taken from [53], no copyright permission required).

Further studies using immunoprecipitation showed that a site within the cytoplasmic domain (including amino acids V2461 and P2462) interacts with the FKBP12.0 protein stabilising the closed state of the RYR1 channel [30, 54, 55]. Disrupting the interaction between RYR1 and FKBP12.0 leads to failure of EC coupling due to the loss of FKBP binding and an increase in RYR1 open probability [31]. Further studies revealed four FKBP12.0 molecules can bind one RYR tetramer. Its binding site is most likely located at the interface between domains 3, 5 and 9 of the surface located cytoplasmic part of RYR1 (figure 1.6). This region includes the MH/CCD causative mutation sites E160, R163, R401 and I403 in human RYR1 that may disrupt the interaction between these two proteins resulting in altered RYR gating [53, 56, 57]. As mentioned above, the α_{1s} subunit of the

dihydropyridine receptor (DHPR) physically interacts with RYR1 and contains a voltage sensor (figure 1.6). Another subunit of DHPR, the β_{1a} subunit, is also believed to interact with high affinity with RYR1. This subunit interacts with the basic RYR1 residues K3495-R3502 [58] and is located at the C-terminus of the full-length DHPR and may contribute to EC coupling since this domain in DHPR is needed for proper skeletal muscle EC coupling [59]. Antibody binding assays have shown that the ryanodine receptor 1 undergoes oligomerisation between the cytoplasmic domains including the 34C antibody binding region 2872–2893 [60]. Amino acid residues ~2700-3000 are possibly surface-exposed since proteolysis experiments showed trypsin was able to cleave this region in native tetrameric RYR1 protein and are therefore unlikely to be involved in forming the core of the tetramer [61, 62].

RYR1 also interacts with many other proteins, including calsequestrin, triadin, junctin and calmodulin (CaM). RYR1 binds 16 CaM (mol/mol) at cytosolic Ca^{2+} concentrations <0.1 μM while it only binds four CaM at 100 μM Ca^{2+} and inhibits the channel at millimolar Ca^{2+} concentrations [63]. CaM is a strong antagonist of RYR when bound to Ca^{2+} but is an agonist in the absence of Ca^{2+}. CaM binds to RYR1 at regions around residues 3614-3643 and/or 2937-3225 which are believed to be in close proximity in the RYR1 tertiary structure (reviewed in [43]). Despite early assumptions, CaM is not necessary for EC coupling [64].

Calsequestrin is a highly acidic protein present in the SR lumen. It has a low Ca^{2+} affinity but a high Ca^{2+} binding capacity and acts as a Ca^{2+} storage protein binding 40-50 Ca^{2+} ions per molecule in skeletal muscle [65]. In the presence of two cofactors, triadin and junctin, calsequestrin inhibits RYR1 activity but it has been suggested that calsequestrin does not bind RYR1 directly [66]. An approximate binding site for triadin to RYR1 was suggested using *in vitro* binding assays, locating its binding site between amino acid residues 4861-4918 in RYR1 [67]. The absence of triadin results in an increased Ca^{2+} leakage from the SR leading to increased cytoplasmic Ca^{2+}

concentrations which suggests negative regulation of RYR1 by this protein [68].

Figure 1.6 shows a summary of RYR1-binding proteins and their predicted three dimensional locations. Some of these proteins i.e. PP1/SP and HRC, were not of interest in this study even though they are important in the regulation of RYRs and Ca^{2+} release, and were therefore not considered here.

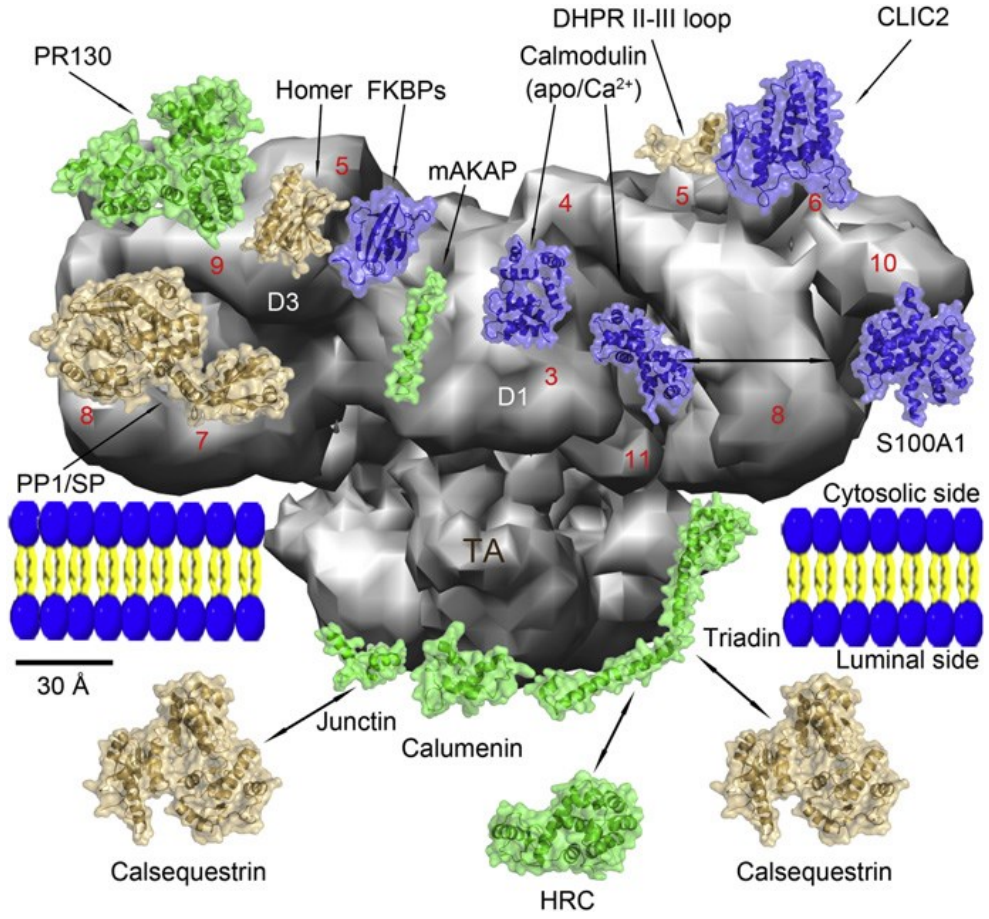

Figure 1.6 Three-dimensional map of the ryanodine receptor 1 assembly.
The cryo-EM map with a side view of the large rabbit RYR1 tetramer in a closed state is shown with its protein interaction partners. Strictly, different subregions are labelled with red numbers 3-11 and correspond to regions in figure 1.5. The three divergent regions are printed in white (D1-3) and the transmembrane domain (TA) is grey (taken from [69], permission for publishing figure was obtained through RightsLink).

Homer interacts at three different positions in RYR1. At low concentrations of homer the open probability of the RYR channel is enhanced and the

frequency of Ca^{2+} sparks, spontaneous Ca^{2+} release in cardiac and skeletal muscle cells, is increased (reviewed in [69]).

Another RYR1 binding protein is CLIC2, a new class of Cl^- channel. This protein appears to act as a RYR1 inhibitor of channel gating when bound to the cytosolic side of RYR1 and it has been suggested that CLIC2 stabilises the closed state of RYR1 (reviewed in [69]). S100A1 is a cytoplasmic Ca^{2+} binding protein and is highly expressed in the SR of skeletal and cardiac muscle regulating SR Ca^{2+} release. It enhances RYR1 open probability at nanomolar concentrations of Ca^{2+} and it is suggested that the S100A1 protein plays a role in RYR1 activation. The S100A1 binding site was localised to residues 3616-3627 and it was shown that S100A1 and calmodulin compete for the same RYR1 binding site although the physiological consequence of this competition to RYR1 is not well understood (reviewed in [43, 69]).

1.5 Other Ca^{2+} release channels

Inositol 1,4,5 triphosphate (IP3) acts as a second messenger which binds to its receptor (IP3R) and releases Ca^{2+} from intracellular stores [70]. The IP3R is a 2749 amino acid protein channel with a molecular mass of 313 kDa. It shows similarities to the ryanodine receptor and is composed of three structural parts: a large cytoplasmic N-terminal (aa 1-2275), a region near the C-terminus which has 6 transmembrane helices (residues 2275–2593) and a short C-terminal tail (aa 2590- 2749) [71]. IP3R also exists as a homo-tetramer, each with an IP3-binding site close to the N-terminus [72] located between aa 226 and 576 [71], as well as a suppressor domain between residues 2-223 which inhibits binding of IP3 to the receptor [73]. The overall 3D structure of IP3R1 is mushroom-like, forming a 190 Å tall structure (figure 1.7A). The central part within IP3R seems to be a so-called “plug” (figure 1.7B), holding the 4 subunits together by oligomerisation. This plug is absent in RYR1, therefore RYR1 must have a different mechanism of oligomerisation. A “window” can be seen in the 3D structure of the individual subunits of IP3R, which is located just above the transmembrane region. This

may allow Ca^{2+} to move freely between the channel domains and cytoplasm [74].

IP3R and RYR1 have structural similarities (figure 1.7A) and exhibit some amino acid sequence homology, especially in the transmembrane domains [75].

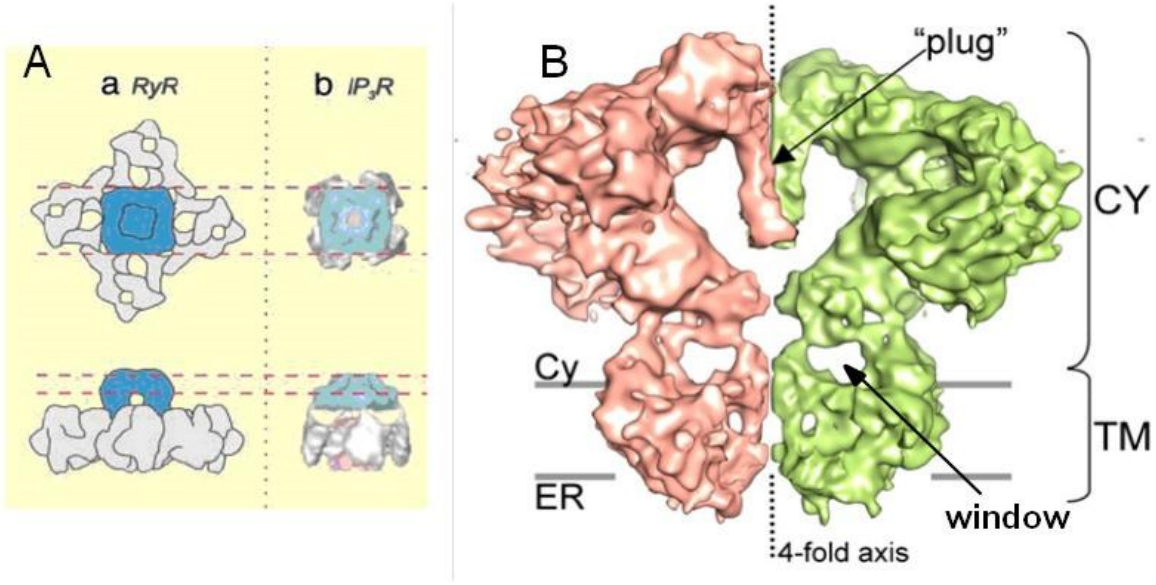

Figure 1.7 3D structure of IP3R and RYR viewed from the ER lumen and membrane.
A) Comparison of the 3D structure of (a) RYR and (b) IP_3R. The upper figures show the view from the lumen and the lower figures show orthogonal view from the membrane. Homologous regions in RYR1 and IP3R are indicated by the same colour.
B) Cross section of the internal structure of IP3R resolved by cryo-EM. The fourfold symmetry axis is indicated by a dashed line and the "plug" involved in oligomerisation is shown. Two different subunits are colour coded. Cy= cytosol, ER= endoplasmic reticulum, CY= cytosolic domain, TM= transmembrane domain. (Figure adapted from [75], no copyright permission to publish required, and [74], permission for publishing figure was obtained through RightsLink).

The N-terminal domain of rabbit RYR1 (aa 1-210) was crystallised by Amador et al. [76] and the RYR1 X-ray protein structure was solved showing that the N-terminal 210 amino acid structure of RYR1 and IP3R are nearly identical. RYR1 and IP3R also show two other homology domains (RIH) one of which is located in the central domain and one in the N-terminus of RYR1 (figure 1.8). These homology domains are located approximately between aa

466-643 and 2157-2365 in RYR1 and between amino acid 499-677 and 1196-1356 in IP3R (source NCBI, [77]).

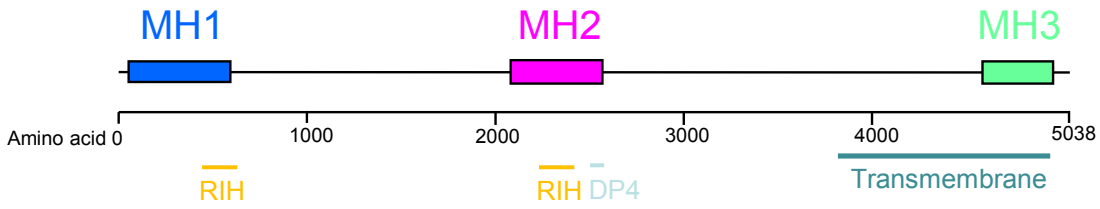

Figure 1.8 Positioning of RYR1 and IP3R homology domains within the ryanodine receptor 1. This schematic diagram is not to scale. RIH= RYR1 and IP3R homology domain, DP4= domain peptide 4.

To verify sequence homology domains, Seo et al. [78] substituted protein domains in the N-terminal region of IP3R with the corresponding region in RYR1 and could still detect functional IP3R suggesting that these domains in each protein have the same function.

1.6 DP4 domain

The DP4 (domain peptide 4) domain was first described by Yamamoto et al. in 2000 [79]. These authors found that this domain corresponds to amino acids L2442 to P2477 in RYR1 (figure 1.8). A DP4 peptide significantly activates RYR1 and induces Ca^{2+} release from the SR when bound to full-length RYR1 microsomal fractions. It increases the sensitivity of RYR1 to agonists and leads to higher Ca^{2+} release. Mutations in this domain lead to two main functional modifications which occur in MH patients; hypersensitivity and hyperactivity [79]. It was suggested that DP4 interacts with the N-terminal domain DP1 (aa 590–628). These two domains were thought to form a complex which has been described as domain-zipping (figure 1.9). This complex could lead to a closed state in the transmembrane region of the Ca^{2+} channel and the close contact between the N- and the C-termini is thought to stabilise the closed state of the pore channel [80].

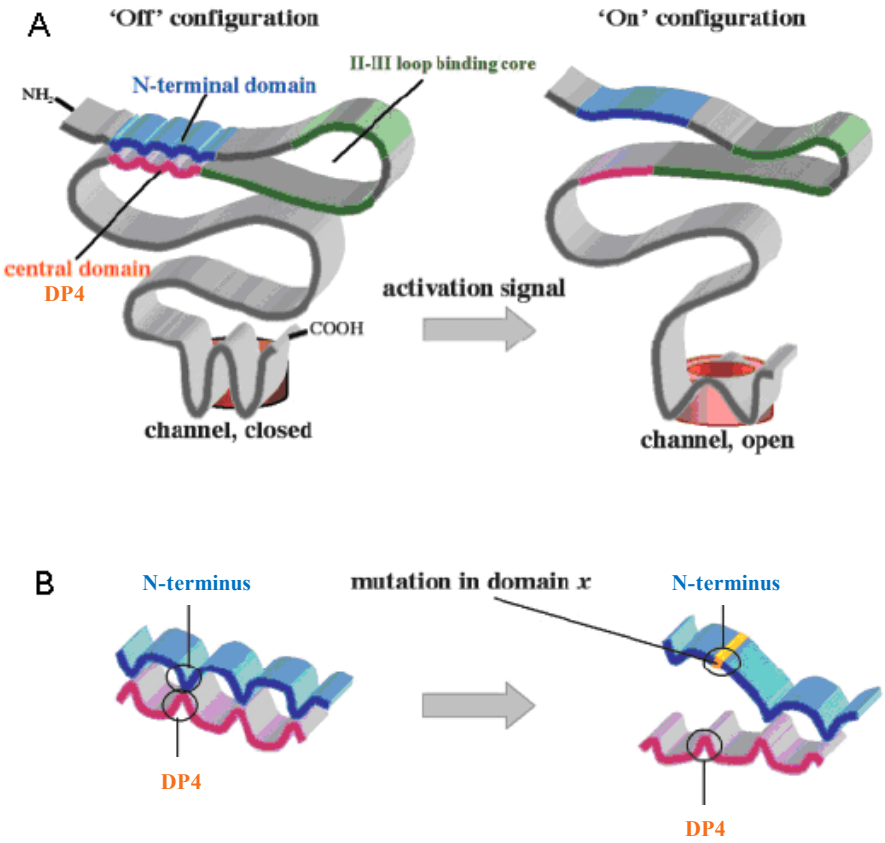

Figure 1.9 Interaction between N- and C-terminal domains in RYR1.
Hypothetical model of opening and closing the RYR1 pore channel as the N-terminus and the DP4 domain interact. A) The model proposes that the interaction between the N-terminus and the central domain stabilises the closed state of the channel. When an activation signal is produced the domains undergo conformational changes, the interaction between the two domains is removed and the channel can switch to the open state.
B) If any mutations occur in either of the domains the interaction of the domains would be weakened (here shown for mutation in N-terminal domain) and the receptor would stay in an open state leading to higher Ca^{2+} release from the SR (taken from [80], permission obtained through RightsLink).

If a mutation occurs in either of the domains, the domain interaction is weakened and the closed state is destabilised. This causes an unzipping of the domains and could lead to an open channel resulting in the hypersensitivity and hyperactivity of the receptor as described above. A recent study supported the model of an N-terminal (aa 35-614) and central domain (aa 2163-2458) interaction by labelling two RYR1 residues in the domains of interest [81-83]. Three dimensional localisation of the DP4 domain showed the N-terminus and the central domain in close proximity, supporting the theory of a "domain zipper-model" (figure 1.9). This model

may also support the suggestion that this domain might be involved in oligomerisation since it is located at the interface between subunits [83]. The crystal structure for the N-terminal amino acids 1-559 has been solved and with the latest results, it has been suggested that not the entire N-terminal domain is involved in a domain zipper model but smaller domains in the N-terminus may be involved in multiple smaller zippers, each separately involved in domain interaction [84]. Another study showed that DP4 binds to the N-terminal region containing the dantrolene binding site (amino acid 590-609) [85, 86]. This may explain why dantrolene, which is administered during MH episodes, can decrease the hypersensitivity of the receptor. The three dimensional structure of DP4 solved via NMR studies (figure 1.10) suggests that the domain contains a helix-turn-helix motif [87].

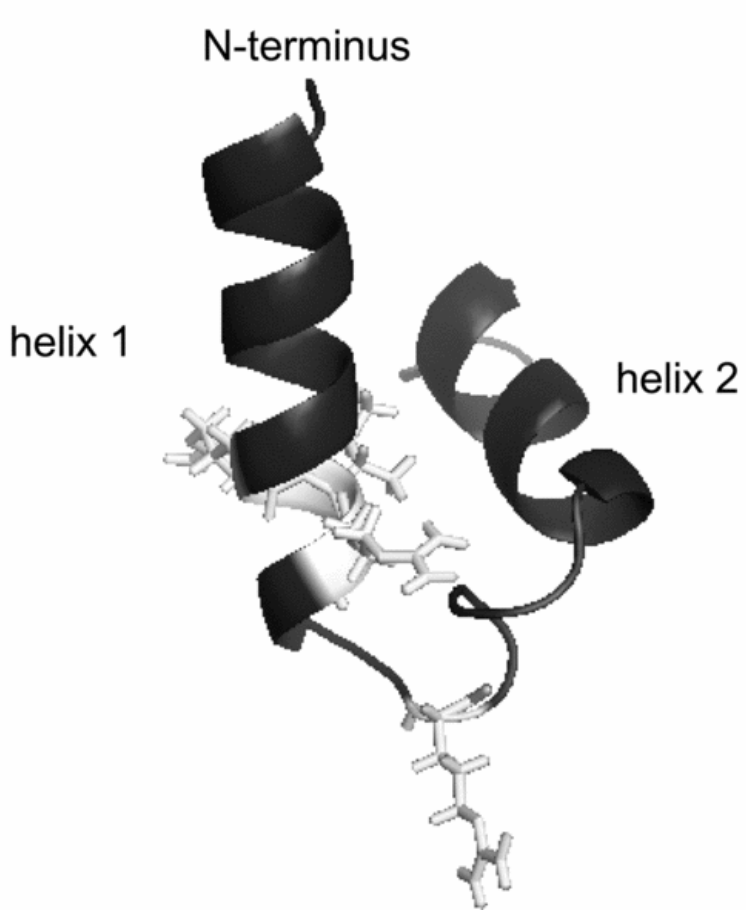

Figure 1.10 NMR structural model of DP4

DP4 contains a helix-turn-helix motif where the N-terminal part of helix 1 acts as a linker between the two helices. Residues 2452 to 2454 (white), are located in the C-terminal part of helix 1 and the connecting turn (taken from [87], no copyright permission required).

1.7 Pharmacology

1.7.1 Dantrolene

Dantrolene is an inhibitor of Ca^{2+} release from the SR, causes relaxation of skeletal muscles, and was first described as a drug to treat MH in 1975 [88]. It was originally synthesized as an antibiotic in 1967 but was never used as such because it was discovered that treatment lead to muscle weakness in animal experiments [89]. Today it is used as a pharmacological antidote to MH as it blocks Ca^{2+} release and inhibits CICR. It was suggested that dandrolene may act upon RYR1 by blocking its interaction with calmodulin and Ca^{2+} while it did not affect the action of the DHPR [90, 91]. Treatment with dantrolene was found to inhibit EC coupling without affecting the muscle itself [92]. To elicit a maximal muscle relaxation in humans, 2.4 mg dantrolene/kg body weight must be given intravenously to result in a final concentration of 4.2 µg/mL in blood [93]. As the dantrolene binding site in RYR1 has been suggested to be between residue L590 and C609 in the N-terminal region, dantrolene could therefore lead to a structural change in RYR1 and stabilise a closed conformation [94]. Dantrolene has been shown to suppress store overload-induced Ca^{2+} release (SOICR) by lowering the threshold for SOICR in studies of the RYR1 mutation R615C, expressed in HEK293 cells. It has been shown that this mutation lowers the threshold for luminal Ca^{2+} activation while volatile anaesthetics further lower the SOICR threshold [95].

1.7.2 Caffeine and halothane

Caffeine and halothane are used in the IVCT and have been well defined as RYR1 agonists by the European MH group since 1984 [15]. The IVCT is based on the hypersensitivity of muscle to these drugs. Caffeine stimulates the central nervous system and can relax smooth muscle cells. It stimulates Ca^{2+} flux from the SR by increasing the Ca^{2+} sensitivity of RYR1, leading to a prolonged open state of the RYR1 channel (reviewed in [96]). A caffeine binding site on the RYR protein has not been located but caffeine EC_{50} values were in the order of 0.2 to 0.5 mM for RYR2 and RYR1, respectively. Caffeine has been shown to increase the frequency and duration of channel

opening in RYR2 incorporated lipid bilayers and caffeine was shown to bind to the receptors cytoplasmic side. It was also shown not to change the channels conductance nor the Mg^{2+} sensitivity [97]. Caffeine and halothane have both been shown to reduce the threshold for SOICR and luminal Ca^{2+} activation in stable transfected HEK293 cells [95]. It was hypothesized that caffeine blocks the conformational change in RYR1 necessary for the inhibitional effect of Ca^{2+} upon the receptor and therefore channel inhibition leading to hyperactivation of muscle [98]. Lopez et al. suggested that in MHS patients caffeine sensitivity is not altered due to mutations but these patients have a higher resting Ca^{2+} level, leading to muscle contraction at lower caffeine concentrations compared to MHN patients [99]. Furthermore caffeine is also known to activate RYR3 [100] which is endogenously expressed in low levels in myocytes possibly explaining why myocytes show a response to caffeine in IVCT but lack a response to other triggering agents [101]. Caffeine was also described to enhance CICR (reviewed in [35]).

Halothane was demonstrated to produce an abnormal response *in vitro* using skeletal muscles from MHS patients. For a long time it was unclear if halothane leads to muscle contraction *in vivo* or if it only blocks the Ca^{2+} uptake from the SR. Studies suggested that halothane induces muscle contraction at 37°C only in MHS patients but does not lead to contractions in MHN patients [102]. Halothane has been described to have two ionotropic effects: a positive effect which is due to sensitisation of CICR from the SR and a negative effect which is due to a decrease in myofibrilic Ca^{2+} sensitivity and lower Ca^{2+} release from the SR [103]. Halothane leads to a longer RYR channel open propability but does not affect channel conductance while it decreases channel closure time. This mechanism is dependent on the pH and Ca^{2+} content in the muscle and can influence ion concentration in the muscle e.g by blocking Na^{+}/Ca^{2+} transport [96, 104]. Experiments using R615C RYR1 transfected HEK293 cells showed enhanced SOICR. This phenomenon suggests a reduction of the luminal Ca^{2+} activation threshold as well as SOICR by volatile anesthetics, which trigger MH.

1.7.3 4-chloro-*m*-cresol (4CmC)

The first time 4-chloro-*m*-cresol (4CmC) was shown to release Ca^{2+} from the SR was in 1993 [105]. It is now known as a potential activator of RYR and can alter the Ca^{2+} permeability of the cell surface membrane and sensitises RYR. Cells are very sensitive to 4CmC and it is active in concentrations 30-40 times lower than observed with other agonists, e.g caffeine. It was also shown that MHS patients have a three to fourfold higher sensitivity to this drug than MHN patients [106]. Studies using ruthenium red to block RYR channels show Ca^{2+} efflux from the terminal cisternae is triggered by CICR [105, 106]. [^{3}H]Ryanodine binding studies have shown that 4CmC decreases the dissociation constant of RYR1 but does not affect the maximal Ca^{2+} binding while it prolongs the channel open probability [107]. Today, 4CmC is used as a preservative in some pharmaceutical preparations, like insulin and heparin. The effect upon MHS patients is therefore important as they may be inadvertently administered pharmaceuticals containing a potential RYR1 agonist. In higher concentrations (>1 mM) 4CmC can also act as an inhibitor of SERCA [108].

It was shown that 4CmC acts in a dose-dependent manner in both MHS and MHN patients *in vitro* [106, 109, 110]. Therefore, studies have proven that 4CmC triggers Ca^{2+} release more specifically from the ryanodine receptor than other agonists, making it a useful tool for research purposes [111]. Since some RYR1 mutations can inhibit the response to 4CmC and voltage-gating but not to caffeine it has been hypothesised that 4CmC may activate RYR1 by a similar mechanism as the voltage sensor [112]. The 4CmC binding site on RYR1 has been mapped between amino acid positions 4007 and 4180 [113].

1.7.4 Other agonists

1.7.4.1 Ca^{2+}, Mg^{2+} and K^+

Cytosolic free Ca^{2+} is important for regulating RYR activity. The channel activity of the receptor is activated by micromolar Ca^{2+} concentrations but inhibited at millimolar concentrations [114]. Cytosolic free Ca^{2+} levels are

~100 nM [99, 115] while free Ca^{2+} levels in the SR stores are between 0.3 and 1 mM [116]. Compared to other cations in a cell such as K^+, Mg^{2+} or Na^+, Ca^{2+} is the only cation which is not evenly distributed across the SR membrane because SERCA pumps Ca^{2+} back into the SR to ensure a trans-SR Ca^{2+} gradient [117].

Mg^{2+} is an inhibitor of Ca^{2+} release through the ryanodine receptor; millimolar concentrations inhibit the receptor because of its high RYR1 pore binding affinity, meaning that Mg^{2+} is preferably bound to RYR1 over Ca^{2+} [116]. It has been suggested that Ca^{2+} and Mg^{2+} interact in the regulation of RYR1. The Ca^{2+} binding sites in the receptor [I (low affinity) and A (high affinity) site] have been identified. The receptor can only bind Ca^{2+} if the channel undergoes a conformational change and weakens the binding of Mg^{2+} to the A-site. If Mg^{2+} is released from the A-site, Ca^{2+} can subsequently bind at this site and induce Ca^{2+} release from the receptor [118, 119]. The RYR1 I-site has a high affinity for Mg^{2+} which inhibits Ca^{2+} release. During EC coupling the DHPR triggers Ca^{2+} release induced by the reduction of Mg^{2+} inhibition in the I- and A-sites. The DHPR controls Ca^{2+} release by having the ability to stop Ca^{2+} release when the surface membrane repolarises after an action potential arrives. This allows a tight control of Ca^{2+} release in the cells. In contrast, in cardiac muscle, the RYR2 I-site has a 10-fold lower Mg^{2+} affinity and DHPR does not influence Ca^{2+} release in these cells. Here, Ca^{2+} release is triggered by Ca^{2+} influx from the surface membrane, while the exact mechanism is unknown (reviewed in [120]). A tetrameric model has been shown for RYR2 including four Ca^{2+}-sensing mechanisms on each subunit: activating luminal L-site (40 µM affinity for Mg^{2+} and Ca^{2+}), cytoplasmic A-site (affinity of 1.2 µM for Ca^{2+} and 60 µM for Mg^{2+}), an inactivating cytoplasmic I_1-site (~10 mM for Ca^{2+} and Mg^{2+}), and an I_2-site (affinity of 1.2 µM for Ca^{2+}). The activation of at least three subunits will lead to channel opening. Mg^{2+} displaces Ca^{2+} from the L- and A-sites while inhibiting the channel, which then fails to open [116]. The Ca^{2+}/Mg^{2+} competition for the RyR pore is mainly responsible for the unitary Ca^{2+} current amplitude [117].

At the resting physiological state there are ~1.5 Mg^{2+} ions and only ~0.5 Ca^{2+} ions bound to the RYR1 selectivity filter indicating the pore region has a higher

affinity for Mg^{2+} than Ca^{2+}. It should be noted that Mg^{2+} is spread evenly across the whole receptor while Ca^{2+} can only be found in the selectivity filter in the pore region [117]. In order to ensure a SR membrane potential near 0 mV and a high ion flux across the membrane, Ca^{2+} needs to have its own countercurrent which is mostly provided by K^+ because its conductivity through RYR1 is 5-10 times higher compared to Mg^{2+} [121]. It should be noted that the molar ratio of Mg^{2+} to K^+ in the selectivity pore is limited to ~4.7 to ensure that K^+ will never be completely displaced from the pore [117]. Mg^{2+} plays a critical role in skeletal muscle contraction and a Mg^{2+} concentration of 1 mM ensures a closed state of RYR1 preventing CICR. It has been suggested that reduced Mg^{2+} regulation can lead to the development of MH and facilitate an MH episode [122, 123].

1.7.4.2 Adenosine triphosphate (ATP)

ATP is known to be an activator of RYR1 *in vivo* and, at concentrations of 5 mM, ATP can fully activate the receptor in muscle cells to release Ca^{2+}. ATP and micromolar concentrations of Ca^{2+} must be present to obtain maximum opening and to stabilize the open state of the RYR1 channel [124]. In the presence of low Ca^{2+} concentrations at least four ATP binding sites per monomer can be found in the RYR1 tetramer identified at amino acid positions 699-704, 701-706, 1081-1084 and 1195-1200, forming the ATP binding pockets. The amino acids at these positions are highly conserved between RYR1, RYR2 and RYR3 suggesting functional conservation. The stimulating effect of ATP on RYR1 was only shown in the presence of Ca^{2+} and it was assumed that this interaction might stabilise the channels open state, however the exact mechanism of the coupled effect upon the channel is still unknown [83]. ATP concentrations in muscle are ~8 mM and could lead to full RYR1 activation but most ATP is bound to intracellular Mg^{2+} (~9 mM). Therefore only small amounts of free ATP are available in the cell and Mg^{2+} acts as an antagonist and prevents ATP-stimulated Ca^{2+} release (reviewed in [120]). Structural studies suggest a mass rearrangement of the RYR channels upon ATP binding leading to opening of the channel and ion flow across the membrane [52].

1.8 RYR1 associated disorder central core disease (CCD)

Some *RYR1* mutations have been linked to MH but others show different functional effects not typical of MH. Central core disease (CCD; OMIM# 117000) was described in 1956 as the first congenital muscle disorder involving structural changes of the muscle fibres [125]. CCD was described as an autosomal dominant disease, characterised by abnormal muscle architecture and sarcoplasmic disorganisation leading to muscle weakness and mild hypotonia in childhood. Further studies have shown that CCD can also be inherited in an autosomal recessive manner [126]. In 1990, Haan et al. were able to link CCD to chromosome 19q13 [127]. Further research and the knowledge that MH susceptible patients have similar phenotypes under anaesthesia to CCD patients, helped to identify *RYR1 as* the CCD locus. CCD mutations occur in hot spot regions in *RYR1* in almost the same regions as for MH (figure 1.4). Interestingly, around 60 % of CCD causative mutations are located at the 3' end of the *RYR1* gene [128]. CCD patients can be identified using IVCT and are therefore diagnosed as MHS. Histology can help to identify whether a patient is MHS or has CCD. Typical skeletal muscle histology in CCD patients shows the absence of oxidative and glycolytic enzyme activity from the central cores of muscle fibres together with a reduction of oxidative activity due to the reduction or absence of mitochondria. In CCD patients, some cores have variable degrees of myofibrillar disorganisation, whereas others might have preserved myofibrillar structure and other cores do not. These two phenomena can be found within a single patient making diagnosis using histology unreliable (reviewed in [129]). MH patients do not show this disorganisation. Even though both disorders are not connected phenotypically, it appears they can co-exist. This is supported by evidence that some mutations can be linked to CCD as well as MH. It is still unknown how these two disorders can co-exist. Research suggests patients with one mutation in *RYR1* could have MH while patients having two mutations in *RYR1* may suffer from CCD due to a compound autosomal-recessive inheritance [130, 131].

1.9 Methodology of functional assays

Since many MH- and CCD-associated mutations have been identified, it is a major goal to characterise these mutations in terms of any functional effect upon RYR1 to be able to offer DNA-based testing for MH mutations rather than IVCT. A range of assays in different cell types have been developed to analyse functional effects of several mutations for MH and CCD. Most assays have been carried out in differentiated muscle cells (myotubes) obtained after an IVCT. These muscle cells express all proteins involved in EC coupling (see chapter 1.2 for details) and therefore closely represent conditions *in vivo.* Results however, can be inconclusive, because if functional studies show abnormal Ca^{2+} release it is still possible that other proteins involved in EC coupling, e.g. DHPR are involved in the abnormal response leading to MH phenotypes. Agonists used in Ca^{2+} release studies only show activation of RYR1 but it cannot be concluded that the abnormal response is due to a defect in RYR1 or in other proteins involved in EC coupling leading to an MHS phenotype. For example, if a mutation in DHPR occurs which leads to defective binding to RYR1 or less Mg^{2+} inhibition, a MHS phenotype can be seen in skeletal myotubes but the cause of the phenotype cannot be determined. Myotubes lacking DHPR expression have been transfected with mutant DHPR cDNA and functional assays were able to show a MHS phenotype [36], showing that care has to be taken when using myotubes in functional assays.

It has been reported that B-lymphocytes, extracted from patients blood, express an alternatively spliced form of RYR1 that lacks amino acids 3481-3485, encoded by exon 70 [132]. It has been speculated that these cells express RYR1 for its involvement in Ca^{2+} regulated signal transduction as well as in cell proliferation [133]. It has been suggested that Ca^{2+} release in lymphocytes is mainly dependent on activation of IP3R by IP3 and store-operated Ca^{2+} entry. Ca^{2+} release is initiated by the cell stimulation of antigen- and Fc-receptors from intracellular ER stores. In addition, activation of the IP3R may coactivate RYR1 (reviewed in [134]). B-lymphocytes have the advantage of better availability compared to myoblasts since they can be extracted from a patient's blood sample and no muscle biopsy is required as

for the extraction of myoblasts. Lymphocytes express RYR1 but no other proteins involved in EC coupling which is an advantage for studying *RYR1* mutations *in vivo* as well as in isolation from the the rest of the channel proteins. Agonist activated lymphocytes showing an MHS phenotype will most likely have a mutation in *RYR1* since no other proteins involved in skeletal muscle contration are involved in Ca^{2+} release in these cells. However, lymphocytes do not represent a physiological system mimicking RYR1 in muscle contraction and therefore may not necessarily demonstrate RYR1 behaviour as seen in muscle cells. Nevertheless these cells are a useful system to study *RYR1* mutations involving patient-derived tissue.

HEK293 cells, transfected with a full-length rabbit or human *RYR1* cDNA clone, have also been used to study Ca^{2+} release previously [135]. HEK293 cells are non excitable cells and their major Ca^{2+} release channel is the IP3R, even though it has been suggested that they express RYR1 and RYR3 at minor levels [136, 137]. These cells show two mechanisms of Ca^{2+} release: receptor-operated Ca^{2+} release, which is triggered by the activation of IP3R by its agonist IP3 and store-operated Ca^{2+} release, triggered by depletion of intracellular Ca^{2+} stores (reviewed in [138]). To be able to use this experimental system however, an MH-associated mutation has to be identified and cloned into an expression vector carrying the full-length *RYR1* cDNA (~15,000 base pairs). HEK293 cells can be transfected with the prepared clones and Ca^{2+} release can be measured in the isolated RYR1. Agonists are used to activate the receptor and the response of RYR1 to the agonist can be measured. Since no proteins involved in EC coupling are expressed in HEK293 cells, Ca^{2+} release is due to a response of RYR1 alone and will not be influenced by other proteins e.g DHPR. If altered Ca^{2+} release is detected in this system, it is most likely due to a *RYR1* mutation. This system however does not represent the biological background of MH patients since transfected HEK293 cells express homozygous *RYR1* mutations while *RYR1* mutations *in vitro* are usually expressed heterozygously [44].

Dyspedic myoblasts, lacking a functional RYR1 protein, are available and can be used for transfections with mutant *RYR1* cDNA to test whether a

mutation alters Ca^{2+} release. This method has the advantage of representing Ca^{2+} release in intact muscle cells as they include all proteins involved in EC-coupling under regulated conditions. In addition since all cells have the same genetic background, the system represents the Ca^{2+} release mechanism *in vivo* by differing only in the expressed *RYR1*. Using dyspedic myoblasts in Ca^{2+} release assays can also help to determine whether *RYR1* mutations have an effect on protein-protein binding and possible disruption of EC coupling mechanisms or signal transduction [139].

A new approach for functional studies has been undertaken by establishing transgenic mice to measure functional effects *in vivo.* It has been shown that the human I4898T mutation, associated with CCD, causes skeletal muscle abnormalities when inherited in a homozygous form accompanied by a delay in embryogenesis leading to developmental defects in the fetus [140]. The heterozygous I4898T mutation in mice however, does not display all the characteristics which can be seen in the human disease and does not show the same severity as do human CCD patients carrying this mutation. Nevertheless, transgenic mice provide valuable information about *RYR1* mutations and their effect *in vivo* on development and embryogenesis, as well as providing information about RYR1 associated protein interactions required for myogenesis but not directly linked to the Ca^{2+} release function of RYR1. RYR1 might rather have a structural role in other protein-protein interactions supporting their function. It has been suggested that the loss of RYR1-mediated Ca^{2+} release might be linked to nerve-induced signal transductions in early embryonic development.

For functional assays, cells are treated with different agonists (e.g. 4CmC or caffeine) and the Ca^{2+} release from the ER/SR is measured using a Ca^{2+} fluorophore, e.g. fura 2-AM. Most MH or CCD associated mutations show an abnormal release of Ca^{2+} in response to the agonists compared to wildtype RYR1. Not all mutations lead to the same phenotype and some mutations (e.g. T4826I in human) show a higher quantitative intracellular Ca^{2+} release compared to wildtype *RYR1* expressing cells [141].

1.10 Functional disorganisation of the RYR1 receptor

1.10.1 Hypersensitive RYR1

MH-associated mutations are thought to cause a hypersensitive ryanodine receptor with hypersensitivity to agonists and hyposensitivity to channel inhibitors, releasing abnormal Ca^{2+} amounts compared to the wildtype receptor [141-143] when exposed to triggering agents (figure 1.11b). Mutant RYR1 proteins have shown channel opening and subsequent Ca^{2+} release at lower agonist concentrations compared to WT RYR1. It has been shown that the threshold for Ca^{2+} release in response to agonists for RYR1 mutations has been lowered from 8 mM to 4.5 mM for halothane in myotubes carrying the R163C mutation, leading to higher channel activation in mutant RYR1 proteins [144]. These values can vary between different patients and different RYR1 mutations. A mechanism to account for Ca^{2+} release in RYR1 relies on the interaction between the N-terminus and the central domain as described in section 1.6. The presence of a mutation in either of these domains weakens their interaction and the channel can release Ca^{2+} in the presence of lower concentrations of agonist. This weaker interaction and hypersensitive receptor results in faster muscle contraction through high Ca^{2+} release into the cytosol, which is a typical symptom of MH patients under general anaesthesia.

1.10.2 Leaky Ca^{2+} channels

Functional studies have shown that not all mutations in *RYR1* lead to a higher response to agonists and therefore higher Ca^{2+} release from the SR. Some mutations appear to result in a leaky channel that causes a depletion of stored Ca^{2+} at the resting state (figure 1.11c). These observations suggest the channel is hyposensitive to agonists and cannot open properly. These defective channels can in part explain the symptoms of CCD patients who show muscle weakness and reduced muscle tension [145]. It was suggested that muscle weakness may be caused by an over active Ca^{2+} channel which is coupled with a steady leakage of Ca^{2+} through the RYR1 (leaky channel hypothesis) and subsequently in Ca^{2+} store depletion. This phenomenon is observed in CCD patients but not in MHN or MHS patients [146-148]. Leakage and a higher resting Ca^{2+} concentration (free cytosolic Ca^{2+}) can be

detected in Ca^{2+} release assays with transfected HEK293 cells bearing the rabbit RYR1 Y523S mutation [146]. The leakage leads to reduced stored Ca^{2+} which may result in insufficient Ca^{2+} release and damage to the core of muscle fibre. As a result the reduced stored Ca^{2+} is insufficient for release of the required Ca^{2+} into the cytosol to elicit proper muscle contraction, resulting in muscle weakness. The best studied mutation for the leaky channel hypothesis is Y523S in rabbit (Y522S in human). Patients with this mutation showed a 25 % reduction of SR Ca^{2+} content while the resting Ca^{2+} concentration significantly increased [149]. Additional mutations have been found by Tong et al. to cause leakage from the SR in transfected HEK293 cells including the human central region mutation R2163H [146] and the rabbit Y4795C mutation, equivalent to the human Y4796C mutation [112].

1.10.3 EC uncoupling

Not all CCD mutations appear to be associated with a leaky channel phenotype. CCD mutations, e.g. I4898T in humans, have also been described to produce the opposite phenotype. These mutations show no response to agonists or membrane depolarisation (figure 1.11d). This phenomenon, described as excitation-contraction uncoupling (EC uncoupling) [150], was first described for the I4898T mutation situated in the C-terminal region of RYR1 (hot spot MH3, figure 1.8). Myotubes, cells isolated and differentiated from muscle samples, expressing this mutation showed a significantly higher resting Ca^{2+} concentration compared to MHN cells but the sensitivity to agonists was even lower [151]. It has been suggested that the receptor is no longer able to respond to the electrical signal sensed by DHPR in muscle. Accordingly, the action potential cannot be passed further and no Ca^{2+} is released through the receptor (reviewed in [152]).

Further mutations have been described which do not respond to activation by caffeine or 4CmC. These mutations are situated in the central domain of RYR1 between amino acids 2370 and 2375. As these mutations occur in a predicted ATP binding site (CCD hot spot region 2), it was concluded that the reduced caffeine sensitivity could be linked to structural changes in the

protein which prohibit caffeine binding. These mutations could not be linked to EC uncoupling [153].

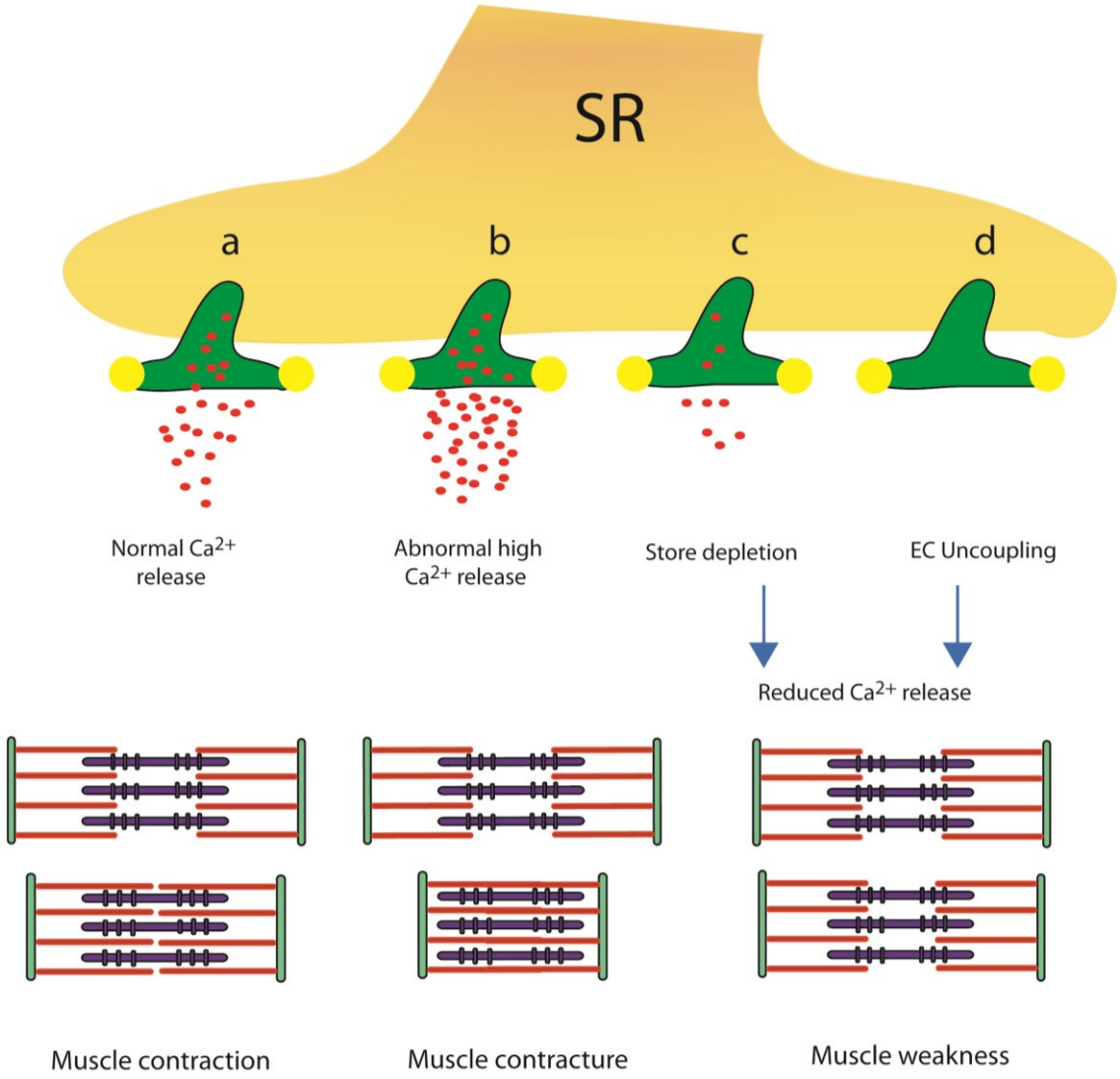

Figure 1.11 Schematic model of abnormal Ca^{2+} release mechanism in RYR1.
Different Ca^{2+} release mechanisms in muscle are shown. The ryanodine receptor (green) is located in the SR membrane (orange). a) Ca^{2+} release in a non mutant RYR1 is shown and leads to normal muscle contraction. After an action potential arrives the receptor releases Ca^{2+} (red dots) leading to muscle contraction. b) If a MH causative mutation occurs in the receptor it leads to a hypersensitive receptor which releases higher amounts of Ca^{2+} resulting in increased muscle contraction. c) If the ryanodine receptor has a mutation leading to a leaky channel phenotype the SR Ca^{2+} stores are depleted. If the receptor is activated RYR1 cannot release the amount of Ca^{2+} needed to form a proper muscle contraction. It can only release a decreased amount of Ca^{2+} and therefore leads to reduced muscle contraction which can be detected as muscle weakness. d) If an action potential arrives at the t-tubule membrane the action potential cannot be transferred to RYR1 due to eliminated interaction between the receptors and uncoupling of DHPR and RYR occurs resulting in a nearly abolished Ca^{2+} release and reduced muscle contractions. (Picture adapted from [154]).

1.11 Reduced RYR1 expression

Studies investigating CCD have shown that some patients show reduced *RYR1* expression. Individuals carrying the CCD-associated human mutations R109W, M402T, A4329D and T4709M express only the mutated allele, indicating allelic silencing of the WT allele. It was proposed that only a small amount of expressed mutant RYR1 is needed to fulfil the function of RYR1 in muscle contraction. It was suggested that some recessive mutations may affect protein stability and assembly which leads to lower *RYR1* expression levels compared to individuals not carrying a *RYR1* mutation. Reduced *RYR1* expression may lead to insufficient Ca^{2+} release in the SR during EC coupling and therefore to the CCD phenotype of muscle weakness [155]. This reduced *RYR1* expression hypothesis is currently only supported by western blotting analysis and needs further functional studies for support. Further studies showed reduced *RYR1* expression due to non-synonymous point mutations introducing a stop codon in one *RYR1* allele leading to lower *RYR1* expression levels in muscle of affected patients, again associated with the CCD phenotype [42].

1.12 Other MH-associated loci

Only 50 % of MH cases appear to be linked to *RYR1* while 1 % are linked to the *CACNA1S* gene (OMIM# 114208). This is another candidate gene for MH, located on chromosome 1q32 and encodes the α_1 subunit of the voltage-gated DHPR. Screening of this gene identified an arginine-histidine substitution at amino acid position 1086 which is linked to MH [156]. This mutation is present in the III-IV loop of the receptor and therefore does not directly interact with RYR1 (refer to section 1.2). Functional studies showed that this mutation leads to a lower threshold for Ca^{2+} release triggered by caffeine and depolarisation [36]. It has been suggested that the R1086H mutation disrupts the negative allosteric regulation of the III-IV loop and RYR1 which is essential for the negative regulation of the Ca^{2+} release channel and therefore leads to excess Ca^{2+} release through RYR1 from the SR. Loss of this feedback mechanism can cause MH reactions where myotubes carrying the *CACNA1S* R1086H mutation showed increased

sensitivity against triggering agents like caffeine [36]. Interestingly another mutation at the same position substituting arginine for serine was identified and is associated with MH in three independent families [157]. A third mutation in the *CACNA1S* was recently identified, R174Y [158]. This is located in a putative voltage sensor domain and therefore a change in charge in this region could alter the voltage sensor mechanism. This mutation has not yet been functionally classified as causative. Four other loci have been associated with MH: MHS 6 (chromosome 5p5), MHS 4 (chromosome 3q13.1), MHS 3 (chromosome 7q21-q22) and MHS 2 (chromosome 17q11.2-q24). These loci were demonstrated by genome-wide linkage studies but no candidate genes have yet been identified [159-162]. *CASQ1* has been shown to cause catecholaminergic polymorphic ventricular tachycardia, a cardiac disorder, mostly associated with RYR2 and can lead to cardiac arrest and sudden death due to extense exercise [163]. *CASQ1* knockout mice showing a MH phenotype in response to heat stress and halothane [164]. To date, no causative mutations have been found in *CASQ1* in human.

1.13 Project outline

In 2000, Chamley et al. reported a novel mutation in the central region of RYR1, R2452W [165]. This mutation was shown to co-segregate with MH in one family and was absent in 100 control genomes. It was therefore classed as MH-associated. Subsequently, a second New Zealand family carrying this mutation was identified. The aim of this project was to functionally characterise the R2452W mutation for inclusion in the EMHG list of causative mutations. This would subsequently allow DNA-based screening for families with this mutation. Functional assays, using Ca^{2+} release assays, were performed to determine whether R2452W is MH causative. Three different cell types were used for this approach:

1. B-lymphocytes, isolated from RYR1 R2452W positive and negative patients. These blood cells express RYR1 but none of the other proteins expressed in skeletal muscle involved in Ca^{2+} release. Immortalized B-lymphoblastoid cells allow measurement of altered Ca^{2+} release from RYR1 alone.

2. Myotubes, obtained from a patient with a positive IVCT. These cells represent the actual events occuring when muscle cells are exposed to triggering agents.
3. A recombinant system, HEK293 cells transfected with R2452W and WT full-length human *RYR1* cDNA. HEK293 cells have been used in various studies to show altered Ca^{2+} release of RYR1 [135, 166]. This system allows the effects of a specific *RYR1* mutation on Ca^{2+} release to be measured in a controlled environment since the WT and R2452W expressed proteins differ only by one amino acid. Therefore altered Ca^{2+} release would be due to altered RYR1 function.

Assay conditions were first optimised in order to determine appropriate conditions and detect Ca^{2+} release from the SR/ER which was measured using a Ca^{2+} specific fluorophore: fura 2. Since lymphocytes are non-adherent cells Ca^{2+} release was measured using a fluorometer. Myotubes and HEK293 cells are adherent therefore a fluorescence-microscope was used to measure Ca^{2+} release. The RYR-specific agonist 4CmC was used for each set of assays. Data for the individual cell lines were compared to cells expressing WT *RYR1* in order to verify altered Ca^{2+} release from the SR/ER by RYR1. Caffeine, a different RYR1 agonist could have been used in this study to obtain additional information about the RYR1 receptor and the R2452W mutation but since this agonist also activates Ca^{2+} efflux through other receptors apart from RYR1, it was decided not to use this agonist and focus on 4CmC only.

To investigate whether the R2452W mutation might alter the overall protein structure of RYR1, the DP4 region together with the RIH region located in the RYR1 central domain were PCR-amplified for cloning and the putative domains were overexpressed in *E. coli*. Soluble protein was purified with the aim of carrying out both stability studies and to subsequently determine the 3D structure by X-ray diffraction of suitable crystals.

Chapter 2 Materials and Methods

2.1 Materials

Commercially purchased kits or products with the supplier names are listed below. All general laboratory chemicals from various suppliers were analytical grade or equivalent.

- Wizard™ SV Gel and PCR purification kit, Promega, Madison, WI, USA
- Turbo DNA free Kit, Ambion Austin, TX, USA
- iScript supermix, BioRad, Hercules, IC, USA
- Fast Start Taq Polymerase, Roche, Mannheim, Germany
- Ssofast Evagreen mix, BioRad, Hercules, IC, USA
- various (restriction) enzymes, New England Biolabs Inc, Ipswich, MA, USA
- Antarctic phosphatase, New England Biolabs Inc, Ipswich, MA, USA
- Taq Polymerase, Roche, Mannheim, Germany
- Fetal calf serum, Gibco, Auckland, New Zealand
- Penicillin/Streptomycin, Gibco, Auckland, New Zealand
- Trypsin, Sigma Aldrich, Steinheim, Germany
- G418, Gibco, Auckland, New Zealand
- Basic human fibroblast growth factor (bhFGF), Sigma, St. Louis, USA
- Opti-MEM I, DMEM high glucose, Ham's F10 media, Sigma, St. Louis, USA
- Insulin, Roche, Mannheim, Germany
- Chamber slide for tissue culture, Lab-Tek II, Naperville, IL, USA
- UV cuvettes 1939, Kartell,Blackburn, Australia
- Spin concentrators Viva Spin, GE Healthcare, Uppsala, Sweden
- Poly-L-lysine, Sigma Aldrich, Steinheim, Germany
- Collagen, calf skin, Calbiochem, Darmstadt, Germany
- Complete mini- EDTA free Protease inhibitor, Roche, Mannheim, Germany
- His-trap HP, GE Healthcare, Uppsala, Sweden
- 35 mm tissue culture plates, Nunclon, Roskilde, Denmark
- T4 Ligase, Roche, Mannheim, Germany
- Pfu Turbo Polymerase, Agilent, Stratagene, La Jolla, CA, USA
- 1 kB + DNA ladder, Invitrogen, Auckland, New Zealand
- High Pure RNA/ Plasmid isolation kits, Roche, Mannheim, Germany

- PureLink™ HiPure Plasmid Midiprep Kit, Invitrogen, Löhne, Germany
- Cell strainer filter cups, Nunc, #9156885, Bedford, MA, USA
- Dispase grade II, Roche, Mannheim, Germany
- Collagense class II, Roche, Mannheim, Germany
- Semi permeable insert, Falcon, #353090, Bedford, MA, USA
- Ficoll-Paque Plus, GE Healthcare, Stockholm, Sweden
- Pluronic F127, Sigma Aldrich, Steinheim, Germany
- 4-chloro-m-cresol, BDH Chemicals, Lutherworth, England
- Tissue culture flasks, 25 cm/ 75 cm, Nunc, Roskilde, Denmark
- T/C 6-well plates, Greiner Bio one, Frieckenhausen, Germany
- UV visible 96 well plates, Greiner Bio one, Frieckenhausen, Germany
- Precision Plus Protein Dual Colour Standard, BioRad, Hercules, CA, USA
- Primary and secondary antibodies used for western blotting were purchased from Sigma-Aldrich, Steinheim, Germany, while secondary antibodies conjugated with FITC and TRITC were purchased from Jackson Immuno Research, PA, USA
- BM Chemiluminescence Blotting Substrate (POD), Indianapolis, IN, USA
- Fugene 6 and HD, Roche Applied Science, Mannheim, Germany
- HisTrap HP 5 mL column, GE Healthcare, Stockholm, Sweden
- Size exclusion column S200 10/300, GE Healthcare, Stockholm, Sweden
- ProlongGold antifade reagent with DAPI, Invitrogen, Eugene, OR, USA
- TrypLE Express, Gibco, Auckland, New Zealand
- Fura-2AM special packaging, Molecular probes, Invitrogen, Eugene, OR, USA

2.2 General Methods

2.2.1 Isolation of genomic DNA from different cell lines

Genomic DNA from B-lymphoblastoid cell lines was isolated using the Wizard™ Genomic DNA extraction kit. Between 1-3x10^6 cells were harvested by centrifugation for 2 min at 13000 x g. The supernatant was removed and the pellet was resuspended in 600 µL Nuclei Lysis Solution™. After addition of 3 µL RNase (20 µg/µL) the sample was inverted 25 times and incubated for 20 min at 37 ˚C. Samples were cooled to room temperature before 200 µL

Protein Precipitation Solution™ was added and mixed vigorously using a vortex mixer for 20 sec. After centrifugation at 16,000 x g the supernatant was collected in a fresh microcentrifuge tube and the DNA was precipitated by addition of 600 µL isopropanol. After mixing the DNA was pelleted by centrifugation for 1 min at 16,000 x g. The pellet was washed with 600 µL 70 % ethanol then centrifuged at 16,000 x g for 1 min. The DNA pellet was air dried and resuspended in 50 µL DNA Rehydration Solution™ at 65 ˚C for one hour.

2.2.2 RNA isolation from different cell lines

The High Pure RNA extraction kit is a column based extraction method and was used to obtain high quality RNA from cell lines according to manufacturer's instructions using $1x10^6$ cells previously washed in PBS before resuspension of the pellet in 200 µL PBS. RNA was eluted in 50 µL elution buffer and the concentration was measured by spectrophotometry at 260 nm using the Nanodrop 1000 before being stored at -80°C.

2.2.3 Reverse Transcriptase PCR

cDNA was prepared using the iScript Reverse Transcriptase Supermix as illustrated in table 2.1, which is based on the iScript RNase H+ MMLV reverse transcriptase. For RT- controls the iScript Supermix without polymerase (supplied in the same kit) was used. cDNA was diluted 1/5 in water for further use and frozen at -20 °C.

Component	Volume (µL)	Final amount
H_2O	variable	
5 x iScript supermix	4	1 x
RNA	variable	1 µg
Total volume	20 µL	

Table 2.1 Reaction components for RT-qPCR.

2.2.4 Polymerase chain reaction (PCR)

PCR was used to amplify cDNA fragments from the cloned human *RYR1* cDNA for sequencing, sub-cloning and colony screening. A standard protocol (table 2.2 and 2.3) was chosen while the annealing temperature varied depending on the primer melting temperatures. The standard volume for a PCR reaction was 50 µL but was reduced to 10 µL for colony PCR.

Component	Volume (µL)	Final concentration/amount
H_2O	27.5	
dNTPs (2 mM)	5	0.2 mM
Polymerase buffer (10 x)	5	1 x
Primer F (10 µM)	5	1 µM
Primer R (10 µM)	5	1 µM
Fast Start Taq Polymerase (5 U/µL)	0.5	2.5 U
DNA template (50 ng/µL)	2	100 ng

Table 2.2 Reaction component for standard PCR.

	Temperature (°C)	Time (mm:ss)	Cycles
Denaturation	94	05:00	1
Denaturation	94	01:00	35x
Annealing	52-83	01:00	
Elongation	72	01:00	
Final elongation	72	07:00	1

Table 2.3 Cycle parameters for standard PCR with varying annealing temperatures.

PCR products (10 % of PCR volume) were analysed for size and purity by agarose gel electrophoresis using TAE buffer [20 mL of 50 x stock (242 g Tris base, 57.1 mL acetic acid, 100 mL 0.5 M EDTA, pH 8) + 980 mL purified water] and the agarose gel percentage depended on the size of the PCR product. Ethidium bromide (0.5 µg/mL) was added to the gel to stain the DNA.

2.2.5 PCR product purification

The Wizard® SV kit, a membrane-based purification method, was used to purify PCR products for sequencing or after enzymatic digestion was performed according to manufacturer's instructions. Products were eluted by the addition of 50 µL of nuclease free water and centrifuged at 16,000 x g for 1 min. DNA was stored at -20 °C.

2.2.6 DNA sequencing

All PCR products or plasmid clones were sequenced by the Massey Genome Service according to their specifications. Sequencing reactions were carried out using the BigDye® Terminator v3.1 Cycle Sequencing Kit and sequences were analysed on the ABI 3730 Genetic Analyser.

2.2.7 High resolution melting (HRM) analysis of genomic DNA

Allele-discrimination was carried out using HRM assays with the LightCycler®480. The High Resolution Melting Master Kit was used as described in the manual and shown in table 2.4. Primers R2452W HRM L forward and reverse were chosen to amplify the region of interest, including the R2452W mutation, in *RYR1*.

Component	Volume (µL)	Final concentration
H_2O	2.3	
$MgCl_2$ (25 mM)	1.2	3 mM
R2452W HRM L forward (5 mM)	0.5	0.25 mM
R2452W HRM L reverse (5 mM)	0.5	0.25 mM
2 x LightCycler®480 HRM Mastermix	5	1 x
Genomic DNA (50 ng/µL)	0.5	2.5 ng

Table 2.4 Standard HRM protocol for primers detecting the R2452W mutation in DNA.

A complete HRM assay program is illustrated in table 2.5.

Target (˚C)	Acquisition mode	Hold (mm:ss)	Ramp rate (˚C/s)	Acquisition (per ˚C)	Sec target	Step size (˚C)
Denaturation						
Cycles	1	Analysis Mode		None		
95	None	10:00	4.40		0	0
Amplification						
Cycles	45	Analysis Mode		Quantification		
95	None	00:10	4.40		0	0
65	None	00:10	2.20		58	0
72	Single	00:04	4.40		0	0
Melting						
Cycles	1	Analysis Mode		Melting curves		
95	None	01:00	4.40		0	0
40	None	01:00	1.50		0	0
76	None	00:01	4.40		0	0
92	Continuous		0.02	25	0	0
Cooling						
Cycles	1	Analysis Mode		None		
40	None	00:30	1.50		0	0

Table 2.5 PCR protocol for HRM assays showing standard parameters.

2.2.8 Restriction endonuclease digest

Restriction endonuclease digestion was used to prepare amplified PCR products and vectors for cloning and to characterise plasmids. Buffers and additives were used as directed in manufacturer's instructions. An example of a restriction endonuclease digest is shown in table 2.6. After digestion for 2 h at 37 °C all enzymes were heat inactivated at either 60 ° or 65 °C, as indicated in the product sheet. Two different enzymes were used to facilitate directional cloning.

Component	Volume (µL)	Final concentration/amount
H_2O	17 - x	
Restriction buffer (10x)	2	1 x
Enzyme 1 (20 U/µL)	0.5	10 U
Enzyme 2 (20 U/µL)	0.5	10 U
DNA or PCR product	x	300 ng

Table 2.6 Protocol for restriction endonuclease digest using two enzymes.
x was dependent on the concentration of the PCR product or vector to be digested.

2.2.9 Antarctic phosphatase treatment of digested vectors

Digested vectors were treated with antarctic phosphatase to prevent re-ligation. The digested vector was incubated for 30 min at 37 °C with antarctic phosphatase. The enzyme was subsequently heat inactivated for 5 min at 65 °C. The final reaction volume was 20 µL. A standard reaction protocol is illustrated in table 2.7.

Component	Volume (µL)	Final concentration/ amount
H_2O	17 – x	
Enzyme buffer (10 x)	2	1 x
Vector DNA	x	300–1000 ng
Antarctic phosphatase (5 U/µL)	1	5 U

Table 2.7 Standard protocol for antarctic phosphatase treatment of digested vector.
x dependent on the concentration of the vector DNA.

2.2.10 Ligation

T4 DNA ligase was used to ligate digested inserts to digested vectors. The ligation mixture (table 2.8) was incubated overnight at 4 °C with an insert: vector ng ratio of 2:1 according to manufacturer's instructions. The final reaction volume was 20 µL.

Component	Volume (µL)	Final concentration
H_2O	17- x- y	
Ligase buffer (10x)	2	1x
Vector DNA	x	50 ng
Insert DNA	y	100 ng
T4 DNA ligase (1 U/ µL)	1	1 U

Table 2.8 Ligation protocol.

x depends on the concentration of the vector DNA, while y depends on the concentration of the insert.

2.2.11 Site-directed mutagenesis

The QuickChange® protocol was used to perform site-directed mutagenesis in plasmids. Thirty nucleotide primers were designed to cover the region of interest and to introduce a modification at this site. PCR was performed using *Pfu*Turbo DNA Polymerase to replicate both plasmid strands and introduce the desired mutation into both strands. The PCR components (50 µL final volume) used are shown in table 2.9.

Component	Volume (µL)	Final concentration/amount
H_2O	31	
dNTP Mix	1	1 µM
Reaction buffer (10 x)	5	1 x
Primer F (10 µM)	5	1 µM
Primer R (10 µM)	5	1 µM
DNA template (50 ng/µL)	2	100 ng
*Pfu*Turbo DNA Polymerase (2.5U/µL)	1	2.5 U

Table 2.9 Mutagenesis PCR protocol.

Since the annealing temperature for the primers used was very high (above 75 °C, see appendix V) the annealing step was omitted from the PCR program and the elongation time was extended (table 2.10).

	Temperature (°C)	Time (mm:ss)	Cycles
Denaturation	95	00:30	1
Denaturation	95	00:30	16x
Elongation	68	16:00	

Table 2.10 Standard protocol used for mutagenesis PCR.

The reactions were chilled on ice for a few minutes prior to the addition of 1 µL (10 U/µL) DpnI to each tube and subsequently incubated for 1 h at 37 °C to digest the methylated, plasmid template. The reactions were used directly for *E. coli* transformation.

2.2.12 Competent *E. coli* cells

2.2.12.1 Ca^{2+} chloride competent cells

Single *E. coli* DH5α colonies were picked from LB plates, used to inoculate 5 mL SOB medium (2 % bacto tryptone, 0.5 % bacto yeast extract, 8.6 mM NaCl, 2.5 mM KCl, 1 mM NaOH, 10 mM $MgCl_2$, 10 mM $MgSO_4$) and then grown at 37 °C for 6 h with constant shaking. One mL was used as a starter culture to inoculate 250 mL SOB which was grown to an OD_{600} of 0.55 at 20 °C. When cultures reached the required OD_{600} they were incubated on ice for 10 min before they were centrifuged at 4,000 x g for 10 min at 4 °C. After washing the pellet in 80 mL ITB medium (10 mM PIPES pH 6.7, 15 mM $CaCl_2$•$2H_2O$, 250 mM KCl, 55 mM $MnCl_2$•$4H_2O$) and centrifugation at 4,000 x g for 10 min at 4 °C, cells were resuspended in 20 mL ice cold ITB and 1.5 mL DMSO was added. The cells were divided into 100 µL aliquots and stored at -80 °C until required.

2.2.12.2 Rubidium chloride competent cells

Single BL21 (DE3) GroEL/ES *E. coli* colonies were picked from LB plates containing 7 µg/mL chloramphenicol and used to inoculate 5 mL LB broth. Cultures were grown overnight at 37 °C under constant shaking to form a starter culture where 1 mL was used to inoculate 200 mL LB broth. This 200 mL culture was grown until an OD_{600} of 0.5 was reached and cells were harvested by centrifugation at 4,000 x g for 10 min at 4 °C. The pellet was

resuspended in 100 mL ice-cold buffer 1 (30 mM KOAc, 100 mM $RbCl_2$, 10 mM $CaCl_2$, 50 mM $MnCl_2$, 15 % (v/v) glycerol, pH 5.8) by vortexing for 30 sec. The cells were chilled on ice for 5 min before they were centrifuged for 10 min at 4 °C at 4,000 x g. Finally the pellet was resuspended in ice cold buffer 2 (10 mM MOPS/KOH pH 6.5, 75 mM $CaCl_2$, 10 mM $RbCl_2$, 15 % glycerol). Cells were chilled on ice before 50 µL aliquots were prepared and then stored at -80 °C until further use.

2.2.13 *E. coli* transformation

Competent *E. coli* strains were thawed on ice before either 1/10 ligation mixture or plasmid (5 ng) was added and incubated on ice between 10 and 30 min, depending on the *E. coli* strain. Competent cells were heat-shocked at 42 °C for 1 to 1.5 min and subsequently incubated on ice for 2 min. DH5α cells (100 µL) were diluted with 900 µL SOC medium and grown for 30 min at 37 °C before aliquots were plated out onto LB-Agar plates containing 100 µg/mL ampicillin. BL21(DE3) GroEL/ES *E. coli* strains were plated directly onto LB-agar plates containing 100 µg/mL ampicillin and 7 µg/mL chloramphenicol and incubated overnight at 37 °C.

2.2.14 Glycerol stocks of transformed DH5α cells

Single cells were picked from LB-agar plates and used to inoculate 5 mL LB broth, containing 100 µg/mL ampicillin, and then grown at 37 °C under constant shaking for 16 h. Glycerol stocks were prepared from these cultures by the addition of glycerol to a final concentration of 10% (v/v).

2.2.15 Rapid boil plasmid isolation

Putative recombinant plasmids were randomly screened using an inexpensive plasmid isolation protocol as follows: a sufficient amount of *E. coli* culture, usually 1.5 mL, was harvested by centrifugation for 1 min at 16,000 x g and the pellet was resuspended in 350 µL STET buffer (50 mM Tris-HCl pH 8, 50 mM Na_2EDTA pH 8, 8 % sucrose, 5 % Triton X-100) and 25 µL of freshly prepared lysozyme (10 mg/mL) was added. After mixing, it

was boiled for 40 sec and centrifuged for 10 min at 14,000 x g. The pellet was removed with a toothpick and 400 µL isopropanol was added to the remaining supernatant and mixed well. The mixture was incubated for 30 min at -20 °C. The precipitated DNA was centrifuged at 14,000 x g for 5 min and washed with 500 µL 95 % ice cold ethanol. After centrifugation the pellet was air dried and resuspended in 50 µL TE buffer (10 mM Tris-HCl, 1 mM EDTA, pH 8).

2.2.16 Isolation of plasmid DNA: small scale

The Roche High Pure Plasmid Isolation kit based on the alkaline lysis method, was used according to manufacturer's instructions to isolate high quality plasmid DNA from *E. coli* DH5α. The required amount of *E. coli* culture, 2-5 mL, was harvested by centrifugation for 2 min at 16.000 x g and the pellet was resuspended in 250 µL suspension buffer. After extraction DNA was eluted in 100 µL elution buffer by centrifugation for 1 min at 16,000 x g.

2.2.17 Isolation of plasmid DNA: medium scale

For larger quantities of plasmid DNA the Invitrogen PureLink™ HiPure Plasmid Midiprep Kit based on anion-exchange chromatography, was used according to manufacturer's protocol. The required volume of *E. coli* culture, between 0.1 and 1.5 L, was harvested at 4,000 x g for 20 min at 4 °C. DNA was resuspended in 200 µL TE buffer.

2.2.18 Protein isolation from mammalian cell lines

2.2.18.1 Preparation of microsomes

Microsomes are vesicle-like cell compartments, formed from the endoplasmic reticulum in broken eukaryotic cells. These vesicles can be isolated by differential centrifugation. Transfected HEK293 cells were washed twice with PBS and harvested in 1.5 mL sucrose buffer (0.25 M sucrose, 10 mM HEPES, pH 7.4, 1x complete mini protease inhibitor). Cells were transferred into a hand-held homogenisor and were homogenised with 100 strokes. The

homogenate was transferred into a microcentrifuge tube and centrifuged at 4 °C at 16,000 x g for 10 min to pellet cell debris. The microsome-containing supernatant was collected and transferred into an ultracentrifuge tube. The supernatant was centrifuged at 100,000 x g in an ultracentrifuge at 4 °C for 1.25 h. The microsome-containing pellet was resuspended in 100 µL sucrose buffer and stored at -80 °C.

2.2.18.2 Crude protein extracts

Transfected HEK293 cells were washed and harvested in PBS followed by pelleting in a microcentrifuge tube for 5 min at 13,000 x g. The supernatant was discarded and the pellet was resuspended in 100 µL cell lysis buffer (0.1 M Tris-HCl pH 7.8, 0.5 % Triton X-100, 1x Complete mini protease inhibitor) and incubated for 15 min at 37 °C to disorganise and lyse cell membranes. Insoluble debris were pelleted by centrifugation at 2000 x g for 10 min at 4 °C. The protein-containing supernatant was stored at –80 °C until further use.

2.2.19 Sodium dodecyl sulfate polyacrylamide gel electrophoresis (SDS-PAGE)

Protein extracts were analysed using either 12.5 % (for proteins <60 kDa) or 7.5 % SDS-PAGE (protein >150 kDa) gels. Protein gels were prepared using the Biorad mini Protean™ gel casting system using components as listed in table 2.11.

Component	7.5 % resolving gel	4 % stacking gel		12.5 % resolving gel	6 % stacking gel
Water (mL)	4.35	3.15		3.35	2.9
40 % Acryl-amide (mL)	1.5	0.5		2.5	0.75
1.5 M Tris pH 8.8 (mL)	2	-		2	-
0.5 M Tris pH 6.8 (mL)	-	1.25		-	1.25
10 % SDS (µL)	80	50		80	50
10 % APS (µL)	80	50		80	50
TEMED (µL)	8	5		8	5

Table 2.11 List of components for either 7.5 or 12.5 % SDS-PAGE gels.

2.2.19.1 Coomassie blue staining

After electrophoresis, gels were stained for 5 min using Coomassie-blue (0.1 % (w/v) Coomassie blue-R250, 45 % methanol, 10 % glacial acetic acid). Destaining was performed by placing the gel in destain solution (15 % methanol, 6 % glacial acetic acid) for 2 h at RT.

2.2.19.2 Silver staining

After electrophoresis, gels were placed in fixing solution (50 % ethanol, 10 % glacial acetic acid) for 1 h with constant shaking. The fixed gel was washed 3 times for 5 min with water and placed in 100 mL 0.8 mM sodium thiosulphate for 4 min. The gel was washed for 5 min in water before it was placed in 100 mL 2 g/L silver nitrate solution for 20 min. Prior to be placed in developer solution the gel was briefly washed with water. Bands were developed for at least 2 min in developer solution (566 mM Na_2CO_3, 0.016 mM sodium thiosulphate, 0.05 % formaldehyde) until the bands of interest were visualised. To stop the staining process the gel was placed in 5 % acetic acid for 5 min.

2.2.20 Western blotting

Sufficient protein (15 µg of microsomal fractions, 70 µg crude extract or ~0.1 µg of purified recombinant RYR1 protein) was incubated with 5 x loading dye [60 mM Tris-HCl, pH 6.8, 25 % glycerol (v/v), 2 % SDS (w/v), 5 % 2-β mercaptoethanol, 0.1 % bromophenol blue (w/v)] at RT for 10 min when western blotting for full-length RYR1 was performed or boiled for 3 min for any other western blot. Protein samples were loaded onto an SDS-PAGE gel and electrophoresis was carried out at 130 V for either 1 h (12.5 % gel) or 1.5 h (7.5 % gel). The gel was soaked in transfer buffer (15.6 mM Tris-HCl pH 8.2, 0.12 M glycine) containing 10 % methanol and was blotted onto a PVDF membrane (precharged by soaking in methanol for 1 min) at 70 mA overnight at 4 °C for full-length RYR1 or 1.25 h at 150 mA at RT for other proteins. The membrane was blocked in 5 % skim milk powder (w/v) in TBST (50 mM Tris, 0.15 M NaCl, pH 7.5, 0.1% Tween-20) for 3 h at RT before the primary antibody (α-RYR1 1:1000, α-His_6-tag 1:3000, α-Tubulin 1:5000) was applied and incubated overnight at 4 °C with constant shaking. The membrane was

washed 4 x 10 min in TBST before the horseradish peroxidase labelled secondary antibody against mouse (1:5000) was applied for 1 h at RT under constant shaking. The membrane was washed 4 x 10 min before it was incubated for 1 min in Roche chemiluminescence blotting substrate and emitted light was detected immediately on X-ray film.

2.2.21 Coating of tissue culture plastic

2.2.21.1 Collagen coating

Tissue culture plastic plates used to grow myoblasts were coated with collagen for more effective cell adhesion and proliferation. Collagen solution (600 µg/mL in 0.1 % acetic acid) was diluted in water to a final concentration of 20 µg/mL and was dispensed into tissue culture plates to sufficiently coat the surface and incubated for 30 min at 37 °C. The collagen solution was removed and plates were washed twice with water and dried in a tissue culture hood. Plates were stored at 4 °C until required.

2.2.21.2 Poly-L-lysine coating

Poly-L-lysine was resuspended in water to a final concentration of 0.01 % (w/v). Tissue culture plastic used for Ca^{2+} release assays for transfected HEK293 cells was coated by the addition of 0.01 % poly-L-lysine and incubated for 1 h at RT under the exposure of UV-light to sterilise the plates. Poly-L-lysine solution was removed and plates washed once with water and were stored at 4 °C until required.

2.2.22 Immunofluorescence staining

Cells grown in chambers were fixed with an ice cold methanol:acetone mixture (v:v,1:1) for 15 min at RT followed by 2 x 10 min wash with PBS. Cells were permeabilised by incubation with PBS containing 0.2 % Triton X-100 (v/v) for 5 min at RT with gentle shaking followed by washing 2 x with PBS. Blocking was carried out in PBS containing 5 % BSA (w/v) and 0.5 % Tween-20 (v/v) for 30 min at RT on a shaker. Primary antibodies [α-RYR1, produced in mouse, 1:500 dilution and α-PDI (protein disulfide isomerase),

used as an ER marker, produced in rabbit, 1:750 dilution] were applied and incubated over night at 4 °C. Cells were washed 3 x 5 min with PBS + 0.5 % Tween-20 (v/v) on a shaker before the secondary antibody was applied [FITC (fluorescein isothiocyanate) labelled goat α-mouse IgG, 1:200, TRITC (tetramethylrhodamine isothiocyanate) labelled goat α-rabbit IgG, 1:200]. Cells were incubated with secondary antibody for 1 h at RT on a shaker followed by 3 x 5 min washing with PBS +0.1 % Triton X-100. The final wash was performed for 5 min with PBS on a shaker before the chamber top was removed from the slide and 10 µL mounting solution (Prolong Gold antifade solution, containing DAPI) was added. Coverslips were placed on top and the edges were sealed with nail polish to keep the coverslip in place. Slides were kept in the dark at 4 °C until used for microscopy.

2.2.23 Establishment of primary lymphocyte cultures from blood

B-lymphocytes were isolated from whole blood using a method previously published [167]. Ten mL of blood was mixed with 25 mL of OptiMEM medium with no additives. To separate the red blood cells the mixed blood (in 4 mL aliquots) was layered onto a 3 mL ficoll-paque and centrifuged at 18 °C for 40 min at 400 x g with no brake activated. The top layer containing blood plasma was discarded while the white blood cells settled at the interface. White blood cells were carefully removed and gently washed twice with 5 mL OptiMEM medium by centrifugation for 10 min at 160 x g. The white blood cells pellet was resuspended in 2 mL lymphocyte proliferation media (table 2.12) in a biohazard hood. The resuspended white blood cells were then mixed with 2.5 mL of filtered (0.2 µm) B95-8 cells supernatant, containing the Epstein-Barr-Virus and were incubated for 2 h at 37 °C. Finally, 5 mL complete medium (table 2.12) containing 1 µg/mL cyclosporin A was added to inhibit the T-cell response and to obtain a culture enriched in B-lymphocytes. Cells were incubated at 37 °C and 5 % CO_2 for ~3 weeks without disturbing. After this time, if immortalisation had occurred the B-lymphocytes tended to aggregate. Media was replenished every 2-3 days by removing ~2 mL media and adding 2 mL of fresh media until visible cell growth occurred.

2.2.24 Isolation of muscle cells from fresh muscle

2.2.24.1 Explant method

Muscle pieces were delivered on ice in sterile 50 mL tubes containing sterile serum free media. A 6-well plate was filled with 1.5 mL of myoblast extraction medium per well (table 2.12). Sterile inserts were placed into the wells and were filled with 0.5 mL of myoblasts extraction medium. Muscle pieces were placed on a sterile petri dish in a biohazard hood and 1x1 mm cubes were cut from the centre of the muscle. One piece of muscle was placed into each insert and incubated at 37 °C, 10 % CO_2 in a humidified atmosphere until muscle cells were visible growing around the block of tissue (~7-12 days). The muscle pieces were then removed and medium from the insert was discarded. The cells were detached by addition of 1 mL TrypLE to the insert and incubated at 37 °C for about 10 min. Detached cells were pooled and transferred into a 3.6 cm diameter collagen-coated tissue culture dish containing 3 mL myoblast separation medium (table 2.12) and placed into the same incubator. When cells reached about 40 % confluence they were trypsinised and transferred into a 10 cm collagen-coated plate containing 10 mL complete myoblast proliferation medium (table 2.12).

2.2.24.2 Collagenase/dispase digest

One gram fresh muscle was weighed and roughly chopped with scissors until a slurry was formed. The slurry was transferred into a sterile 15 mL tube containing 1 mL collagenase/dispase mixture (1 g of collagenase class II to 100 mL of dispase grade II with a final concentration of 2.5 µM $CaCl_2$) followed by incubation for a total of 1 hour in a 37 °C water bath. Every 10 min the slurry was titurated using a 5 mL pipette. The digested mixture was filtered through a 0.7 µm filter cup and centrifuged at 400 x g for 10 min. The supernatant was removed and the cell pellet resuspended in 10 mL myoblast proliferation media and plated into an uncoated 10 cm tissue culture dish. Fibroblasts adhere more quickly than myoblasts and therefore can be removed from the media. Therefore the supernatant was removed every 30 min over a period of 3 hours and plated into a new plate. The previous plates were replenished with 10 mL myoblast proliferation media (table 2.12) and placed in the 37 °C incubator containing 10 % CO_2. For the final plating the

medium was dispensed into a collagen-coated plate. Most fibroblasts will be removed by this stage and thus the cell suspension should be highly enriched for myoblasts.

2.2.24.3 Enrichment of myoblasts

Fibroblasts adhere very strongly to surfaces while myoblasts do not. Therefore another method to enrich for myoblasts was to take advantage of this behaviour. When the freshly isolated myoblast cultures were 50 % confluent the media was removed and replaced by 4 mL of PBS (0.14 M NaCl, 2.7 mM KCl, 10 mM Na_2HPO_4, 1.8 mM KH_2PO_4). Cells were incubated for at least 10 min at 37 °C. Myoblasts were released rapidly from the tissue culture plastic freely while fibroblasts remained adherent. The cell-containing PBS was placed into another collagen-coated dish containing 8 mL myoblast proliferation media. This step was repeated for 3 weeks until no signs of fibroblasts could be detected.

2.2.25 Reviving frozen cell stocks

Cell stocks from all cell lines were either stored in a -80 °C freezer for short term storage or in liquid N_2 for long term storage. A vial of cells was thawed rapidly in a water bath (37 °C) and mixed with 5 mL completed media (see table 2.12 for the cell specific media and incubator conditions) followed by centrifugation for 4.5 min at 200 x g. The supernatant was removed and cell pellets were resuspended in 5-10 mL complete media, seeded into tissue culture plasticware and placed in an incubator.

Cell lines	Media + components (v/v)	CO_2 concentration
Lymphocyte proliferation medium	OptiMEM medium + 2 % fetal bovine serum (FBS) + 1 % penicillin/ streptomycin (P/S)	5 %
Myoblast proliferation medium	Hams F-10 medium + 20 % FBS + 1 % P/S + 5 ng/mL bhFGF (basic human fibroblast growth factor)	10 %
Myoblast differentiation medium	DMEM medium + 2 % horse serum (HS) + 1 % P/S	10 %
Normal HEK293 cell growth medium	DMEM medium + 10 % FBS + 0.5 % P/S	5 %
Stable HEK 293 cell growth medium	DMEM medium + 10 % FBS + 400 µg/mL geneticin	5 %
Myoblast separation medium	DMEM medium + 10 % horse serum (HS) + 1 % P/S, 5 ng/µL Insulin	10 %
Myoblast extraction medium	DMEM medium + 20 % FBS + 1 % P/S + 5 ng/µL Insulin	10 %

Table 2.12 Media and CO_2 concentrations used to cultivate different cell lines.

2.2.26 Passage of cells

When passaging cells all solutions and media were preheated to 37 °C.

2.2.26.1 Lymphocytes

Lymphocytes are non-adherent cells and when immortalised to B-lymphoblastoid cell lines form clumps. One rapid and reliable criterion for passaging lymphocytes is the colour of the medium containing phenol red as pH indicator. If the medium becomes slightly yellow due to a reduced pH (usually every 3 days) the cells need medium replenishment. If colour change occurs faster than every ~3 days cells require passage. For this purpose cells were completely resuspended in medium and divided into 2 or 3 flasks and replenished with 5-10 mL lymphocyte proliferation medium depending on the flask size and cell number (table 2.12) and flasks were placed at 37 °C with 5 % CO_2 in an upright position.

2.2.26.2 HEK293 cells

HEK293 cells are adherent cells but adhere poorly to tissue culture flasks. Media was removed and 0.5 mL TrypLE was added to the cells and left for 5 sec before it was removed. Two mL fresh HEK293 growth medium (table 2.12) was added and the cells were shaken gently to detach them from the surface. Cells were passaged by transferring one fifth (0.5 mL) of the cell suspension into a new T25 flask into an additional 4.5 mL fresh medium.

2.2.26.3 Myoblasts

Myoblasts adhere to tissue culture dishes and cells should not be grown to confluence as this encourages differentiation. Therefore they were passaged at about 60 % confluence by removing the media and the addition of 2 mL TrypLE to the 10 cm diameter dish. The cells were incubated for 5 min in the 37 °C, 10 % CO_2 incubator until all cells were dislodged. Proliferation medium (5 mL) was added and 2 mL of cell suspension was placed into a new 10 cm dish containing 9 mL of proliferation medium.

2.2.27 Freezing cells

Cells were harvested by centrifugation at 200 x g for 4.5 min. The cell pellet was resuspended in FBS containing 10 % (v/v) DMSO and transferred into a cryo-vial. Vials were placed in a CoolCell (Biocision) and placed in the -80 °C freezer to allow slow freezing of cells. After a week they were either stored at -80 °C or transferred in liquid N_2 for long-term storage.

2.2.28 Transfections

Transient transfections were carried out using either Fugene HD for Ca^{2+} release assays or Fugene 6 for immunostaining. Cells used for Ca^{2+} release assays were grown to 90 % confluence in poly-l-lysine coated 96 well plates and transfected with a Fugene HD (µL): DNA (µg) ratio of 8:2 according to manufacturer's instructions while 150 ng DNA was used in total per well and incubated for 72 h. For immunostaining, cells were transfected at a confluency of 10 % with the same ratio and amount as described earlier.

2.2.29 Ca^{2+} release assays

2.2.29.1 B-lymphoblastoid cells

B-lymphoblastoid cells were counted to obtain $1.2x10^7$ cells and harvested by centrifugation for 4.5 min at 200 x g. The cell pellet was washed once with 1 x BSS plus Ca^{2+} buffer (140 mM NaCl, 2.8 mM KCl, 1 mM $MgCl_2$, 2 mM $CaCl_2$, 10 mM glucose, 10 mM HEPES, pH 7.25), loaded with 2 µM fura 2-AM and 0.01 % pluronic F127 and incubated for 1 h at 37 °C in the dark. Cells were washed once with 1 x BSS plus Ca^{2+} and once with 1x BSS with 20 µM free Ca^{2+} (140 mM NaCl, 2.8 mM KCl, 1 mM $MgCl_2$, 2 mM $CaCl_2$, 2 mM EGTA, 10 mM glucose, 10 mM HEPES, pH 7.25) and kept in this buffer for fluorometry. Free Ca^{2+} concentrations in this buffer were calculated using the free internet software Ca-EGTA Calculator v1.3 (http://www.stanford.edu/~cpatton/CaEGTA-TS.htm) based on the Theo Schoenmakers' Chelator [168]. Fura 2 loaded B-lymphoblastoid cells were dispensed at a density of $2x10^6$ cells per UV transparent cuvette and made up to a final volume of 2 mL. A 0.5 cm flea was added to each cuvette and Ca^{2+} release was detected using a fluorometer (Luminescence spectrometer LS50B, Perkin Elmer, using the FL WinLab software) at the excitation wavelength of 340 and 380 nm with emission at 509 nm. Measurements were taken every 2 sec for each wavelength over ~10 min, at RT by the addition of the agonist 4CmC with constant stirring.

2.2.29.2 Myotubes/ transfected HEK293 cells

Ca^{2+} release assays were carried out in UV-transparent 96-well plates for both differentiated myoblasts and transfected HEK293 cells. The fura 2-AM loading protocol for myotubes/HEK293 cells is identical to that for lymphocytes loading and can be found in section 2.2.29.1. Fura 2 loaded cells were finally stored in 100 µL 1x BSS with 20 µM free Ca^{2+} and Ca^{2+} release in response to the agonist 4CmC was measured at RT using a fluorescence microscope (Olympus IX81) with 16 x magnification containing a filterset for the excitation wavelengths of 340 and 380 nm. Emission was detected at 509 nm every 0.5 sec. The Metafluor software was used for data analysis.

2.3 Protein purification methods

2.3.1 Induction of transformed *E. coli*

A single transformed *E. coli* BL21(DE3) GroEL/ES colony was picked and used to inoculate a 5 mL LB broth containing 100 µg/mL ampicillin and 7 µg/mL chloramphenicol and grown for 4 h at 37 °C. Starter cultures (5 mL) were used to inoculate 500 mL LB containing 100 µg/mL ampicillin and 7 µg/mL chloramphenicol and grown at 37 °C under constant shaking to an OD_{600} of 0.4 before they were induced with 0.1 mM IPTG. For protein overexpression the cultures were grown at 20 °C for 3 h (optimised condition) with constant shaking before they were harvested by centrifugation (4000 x g for 15 min). The pelleted *E. coli* culture was frozen at -20 °C until further use.

2.3.2 Protein extraction from induced *E. coli*

An *E. coli* pellet (9 L culture volume) was resuspended in 30 mL cell lysis buffer (0.1 M Tris HCl, 0.5 M NaCl, pH 7.8, 50 mM imidazole) and well mixed. Cells were lysed using a French press at 5,000 psi twice and chilled on ice in between. Lysed cells were centrifuged at 4°C for 15 min at 16,000 x g to pellet cell debris and insoluble proteins.

2.3.3 His_6-tag purification via Ni^{2+}-NTA affinity column

A Ni^{2+}-NTA agarose filled 5 mL HisTrap HP column (GE Healthcare) was used for His_6-tag affinity purification. The column was equilibrated with 5 column volumes of lysis buffer containing 0.1 M Tris HCl, pH 7.8, 0.5 M NaCl, 20 mM ATP and 50 mM imidazole to reduce non specific binding. ATP was added to weaken the binding of GroELS to overexpressed RYR1. Soluble protein was loaded onto the column at a flow rate of 2 mL/min before the column was washed with 10 column volumes of equilibration buffer containing 100 mM imidazole to elute unspecifically bound protein. RYR1 protein was eluted using a gradient ranging from 100 mM to 400 mM imidazole as a first purification step. For further purification protein was loaded again onto the column equilibrated with lysis buffer as described

above and eluted using a step gradient with two elution steps at 155 mM and 400 mM imidazole in the previously mentioned buffer.

2.3.4 Size exclusion purification for RYR1 central domain

To prevent blockage of the FPLC ÄKTA system all reagents were filtered before use. Concentrated protein was centrifuged at 100,000 x g for 10 min to pellet any insoluble particles in the protein solution. The size exclusion column Superdex 200 10/300 GL (GE Healthcare) was washed with 1.5 column volumes of water (flow rate 0.6 mL/min) followed by equilibration with buffer containing 20 mM Tris-HCl, pH 7.9, 20 mM NaCl. Concentrated protein was loaded into a 500 µL loop and loaded onto the column. Proteins were eluted using a flow rate of 0.6 mL/min for 1.2 column volumes while fractions of 300 µL were collected throughout elution. The gel filtration column was calibrated using different sized proteins. Protein standards at 0.5 mg/mL were loaded onto the column and the calibration curve is included in appendix VII.

2.3.5 Cleavage of affinity tag using enterokinase

Fractions containing purified Ni^{2+}-affinity eluted protein were concentrated using a spin Viva Spin concentrator, to a final volume of 500 µL and protein concentration was estimated using spectrophotometry measuring light absorbance at 280 nm using the extinction coefficient of the overexpressed protein. For every 25 µg protein 0.1 µL enterokinase (1 µg/mL stock solution) was added to the concentrated protein and incubated for 3 h at RT.

2.3.6 Circular dichroism spectroscopy

Concentrated purified protein was used in circular dichroism spectroscopy (CD) as a means of determining a distinctive secondary structure and as a measure of protein folding. CD spectra in the far UV light range (260-180 nm) were measured using a Chirascan CD spectrometer (Applied Photophysics) using a 1 mm path cell and protein concentration of 0.1 mg/mL at 20 ºC in buffer containing 10 mM phosphate buffer pH 7.9, 10 mM NaCl, 1 mM DTT.

Protein measurements were recorded 5 times with a band width of 1 nm and 0.5 nm increments and readings taken every 1 second before being averaged and smoothed curves were calculated. For thermal stability assays CD spectra were measured from 5° to 90°C in 5°C increments and a 1 min equilibration time and a tolerance level of 0.2 °C. Deconvolution of the CD spectra was carried out using the CDNN software (Applied Photophysics).

2.3.7 Mass spectrometry

Mass spectrometry was kindly carried out as a service by Trevor Loo, IMBS, Massey University.

2.3.7.1 Desalting of samples

A 200 µL gel-load tip (GR770290, Raylab, NZ) was self packed with POROS 20 R2 medium slurried in 100 % methanol. The packaged medium was washed once with 70% acetonitrile (ACN), 0.1% formic acid (FA) and then with water containing 0.1% FA before the appropriate amount of protein sample (20 pmol) was slowly loaded onto the media. Protein was washed once with water containing 0.1% FA and eluted in 30 µL 70% ACN, 0.1% FA and stored at -80 °C for mass spectrometry to detect the exact mass of intact proteins.

2.3.7.2 In-gel digestion

Bands on colloidal Coomassie (G250)-stained SDS-PAGE gels were cut and destained using 50 mM ammonium bicarbonate three times for 20 min at 37 °C before 100 % ACN was applied for 10 min as a final washing step. The supernatant was removed and gel pieces were dried for 10 min using a centrifugal evaporator. Protein in the gel pieces was reduced by the addition of 30 µL fresh 10 mM DTT for 1 h at 50 °C. To alkylate the protein 30 µL of freshly prepared iodoacetamide (0.5 mM in 100 mM ammonium bicarbonate) was added and incubated for 30 min at 37 °C in the dark. The supernatant was removed and gel pieces were washed twice for 5 min with 100 µL Coomassie destain solution before gel pieces were dehydrated by the addition of 100 µL 100 % ACN for 15 min. Supernatant was removed and the gel pieces dried for 10 min using a centrifugal evaporator. Dried gel pieces

were rehydrated by using enough ice-cold trypsin solution to cover them (15 ng/µL sequencing grade trypsin, Sigma Aldrich, in 3 mM acetic acid and 25 mM ammonium bicarbonate buffer) and incubated at 37 °C in the dark overnight. Protein from the digested gel pieces was eluted twice by the addition of 60 µL 60% ACN, 0.1% FA and sonicated in a water bath for 1 min before a final elution was done in 100% ACN followed by 1 min sonication. Eluted fractions were pooled and the volume was reduced to 20 µL using a centrifugal evaporator. Samples were stored at -80 °C.

2.3.7.3 In-solution digestion

Concentrated protein sample (10 µg in 50 µL) was mixed with 30 µL of 20% ACN in 50 mM ammonium bicarbonate containing 2 mM $CaCl_2$ and incubated for 20 min at room temperature (RT). To reduce the disulphide bonds in proteins, 6 µL 200 mM freshly prepared DTT (final concentration 15 mM) was added and incubated for 1 h at 37 °C. For protein alkylation 8 µL of 100 mM iodoacetamide in ammonium bicarbonate buffer (final concentration 10 mM) was added and incubated for 15 min at RT in the dark. The protein digest was carried out overnight at 37 °C by the addition of 2 µL trypsin (200 ng/µL stock in 3 mM acetic acid and 25 mM ammonium bicarbonate buffer). To stop the digest 1 µL ~ 98% FA was added to acidify the samples prior to storage at -80°C until further use.

Chapter 3 Functional characterisation of the RYR1 R2452W mutation using patient-derived cells

3.1 Introduction

Malignant hyperthermia (MH) has a relatively high incidence worldwide with an approximate frequency of 1 in 15,000 surgeries. The lower part of the North Island of New Zealand has an even higher incidence with one in every ~200 anaesthetics at Palmerston North hospital being administered to a patient classified as MHS. In the whole of New Zealand, 55 families to date are known to have an MH background and of these, RYR1 mutations have been identified in 27. Two of these unrelated families carry the R2452W mutation which to date has not been demonstrated to be causative of MH. This chapter describes the use of patient-derived cells from these families in functional agonist-stimulated Ca^{2+} release assays with the ratiometric Ca^{2+} indicator fura 2-AM. This esterified fluorophore is membrane permeable and allows the dye to enter the cytosol of cells where it is hydrolysed to fura 2 by cytosolic esterases. Fura 2 was then used to monitor changes in cytosolic Ca^{2+} using a fluorescence microscope or fluorometer. The fluorophore fura 2 is excited at wavelengths of 340 and 380 nm with emission measured at 509 nm. In the absence of Ca^{2+} the excitation maximum is monitored at 380 nm but once Ca^{2+} has bound to fura 2 the excitation maximum shifts to 340 nm. Fura 2 has a high affinity for Ca^{2+} and a low affinity for Mg^{2+} [169]. The RYR1 (and RYR2) specific agonist 4-chloro-*m*-cresol (4CmC) was used together with fura 2 in functional assays to specifically detect altered Ca^{2+} release from the ER/SR by RYR1 in either B-lymphoblastoid cells or myotubes established from patient samples.

Informed consent was contained from patients under human ethical approval from the Central Region (Wellington, New Zealand) and Massey University (Palmerston North, New Zealand) human ethics committees and handled under number MWH0010051. Ethical approval to construct the human *RYR1* cDNA clone was obtained from the Massey University Genetic Technology Committee acting as the Institutional Biological Safety Committee for the National Advisory Environmental Risk Management Authority.

3.1.1 B-Lymphoblastoid cells

B-lymphocytes express RYR1 endogenously although its function in these cells is currently unclear. It has been suggested that RYR1 is involved in intracellular Ca^{2+} regulation and signal transduction [133]. In recent years B-lymphocytes have become a model system for functional studies of RYR1-mediated Ca^{2+} release since the expression levels are moderate and lymphocytes can be easily extracted from patient blood samples. Lymphocytes express an alternatively spliced form of RYR1 missing exon 70, encoding 5 amino acids but the functional reason for this is unknown [132]. Alternative splicing also occurs in skeletal muscle thus the amino acids encoded by exon 70 are not thought to be essential for function. B-lymphocytes do not express the other proteins associated with the skeletal muscle triad, which could influence Ca^{2+} release from the SR through the ryanodine receptor. Using B-lymphoblastoid cells as a system to measure Ca^{2+} release from RYR1 has the advantage that Ca^{2+} is released in the absence of other proteins used in skeletal muscle contraction and a functional effect of *RYR1* mutations can therefore be detected independently. If there is any abnormal Ca^{2+} release detected in lymphocytes it can be concluded that it is most likely due to a mutation in the *RYR1* gene. If, however an *RYR1* mutation alters Ca^{2+} release due to a defective coupling of e.g. DHPR in muscle cells, Ca^{2+} release assays in B-lymphoblastoid cells will appear to be MHN leading to a false negative result, which may suggest there is no mutation in *RYR1*.

B-lymphocytes used in this study where isolated from patient blood samples. Blood samples of MH-associated families as well as control patients were collected by staff members of the Palmerston North Hospital and B-lymphocytes were extracted at Massey University and established as continuous cultures of B-lymphoblastoid cell lines.

3.1.2 Myoblasts

Muscle cells contain several different cell types including fibroblasts and myoblasts. Fibroblasts are responsible for the maintenance of cell integrity

and to form connective tissue while myoblasts are the actual muscle cells that differentiate to form myofibrils. Satellite cells were first discovered in 1961 by Mauro et al. [170] and are located at the periphery of myofibres. These cells are myogenic stem cells and are responsible for growth and regeneration. They are activated when the tissue is injured and proliferate as new myoblasts. To fulfil their muscle function, myoblasts need to be differentiated into myotubes, forming long cells by fusion of multiple myotubes eventually forming a myofibril. The formation of these cells can be monitored *in vivo* by microscopy since they become multinucleate cells due to the fusion of single cells [143, 171, 172]. Myotubes express *RYR1* as well as other components of the skeletal muscle Ca^{2+} release channel, while the precursor myoblasts do not express *RYR1*. Myotubes are therefore the preferred cells to investigate altered Ca^{2+} release for MHS patients as they are a close physiological system to that of muscle and they should reflect the function of the complete muscle contraction cascade, not just RYR1. Altered Ca^{2+} release in these cells could be due to either mutations in *RYR1* or any other of the proteins involved in Ca^{2+} release and excitation-contraction (EC) coupling e.g. DHPR. Myotubes also have the advantage of reflecting the patient's genetic background and represent a useful experimental system for the study of mutations in all proteins expressed in skeletal muscle.

3.2 Patient samples

B-lymphoblastoid cells and myoblasts from MHS, MHN and MHE patients (table 3.1) were used for Ca^{2+} release assays in an attempt to use these cells to discriminate between different genotypes. Lymphocytes for patients carrying the R2452W mutation were immortalised from two different families (A and B). Samples for family B (figure 3.1) were only available for the mother BI and her three children where one child (BII:1) is not a carrier for this mutation (-). No information (nt) was available for the father. Sibling BII:1 was used as an internal negative control since the genetic background of the siblings is the same. If the mutation-carrying family members show a hypersensitive receptor compared to BII:1 it would be most likely due to the R2452W mutation in RYR1. Mutation information due to DNA screening for

this mutation was available for patient BIs sibling and nephews but unfortuantely no lymphocytes could be extracted from these patients.

Patient	IVCT result	RYR1 mutation	Gender	Age	Contraction (g) at 2 % Halothane	Contraction (g) at 2 mmol/L Caffeine
A	MHS	R2452W	male	36	2.5	2.4
B I	MHS	R2452W	female	50	4.3	3.7
B II: 1	nt	negative	female	25	nt	nt
B II: 2	nt	R2452W	male	29	nt	nt
B II :3	MHS	R2452W	male	27	6.4	5.1
C1	MHN	negative	female	50	0.2	0.1
C2	MHN	negative	female	40	0	0.1
C3	MHS	H4833Y	female	32	nt	nt
U1	MHE_h	negative	male	40	0.6	0.4
U2	MHE_h	negative	female	65	0.7	0.2

Table 3.1 Patient-derived samples used in Ca^{2+} release assays.
Stated above are patient sample, IVCT results (when applicable) as well as age and gender. Patients not tested by IVCT are indicated as nt and therefore no data was available. The threshold for MHS is 0.4 g for 2 % halothane and 0.2 g tension for 2 mmol/L caffeine. Patients U1 and U2 had a positive reaction to halothane (h) and are therefore classed as MHE_h, indicating a positive halothane response.

Patient A is from a family unrelated to family B and therefore does not share the same genetic background. Unfortunately no information about any other family member of patient A was available.

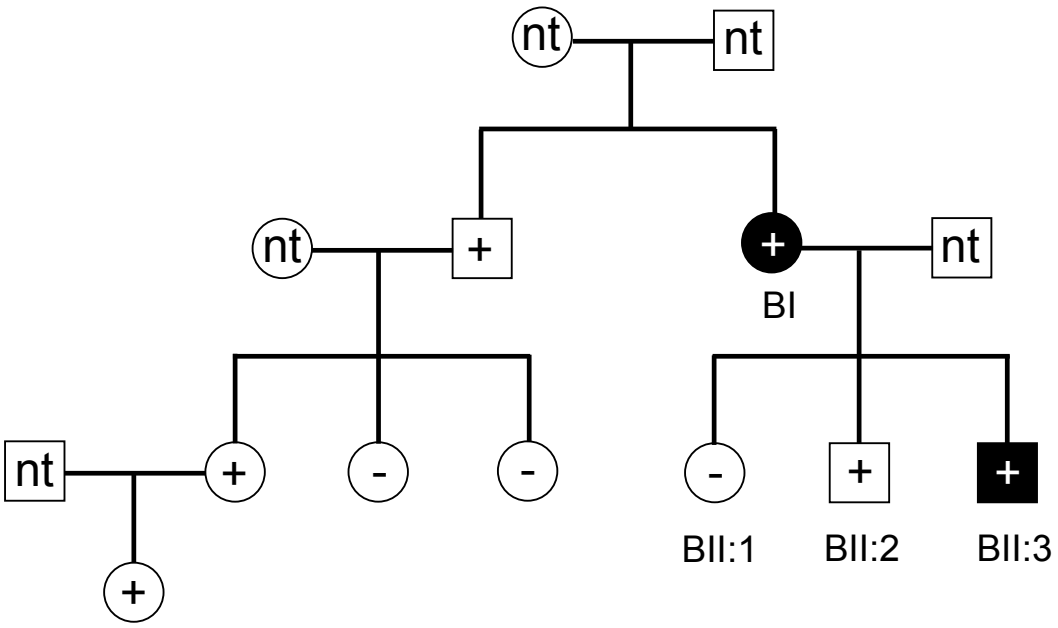

Figure 3.1 Pedigree of family B.
Black symbols represent patients who underwent an IVCT and were classified as MHS while white symbols represent family members that did not undergo an IVCT. + indicates the presence of the R2452W mutation in the patients DNA while – represent the absence of the mutation. Patients not tested for the mutation in their DNA are labelled as nt.

Altogether three controls were chosen. Additional to the control patient BII:1, two more unrelated patients (C1 and C2) with different genetic backgrounds and a previously negative IVCT were chosen. As a positive control for Ca^{2+} release assays in B-lymphoblastoid cells, a RYR1 H4833Y carrier (C3) was chosen. The H4833Y mutation is associated with MH and has been shown to result in a hypersensitive receptor [8, 166]. The two control patients C1 and C2 belong to families with an MH history and therefore underwent an IVCT with a negative result.

The IVCT does not always result in a clear classification of MHS or MHN. Two additional MHE patients (U1 and U2) were included in this study. The MHE clinical phenotype is unclear and any abnormal reactions to RYR1 agonists may assist in understanding the molecular basis underlying this classification.

3.3 Results

3.3.1 Confirmation of the presence of R2452W mutation in assayed samples

The presence (or absence in negative controls) of mutations in *RYR1* was determined before and after each set of B-lymphoblastoid Ca^{2+} release assays to eliminate possible contamination of the different cell lines. HRM (high resolution amplicon melting) assays were carried out to detect the R2452W mutation. These assays are based on different melting behaviours of an amplified PCR product in the presence or absence of mutations. Positive and negative controls were used to confirm amplification and allele-specific discrimination. The H4833Y mutation (used as a positive control in Ca^{2+} release assays) was detected using a hybridisation probe assay. This assay makes use of fluorescent probes as well as unlabelled primers which amplify the DNA and incorporate the probes at the annealing step of the amplification protocol. Assays were carried out on a Roche Lightcycler 480 using the Roche analysis software for allelic discrimination. Results showed that the R2452W mutation was present in all positive B-lymphoblastoid cell lines used (BI, BII:2, BII:3, A, shown blue in figure 3.2A) while the negative controls (BII:1, C1 and C2), unknown controls (U1, U2) as well as the H4833Y control (C3) were negative for R2452W (red trace for patient BII:1 and C1 in figure 3.2A). The hybridisation probe assay showed that the H4833Y mutation was present in the positive control C3 (red line in figure 3.2B) and absent in all other samples used. For discrimination purposes, positive (PC) and negative (NC) controls were included in each assay performed and are indicated in figure 3.2.

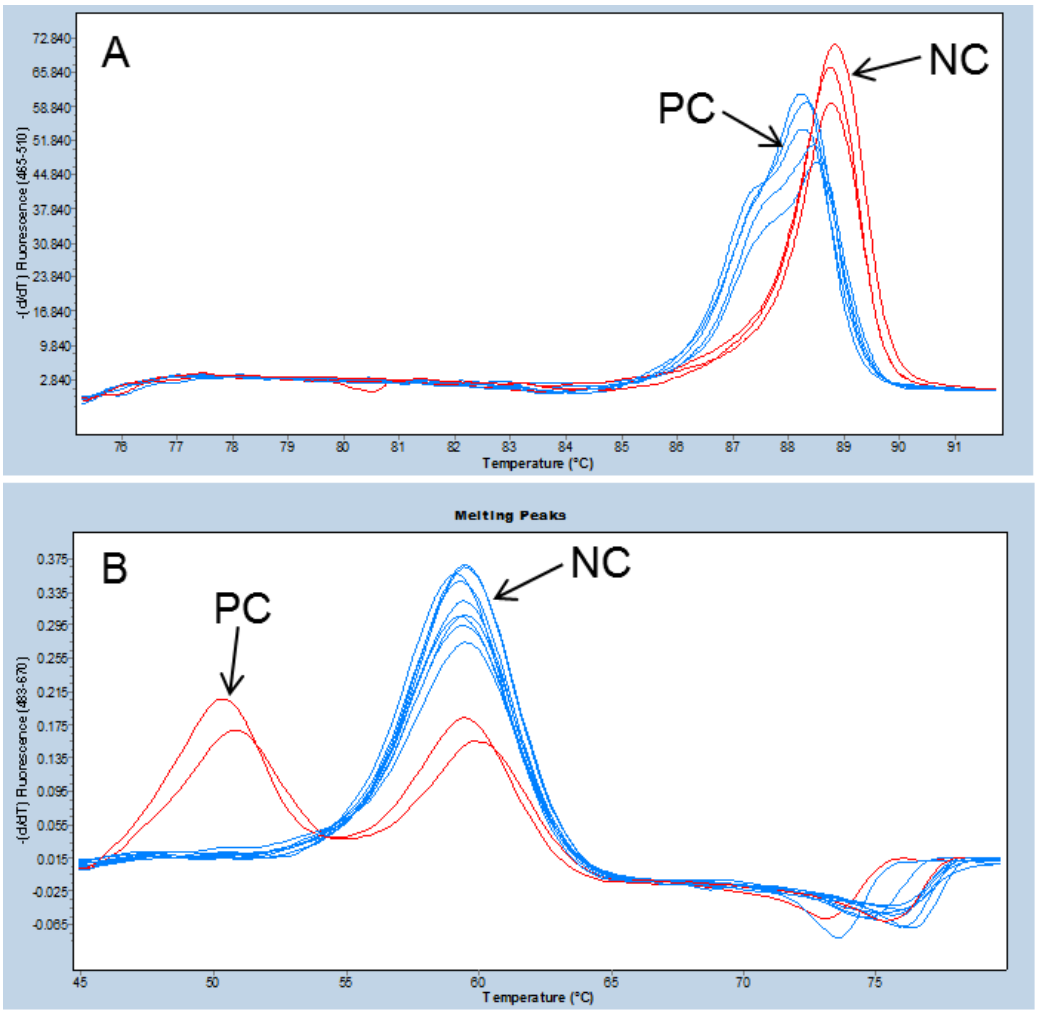

Figure 3.2 HRM and hybridisation probe assays to detect R2452W and H4833Y mutations in B-lymphoblastoid cells.

A) Results for the HRM assays detecting the mutated allele causing the R2452W mutation. Blue lines indicate R2452W positive samples while red curves indicate the absence of this mutation and are therefore classed as WT. The shoulder on the melting curve indicates a heterozygous sample. B) Melting curves for hybridisation assays for the H4833Y mutation. Red lines indicate alleles carrying the mutation leading to H4833Y mutation while blue curves indicate the absence of the mutation. Only patient C3 carries the alleles expressing the H4833Y mutation, showing the same curve as the positive control (PC).

3.3.2 Optimisation of myoblast extraction

Several methods have been reported for the preparation of skeletal muscle myoblasts [144, 172]. Some of these methods were trialled and optimised to develop methods that were generally successful in obtaining cultures enriched with myoblasts.

3.3.2.1 Enzymatic digest of biopsy material

This method has been described in chapter 2.2.24.1. After pre-plating, plate 1 and 2 normally contained high amounts of fibroblasts while the last plate should contain myoblasts only. Using this protocol, many cells were extracted from the biopsy tissue and viable cells were regularly obtained. Unfortunately this method did not yield pure myoblast cultures but significant contamination with fibroblasts. Attempts to separate myoblasts from fibroblasts were made by using PBS as described in 2.2.24.3 but fibroblasts were still abundant. With a high abundance of fibroblasts in the culture it became very difficult to differentiate myoblasts as they became quickly overgrown by fibroblasts. Therefore this tissue disruption method was abandoned.

3.3.2.2 Explant method

After an IVCT was performed, cells were extracted using the explant method described in 2.2.24.2. Enriched myoblasts were trypsinised and cultured in a 10 cm collagen-coated plate, which facilitates adherence by myoblasts. In order to separate residual fibroblasts and myoblasts, cells were grown on collagen-coated plates for myoblast proliferation due to the different adhesion properties of the two cell types [173]. Cells were passaged using PBS while growth media was removed and replaced with PBS. Myoblasts tend to detach from the collagen-coated plate when incubated in PBS, due to different surface adhesion of the two cells types [174], while fibroblasts attached to collagen-coated plates remain adherent due to stronger surface-attachment [175]. The myoblast detachment is probably due to the withdrawal of Ca^{2+} from the media which supports cell adhesion [176]. Myoblasts were then transferred into a new collagen-coated dish for further proliferation. This optimised method resulted in mostly pure myoblast cultures and these cells were further used for differentiation and functional studies.

3.3.3 RYR1 detection in different cell types

3.3.3.1 Immunodetection of RYR1 in B-lymphoblastoid cells

To confirm RYR1 expression in B-lymphoblastoid cells, protein was extracted for subsequent analysis using western blotting. Microsomes were extracted

from ~1x10^7 cells and 15 µg of microsomal protein was analysed on a 7.5 % SDS-PAGE gel followed by western blotting onto nitrocellulose membrane. Membranes were incubated with 34C antibody overnight at 4 ºC and detected the next day using an anti mouse 2º antibody.

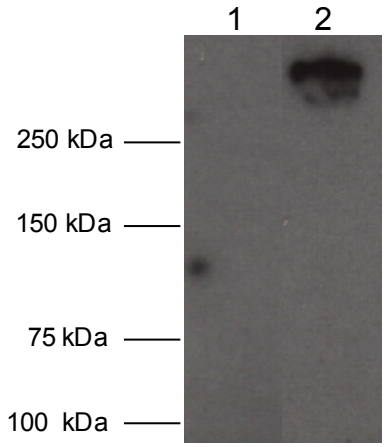

Figure 3.3 Immunoblotting for RYR1 using immortalised B-lymphocyte microsomes extracts. SDS-PAGE gel (7.5 %) was electrophoresed for 1.5 h before transfer overnight at 70 mA onto a nitrocellulose membrane. Lane 1: microsomes of untransfected HEK293 cells; Lane 2: microsomes of lymphoblastoid cells. Western blots were developed using Roche Chemiluminescence solution and emitted light was detected by X-ray film.

The immunoblot showed a band for RYR1 above 250 kDa which represents the ryanodine receptor 1 with a predicted size of 560 kDa (figure 3.3, lane 2). A faint band with higher mobility was also detected most likely indicating degradation of the RYR1 protein. Microsomes extracted from human embryonic kidney cells (HEK293) were used as a negative control (figure 3.3, lane 1) as these cells do not express detectable amounts of RYR1.

B-lymphoblastoid cells were used as a positive control for RYR1 immunofluorescence staining since lymphocytes express the ryanodine receptor 1 endogenously. This method is also useful to confirm localisation of RYR1 in these cells. After fixing B-lymphoblastoid cells onto coverslips coated with 0.01 % poly-L-lysine for 10 min at 37 ºC, the ryanodine receptor 1 was stained using the 34C antibody. The protein disulphide isomerise (PDI) protein, expressed in the ER, could not be used for co-localisation studies in B-lymphoblastoid cells since these cells also express PDI on their surface [177]. The immunostaining showed that RYR1 (figure 3.4b) is not expressed

in the nuclei, represented by DAPI staining (figure 3.4A) but in other cellular compartments.

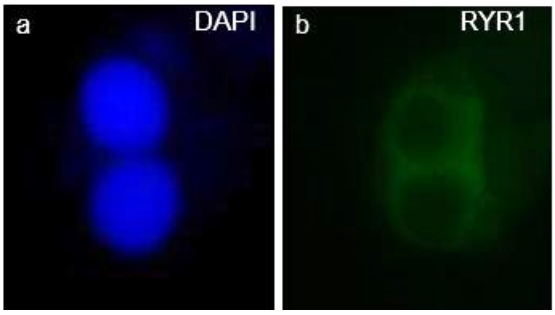

Figure 3.4 Immunostaining of B-lymphoblastoid cells.
DAPI showed staining of the nuclei (a) while image b showed RYR1 staining in B-lymphoblastoid cells which is expressed in regions around the nucleus. Images were taken at 100 x magnification.

3.3.3.2 Immunostaining to confirm the presence of myoblasts

Cells obtained from a muscle biopsy were tested by immunofluorescence to verify myoblast enrichment. Two different antibodies were used: α-desmin and 34C for RYR1 staining. Desmin is an intermediate filament found in muscle around the Z interfilament. To confirm the presence of myoblasts derived from the explant method as well as the absence of fibroblasts, cells were stained with an α-desmin antibody and visualised using a FITC-conjugated secondary antibody (figure 3.5). Desmin is expressed in muscle cells but is absent from fibroblasts. Cells were stained as described in 2.2.22 and fixed in mounting solution containing DAPI for nuclei staining. Desmin is expressed throughout the cells, meaning that co-localisation studies could not be done. Figure 3.5 shows myoblasts stained with desmin (green) and DAPI (blue) and confirmed the presence of myoblasts in the extracted culture. The merged figure shows that desmin is not expressed in the nuclei but within other cell compartments and that extracted cells are myoblasts.

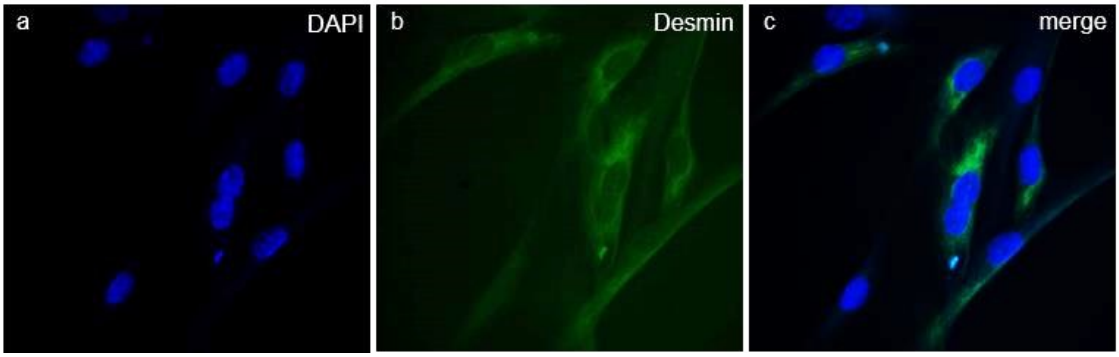

Figure 3.5 Immunostaining of myoblasts using α-desmin antibody.
a) Nuclei staining using DAPI. b) Cells stained with desmin representing the presence of myoblasts. One cell in the centre of the merged image c shows a cell with two nuclei. This cell has already undergone differentiation and is therefore called a myotube. Images were taken at 100 x magnification.

Differentiated myoblasts (myotubes) should express RYR1. Therefore to verify RYR1 expression in myotubes, immunostaining and co-localisation studies were carried out using antibodies against RYR1 and the ER marker PDI. Cells were differentiated in collagen-coated plates, fixed and stained for co-localisation of RYR1 in the ER (figure 3.6).

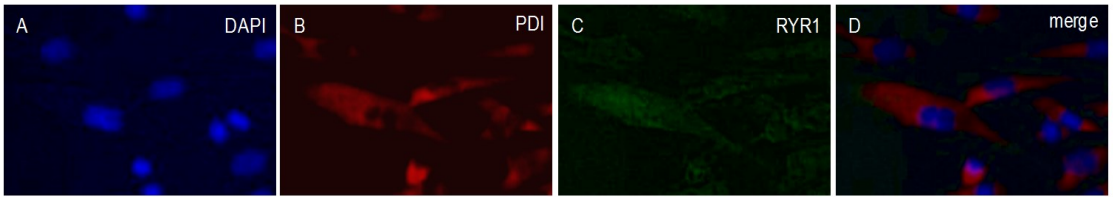

Figure 3.6 Co-localisation studies using PDI and RYR1 antibody in myotubes.
A) Nuclei stained with DAPI. B) SR staining using a PDI antibody. This shows PDI is not expressed within the nuclei. RYR1 is weakly expressed and represented by a faint green stain of the cell in the middle of panel C having two nuclei. Merged figures show co-localisation of SR (PDI) and RYR1 (panel D). Images were taken at 40 x magnification.

Although the sensitivity of fluorescence detection was low figure 3.6 shows that RYR1 was expressed in low levels in myotubes and co-localised with the SR.

3.3.4 Optimisation of Ca^{2+} release assays

Many types of buffers and conditions have been used to perform Ca^{2+} release assays in various cell types. In order to optimise assay conditions and to show that free Ca^{2+} would not interfere with the reliability of the results a number of initial tests were carried out on the same sample of cells (MHN sample C1). Ca^{2+} release of fura 2 loaded B-lymphoblastoid cell line C1, triggered by 4-chloro-*m*-cresol (4CmC), was tested in the presence of buffer containing different concentrations of external Ca^{2+} and EGTA. The different conditions were as follows:

1. 1x BSS + 2 mM Ca^{2+}
2. 1x BSS + 0.1 mM EGTA
3. 1x BSS + 1 mM EGTA
4. 1x BSS + 2 mM EGTA

The baseline fluorescence, representing the ratio of the emission at the two excitation wavelengths 340/380 nm, was recorded using a fluorometer for ~ 2 min before the addition of 900 µM 4-chloro-*m*-cresol (4CmC) that causes the 340/380 ratio of the two wavelengths to increase due to Ca^{2+} release from the stores, and subsequently the maximum amount of Ca^{2+} released was recorded. The difference between the baseline and the peak Ca^{2+} release (Δ) was recorded by subtracting the baseline ratio from the peak ratio (see figure 3.7) as well as the difference induced by the addition of 200 nM thapsigargin, an inhibitor of the Ca^{2+}-ATPase SERCA, to provide an indication of the ER Ca^{2+} store size (table 3.2).

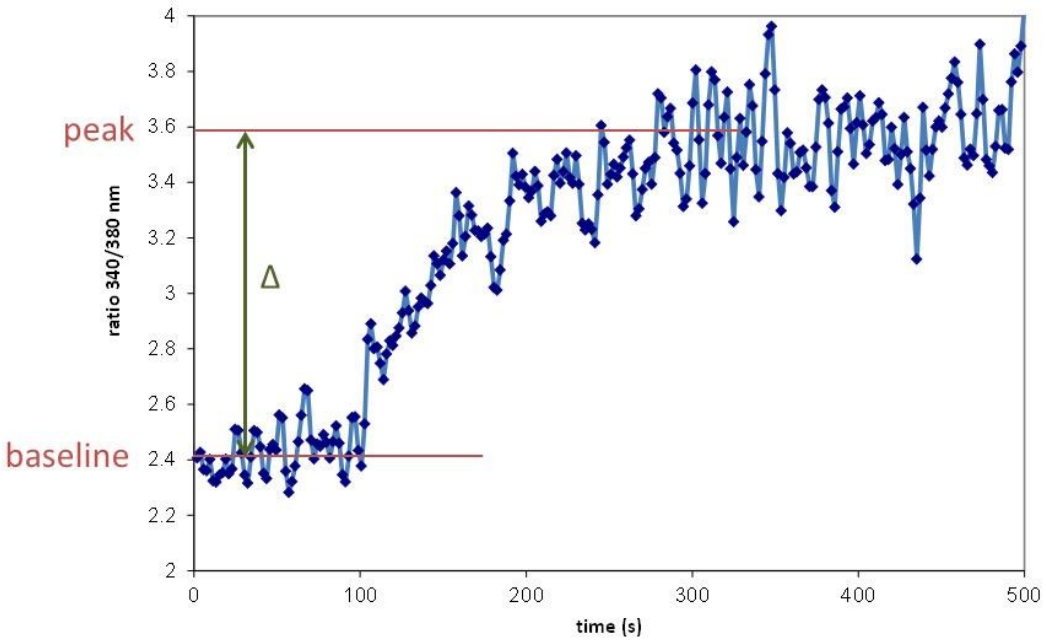

Figure 3.7 Raw data of the 340/380 nm ratio change after the addition of 4CmC.
Average baseline values can be determined from the above graph for fura 2-AM loaded B-lymhoblastoid cells before 900 µM 4CmC was added to stimulate RYR1 Ca^{2+} release. While the ratio of 340/380 nm increases the peak Ca^{2+} release in B-lymphoblastoid cells can be determined. Subtracting the peak Ca^{2+} release from the baseline gives the Δ ratio for each individual cell line.

1 x BSS	Δ ratio induced by 900 µM 4CmC	Δ ratio induced by 200 nM thapsigargin
+ 2 mM Ca^{2+}	0.9	1.64
+ 0.1 mM EGTA	0.75	1.7
+ 1 mM EGTA	0.72	1.1
+ 2 mM EGTA	0.2	0.5

Table 3.2 Influence of different Ca^{2+} concentrations in buffer on Ca^{2+} release in B-lymphoblastoid cells in response to 4CmC.
Addition of a high concentration of EGTA (2 mM) into Ca^{2+} imaging buffer leads to a decrease of mobile Ca^{2+} released by the addition of 4CmC. Furthermore the addition of high amounts of EGTA (1 and 2 mM) reduces the Ca^{2+} store size measured by the addition of thapsigargin.

This experiment was performed only once to assess the effects of external Ca^{2+} and EGTA on Ca^{2+} release from B-lymphoblastoid stores while the cells were only transferred into the measuring buffer just prior to measurements to prevent any effects the EGTA might have upon the cells. The results showed

that the buffer containing 2 mM EGTA significantly reduces the releasable Ca^{2+} amount as well as the size of the Ca^{2+} containing stores. Even though RYR1 was activated with a high amount of 4CmC, Ca^{2+} released was negligible in buffer containing 2 mM EGTA (table 3.2). This effect was not as strong with 0.1 and 1 mM EGTA although it can be concluded that the Ca^{2+}-containing stores appear to decrease in buffer containing 1 mM EGTA. Assays in BSS containing 0.1 and 1 mM EGTA gave almost the same Ca^{2+} release triggered by 4CmC as the 1 x BSS buffer containing 2 mM free Ca^{2+} (ratio ~0.8, see table 3.2). Therefore it was concluded that small amounts of free Ca^{2+} or EGTA do not significantly affect Ca^{2+} release assays. This experiment showed that it is important to use identical buffer conditions for every assay since changes in external Ca^{2+} concentration can influence the results of the assays. To assure that the EGTA does not damage the cells even before the assays were started, cells were kept in plus Ca^{2+} buffer until immediately before the experiment was carried out. The differences in ratio for 200 nM thapsigargin induced Ca^{2+} release is an indicator of the amount of Ca^{2+} stored in the ER since thapsigargin blocks SERCA leading to an indirect depletion of the ER stores. According to the data shown in table 3.2 there is almost no difference in the Ca^{2+} store size of B-lymphoblastoid cells measured in buffer containing 2 mM free Ca^{2+} (Δ ratio = 1.64) and 0.1 mM EGTA (Δ ratio = 1.7). Addition of 1 mM EGTA into 1 x BSS buffer diminished the Ca^{2+} store size to around 70 % (Δ ratio = 1.1 compared to assays in buffer containing 2 mM free Ca^{2+}) while Ca^{2+} release assays performed in buffer containing 2 mM EGTA diminished the Ca^{2+} store size even further to around 30 % (Δ ratio = 0.5).

To further test the effect of external Ca^{2+} on 4CmC activation, concentration-response curves using 100–1000 µM 4CmC were obtained. The following combinations of Ca^{2+} and EGTA were used to measure concentration-response curves in the MHN cell line C1:

1. 1x BSS + 2 mM Ca^{2+}
2. 1x BSS + 2 mM Ca^{2+} + 2 mM EGTA (20 µM free Ca^{2+})
3. 1x BSS + 0.1 mM EGTA
4. 1x BSS + 2 mM EGTA

Results are shown in figure 3.8.

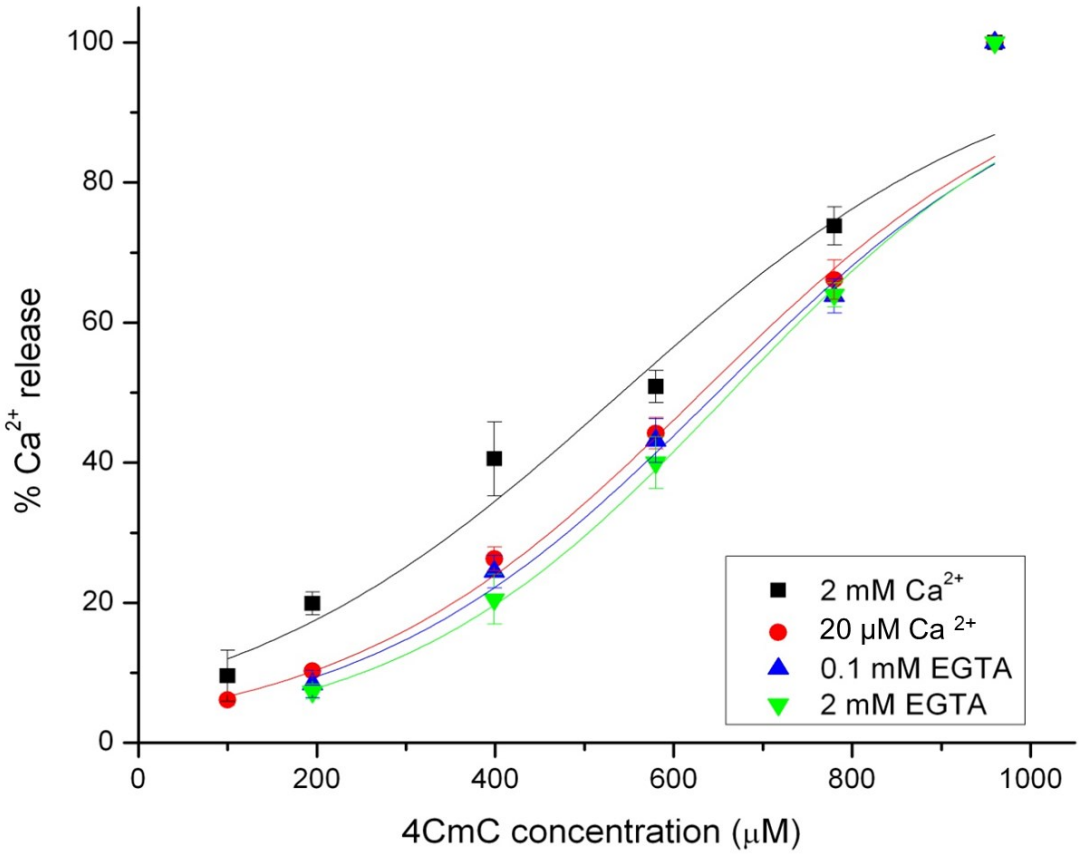

Figure 3.8 Ca^{2+} release assays for the MHN patient C1 in buffers containing different Ca^{2+} and EGTA concentrations in response to 4CmC.
Ca^{2+} release was calculated as a percentage of Ca^{2+} released by the addition of 1 mM 4CmC. Error bars represent the SEM (n= 5-8).

Ca^{2+} release was calculated as a percentage of Ca^{2+} released in response to the addition of 1 mM 4CmC and concentration-response curves were drawn using sigmoid curve fitting using the Origin 8.6 software. The deltas for all cell lines used in this study activated with 1 mM 4CmC are shown in appendix III. Figure 3.8 shows there is no significant difference (calculated using One-Way ANOVA with Bonferroni post hoc analysis) in the concentration-response curves for all buffers except for 1x BSS buffer containing 2 mM external Ca^{2+} which showed a decreased EC_{50} value (table 3.3).

1x BSS buffer	EC_{50} values (µM 4CmC) ±SEM
+ 2 mM Ca^{2+}	560±12 *
+ 2 mM Ca^{2+} + 2 mM EGTA (20 µM free Ca^{2+})	652±14
+ 0.1 mM EGTA	665±11
+ 2 mM EGTA	681±17

Table 3.3 EC_{50} values for 4CmC stimulation obtained in different buffer conditions. Significant differences were calculated using One-Way ANOVA and are indicated with an asterisk. EC_{50} are shown ±SEM (n=4-8).

The EC_{50} values calculated for buffer conditions 2, 3 and 4 are all within the same range and do not show a significant difference compared to each other. A significant difference of EC_{50} values was obtained for conditions 2-4 compared to condition 1 (1x BSS containing 2 mM Ca^{2+} [$p< 0.011$]). Taking these results into account it was decided to use a buffer containing 20 µM free Ca^{2+} for further assays. For curve fitting a sigmoid model was chosen in order to represent concentration-response curves and calculate EC_{50} values (table 3.3). Since EC_{50} represents the half maximal effective concentration of an agonist, the lowest and the highest points of a sigmoid curve need to be defined to fit a sigmoid curve, in order to calculate EC_{50}. The resulting fitted curves do not pass through the 100 % value because the data set does not include enough data points to create a sigmoid model. The curve rather represents a polynomial distribution. In order to obtain better fitting sigmoid curves 4CmC concentrations >1 mM needed to be measured to obtain a value for the maximum Ca^{2+} release which would be shown by a plateau in the concentration-response curve. Using 4CmC concentrations above 1 mM can result in unspecific Ca^{2+} release due to SERCA inhibition and therefore store depletion resulting in non-reliable data [108]. Polynomial curve fitting can be used to obtain curves passing through the 100 % value but because EC_{50} values were to be calculated, sigmoid curves need to be fitted since polynorminal curves do not represent any biological background. When using polynomial curves half maximal activation can be reported instead of EC_{50}.

3.3.5 Results for Ca^{2+} release assays in lymphoblastoid cell lines

Ca^{2+} release assays were carried out in B-lymphoblastoid cells carrying the R2452W mutation as well as control B-lymphoblastoid cells derived from MHN individuals (WT), see table 3.1. Cells were counted in order to ensure the same number of cells was measured in each assay and to achieve a standard fura 2 concentration in each cell since fura-2 is an EGTA-based salt and therefore influences the amount of free Ca^{2+} in the cell. The order of addition of various 4CmC concentrations (100-1000 µM) for each measurement was randomized to exclude artefacts arising from cells being incubated for different times before measurements could be undertaken. The difference between emission ratios for baseline and peak Ca^{2+} release were calculated and Ca^{2+} release was expressed as a percentage of the highest amount of Ca^{2+} released (1 mM 4CmC used in this study) since different cell lines released different amounts of Ca^{2+}. EC_{50} values were calculated using the Origin 8.6 software (table 3.4) while the average raw data for the delta Ca^{2+} release of lymphocytes from patients C1 in 20 µM Ca^{2+} can be found in appendix I.

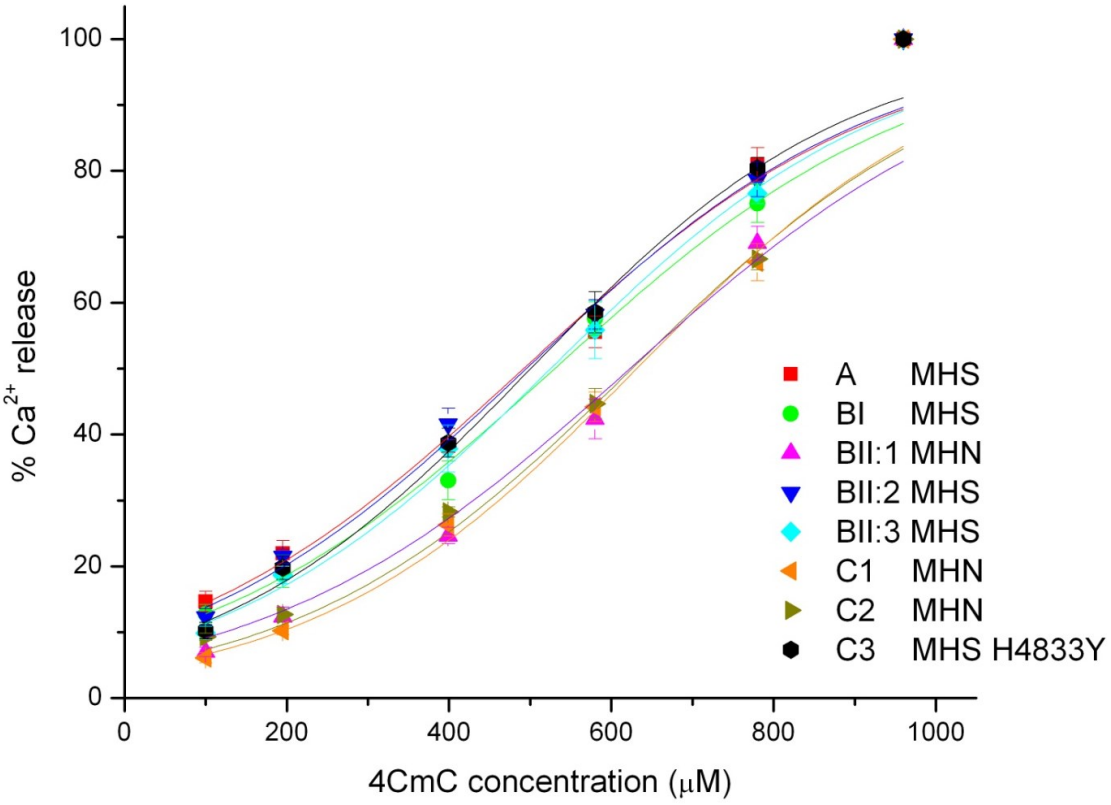

Figure 3.9 Concentration-response curve using B-lymphoblastoid upon 4CmC stimulation. Sigmoid fitted curves were used to calculate EC_{50} values. MH status of each patient is given on the right hand side. Error bars represent the SEM (n= 5-8).

Ca^{2+} release assays demonstrate that B-lymphoblastoid cells carrying the R2452W mutation were more sensitive to 4CmC stimulation compared to MHN samples (figure 3.9). The curve was shifted to the left for B-lymphoblastoid cells carrying R2452W as well as those carrying the H4833Y mutation. This is indicative of calcium release at lower concentrations of 4CmC. EC_{50} values were calculated using One-Way ANOVA with Bonferroni post-hoc analysis to confirm significance levels of differences between MHS and MHN samples. EC_{50} values for MHS patients were lower than for MHN samples (table 3.4) and statistically significant at the 95 % confidence interval ($p< 0.05$ *).

patients	EC_{50} values (µM 4CmC) ±SEM	MH status
A	506±11 *	MHS
BI	544±15 *	MHS
BII:1	641±8	MHN
BII:2	509±23 *	MHS
BII:3	532±23 *	MHS
C1	652±14	MHN
C2	642±10	MHN
C3	505±19 *	MHS

Table 3.4 EC_{50} values for B-lymphoblastoid cell lines upon 4CmC stimulation.
Significant differences calculated using One-Way ANOVA compared to MHN samples are indicated by an asterisk. EC_{50} are shown ± SEM (n=5-8).

Importantly it was observed that lymphoblastoid cells from both families A and B, carrying the R2452W mutation showed almost the same EC_{50} values as the positive control C3 (H4833Y) and show no significant difference. It can be concluded that the R2452W mutation alters Ca^{2+} release through the ryanodine receptor 1 and is likely to result in susceptibility to MH.

B-lymphoblastoid cells from both MHE patients U1 and U2 were extracted and were measured in the same way as MHS and MHN patients. B-lymphoblastoid cells derived from these patients showed an MHN phenotype compared to MHS patient A and resulted in a similar curve shape as MHN patient C1 (figure 3.10).

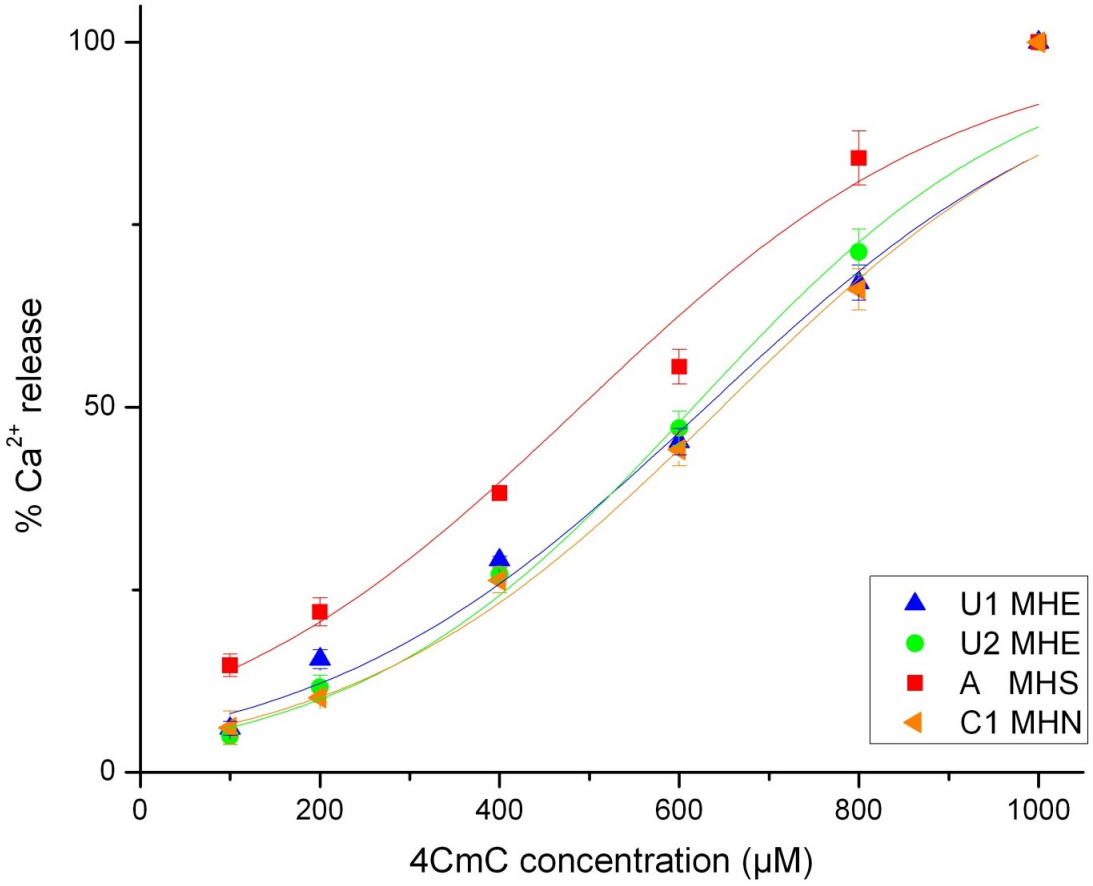

Figure 3.10 Concentration-response curve of B-lymphoblastoid cells from MHE patients upon 4CmC stimulation.

Ca^{2+} release was measured in response to 4CmC and normalised to the highest amount of Ca^{2+} released by the addition of 1 mM 4CmC. Error bars represent SEM for n= 6- 8 measurements.

Some individual data points for patient U1 (200 and 400 µM 4CmC) and U2 (800 µM 4CmC) were higher compared to patient C1 but using the Origin 8.6 software and sigmoid curve fitting resulted in almost the same curves. EC_{50} values for MHE B-lymphoblastoid cells were slightly higher compared to C1 but no significant difference for U1 or U2 was determined compared to MHN patient C1 ($p>0.77$) using One-Way ANOVA (table 3.5). A significant difference was calculated for U1 and U2 compared to MHS patient A ($p< 0.0003$).

patients	EC_{50} values (µM 4CmC) ±SEM	MH status
A	506±11 *	MHS
C1	652±14	MHN
U1	645±38	MHE_h
U2	632±39	MHE_h

Table 3.5 EC_{50} values for 4CmC stimulation in B-lymphoblastoid cells of MHE patients showing a positive reaction to halothane (h).
Significantly different EC_{50} values compared to MHN control C1 are marked with an asterisk. Error bars represent SEM for n= 6- 8 measurements.

Therefore, it was concluded that patients U1 and U2 could be classed as MHN using B-lymphoblastoid cells and a mutation in RYR1 is unlikely. It is however possible that the MHE results in the IVCT were caused by an abnormality in another gene, so this *in vivo* test cannot be used diagnostically to rule out MH-susceptibility.

3.3.6 Ca^{2+} release assays using myotubes

Ca^{2+} release assay conditions in myotubes were chosen to be the same as for B-lymphoblastoid cell assays. They were carried out for cells derived from patient A and for control patients C1 and C2 only since no cells were available from any other patients carrying the R2452W mutation. Myoblasts were seeded into collagen-coated 96-well plates and grown to about 70 % confluence before the medium was changed to differentiation medium containing 2 % horse serum and 1 % penicillin/streptomycin. Cells were left to differentiate for 2 to 3 weeks depending on the cell line.

For Ca^{2+} release assays, individual cells were selected under the microscope and Ca^{2+} release was measured in response to different concentrations of 4CmC. Results from individual cells were combined and the average of Ca^{2+} released in response to 4CmC was calculated. Ca^{2+} release was calculated as the % of Ca^{2+} released normalised to 1 mM 4CmC. This is shown in figure 3.11A while an example of raw data for Ca^{2+} release of patient C1 in response to 1 mM 4CmC is given in figure 3.11B.

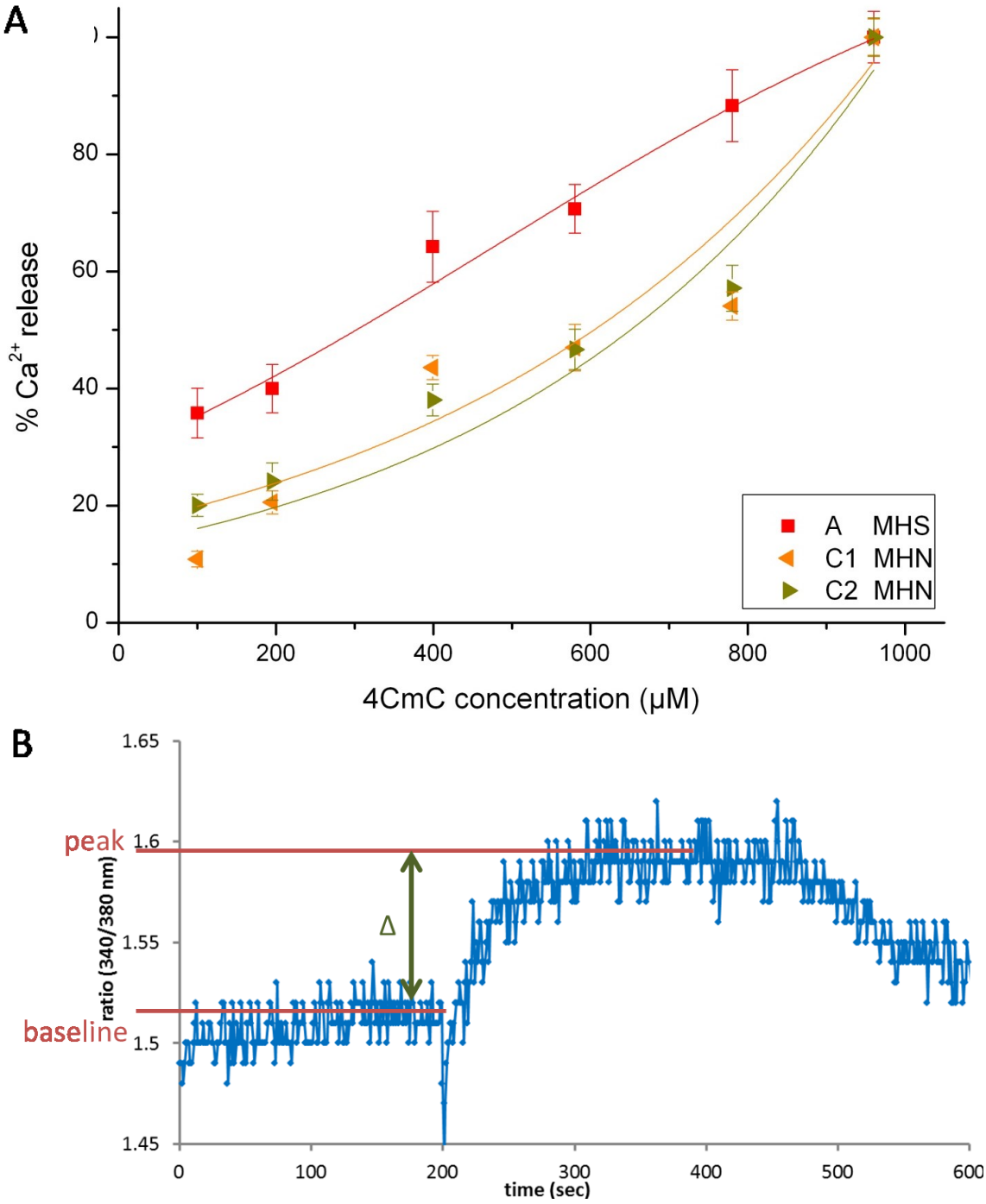

Figure 3.11 Ca^{2+} release data and concentration-response curve for myotubes upon 4CmC stimulation.

A) Ca^{2+} release data normalised to 1 mM 4CmC. Values are given as the average of all measurements ± SEM (n= 14-30) depending on myotubes availability. B) shows an example of raw data from Ca^{2+} release assays in myotubes when stimulated with 1 mM 4CmC. As previously shown for B-lymphoblastoid cells, the baseline ratio of 340/380 nm was determined before the addition of the agonists. The peak Ca^{2+} release was determined and subtracting the ratio for the peak Ca^{2+} release from the baseline ratio yields the Δ Ca^{2+} release.

Because of high variability between Ca^{2+} releases of individual cells, which could be at different stages of differentiation, results of all individual cells were averaged and one sigmoid fitted curve was obtained and the EC_{50} read from the graph. The resulting EC_{50} values are shown in table 3.6.

patients	EC_{50} values (µM 4CmC) ±SEM	MH status
A	309±45 *	MHS
C1	612±54	MHN
C2	638±11	MHN

Table 3.6 EC_{50} values for 4CmC stimulation calculated from concentration-response curves using myotubes.

EC_{50} values were calculated from a sigmoid fitted curve and expressed as the average EC_{50} value ± SEM (n=14-30). Significantly different EC_{50} values compared to MHS controls C1 and C2 are marked with an asterisk.

The EC_{50} value for patient A was significantly lower using One-Way ANOVA with Bonferroni post-hoc analysis when compared to both control individuals ($p< 0.005$) whereas there was no significant difference between samples C1 and C2 ($p>0.05$). Ca^{2+} release for myotubes shows activation at lower 4CmC concentrations indicating higher Ca^{2+} release compared to both control patients. Concentration-response curves for C1 and C2 result in different EC_{50} values but are not statistically different. Since these two patients are not related the differences could be due to the genetic background or within experimental error.

Ca^{2+} release assays for the MHE samples were carried out as described above but cells of patient U1 were differentiated for 2 weeks whereas cells of patient U2 took almost 5 weeks to differentiate into myotubes.

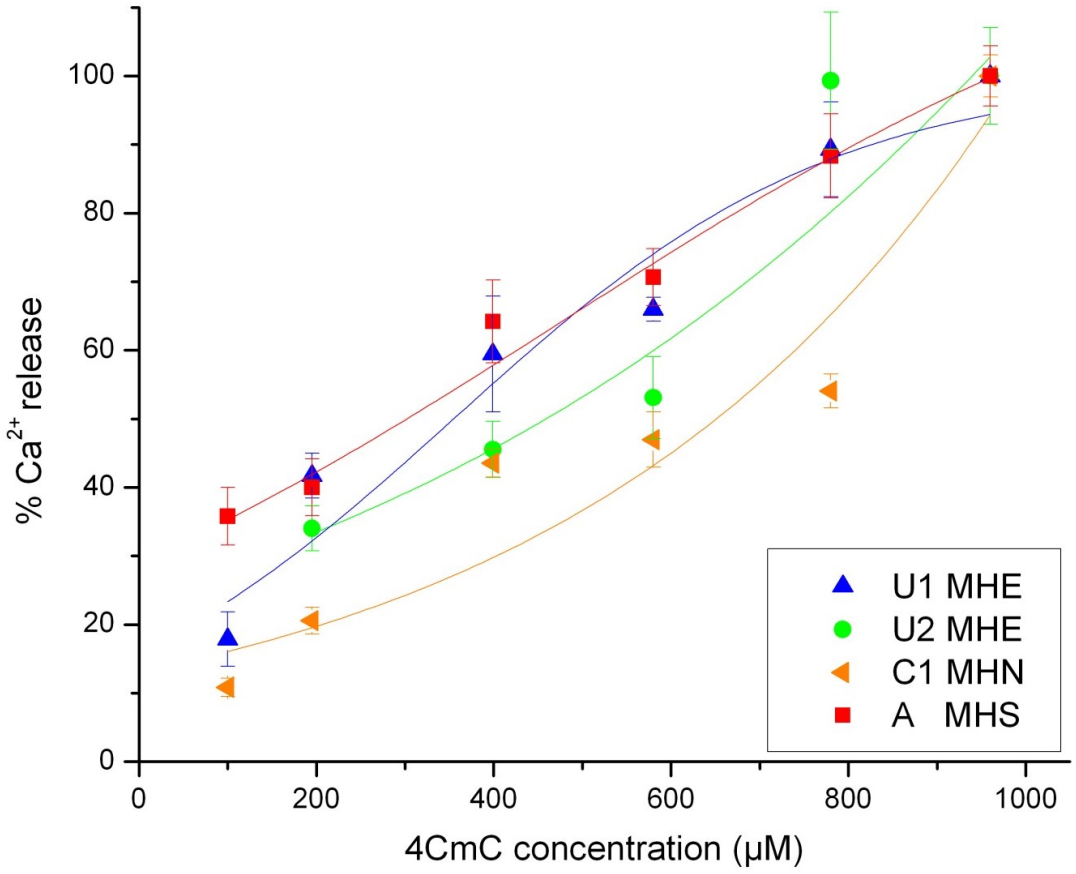

Figure 3.12 Concentration-response curve using myotubes of MHE patients after 4CmC stimulation.

Values are presented as the average of all measurements ± SEM (n= 6-30) and are normalised to 1 mM 4CmC.

Figure 3.12 shows concentration-response curves fitted using a sigmoid curve function. Myoblasts for patient U1 showed similar Ca^{2+} release as MHS patient A however Ca^{2+} release in response to 100 µM 4CmC was lower. Ca^{2+} release for patient U1 was high for all 4CmC concentrations above 100 µM which would class this patient as MHS (compared to MHS individual A). The sigmoid curves for both patients were similar suggesting patient U1 has a MHS phenotype in muscle cells. On the other hand patient U2 showed similar Ca^{2+} release for 400 and 600 µM 4CmC as the MHN control whereas Ca^{2+} release is much higher for 200 and 800 µM 4CmC where values are similar to MHS patient A. Therefore patient U2 cannot be classified as either MHN or MHS using this assay. EC_{50} values for all samples were calculated and are listed in table 3.7.

patients	EC_{50} values (µM 4CmC) ±SEM	MH status
A	309±45 *	MHS
C1	612±54	MHN
U1	334±87 *	MHE_h
U2	473±11	MHE_h

Table 3.7 EC_{50} values for myotubes of MHE patients upon 4CmC stimulation.
Values are presented as the average of all measurements ± SEM (n= 6-30) and are normalised to 1 mM 4CmC. Significantly different EC_{50} values compared to MHN control C1 are marked with an asterisk.

Results were subject to One-Way ANOVA for each individual 4CmC concentration measured using a Bonferroni post-hoc analysis to determine significant differences between either MHN and MHE or MHS and MHE samples. A significant difference was found between samples from patient A and C1 ($p<0.05$) for all 4CmC concentrations used. U1 and C1 showed significant differences for all concentrations apart from 100 µM 4CmC at a confidence interval of 95 %. U1 compared to C1 showed significant differences for most 4CmC concentrations measured, apart from 100 and 600 µM 4CmC which could be due to the smaller sample size used (n=6), therefore patient C1 could be classed as MHS.

3.4 Discussion

3.4.1 B-lymphoblastoid cells

3.4.1.1 R2452W mutation confirmation

Lymphocytes express RYR1 endogenously and are therefore a suitable model to study the function of RYR1 *in vivo* since only a patient's blood sample is required. HRM assays were carried out before and after Ca^{2+} release assays to confirm presence or absence of the R2452W mutation in samples from each patient. This qualitative control procedure ensures that contamination between positive and negative cell lines does not occur as well as a check for potential loss of mutation due to DNA recombination. DNA was extracted from cultured B-lymphoblastoid cells and all samples were

analysed. HRM assays confirmed the presence of the R2452W mutation in all positive samples and absence in all MHN samples before and after the Ca^{2+} release assays were performed. Therefore contamination of the B-lymphoblastoid cell lines could be excluded. Furthermore all cell lines used were tested negative for the H4833Y mutation apart from control 3 known to carry the H4833Y mutation. Even though it is well established that RYR1 is expressed in lymphocytes [133], western blot and immunofluorescence staining were carried out to confirm RYR1 expression in B-lymphoblastoid cells which were prepared at Massey University and used in this study.

3.4.1.2 Ca^{2+} release assays

Since the literature describes many different buffers used for *in vivo* Ca^{2+} release studies, initial tests were performed to determine whether external Ca^{2+} influences the function of RYR1 upon 4CmC-induced Ca^{2+} release from the ER. Table 3.2 shows that Ca^{2+} released by the addition of 4CmC was drastically reduced by the addition of 2 mM external EGTA while the release of Ca^{2+} in all other buffers containing lower EGTA concentrations was similar. Furthermore the experiment showed a reduction of the ER Ca^{2+} stores indirectly measured by the addition of thapsigargin. The ER Ca^{2+} stores had a similar size measured in buffer with 2 mM Ca^{2+} as well as in buffer containing 0.1 mM EGTA but with the addition of higher EGTA concentrations, Ca^{2+} appeared considerably reduced (table 3.2). Therefore it was concluded that higher concentrations of EGTA influence the Ca^{2+} stores in the cells but up to external 2 mM Ca^{2+} in the measurement buffer does not influence Ca^{2+} stores in lymphoblastoid cells. The effect of high external Ca^{2+} was also tested in a concentration dependent manner. Concentration-response curves for cells from control patient C1 were measured five times using four different buffers (figure 3.8). Results showed that concentration-response curves as well as calculated EC_{50} values do not significantly differ in all buffers used except for buffer containing 2 mM free Ca^{2+} which significantly decreased EC_{50} values in B-lymphoblastoid cells. It is hypothesised that high amounts of external Ca^{2+} may increase Ca^{2+} induced Ca^{2+} release. McKinney et al. reported experiments using buffers containing various amounts of Ca^{2+} which showed the higher the external Ca^{2+}

concentration in cells, the higher the Ca^{2+} release in response to 4CmC [178]. These results agree with the results found in this study showing decreased EC_{50} values for Ca^{2+} release measured in buffer containing 2 mM Ca^{2+}. Sei et al. reported caffeine stimulation of B-lymphoblastoid cells in buffer containing either 2 mM Ca^{2+} or ~3 mM EGTA and showed that Ca^{2+} release in response to caffeine in EGTA buffer was significantly decreased [179] which is again in agreement with the results found in this study. EGTA should not be able to enter the cell as it cannot pass through the outer cell membrane due to the absence of transporter proteins. Therefore it is assumed that EGTA takes away Ca^{2+} substrate from the transporter and might result in a decreased amount of Ca^{2+} within the cell and reduced ER Ca^{2+} content.

Concentration-response curves were measured for all patients listed in table 3.1. The 4CmC activation threshold for cells carrying the R2452W mutation and EC_{50} values for R2452W positive cell lines were significantly lower compared to WT cell lines. Cells of MHS patients from family B showed a different strong response to 4CmC with family members BI (MHS) and BII:2 showing a lower EC_{50} value compared to family member BII:3. Comparing the IVCT results, BII:3 had a higher response to caffeine and halothane compared to patient BI (table 3.1). This could explain the higher EC_{50} value for patient BII:3 even though it is still not clear whether there is a relationship between IVCT results and EC_{50} values obtained by *in vivo* tests.

A positive control was included using patient B-lymphoblastoid cells carrying the H4833Y mutation, previously associated with MH susceptibility. This mutation shows a positive response to the triggering agent and yielded a similar EC_{50} value as the R2452W positive patients, supporting the recommendation that the R2452W mutation can be classed as MH causative. Previous publications using B-lymphoblastoid cells carrying the H4833Y mutation determined the half-maximal release using $^{45}Ca^{2+}$ studies with a value of 370 µM 4CmC for cells carrying the H4833Y mutation compared to WT cells with EC_{50} value of 670 µM [8]. These values differ from the EC_{50} values obtained in this study which are higher for MHS lymphocytes (505 µM

in this study, see table 3.4). Since different methods were used in the present study and the study by Anderson et al., the results cannot be compared directly but it shows that both studies indicate altered Ca^{2+} release through RYR1 in the presence of the H4833Y mutation and a hypersensitive channel.

Ca^{2+} release assays using B-lymphoblastoid cells have been carried out by many groups and yielded similar EC_{50} values to the current study [109, 180]. Discrepancies between EC_{50} values can occur because of the genetic background of each individual as well as the assay conditions, as discussed above. It should be noted that different research groups use different amounts of fura 2-AM in Ca^{2+} release assays. As mentioned earlier, fura 2-AM is an EGTA-based fluorophore and its concentration can influence the amount of free Ca^{2+} measured. As shown by Vukcevic et al. [109] in B-lymphoblastoid cells, different mutations also resulted in different responses in Ca^{2+} release triggered by 4CmC. The RYR1 H382N mutation resulted in an EC_{50} value of 615 µM while A2508G gave an EC_{50} value of 501 µM. The difference in EC_{50} value could be explained by the different position of each mutation in the three dimensional structure of RYR1 and the overall effect each mutation may have upon the receptor could therefore differ. The EC_{50} value for A2508G is similar to that obtained for the R2452W mutation (~520 µM 4CmC) in the current study (table 3.4).

Comparing EC_{50} values obtained for cells from patients U1 and U2, there is no significant difference between Ca^{2+} release of the two samples and cells from the control patient C1 whereas a significant difference was obtained compared to cells from MHS patient A. The two MHE patients may have had a false positive reaction in the IVCT or they may carry a mutation in a different protein involved in muscle contraction (not RYR1). These results could indicate that either it is unlikely these two patients carry a MH causative mutation in *RYR1* or they carry a mutation which cannot be characterised using B-lymphoblastoid cells because of position effects in the protein or maybe alternative splicing in lymphocytes. Some RYR1 mutations e.g. R4892W respond to caffeine activation only rather than either membrane depolarisation or 4CmC activation [112]. Other mutations may respond only

to membrane depolarisation. Patients U1 and U2 might carry a mutation that does not affect 4CmC activation and therefore could show an MHN phenotype in Ca^{2+} release assays.

3.4.2 Myotubes

3.4.2.1 Myoblast extraction optimisation

In order to obtain high quality and quantity myoblast cultures extracted from muscle biopsies the method was first optimised comparing two different methods. Cells were extracted using the modified method described by Wehner et al. [143]. Myoblasts were enriched but the population of fibroblasts was too high so cells could not be readily differentiated as fibroblasts tended to overgrow the myoblasts. Therefore the explant method was used to prepare myoblasts. This method was optimised to support rapid myoblast proliferation and generally pure myoblast cultures were obtained. The literature described growing myoblasts in DMEM supplemented with 20 % FCS and 1% penicillin/streptomycin but this seemed to improve fibroblast proliferation. The use of Ham's F10 medium supplemented with 20% FCS, 1% P/S and 40 ng/µL rhFGF seemed to be an optimal growth medium for myoblasts (adapted from [175]) and has been described for primary myoblast cultures previously [181, 182]. Separation of myoblasts and fibroblasts by the addition of PBS [175] was trialled and found to be suitable because myoblasts would detach and could be removed for separate cultures while fibroblast-like cells remained attached to the plate. This optimised protocol led to relatively pure myoblast cultures which could be used for differentiation into myotubes and subsequent use in Ca^{2+} release assays. Immunostaining, using the myocyte-specific antibody desmin, was carried out to confirm success of the myoblast extraction protocol.

3.4.2.2 Ca^{2+} release assays

For Ca^{2+} release assays collagen-coated 96-well plates were used. Differentiation took, depending on the cell line, between 1 and 5 weeks and progress was monitored regularly. Multiple differentiated myotubes were present in a single well and were observed under the microscope simultaneously and stimulated with 4CmC. Cells, depending on their

differentiation state and also the size and the number of nuclei, reacted with different intensities to the agonist. Therefore averaged results for one given 4CmC concentration were calculated in an attempt to obtain robust data. The SEM (between 14 and 30 myotubes for each 4CmC concentration) was also calculated. Data showed that R2452W positive cells responded to much lower 4CmC concentrations compared to MHN cells C1 and C2. The EC_{50} value for patient A was approximately half that of control patients C1 and C2 (table 3.6).

Ca^{2+} release assays for patients carrying the adjacent I2453T mutation [110], estimated the EC_{50} value at 93.9 μM 4CmC compared to EC_{50} values for MHN patients ranging between 192.5 and 352.3 μM 4CmC. While these values are different to those observed in the current study the functional assays for myotubes carrying the I2453T mutation were carried out in buffer containing 2 mM free Ca^{2+}. This could influence the amount of Ca^{2+} released from the stores as demonstrated previously for B-lymphoblastoid cells. Nevertheless the difference in EC_{50} values between MHN and MHS cell lines were relatively similar, being approximately threefold.

Ca^{2+} release in myotubes measured using Krebs-Ringer solution containing 0.5 mM EGTA was studied by Ducreux et al. [151]. EC_{50} values of 10 μM 4CmC for cells carrying an MH-associated mutation V2168M and 50 μM for the CCD-associated mutation I4898T have been found as well as EC_{50} value of 120 μM 4CmC for a MHN control individual. Wehner et al., using an imaging buffer containing 2 mM Ca^{2+}, obtained EC_{50} values of 118 μM 4CmC for MHS and 210 μM 4CmC for MHN individuals [183]. Discrepancies between different studies cannot be easily explained but indicate the importance of standard assay conditions to accurately compare MHN and MHS samples.

Ca^{2+} release assays using myotubes have also been studied by Kaufmann et al. [184] using 4CmC as well as caffeine and halothane as RYR1 agonists. Their study showed EC_{50} values of 100 μM 4CmC for MHN control individuals and 40 μM for MHS patients. Interestingly, the study failed to

show a hypersensitive ryanodine receptor 1 for myotubes carrying the R2458H mutation when using 4CmC as agonist. Nevertheless the R2458H mutation has already been classed as MH causative by the EMHG according to Yang et al. [141].

These examples indicate that even though relative EC_{50} values differ between different assays and conditions, in general a two- to threefold decrease in EC_{50} for MH or CCD causative mutations is observed compared to WT RYR1. This conclusion is supported by the present study where EC_{50} values were halved, compared to MHN cells, in patient A carrying the R2452W mutation (table 3.6). Ca^{2+} release in both myotubes and lymphocytes from patient A was altered. Since B-lymphoblastoid cells from two unrelated families with the R2452W mutation gave a MHS phenotype in Ca^{2+} release assays it is likely that the R2452W mutation is responsible for this phenotype since lymphocytes do not express any other proteins associated with muscle contracture or the muscle triad. This leads to the conclusion that R2452W can be classed as an MH causative mutation.

Ca^{2+} release assays for myotubes from two unrelated MHE patients U1 and U2 gave less clear results. EC_{50} values were determined and showed that values for patient U1 were in the same range as for MHS patient A. The error bars obtained for these measurements are small and not overlapping with the control patient and statistical analysis of the results show a significant difference between U1 and C1, classing this patient as MHS using myotubes, indicating a hyperactive RYR1 channel. Therefore the MHE classification from the IVCT may have been incorrect. Taking the results for the B-lymphoblastoid cell Ca^{2+} release assays into account, RYR1 can be excluded as candidate gene for MH in patient U1. Ca^{2+} release data for patient U2 are equivocal. Sigmoid curve fitting for myotubes Ca^{2+} release data resulted in a curve intermediate between those of MHN and MHS samples (figure 3.12). Considering the individual data points, only Ca^{2+} release in response to 800 µM is significantly increased to the level observed for MHS samples. For other 4CmC concentrations the measured Ca^{2+} release appeared similar to MHN patients. Taking into account the B-lymphoblastoid Ca^{2+} release data, it

is unclear whether this patient had a false positive IVCT result, a mutation in a gene other than RYR1, involved in Ca^{2+} release in muscle cells or this patient is correctly classified as MHE and may or may not be susceptible to triggering agents.

There are several reports showing that 4CmC is not able to discriminate between MHE and MHS cells [185, 186]. Weigl et al. [186] failed to demonstrate altered Ca^{2+} release in MH equivocal myotubes with caffeine leading to the assumption that neither 4CmC nor caffeine can be used as agonist to demonstrate functional effects in MHE cells. If both agonists failed to show altered Ca^{2+} release it is possible that the IVCT gave a false positive result. Kaufman et al. [184] showed that R2458H positive myotubes failed to show a hypersensitive Ca^{2+} release with 4CmC, but altered Ca^{2+} was shown when stimulated with caffeine. This suggests that some patients might carry mutations which can only be detected with Ca^{2+} release assays using caffeine as agonist which might be the case for patient U2. To obtain further information about Ca^{2+} release in myotubes of patient U2, further assays could be performed using caffeine as the agonist. Caffeine also activates RYR3 and therefore a more non-specific reaction may be detected [100, 101] which may confound results.

In summary, patient B-lymphoblastoid cells and/or myoblasts can be used in Ca^{2+} release assays to determine whether a RYR1 mutation alters Ca^{2+} release from the SR. This study shows that patients from two unrelated families carrying the R2452W mutation show altered Ca^{2+} release resulting in a hypersensitive receptor phenotype. These results confirm that the R2452W is causative of MH and this study can be used to support the addition of the R2452W mutation to the list of MH causative mutations. MHE samples used in this study did not show altered Ca^{2+} release in B-lymphoblastoid cells and therefore may not carry a mutation in RYR1. Myotube Ca^{2+} release assays did not yield a clear result for patient U2 while patient U1 can be classed as MHS according to myotube assays. Since this patient showed a negative phenotype in B-lymphoblastoid cells this patient is likely to carry a mutation in a different, as yet unidentified, gene involved in Ca^{2+} release in muscle cells.

Chapter 4 Functional characterisation of the R2452W mutation using a recombinant system

4.1 Introduction

Human Embryonic Kidney (HEK) 293 cells do not express functional RYR1 endogenously in measurable amounts and therefore are a useful system to study altered Ca^{2+} release from the endoplasmic reticulum (ER) through transfected mutated ryanodine receptor channels. HEK293 cells normally use an alternative mechanism for Ca^{2+} release involving the inositol 1,4,5-trisphosphate (IP3) receptor. This Ca^{2+} channel is the favoured channel over the ryanodine receptor for release of stored Ca^{2+} from the ER in many non-excitable mammalian cell lines e.g. HeLa or fibroblast cells. It has been suggested however that RYR1 might play an important role in intracellular Ca^{2+} signalling in these cells e.g. signal transduction or hormone-evoked Ca^{2+} response [136, 137].

HEK293 cells can be transfected with *RYR1* cDNA cloned into an mammalian expression vector and expressed protein can be activated with a specific ryanodine receptor agonist like 4-chloro-*m*-cresol (4CmC), halothane or caffeine [135]. In this study transfected HEK293 cells, either transiently or stably expressing RYR1, were loaded with the fluorescent Ca^{2+} indicator fura 2-AM and Ca^{2+} release was measured in response to various concentrations of the specific ryanodine receptor agonist 4CmC. Changes in fura 2 fluorescence were detected using a fluorescence microscope and Ca^{2+} release was normalised to the amount released at 1 mM 4CmC which was set to 100%.

4.2 Results

4.2.1 Full-length R2452W mutant *RYR1* cDNA

The full-length human wildtype *RYR1* cDNA had been previously cloned and sequenced by Keisaku Sato [166] while the full-length human *RYR1* cDNA carrying the R2452W mutation had been prepared by Alexandra Schulz and

Lili Alana Rhodes (IMBS, Massey University Palmerston North). Prior to beginning functional analysis, it was necessary to completely sequence this clone to confirm the presence of R2452W which had been introduced by PCR-based site-directed mutagenesis, as well as the absence of any random PCR-induced mutations.

4.2.1.1 Confirmation of the R2452W mutation in the pcRYR1-R2452W plasmid

Full-length human WT (pc*RYR1*) and R2452W mutant *RYR1* (pc*RYR1*-R2452W) cDNA constructs were prepared in the pcDNA3.1(+) vector and then used to transform *E. coli* DH5α competent cells in order to obtain single colonies for propagation of the two recombinant plasmids. These cultures were used for the extraction of plasmid DNA of both high quality and quantity. Control restriction endonuclease digests were carried out as a first step to confirm the size and the identity of each plasmid construct. The 20.6 kb pc*RYR1* and pc*RYR1*-R2452W cDNA constructs contain five XhoI restriction sites within the *RYR1* sequence (red, figure 4.1A) which can be used to confirm the identity of each plasmid. The resultant restriction fragments were of different sizes and could be used to identify the plasmid.

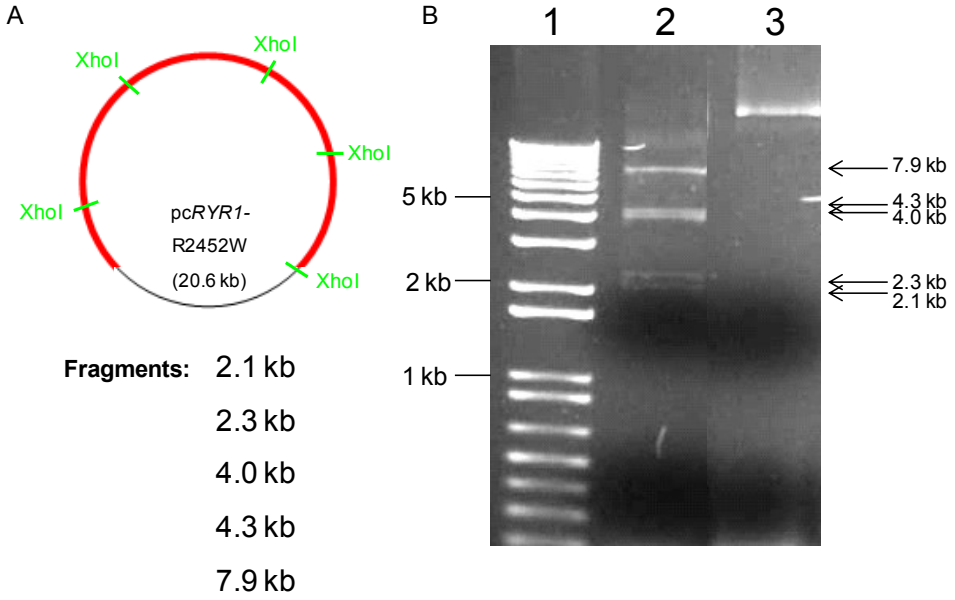

Figure 4.1 Restriction endonuclease digest of the pc*RYR1*-R2452W plasmid.

A) XhoI recognition sites within the pc*RYR1*-R2452W plasmid (pcDNA3.1(+) vector backbone is shown in black). The *RYR1* coding sequence is shown in red. B) Electrophoresis of an XhoI control digest to resolve the five resulting bands loaded onto a 1 % agarose gel and electrophoresis was carried out for 1 h at 80 V in 1x TAE buffer and stained with 0.5 µg/mL ethidium bromide. Lane 1 shows the 1 kb+ size marker, lane 2

contains XhoI digested pc*RYR1*-R2452W and lane 3 shows the undigested pc*RYR1*-R2452W plasmid.

The control which consists of 1 µg pc*RYR1*-R2452W plasmid digested with 10 U of XhoI for 30 min at 37 ºC shows the presence of all five bands of the expected sizes (Figure 4.1B) confirming the identity of the plasmid. The separation between 4.0 and 4.3 kb bands is marginal but a brighter band can be observed at this location suggesting it contains two similar sized bands.

In order to confirm the presence of the R2452W mutation in the plasmid and to exclude any other mutations within the insert, both strands were fully sequenced by di-deoxy chain termination using BigDye Version 3.1 by the Massey Genome Service. It was confirmed that the R2452W mutation (g.G7354T) was present in the plasmid and the insert cDNA had been cloned in frame. Figure 4.2 shows the sequencing results for the R2452W mutation carrying plasmid indicating the nucleotide change from cytosine to thymine by an arrow. The associated base is coloured in grey.

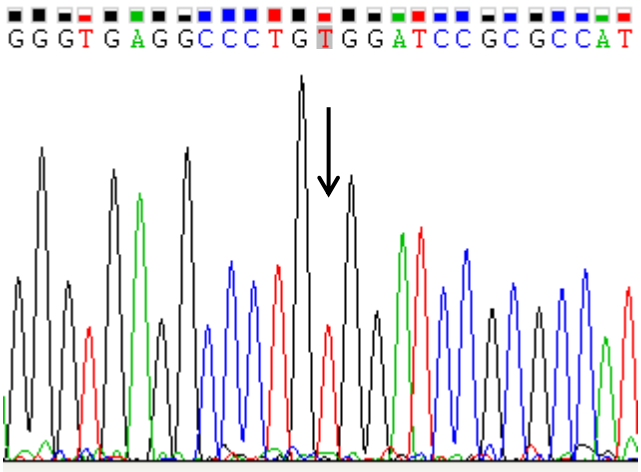

Figure 4.2 Sequencing result of pc*RYR1*-R2452W to confirm the presence of R2452W. The forward sequence of pc*RYR1*-R2452W cDNA contains the c.C7354T mutation, coding for the R2452W mutation (indicated by an arrow).

Fourteen single base pair changes were found by sequencing the plasmid but they were all synonymous and did not lead to amino acid substitutions. Some of the changes had been recorded in the SNP database [187] and all are listed in table 4.1. All other variants are likely to be novel polymorphisms

found in human *RYR1* cDNA or are PCR-induced changes. All variants are in the 3rd position of the codon so they are likely to be natural variants.

Amino acid and position	Codon change	SNP database
A359	GCC -> GC**T**	rs10406027
D993	AAC -> AA**T**	rs2228070
H2621	CAC-> CA**T**	rs2229142
T2659	ACG -> AC**A**	rs2229144
D2705	ATT -> AT**C**	
D2730	GAT -> GA**C**	rs2915951
E2779	GAG -> GA**A**	rs2915952
P3062	CCA -> CC**G**	rs2071089
D3396	GAC -> GA**T**	rs2229145
G3893	GGG -> GG**A**	
A4116	GCG -> GC**A**	
I4317	GTG -> GT**A**	
S4584	TCA -> TC**G**	
L4687	CTG -> CT**A**	

Table 4.1 List of synonymous polymorphisms found in the pc*RYR1*-R2452W plasmid. Amino acid positions are listed on the left-hand side while codons including base changes are listed in the middle panel. The mutated base has been highlighted. Corresponding rs numbers (RefSNP numbers) when applicable, have been listed on the right-hand side.

4.2.1.2 Optimisation of RYR1 expression in HEK293 cells

The ratio between Fugene HD transfection reagent and pc*RYR1*-R2452W cDNA was first optimised in order to obtain measurable expression of human RYR1 in human embryonic kidney (HEK293) cells. Cells were grown in 3.5 cm plates and transfected at ~90 % confluency with a 0:2 (no DNA control) 6:2, 8:2 and 10:2 ratio of Fugene HD (in µL): pc*RYR1*-R2452W (in µg) and HEK293 cells treated only with transfection reagent (2:0) were used as a negative control. Microsomes were extracted 72 h post transfection and used in western blotting to detect ryanodine receptor 1 protein using the 34C anti-ryanodine receptor antibody with anti-mouse HRP as the secondary antibody. Tubulin was used as the internal loading control.

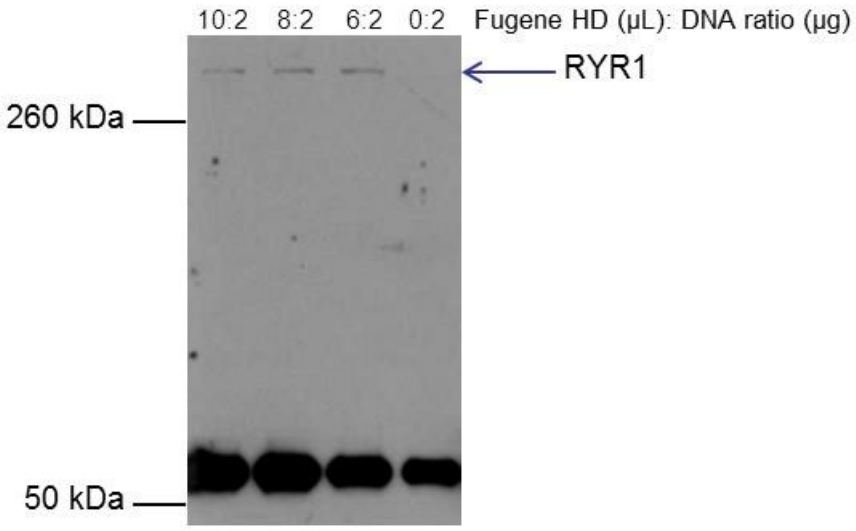

Figure 4.3 Western blotting for transfected HEK293 cells using different ratios of pc*RYR1*-R2452W cDNA and FugeneHD.

Microsomes (15 µg) were loaded onto a 7.5 % SDS-PAGE gel which was electrophoresed for 1.5 h at 120 V before transfer at 70 mA overnight onto a nitrocellulose membrane. The blot shows a band higher than 250 kDa representing RYR1 and is expressed in all RYR1 transfected HEK293 cells. Tubulin can be detected at ~55 kDa in all lanes.

Western blotting (figure 4.3) showed RYR1 was expressed at all different ratios of transfection reagent: *RYR1* plasmid DNA tested and expression levels were similar. Mock transfection (0:2) showed no ryanodine receptor 1 expression. Therefore HEK293 do not endogenously express detectable amounts of RYR1 and the antibody used for western blotting recognises RYR1. As a result a 8:2 ratio of Fugene HD to plasmid DNA was used for further transfections.

4.2.2 Transient transfected HEK293 cells

While western blotting was used to confirm expression of pc*RYR1*-R2452W, immunoblotting and immunofluorescence were used to confirm both expression and cellular localisation, respectively, of both WT and R2452W mutant RYR1 proteins.

4.2.2.1 Immunoblotting to confirm RYR1 expression

HEK293 cells transfected with empty pcDNA3.1(+) vector were used as a negative control. Whole cell lysates of transient transfected HEK293 cells grown in 3.5 cm plates were prepared 72 h post transfection and loaded onto

a 7.5 % SDS-PAGE gel. Endogenous tubulin protein was used as a loading control showing that all lanes had equal amounts of protein (70 µg of crude protein extract) but differ in RYR1 levels.

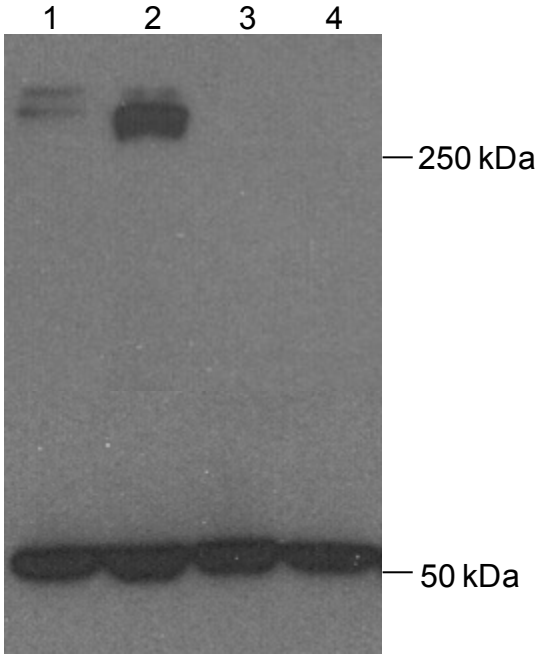

Figure 4.4 Western blotting for detection of transiently expressed RYR1 protein in HEK293 cells.

Lane 1: HEK293 cell lysate expressing WT RYR1 (70 µg); Lane 2: cell lysate representing R2452W mutant RYR1 of transient transfected HEK293 cells (70 µg); Lane 3: HEK293 cell lysate transfected with empty pcDNA3.1(+) vector (70 µg); Lane 4: cell lysate of untransfected HEK293 (70 µg). The 7.5 % SDS-PAGE gel was electrophoresed for 1.5 h at 120 V and transferred overnight at 70 mA onto a nitrocellulose membrane.

Western blotting (figure 4.4) shows bands at lower mobility than 250 kD representing RYR1, as well as a faint band at the top of the gel which could be aggregated or non-denatured RYR1 too large to enter the gel since samples were not boiled prior to gel loading. The blot indicated that R2452W mutant RYR1 is expressed at higher levels than WT RYR1 resulting in a darker band for the mutant (figure 4.4, lane 2). Western blots were performed for two independent transfections with WT and mutant RYR1 simultaneously and yielded the same result. No bands at >250 kDa were detected for lysates from HEK293 cells untransfected or transfected with pcDNA3.1(+) vector, suggesting that vector alone does not enhance RYR1 expression and also that HEK293 cells do not express detectable amounts of endogenous RYR1. It is unknown why mutant RYR1 is expressed at higher levels compared to

WT, however it could be that the quality of the mutant plasmid was higher and therefore yielded higher expression levels in HEK293 cells. This experiment was performed twice and the same result was obtained both times.

4.2.2.2 Immunofluorescence studies for localisation of RYR1 in transiently transfected HEK293 cells

In order to release Ca^{2+} from the SR/ER into the cytosol RYR1 must be expressed in SR/ER membranes. Co-localisation studies using confocal microscopy were therefore carried out to confirm appropriate localisation of expressed RYR1 in HEK293. Fixed transient transfected cells were stained with α-RYR1 antibody (34C) and α-PDI as an ER-marker. A FITC conjugated secondary antibody was used to detect ryanodine receptor (green colour, figure 4.5C) while a TRITC conjugated secondary antibody was used to stain the ER (red, figure 4.5B). DAPI was used as a control to stain nuclei (blue, figure 4.5A). Immunostaining (figure 4.5) indicated that very few cells expressed RYR1. A negative control was not performed for this experiment since untransfected cells represented an internal negative control. Merged images (figure 4.5D) show co-localisation of PDI and RYR1 suggesting RYR1 was expressed and correctly targeted to the ER. HEK293 cells transfected with either pc*RYR1* or pc*RYR1*-R2452W showed no difference in expression localisation using this method of detection. Histogram plots were made and are shown in appendix II. These provide additional evidence of co-localisation of RYR1 and PDI in transiently transfected HEK293 cells. These experiments cannot be used to distinguish expression efficiency because these experiments were carried out with Fugene 6, which is used for low cell densities, while Fugene HD is used a high cell densities in order to drive high expression of the target protein.

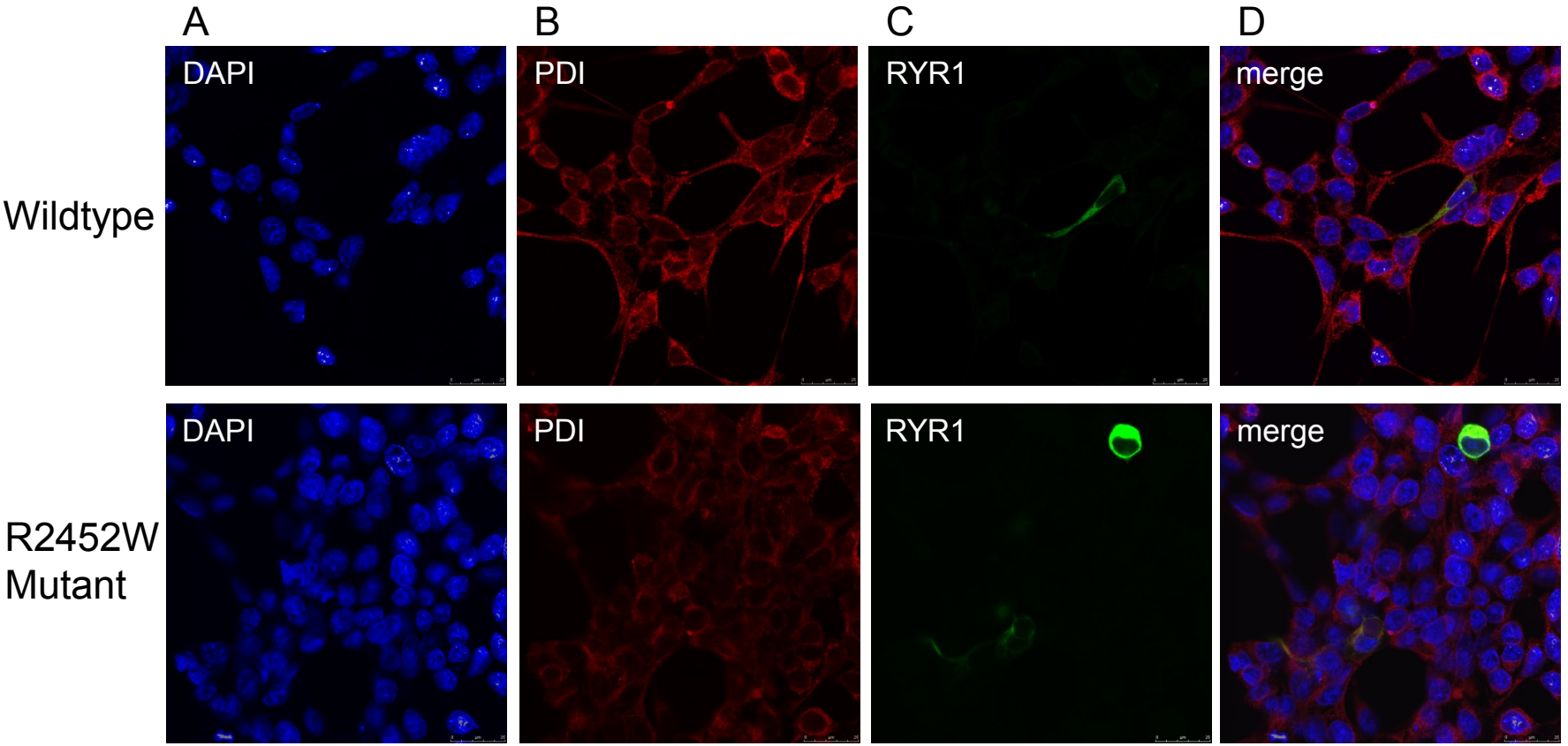

Figure 4.5 Immunofluorescence of transient transfected WT and R2452W mutant RYR1.

The top panel shows immunostaining for HEK293 cells transiently transfected with pc*RYR1* while the lower panel represents cells transfected with pc*RYR1*-R2452W. DAPI (A) is shown in blue, while the ER marker PDI (B) is coloured red and RYR1 green (C). Overlaid images (D) showed co-localisation of RYR1 and PDI. Images were taken at 100 x magnification.

4.2.2.3 mRNA level detection

Western blotting could not be used on transient transfected HEK293 cells that had been used for Ca^{2+} release assays as these were carried out in 96-well plates that contained insufficient cells to yield enough protein for detection. Expression at the mRNA level could be detected, however, as an additional check. Therefore, RNA was extracted from 6 wells (of a 96 well plate) of transient transfected HEK293 cells previously used in Ca^{2+} release assays. RNA was extracted using the Roche High Pure RNA Extraction kit and cDNA was synthesised using the iScript cDNA kit with 1 µg RNA per reaction. RNA from untransfected HEK293 cells from the same passage number as transfected cells, was extracted as a control for endogenous *RYR1* levels. RT- controls were included using equal amounts of RNA as in the RT+ samples to check for DNA contamination. Primer pairs binding to different regions of the RYR1 cDNA were chosen for RT-qPCR. One set detected mRNA expression levels using the central domain (primer pair 1) covering the region including the C7354T mutation (translated into p.R2452W) and the second set (primer pair 2) targeted the C-terminal region (figure 4.6). HPRT (hypoxanthine phosphoribosyltransferase) was used as a reference gene since its endogenous expression is low [188] and was expected to have similar expression levels to *RYR1* in transiently transfected HEK293 cells.

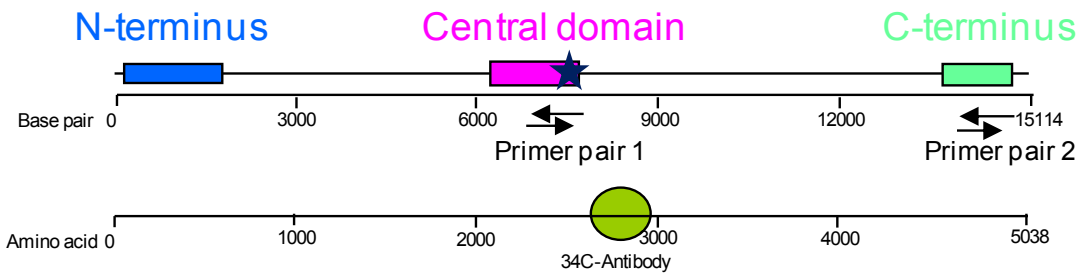

Figure 4.6 Primer design for RT-qPCR using two different primer pairs.
Primer pair 1 was located in the central region while primer pair 2 was located in the cDNA representing the C-terminus. The 34C antibody used in western blotting binds around amino acid position ~2750. The star represents the location of the p.R2452W/c.C7354T mutation in the central domain. This schematic diagram is not drawn to scale.

PCR products for primer pairs 1 and 2 were loaded onto a 2 % agarose gel to verify the correct product size and products for primer pair 1 were sequenced to confirm identity. Products for primer pair 2 were not sequenced since these amplicons had been verified in previous work [189]. Standard curves for primer efficiencies were obtained using B-lymphoblastoid cell cDNA since these cells endogenously express *RYR1* (appendix XII). PCR efficiencies were calculated using the REST 2009 gene expression software [190] and are considered as reliable for values <1 (table 4.2).

Primer pair name	PCR Efficiency
RYR1 primer pair 1	0.982
RYR1 primer pair 2	0.9541
HPRT	0.9994

Table 4.2 PCR efficiencies for three primer pairs calculated by the REST 2009 software. Primer efficiencies were determined from standard curves for four different concentrations of B-lymphoblastoid cell cDNA, amplified in triplicate.

RT-qPCR was carried out for HEK293 cells transfected with pc*RYR1* and pc*RYR1*-R2452W as well as for untransfected HEK293 cells. Crossing points (Cp), where the fluorescence detected was higher than the baseline threshold, were measured in all three samples. The lower the Cp value, the higher the abundance of cDNA. Results showed a higher abundance of R2452W mutant cDNA compared to WT of ~6 cycles indicating a 100 fold higher abundance of mutant cDNA (table 4.3).

Sample	Primer pair 1		Primer pair 2		HPRT	
	Mean Cp	Stdev.	Mean Cp	Stdev.	Mean Cp	Stdev.
HEK293	33.36	0.13	30.90	0.05	23.16	0.15
R2452W mutant	20.79	0.10	20.61	0.10	24.36	0.06
WT	27.11	0.03	26.67	0.09	23.77	0.12

Table 4.3 Cp values obtained for three samples used in one real-time PCR experiment. Average Cp values resulting from analysing triplicate of one biological cDNA sample, including the standard deviation (stdev), were calculated.

The REST2009 software [191] was used to calculate expression levels. This software uses the PCR efficiencies calculated from the standard curves to convert Cp values into relative expression values of cDNA transcripts. Relative expression was then calculated by the REST2009 software normalising Cp values for WT and R2452W for primer pairs 1 and 2 to Cp values of HPRT, which acts as a housekeeping gene with a stable expression profile. Expression of *RYR1* in untransfected HEK293 cells was set as 1 and relative expression to untransfected cells was calculated together with statistical analysis was carried out using a randomization test with a 95 % confidence interval as well as a hypothesis test.

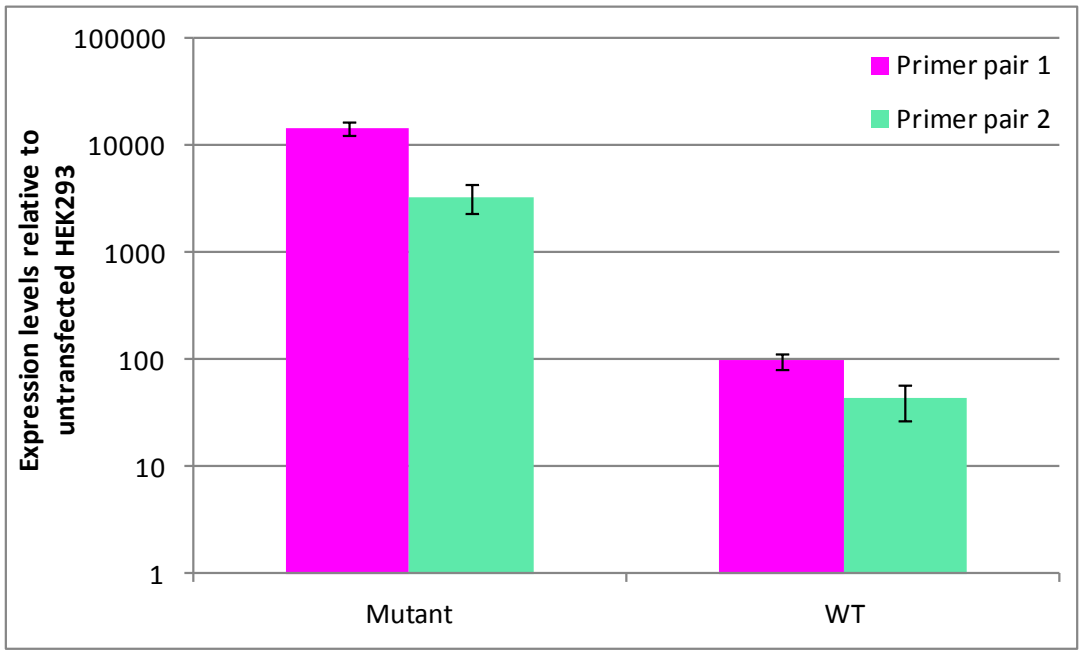

Figure 4.7 mRNA *RYR1* expression levels in transient transfected HEK293 cells. Expression levels were calculated relative to the expression of untransfected HEK293 cells. Expression levels compared to untransfected HEK293 cells analysed using primer pair 1 are shown in pink and expression levels using primer pair 2 in green. Error bars represent standard error of the mean of cDNA triplicates obtained from two different transfection experiments.

The relative expression was significantly higher for R2452W *RYR1* ($p<0.04$) compared to WT *RYR1* (figure 4.7). Furthermore a difference in expression levels detected by primer pair 1 (central region) and 2 (C-terminal region) could be seen. Since only 2 biological replicates were performed no statistical analysis could be performed. These results confirm western

blotting experiments showing that R2452W mutant *RYR1* is expressed in higher levels compared to WT *RYR1*.

4.2.2.4 Optimising Ca^{2+} release assays using different Ca^{2+} concentrations

To confirm whether 1x BSS buffer containing different Ca^{2+} concentrations alters Ca^{2+} release from the ryanodine receptor 1, HEK293 cells were transfected with a control plasmid carrying the human *RYR1* cDNA containing the H4833Y mutation and Ca^{2+} release was measured in duplicate in the following buffers:

1. 1x BSS + 2 mM Ca^{2+}
2. 1x BSS + 2 mM Ca^{2+} + 2mM EGTA (20 µM free Ca^{2+})
3. 1x BSS + 0.1 mM EGTA

Graphs were plotted using the Origin 8.6 software applying a concentration-response curve fitting and are shown in figure 4.8. Results showed that Ca^{2+} release and EC_{50} values for buffers containing very little Ca^{2+} (condition 2 and 3) were almost the same within experimental error. Therefore a small amount of external Ca^{2+} did not appear to influence the accuracy of the results (figure 4.8). Error bars represent the SEM for two measurements.

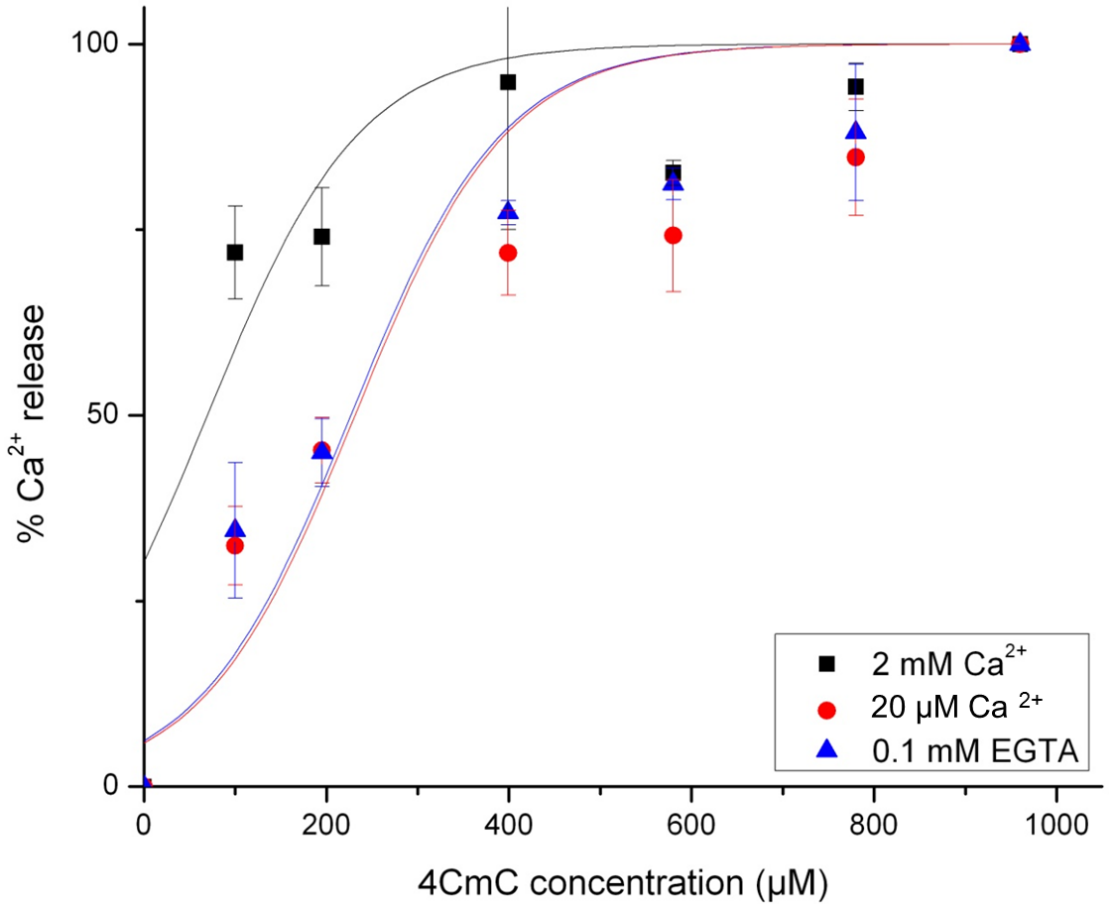

Figure 4.8 Concentration-response curve of H4833Y transient transfected HEK293 cells in different imaging buffers upon 4CmC stimulation.
Average Ca^{2+} release values are shown ± SEM (n=2) and sigmoid fitted curves were used, using 1 mM 4CmC as the maximum value of Ca^{2+} release.

The obtained EC_{50} value in buffer containing 2 mM Ca^{2+} was lower compared to EC_{50} value for Ca^{2+} release in buffers containing low Ca^{2+} or 0.1 mM EGTA (figure 4.8). Ryanodine receptor stimulation using 4CmC was high even at low concentration (<200 µM). In contrast, Ca^{2+} release from RYR1 at 200 µM 4CmC was 45 % for 20 µM free Ca^{2+} but was 75 % for the buffer containing 2 mM free Ca^{2+}. In order to obtain a more accurate concentration-response curve for the Ca^{2+}-containing buffer, lower concentrations of 4CmC could have been used to determine Ca^{2+} release. Since it was decided to perform Ca^{2+} release assays in the buffer containing 20 µM free Ca^{2+} no further studies were undertaken using the buffer containing 2 mM free Ca^{2+}. EC_{50} values for all assays were obtained from the above graph and are listed in table 4.4.

1x BSS buffer	EC_{50} (µM 4CmC) ±SEM
+ 2 mM Ca^{2+}	63±14
+ 2 mM Ca^{2+} + 2mM EGTA (20 µM free Ca^{2+})	232±20
+ 0.1 mM EGTA	207±5

Table 4.4 EC_{50} values of transient transfected H4833Y mutant RYR1 in different buffers upon 4CmC stimulation.

Since the Ca^{2+} release in buffers 2 and 3 gave similar results, buffer 2 (20 µM free Ca^{2+}) was used for all further measurements. This is also the same condition as used for Ca^{2+} release assays of B-lymphoblastoid cells and myotubes (chapter 3).

4.2.2.5 Ca^{2+} release assays

HEK293 cells were transiently transfected with pc*RYR1* or pc*RYR1*-R2452W and incubated for 72h to obtain optimal RYR1 expression. Ca^{2+} release assays were performed in BSS buffer containing 20 µM free Ca^{2+}. Assays were carried out using different concentrations of 4CmC with concentrations ranging from 100 to 1000 µM. Since expression levels were quite variable between different transfection experiments for both WT and R2452W mutant plasmids, Ca^{2+} release was calculated as a percentage of the maximal Ca^{2+} released by the addition of 1 mM 4CmC, while the average raw data set for WT and mutant RYR1 are shown in appendix III. EC_{50} values were calculated from measurements of six biological replicates for WT and R2452W mutant RYR1. Two biological replicates were performed for H4833Y mutant RYR1 as a control. Graphs were drawn using the Origin 8.6 software and sigmoid curves were fitted (figure 4.9). Non-transfected HEK293 control cells were also assayed and showed no stimulation by 4CmC. This suggests that even though they express low amounts of *RYR1* mRNA endogenously (table 4.3), it is not functional in this experimental system.

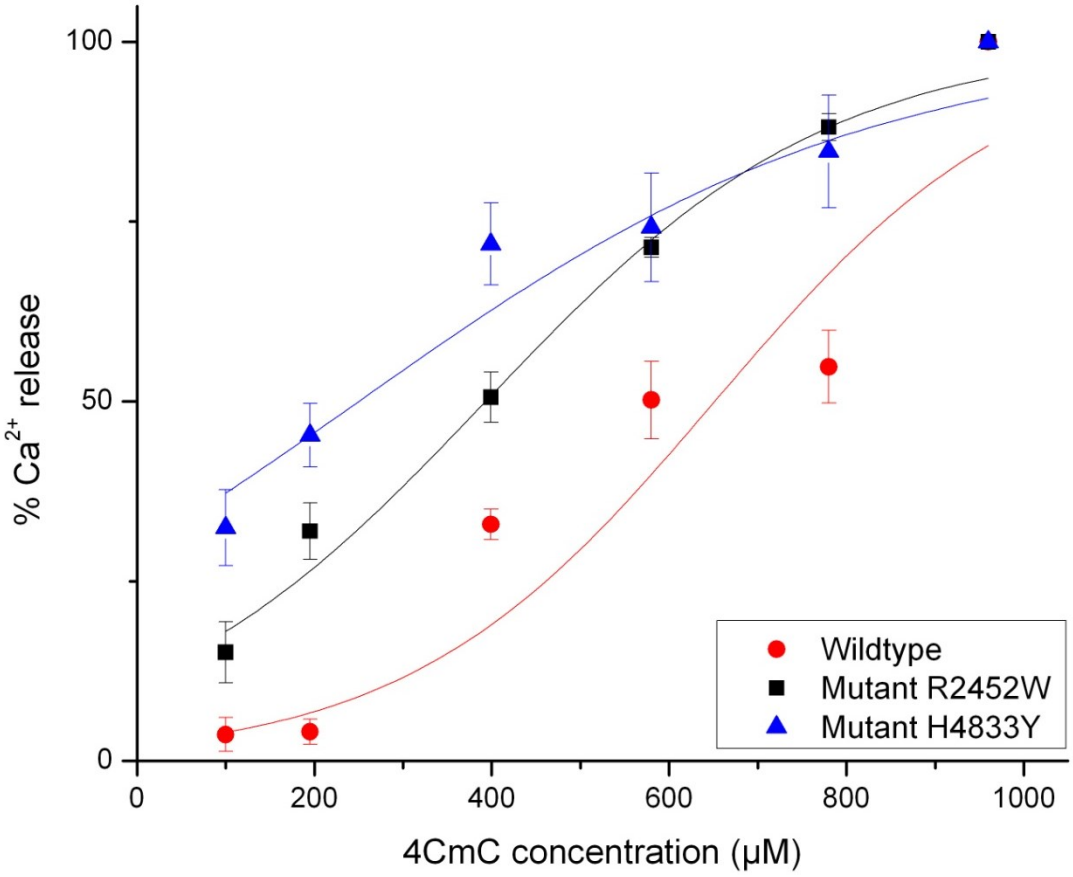

Figure 4.9 Concentration-response curve for *RYR1* transient transfected HEK293 cells upon 4CmC stimulation.

Results are shown as the average of all measurements ± SEM (n=6 for WT and R245W mutant RYR1, n=2 for H4833Y mutant RYR1) and sigmoid curves were fitted.

Ca^{2+} release in pc*RYR1* transfected HEK293 cells was significantly less in comparison to pc*RYR1*-R2452W transfected HEK293 cells at the same 4CmC concentrations. Ca^{2+} release for pc*RYR1*-R2452W transfected cells increased in a concentration-dependent manner, while in WT RYR1 expressing cells, Ca^{2+} released was barely detectable for 4CmC concentrations at 200 µM and below. Raw data for Ca^{2+} release of WT and R2452W mutant RYR1 at the individual 4CmC concentrations can be found in appendix IV. EC_{50} values were determined to be significantly higher for WT compared to R2452W mutant expressing cells (see table 4.5) using One-Way ANOVA with Bonferroni post hoc analysis (p=0.0005). Ca^{2+} release for pc*RYR1*-R2452W and pc*RYR1*-H4833Y transfected cells yielded no significant difference using One-Way-ANOVA with Bonferroni post hoc analysis (p=0.066). This may be due to the limited sample size of Ca^{2+} release measured for pc*RYR1*-H4833Y transfected cells.

RYR1 mutation	EC_{50} (μM 4CmC) ±SEM
R2452W	391±16 *
WT	650±42
H4833Y	223±15 *

Table 4.5 EC_{50} values for 4CmC stimulation of *RYR1* transient transfected HEK293 cells. EC_{50} values for cells expressing either WT RYR1 or a RYR1 mutation are shown including the standard error of the mean for n=6 and for H4833Y n=2. An asterisk indicates a significant difference, with a confidence interval of 95 %, compared to WT.

4.2.3 Stable transfected HEK293 cells

Stable transfection of HEK293 cells was used as an alternative system to transient transfections where only a small proportion of cells actually express recombinant protein. The potential advantage of stable expression is consistent expression of RYR1 and the availability of stable cell lines. Conversely, copy number and position effects of integration into the host genome can alter expression. This potential confounding effect was controlled by normalising all data to the highest amount of Ca^{2+} release measured after the addition of 1 mM 4CmC.

Stable HEK293 cell lines were obtained by transfection with pc*RYR1* or pc*RYR1*-R2452W, followed by selection with 800 ng/μL G418 as the pcDNA3.1(+) vector confers geneticin resistance. After 5-6 days single colonies could be observed on plates and single colonies were trypsinised and transferred into individual plates for further proliferation to ensure clonal selection. Colonies were checked for RYR1 expression in the ER before being used for Ca^{2+} release assays.

4.2.3.1 Confirmation of ER-localisated RYR1 expression

Immunostaining and co-localisation studies using a confocal microscope were carried out. Fixed stably transfected cells were stained with α-RYR1 antibody (34C) and α-PDI was used as an ER marker. A FITC-conjugated secondary antibody was used to detect ryanodine receptor 1 (green, figure 4.10) while a TRITC-conjugated secondary antibody was used to indicate the

ER (red, figure 4.10). DAPI was used as a control to stain nuclei. Merged images show both RYR1 and PDI are located in the same cellular compartment i.e. the ER. RYR1 can be detected in every cell since stable transfected HEK293 cells were used (figure 4.10). Untransfected HEK293 cells were used as a negative control for RYR1 but show PDI staining as expected. Low background staining for RYR1 could be seen in untransfected HEK293 which may suggest either RYR1 expression in low levels or nonspecific background fluorescence.

The fluorescence intensity of HEK293 cells transfected with pc*RYR1*-R2452W was higher compared to untransfected HEK293 cells indicating appropriate expression of R2452W RYR1 in the ER. Expression of pc*RYR1*-R2452W appeared to be lower than in HEK293 cells transfected with pc*RYR1*. Histogram plots were made to show co-localisation of the RYR1 with PDI in untransfected, WT and R2452W mutant RYR1 and are shown in appendix II. This representation also shows increased RYR1 staining in the ER compared to the nuclei in mutant stable cell lines while no staining was detected in untransfected HEK293 cells.

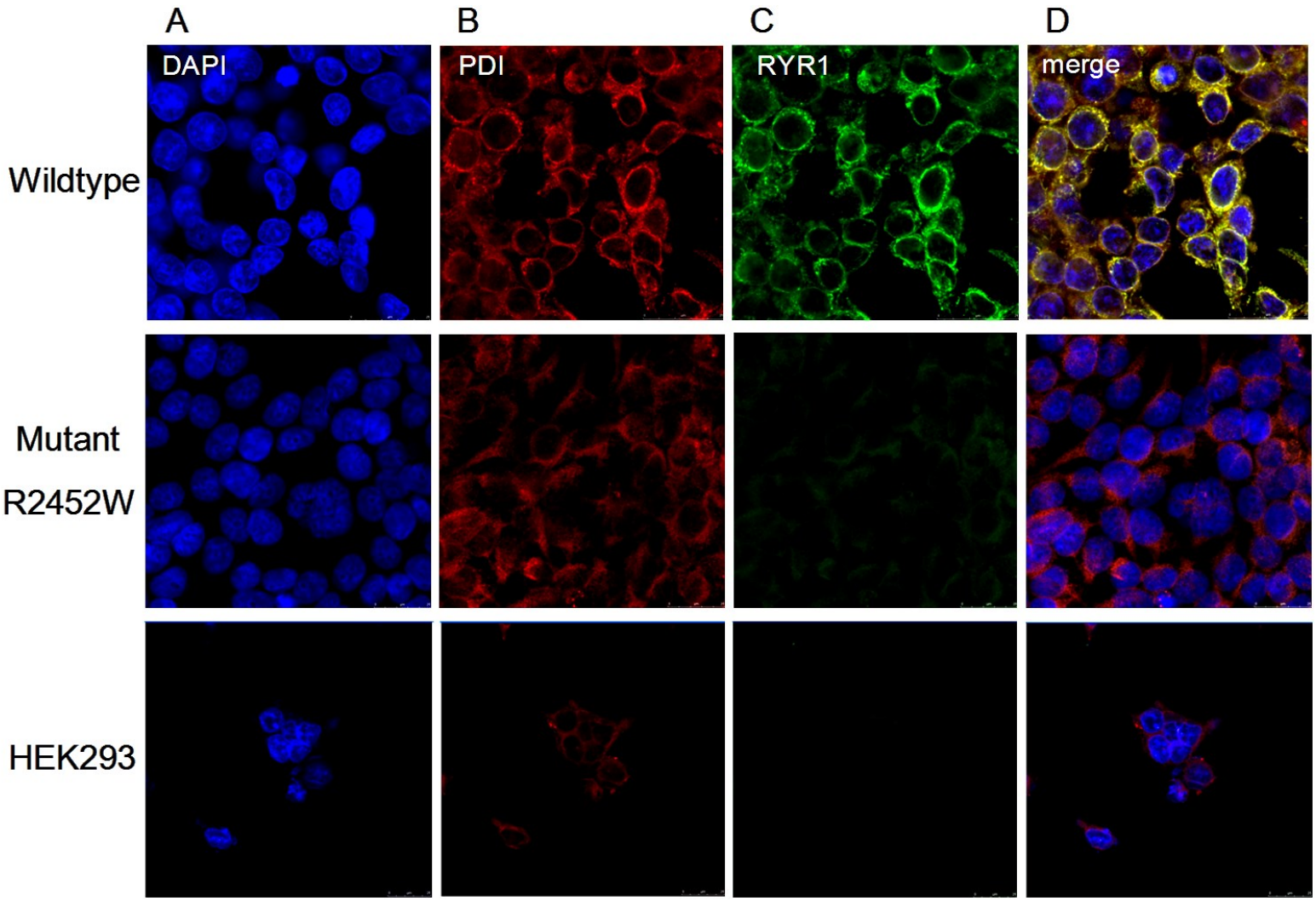

Figure 4.10 Immunostaining of stably transfected and untransfected HEK293 cells.

Merged images (D) show PDI (red, B) and RYR1 (green, C) co-localise into the same cell compartment, the ER. RYR1 stained untransfected HEK293 cells show only very low levels of RYR1 expression and were used as a negative control. Images were taken at 100 x magnification.

4.2.3.2 Immunoblotting to confirm RYR1 expression in HEK293 cells

Total protein was extracted from stably transfected HEK293 cells, grown in T25 flasks as described in section 2.2.18.2. Expression of WT and R2452W mutant RYR1 was detected using immunoblotting with the polyclonal 34C antibody while α-tubulin was used as a loading control. In accordance with the results from immunofluorescence, figure 4.11 shows that WT RYR1 is expressed at much higher levels compared to R2452W RYR1 where R2452W mutant RYR1 cannot be detected using western blotting. No signal was observed for untransfected HEK293 cells, as shown previously (figure 4.4). WT RYR1 appears as a double band, one at 250 kDa and one >250 kDa. The band with lower mobility is likely to represent full-length RYR1 while the higher mobility band may represent a truncated form of RYR1 or protein degradation. Protein extracted from HEK293 cells transiently transfected with pcDNA3.1(+) was used as a negative control, showing no expression of RYR1. Faint bands at high mobility can be detected on the blot which are probably due to unspecific binding of the 34C antibody and may represent background noise or degraded protein. Since expression of RYR1 was weaker compared to tubulin the immunoblots were developed independently to prevent over-exposure of tubulin bands visible at 55 kDa. The tubulin control shows that equal protein amounts (70 µg) were loaded into each well.

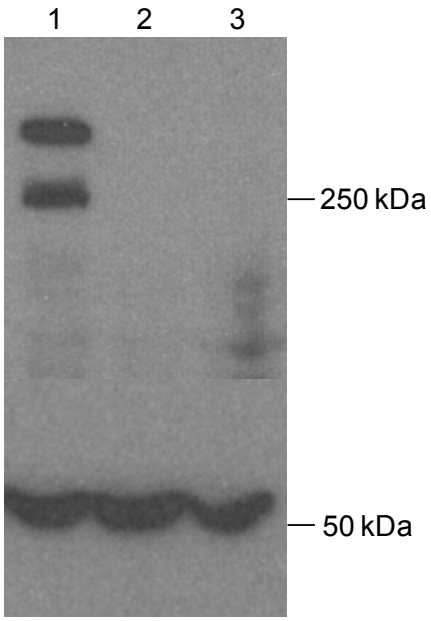

Figure 4.11 Western blotting showing RYR1 protein in stable transfected HEK293 cells.
Lane 1: protein extract of WT RYR1 expressing stable transfected HEK293 cells, lane 2: protein extract of R2452W mutant RYR1 expressing stable transfected HEK293 cells, lane 3: negative control containing protein extract of HEK293 cells transiently transfected with pcDNA3.1(+) vector only. The 7.5 % SDS-PAGE gel was electrophoresed for 1.5 h at 120 V and transferred overnight at 70 mA onto a nitrocellulose membrane.

It is possible that R2452W is less stable than WT RYR1 in stably transfected HEK293 cells and therefore expression is difficult to detect. Alternatively, integration of the mutant construct may have occurred in a region of the genome where transcription is less likely to occur or copy number differences resulted in different levels of expression.

4.2.3.3 mRNA analysis of stable transfected HEK293 cells

Expression levels of R2452W mutant stable transfected cells could not be detected using western blotting. Therefore, RNA was extracted from HEK293 cells stably transfected with either pc*RYR1*-R2452W or pc*RYR1,* as well as from untransfected HEK293 cells in an attempt to detect expression of endogenous *RYR1* mRNA by RT-qPCR. cDNA was prepared in analytical duplicates and each sample was measured in triplicate in order to obtain more accurate results.

Expression levels were calculated using the REST2009 software comparing a stably transfected cell line to an untransfected cell line as explained in 4.2.2.3. Results for the RT-qPCR are shown in figure 4.12.

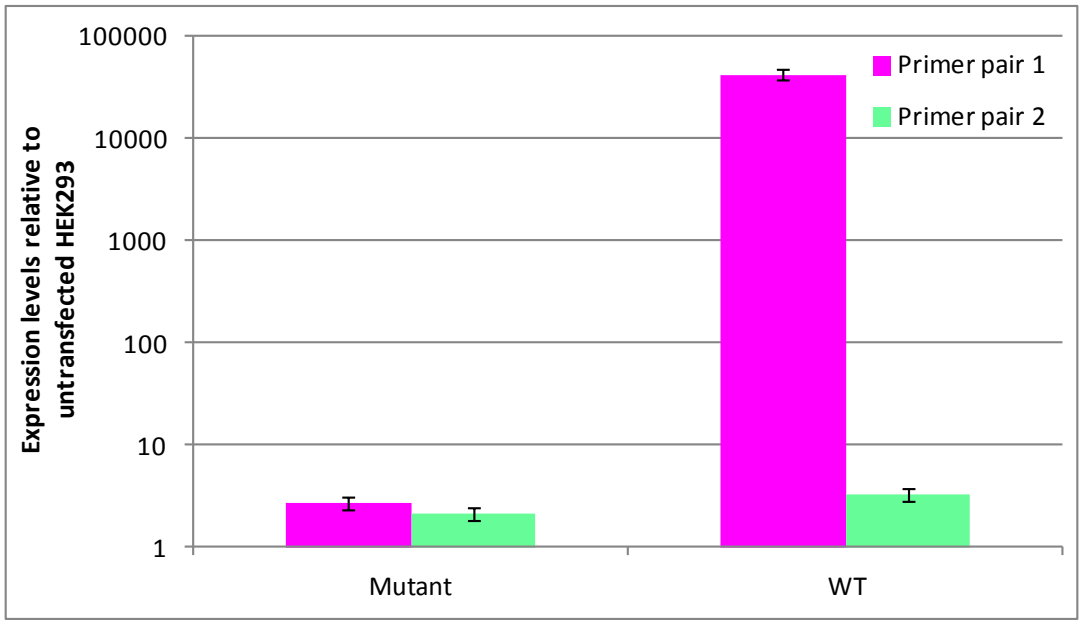

Figure 4.12 mRNA expression levels of *RYR1* in stable transfected HEK293 cells. Expression levels relative to untransfected HEK293 cells were calculated for each individual LightCycler assay and the average of all assays (n=6, each in triplicate) was calculated. Error bars represent the SEM of all samples.

The REST 2009 software calculated a significant increase ($p<0.05$) in R2452W mutant *RYR1* expression as well as in WT *RYR1* expression compared to untransfected HEK293 cells. Expression levels of *RYR1* detected by using primer pair 1 in the WT *RYR1* cell line was much higher compared to expression levels detected using primer pair 2 amplifying the same cDNA. These results suggest multiple insertion of the WT cDNA into the genome including a higher abundance of central region cDNA with truncated cDNA that does not express the 3' end region. PCR efficiencies, as discussed earlier, are different for both primer pairs used, resulting in a different relative expression detected from each primer set. This was sufficiently different to account for the different levels of expression observed for WT *RYR1*.

4.2.3.4 Confirmation of the R2452W expressing cDNA in stably transfected cell lines by sequencing

Because expression levels for R2452W *RYR1* are very low, it was necessary to confirm that HEK293 cells stably transfected with pc*RYR1*-R2452W carry this mutation as well as being absent in HEK293 cells stably expressing WT *RYR1*. Genomic DNA of untransfected HEK293 cell DNA as well as cDNA of cells transfected with pc*RYR1*-R2452W and pc*RYR1* was extracted. PCR-primers were designed to amplify the region corresponding to R2452W in gDNA as well as the mutated region in cDNA, resulting in two different sized bands (figure 4.13).

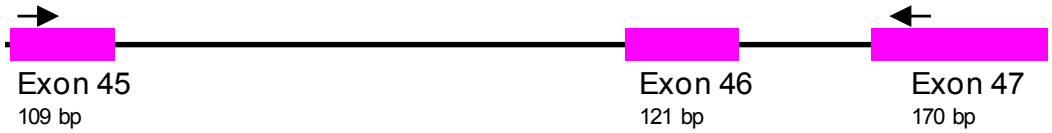

Figure 4.13 Binding sites of LC primer pair 1 in *RYR1* gDNA.
Exons 45-47 are represented by pink rectangles and connected by intron 45 and 46 (black lines). Primer pair 1 binding sites are indicated with arrows in exon 45 and 47. The schematic diagram is not drawn to scale.

Primer pair 1 has been used previously to amplify cDNA (chapter 4.2.2.3). This primer pair binds within exons 45 and 47 (figure 4.13) and could therefore amplify gDNA as well as cDNA yielding a PCR product of 1024 bp for gDNA and 265 bp for cDNA.

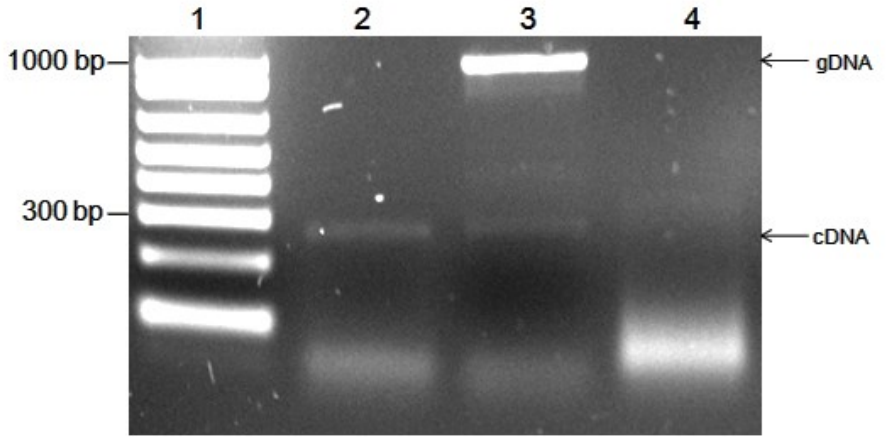

Figure 4.14 PCR products for gDNA and cDNA of stable transfected R2452W *RYR1*.
Lane 1: 1 kb+ DNA ladder, Lane 2: cDNA of pc*RYR1*-R2452W stably transfected cells, Lane 3: gDNA of pc*RYR1*-R2452W stably transfected cells, Lane 4: negative control water. Products were loaded onto a 2 % agarose gel, electrophoresed for 1h at 80 V in 1x TAE buffer and DNA bands were stained with 0.5 µg/mL ethidium bromide.

The PCR using cDNA as template yielded one band (265 bp) while two bands were obtained from HEK293 cells stably expressing pc*RYR1*-R2452W (figure 4.14). Since amplification of gDNA extracted from pc*RYR1*-R2452W transfected cells yielded two bands representing cDNA and gDNA amplicons, it can be concluded that cDNA had been integrated into the host genome. Since the bands do not appear in a 1:1 ratio some cells may not have integrated the full-length *RYR1* cDNA. This could be due to the failure of clonal selection or some cells may shed the *RYR1* cDNA during proliferation. PCR products for no DNA template control showed no amplification. Amplified cDNA (figure 4.14, lane 2) was purified using the Wizard kit prior to sequencing. Sequencing of the cDNA of HEK293 cells stably transfected with pc*RYR1*-R2452W, shown in figure 4.15, confirmed the presence of the R2452W mutation in the cDNA incorporated into the host DNA and subsequent expression. Sequencing also revealed that the WT *RYR1* expressing HEK293 cells do not express the R2452W mutation.

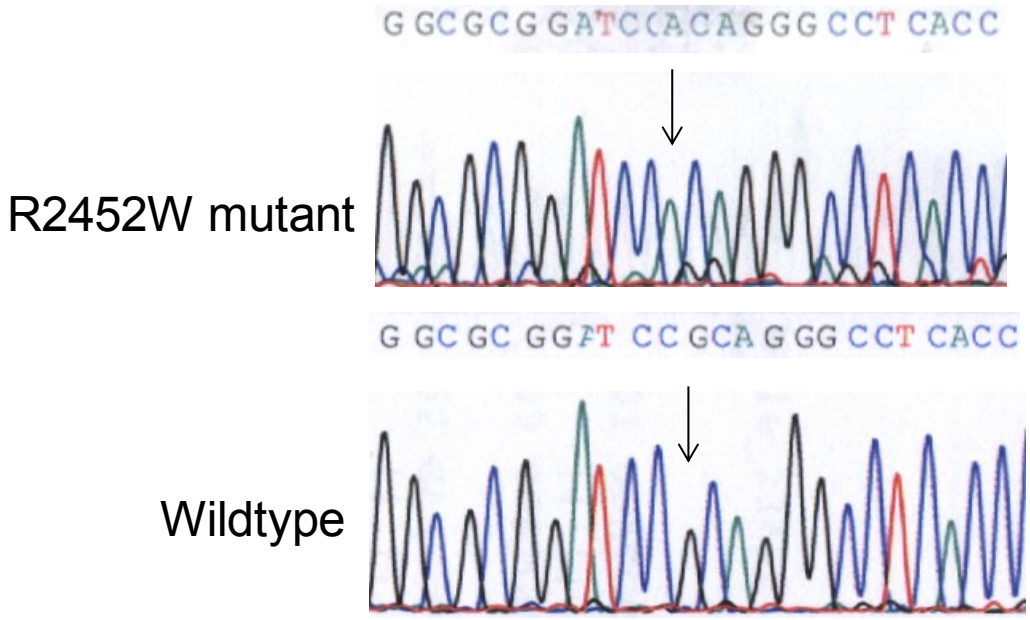

Figure 4.15 Sequencing results for cDNA of HEK293 cells stably transfected expressing R2452W and WT RYR1.

An arrow indicates the location of the R2452 amino acid (c.C7354T) in both WT and R2452W mutant expressing *RYR1* cell lines. This indicates the presence of R2452W in the mutant cell line and the absence in the wildtype transfected cell. The sequence shown represents the reverse strand and therefore indicates a change from G to A.

4.2.3.5 Ca^{2+} release assays

Stably transfected HEK293 cells were grown in media supplemented with 400 ng/µL G418 when Ca^{2+} release assays were about to be carried out. G418 is a blocker of Ca^{2+} release through of the IP3 receptor (IP3R), which is the main Ca^{2+} channel used in HEK293 cells. Phosphatidylinositol 4,5 bisphosphate (PIP2) within the cytosol of cells is cleaved by members of the phospholipase C (PLC) family into diacylglycerol (DAG) and inositol-1,4,5-trisphosphate (IP3) while IP3 functions as the activator of the IP3 receptor. Because phospholipase C is inhibited by G418 (figure 4.16) IP3 levels are low and therefore unable to activate the IP3R to release Ca^{2+} from the ER [70, 192]. Hence when cells are activated with 4CmC, Ca^{2+} can only be released through the ryanodine receptor 1. Therefore the use of stably transfected HEK293 cells, grown in selection medium, had the advantage of a higher specificity for measuring Ca^{2+} released by the ryanodine receptor 1 and should therefore provide more specific and reproducible results.

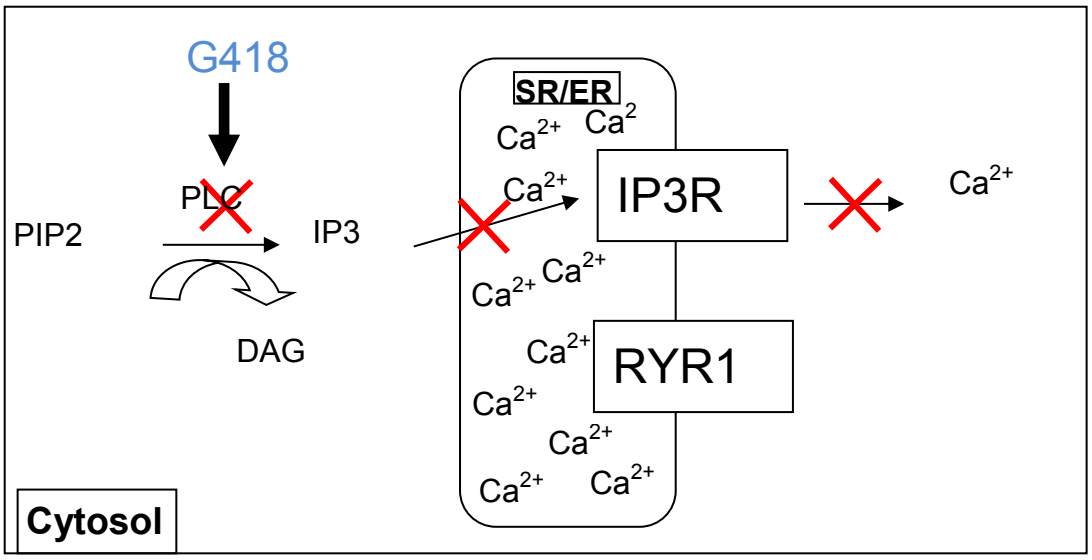

Figure 4.16 IP3R Ca^{2+} release pathway inhibited by G418.

G418= geneticin, PLC= Phospholipase C, IP3= Inositol 3 phosphate, IP3R= IP3 receptor.

HEK293 cells were loaded with the Ca^{2+} indicator fura 2-AM in order to detect Ca^{2+} release triggered by the addition of various concentrations of 4CmC. Free Ca^{2+} concentrations in the buffers used, were controlled at 20 µM as described previously. Untransfected HEK293 cells were used as a negative control for Ca^{2+} release. Biological replicates were performed five times to obtain statistically reliable results. Data are shown as mean ± SEM

(n=5) in figure 4.17. Ca^{2+} release was calculated as a percentage of the maximal Ca^{2+} released with the addition of 1 mM 4CmC. This approach allowed normalisation of data necessary for comparison since expression levels for WT and R2452W mutant RYR1 were quite different. The 4CmC concentrations used ranged between 100 µM and 1000 µM and EC_{50} values were calculated applying a sigmoid fitted curve using the Origin 8.6 software. Raw data for the maximal Ca^{2+} released by the addition of 1 mM 4CmC are given in appendix III.

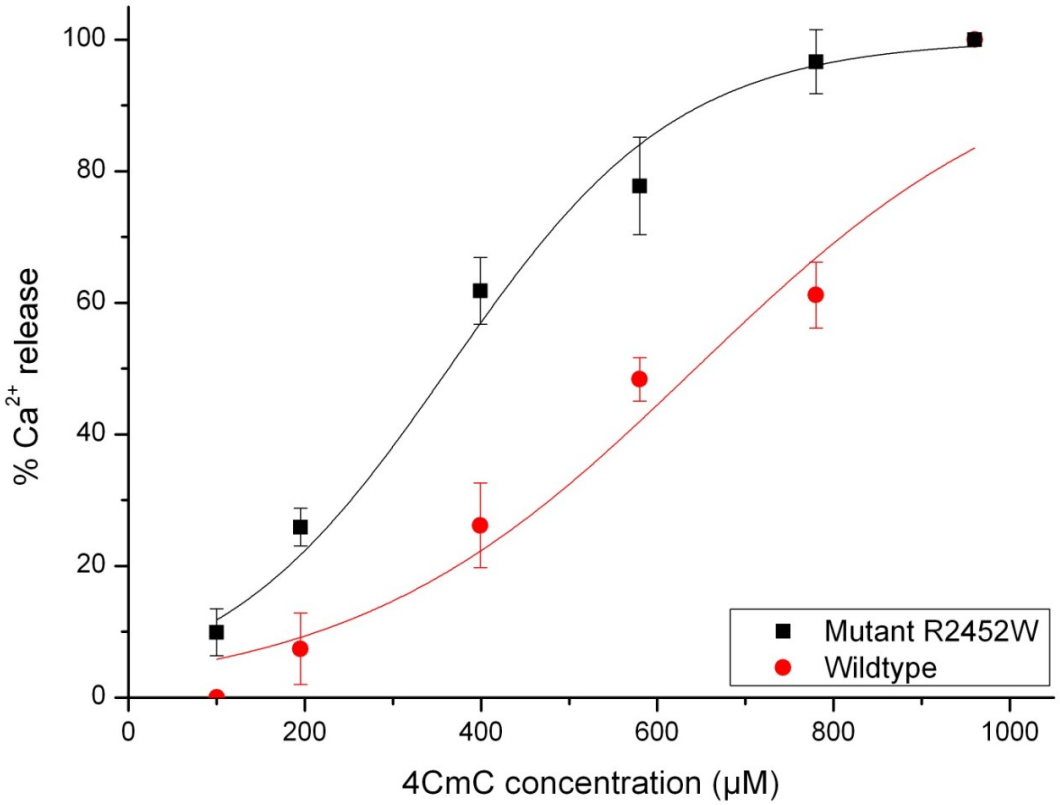

Figure 4.17 Concentration-response curve for stably transfected HEK293 cells upon 4CmC stimulation.
Data are represented using a sigmoid curve fitting showing the average Ca^{2+} release ± SEM (n=5).

Figure 4.17 shows the fitted sigmoid curves of the generated data set. Results indicate that cells expressing the R2452W mutant RYR1 show a hypersensitive response to the agonist 4CmC in comparison to WT RYR1. EC_{50} values were compared using One-Way ANOVA with Bonferroni post hoc analysis. Accordingly, cells expressing pc*RYR1*-R2452W have a significantly lower EC_{50} value compared to pc*RYR1* expressing cells (p= 0.00009, table 4.6).

RYR1 mutation	EC_{50} (μM 4CmC) ±SEM
WT	665±29
R2452W	363±25 *

Table 4.6 EC_{50} values for 4CmC activation of WT and R2452W mutant RYR1 stable transfected HEK293 cells.
Asterisk indicates a significant difference compared to WT RYR1.

This suggests the R2452W mutation could trigger abnormal Ca^{2+} release *in vivo* and thus is likely to be causative of MH.

4.3 Discussion

4.3.1 Cloning

RYR1 cDNA carrying the R2452W mutation was cloned and confirmed by sequence analysis. Furthermore sequencing excluded other non-synonymous mutations or cloning artefacts in the plasmid. While sequencing the plasmid, synonymous variants were identified and these are listed in table 4.1. Many of these variants could be found in the SNP database and are therefore likely to be carried by the individual person the cDNA was extracted from. Other synonymous changes might have been introduced by PCR error. Since these potential PCR errors introduced only synonymous variants, they were not corrected.

4.3.2 RYR1 Expression

Transfection was optimised to achieve adequate expression of RYR1 in HEK293 cells. Different ratios of transfection reagent to DNA were used and expression was detected using western blotting. All different ratios yielded RYR1expression so a ratio of 8:2 [Fugene HD: plasmid (μg)] was used for further experiments. Immunofluorescence was used to confirm RYR1 expression in the ER in both stable and transient transfected HEK293 cells. RYR1 protein is expected to be in the ER since the ryanodine receptor 1 is normally located in the SR membrane of skeletal muscle cells and can only release Ca^{2+} once it is located in the SR/ER membrane. This result was

crucial to be able to use the *RYR1* plasmids in further experiments and to be able to detect Ca^{2+} release in functional studies.

Western blotting was used to confirm expression of RYR1 in stably and transiently transfected cells. Transiently transfected cells expressed RYR1 in high levels but the mutant protein appeared to be expressed more efficiently than WT. Protein, as well as RNA, was extracted twice on separate occasions and analysed. Transiently expressed mutant *RYR1* is expressed at least 50 times higher than WT according to RT-qPCR results. Both primer pairs detected different expression levels of *RYR1*. Different efficiencies might occur during cDNA synthesis, where some regions might be transcribed into cDNA because they contain a polydT sequence. If the R2452W mutation is located near these regions the RNA might preferentially be transcribed into shorter cDNA. Since *RYR1* cDNA consists of ~16,000 base pairs, a mixture of random and oligodT primers have been used to prevent position effects in cDNA synthesis. Different expression levels could also be artefacts resulting from different qPCR primer efficiencies (table 4.2), however these differences are not marked. Also since the binding sites for primer pair 2 are located at the far end within the 3' end cDNA region it is possible that the mRNA has degraded. Since degradation of mRNA/cDNA occurs more likely from either the 5'- or the 3' end rather than in the central region of the transcript, it is possible that lower levels of full-length cDNA were detected. PCR efficiencies as well as the amplicon size of both primer pairs (270 bp for primer pair 1 vs. 80 bp for primer pair 2) used were different and these factors may be involved in the production of apparently different expression levels in *RYR1*.

Western blotting showed an estimated 10 times higher amount of protein for the R2452W mutant compared to WT RYR1 in transient transfections, supporting the results obtained with RT-qPCR. Both proteins were overexpressed *in vivo* and co-localisation studies confirmed expression in the ER. Different expression levels of WT and R2452W RYR1 might be due to different transfection efficiencies of the two plasmids used since the same amount of plasmid DNA was used in HEK293 cells transfection experiments.

It is possible that the cells preferably express R2452W RYR1 over WT since it is assumed that this mutation leads to a gain-of-function and may support cell growth and viability. Nevertheless this seems to be rather unlikely since it was shown that in muscle *in vivo*, mutant RYR1 expression levels tend to be lower compared to WT, however this has only been shown in western blots [155].

Expression levels of stably transfected HEK293 cells were detected using western blotting but only RYR1 expression of pc*RYR1* transfected cells was visualised, showing two bands at 250 and >250 kDa, representing full-length RYR1 (~500 kDa) and truncated RYR1 (250 kDa) but the bands had roughly the same intensity. The origin of the second band at 250 kDa is unknown and it was suspected that either a truncated *RYR1* cDNA fragment as well as *RYR1* full-length cDNA may have been inserted into the host gDNA or that the WT protein is not stable in HEK293 cells and becomes degraded, showing a second, smaller band. RYR1 in R2452W mutant stable cell lines was not detectable using western blotting. Nevertheless, RYR1 expression in stably transfected HEK293 with pc*RYR1*-R2452W cells could be detected at low intensity in immunofluorescence studies. To prevent false positive results, laser intensity settings for non-transfected HEK293 cells and R2452W mutant cells were identical. Low fluorescence levels were detected for RYR1 in R2452W mutant cells whereas a very low signal was detected for untransfected cells. It was concluded that protein expression levels in R2452W mutant cells were low. RNA from both stably transfected cell lines was extracted in order to evaluate expression of *RYR1*. RT-qPCR results for stably transfected HEK293 cells revealed that R2452W *RYR1* expression was increased by a magnitude of two compared to untransfected HEK293 cells for both primer pair 1 and 2 (figure 4.12), confirming expression of the R2452W mutation. Reasons for this low expression could be that the R2452W mutation leads to a hypersensitive receptor and therefore expression levels in cells were kept low in order to prevent too much Ca^{2+} being released from the ER. This hypothesis is supported by the finding of Zhou et al. who found allele silencing of RYR1 in CCD patients, and therefore lower RYR1 expression. It was hypothesised that only a small amount of

functional RYR1 is required to maintain a normal phenotype in cells from CCD patients [155]. The R2452W mutation however has not been linked to CCD and these results were not obtained in transiently transfected cells. Therefore, it was concluded that position effects are more likely to cause lower expression of pc*RYR1*-R2452W in HEK293 cells. Another reason for low expression levels of mutant RYR1 might be the position of insertion of the cDNA into the host gDNA. If this region is not very transcriptionally active e.g. because of the presence of insulator elements or located far from a promoter, the inserted cDNA may have a very low expression profile leading to low RNA levels.

Results obtained for stable transfected WT *RYR1* by RT-qPCR were controversial since the expression detected using primer pair 1 (central domain, see figure 4.6) showed high expression levels, up to 10,000 times higher than those detected by primer pair 2 (3' end). The position where primer pair 1 binds in the cDNA and the antibody binding site in the corresponding protein sequence (figure 4.6) are very close and are therefore likely to give the same order of expression when analysing either cDNA or protein. Primer pair 2 binds at the 3' end of the *RYR1* cDNA and a lower expression of *RYR1* cDNA was obtained, perhaps due to RNA degradation or poor efficiency of cDNA synthesis. As mentioned for cells transiently transfected with *RYR1* cDNA, PCR efficiencies and instability of cDNA might be a reason for the discrepancy between expression levels but it cannot explain the 10000 fold expression differences detected using primer pair 1 and 2. These large differences suggest insertion of a truncated *RYR1* cDNA into a highly expressed region of the host genome and therefore higher expression levels observed using primer pair 1. Expression levels appeared low when measuring the 3' end of the mRNA compared to expression levels of the central domain, leading to the assumption that only low levels of full-length functional RYR1 are expressed. This in turn suggests that only low levels of protein will be located within the ER membrane since the C-terminus part of RYR1 is important in anchoring the protein into this membrane.

Comparing expression level results of RT-qPCR and western blotting for cells stably expressing pc*RYR1,* supports the hypothesis of a truncated RYR1 form, as well as a full-length RYR1 being expressed. Immunofluorescence is not able to distinguish between protein located in the ER membrane or ER compartment and therefore cannot be used to investigate the presence of the truncated RYR1 form within the ER. In order to detect whether this form is located in the ER or the ER membrane another antibody to label the ER membrane e.g. Calnexin, would need to be used for co-localisation studies. If the C-terminus is still present in the putative truncated form it is likely to be expressed within the ER membrane. Alternatively, RYR1-antibodies that recognize different epitopes could be used in solving this issue. Finally, expression of R2452W mutant *RYR1* in stably transfected pc*RYR1*-R2452W cells was confirmed by cDNA sequencing, also revealing the absence of R2452W in stable WT *RYR1* cells.

The 34C antibody binds between aa position 2756 and 2803 [55] whereas the primers bind cDNA in the corresponding protein sequence at either upstream (aa 2405-2493) or downstream (aa 4826-4850) of the antibody binding site (figure 4.6). Therefore the antibody binding site is located closer to the position corresponding to that amplified by primer pair 1, showing similar results (high expression levels of WT RYR1 plasmid in western blots as well as in RT-qPCR). Primer pair 2 binds close to the mRNA 3' end, representing the C-terminus of the RYR1 protein. mRNA as well as cDNA could be subject to degradation, possibly resulting in the low expression levels detected with primer pair 2. Furthermore, cDNA from the R2452W *RYR1* stably transfected cell line was sequenced, thus confirming that the expressed *RYR1* cDNA contained the c.C7354T/p.R2452W.

4.3.3 Ca^{2+} release assays

Cells transiently transfected with pc*RYR1*-R2452W release more Ca^{2+} compared to pc*RYR1* transfected cells when stimulated with the agonist 4CmC. Because expression levels appeared to be different between WT and R2452W RYR1, results of Ca^{2+} release assays were normalised to 1 mM 4CmC. Normalisation gives a more accurate indication of whether the

R2452W mutant RYR1 protein leads to a hypersensitive channel. EC_{50} values for R2452W mutant cells were almost half those of WT transfected cells (table 4.4). These differences were statistically significant ($p<0.0005$).

The pc*RYR1*-H4833Y plasmid was used as a positive control for transiently transfected cells since this mutation is described in the literature to express a hypersensitive RYR1 protein associated with MH [166]. Comparing EC_{50} values for R2452W and H4833Y mutations to RYR1 WT expressing cells revealed that the R2452W mutation alters Ca^{2+} release and leads to a hypersensitive channel when stimulated with 4CmC, but showed higher EC_{50} values compared to that obtained for H4833Y ($p=0.066$). One reason for this phenomenon could be the location of each of the R2452W and H4833Y mutations. The R2452W mutation is located in the central domain of RYR1, which is predicted to be part of the "domain-zipper complex" [85]. A mutation in this region could weaken the interaction between the N-terminal and the central domain, leading to an unstable closed RYR1 pore complex and therefore to a hypersensitive, as well as hyperactive, ryanodine receptor. H4833Y however, is located in the C-terminal domain. RYR1 C-terminal mutations have been suggested to have a higher channel open probability since this region is believed to be involved in forming the homo-tetramer protein and a higher sensitivity against agonists like 4CmC has been predicted [193]. Because of the different structure and function of central and C-terminal domains, mutations in these different regions are likely to influence the RYR1 function differently. Since the 3D structure has not been solved yet, no judgement can be made on position effects of these two mutations. Nevertheless, Ca^{2+} release assays showed that the R2452W mutation results in a hypersensitive receptor leading to a significantly higher Ca^{2+} release from the ER compared to WT RYR1.

Many studies have been carried out using rabbit *RYR1* cDNA in transient transfection experiments to show hypersensitive RYR1 mutations. EC_{50} values in these studies for WT and mutant constructs tended to be lower compared to the values found in this study [135]. These other studies have been performed using imaging buffer containing 2 mM Ca^{2+} while the present

study was done using buffers containing 20 µM Ca^{2+}. As shown in figure 4.8, high external Ca^{2+} concentrations increase Ca^{2+} release, resulting in lower EC_{50} values. This also shows that small amounts of external free Ca^{2+} (20 µM) do not significantly influence Ca^{2+} release from RYR1 or EC_{50} values. These results are in agreement with Ca^{2+} release assays using the same buffer systems in B-lymphoblastoid cells (see chapter 3.3.4). Both systems result in lower EC_{50} values obtained when 2 mM Ca^{2+} was present in the imaging buffer. This suggests that high amounts of extracellular Ca^{2+} may increase Ca^{2+} induced Ca^{2+} release resulting in lower EC_{50} values.

Ca^{2+} release assays for stably transfected cells also confirmed a hypersensitive ryanodine receptor 1 when carrying the R2452W mutation. EC_{50} values for the R2452W mutant cell line were halved, compared to WT RYR1 cell lines (table 4.6) and are therefore more sensitive to agonists. While pc*RYR1* transfected cells did not respond significantly to 4CmC concentrations <400 µM, the R2452W mutant RYR1 gave a high response at 200 µM 4CmC (figure 4.17).

Interestingly, EC_{50} values obtained in Ca^{2+} release assays for stably and transiently transfected HEK293 cells (figure 4.9 and 4.17) are very similar for either WT (665±29 µM for stable transfection vs 650±42 µM for transient transfection) or R2452W mutant cells (363±25 µM for stable transfection vs 391±16 µM for transient transfection). These observations confirmed that both systems give essentially the same results, within experimental error and either system can be used to demonstrate that the R2452W mutation results in a hypersensitive channel to 4CmC activation and is therefore likely to cause MH. Even though expression levels in stably transfected HEK293 cells were lower, compared to transiently transfected cells, these cells gave reproducible results with similar EC_{50} values. This suggests that stably transfected cell lines are useful in Ca^{2+} release assays, as they avoid new transfections for every experiment, once the cell line has been established.

Comparing results obtained for either transiently or stably transfected HEK293 cells to Ca^{2+} release data obtained from patient-derived cells

(chapter 3), showed that EC_{50} values of myotubes were very similar to values for transfected cells (table 4.7). Since both methods used the same imaging buffer and microscope, it can be assumed that either of the two methods can be equally effective in detecting altered Ca^{2+} release resulting from mutations in RYR1. Since HEK293 cells do not express any muscle proteins apart from overexpressed RYR1, it can be concluded that pc*RYR1*-R2452W transfected HEK293 cells showed altered Ca^{2+} release compared to WT because they express a hypersensitive receptor when stimulated with 4CmC. The transfected HEK293 cells share the same genetic background, differing only by the overexpressed *RYR1* plasmid. To be able to use transfected HEK293 cells for Ca^{2+} release assays however, a RYR1 mutation needs to be identified which then has to be cloned and overexpressed. As ~50 % of MHS patients do not carry mutations in RYR1, the use of transfected HEK293 cells is somewhat limited.

patients	Lymphocytes EC_{50} (µM 4CmC) ±SEM	Myotubes EC_{50} (µM 4CmC) ±SEM	HEK293 EC_{50} (µM 4CmC) ±SEM		
A	506±11	309±45	plasmid	stable	transients
BI	544±15	na	Wildtype	665±29	650±42
BII:1	641±8	na	Mutant	363±25	391±16
BII:2	509±23	na			
BII:3	532±23	na			
C1	652±14	612± 54			
C2	642±10	638±11			

Table 4.7 Summary of EC_{50} values for 4CmC activation obtained from concentration-response curves of either B-lymphoblastoid cells, myotubes or transfected HEK293 cells. EC_{50} values are given as the average 4CmC concentration (µM) ±SEM. na= no availability of data.

Results using myotubes suggest intact muscle cells show altered Ca^{2+} release in patients carrying the R2452W mutation, however because more proteins are involved in Ca^{2+} release in this cell type, it cannot be ruled out that other proteins might also influence release. As mentioned earlier, transfected HEK293 cells differ only in the expression of different RYR1 constructs and RYR1 function can be assessed independently. Taken together, the experimental results using myotubes and the recombinant

system suggest that the R2452W mutation causes altered Ca^{2+} release from RYR1 when activated with 4CmC. The results obtained by Ca^{2+} release assays in B-lymphoblastoid cells, also showing a hypersensitive receptor while 4CmC activation, indicate very strongly that the R2452W mutation alters the function of RYR1 *in vivo.*

HEK293 cells do not express any other skeletal muscle proteins and can therefore not be used to analyse mutations which may lead to altered Ca^{2+} release due to altered interactions between RYR1 and other proteins involved in EC coupling. To study these mutations, or mutations only responding to depolarisation, *RYR1* cDNA could be expressed in IB5 cells, isolated from the dyspedic mouse [194]. Since these cells are intact muscle cells lacking only RYR1, the function of a mutation in the ryanodine receptor can be monitored in a more physiological system.

In summary, the use of patient derived cells and HEK293 cells transfected with WT or R2452W mutant RYR1 gives an indication that cells carrying the R2452W mutation show a hypersensitive phenotype in response to 4CmC activation. Differences between EC_{50} values of WT and mutant RYR1 expessing cells are between two and threefold, indicating a significant increase in Ca^{2+} activation. Results obtained in this study and the use of three different systems to detect altered Ca^{2+} release, suggest that the R2452W mutation is likely to be causative of MH.

Chapter 5 Overexpression and purification of the ryanodine receptor 1 central domain

5.1 Introduction

The RYR1 central domain containing the R2452 residue was chosen for overexpression and purification studies in order to understand protein stability and structure. This domain is potentially very important since it is proposed to be involved in domain interactions and in channel opening and closing [85]. In support of this, over 50 mutations have been found in this domain, many of which have been linked to MH (reviewed in [43]). RYR1 is a membrane-bound protein of 5038 amino acids forming a homotetramer of four 560 kDa subunits. Because of these properties overexpression, purification and crystallisation of the whole protein are technically very difficult. Previous studies reported high-resolution crystal structures for the N-terminal domain of RYR1 encompassing amino acids 1-604 [78]. Furthermore, the structure of the RYR1 domain containing the phosphorylation site (aa 2734-2940) has been solved, showing a two-fold symmetry within this domain [195]. Studies carried out in 2001 using parts of the central domain, and investigating the effect of the V2461I RYR1 variant, revealed that this mutation might affect the binding of FKBP12, stabilising the closed state of RYR1 by altering its binding site [196]. A recent study using small peptides corresponding to RYR1 and an IP3R homology domain indicates that the amino acids between 2459 and 2473 in RYR1 are important for FKBP12 binding [197].

To date, there have been no reports for structural determination of the central domain of RYR1. Furthermore, this domain contains the R2452W mutation which is linked to malignant hyperthermia (MH) and was functionally characterised earlier in this study with results suggesting that this mutation is likely to be causative of MH. Therefore, cDNA representing the central domain was cloned with the aim of carrying out X-ray crystallographic structural studies to aid in understanding the molecular basis for altered function of the protein. The R2452W mutation is located within the DP4

domain as part of the central domain, which is thought to be involved in "domain-zipping" of the N-terminus and central domain in RYR1 [85].
Primer pairs were designed to amplify the human *RYR1* central domain cDNA including an IP3R homology domain (1000 bp) which, when overexpressed in *E. coli,* would result in an RYR1 polypeptide representing amino acid sequence 2157-2489. One of the RYR1 and IP3R homology domains (RIH) located in the central domain (amino acid 2157-2365) was included for expression of soluble protein and as an aid in solving the secondary and tertiary structure as the 3D structure of the N-terminal IP3R domain is known [198]. N- and C-terminal tags were included in the cloning strategy to assist in both expression and purification of the RYR1 protein (figure 5.3). The N-terminal tags were followed by a cleavage site for removal of the tags.

5.2 Bioinformatics

Previous reports suggest two homology domains between RYR1 and IP3R (RIH) occurring within different regions of each protein. The first of these domains is in the N-terminal region of each protein and comprises amino acids 439–643 of RYR1, while the second is near the central domain of RYR1, comprising amino acids 2157-2365 which are homologous to IP3R amino acids 499–677 and 1196–1356, respectively. Studies of the IP3R included binding assays of the IP3 ligand as well as structural determination by X-ray crystallography (reviewed in [199]). Mignery et al. [200] expressed full-length IP3R, as well as a deletion mutant in COS cells and were able to obtain soluble protein with a deleted membrane helix. Since the goal of this study was to obtain soluble protein, the RIH domain was included in the clone representing the RYR1 central domain to potentially support solubility.

5.2.1 Mobyle portal

Protein structure prediction programs were used to help investigate the secondary structure of the RIH domain as well as the DP4 domain. The program Mobyle portal [201] predicts helix domains (H) as well as β-strands (E), coils (C) or turn (T) motifs, using the amino acid sequence as a reference.

Figure 5.1 shows the predicted secondary structure for the WT (A) or R2452W mutant (B) RYR1 central domain (amino acids 2101-2500). Results indicate that the R2452W mutation (asterisk) is located within a predicted helix motif and could therefore potentially disrupt this motif.

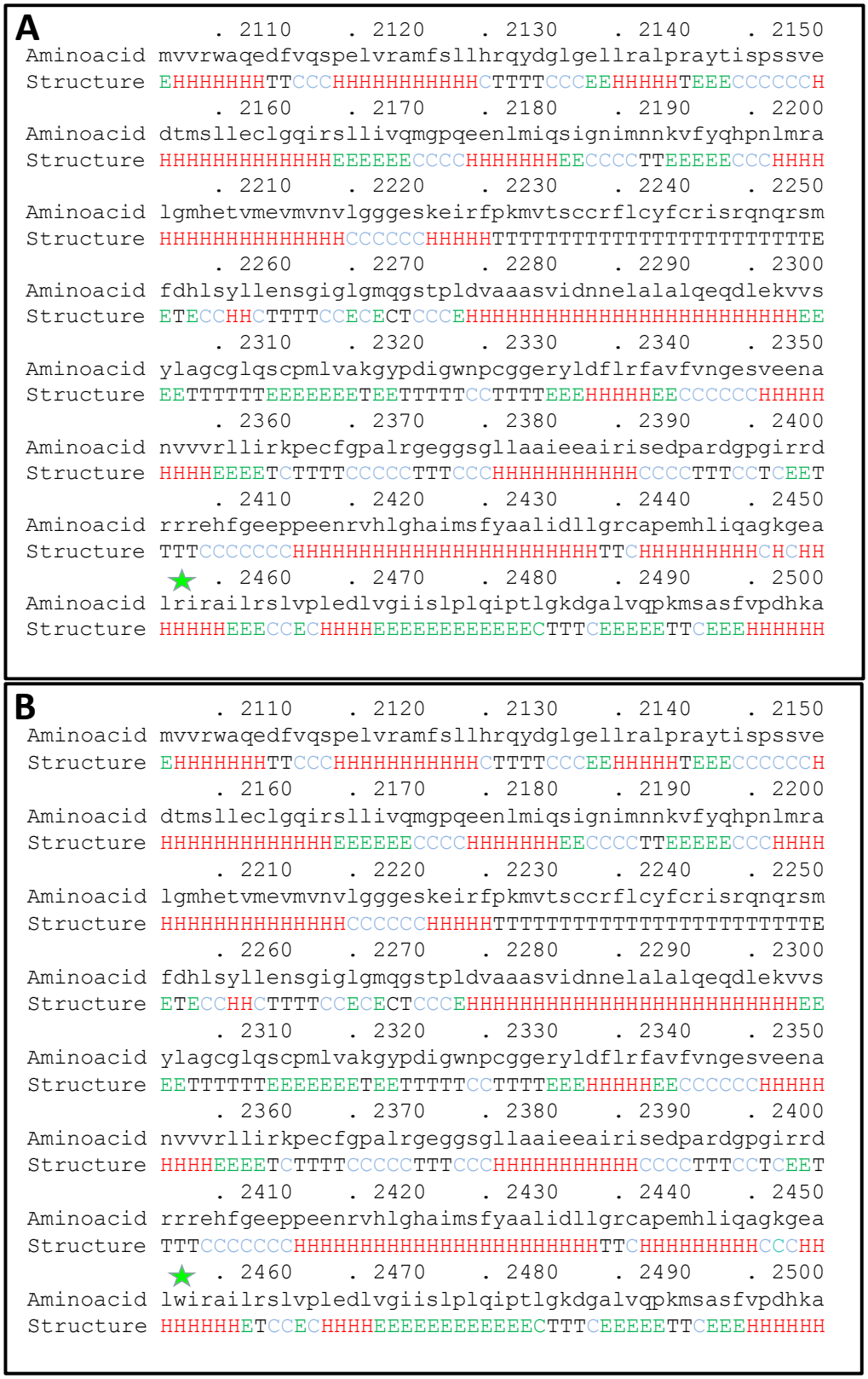

Figure 5.1 Secondary protein structure prediction for WT (A) and R2452W mutant (B) RYR1 central domain using Mobyle portal.
The figure was adapted from the output results of the Mobyle portal software and amino acids 2101 to 2500 of RYR1 are shown. Structures predicted to form helices (H) are red, β-sheets (E) are green, turns (T) are black and coiled structures (C) are blue. The position of the R2452W mutation is marked with an asterisk.

The amino acid sequence 2101 to 2500 for either WT or R2452W variant (ensemble genome browser protein ID ENSP00000352608.2) were entered into this program to obtain predicted percentage for different secondary structure motifs and results are shown in table 5.1. Unfortunately, Mobyle Portal does not give a confidence/reliability interval for the predicted structures.

Motif	WT (%)	R2452W mutant (%)
α-helix	44.7	44.7
β-sheet	17.9	17.7
turns	19.9	20.1
coiled	20.7	20.9

Table 5.1 Predicted secondary structure motifs for WT and R2452W mutant RYR1 domain.
Secondary structure motifs are listed on the left-hand side and their predicted percentage for WT and R2452W mutant are listed in percent of the full-length protein.

cDNA sequences for cloning were designed so that putative secondary structure motifs should not be disrupted when overexpressed in *E. coli*. Furthermore the same sequences were also used in the SWISS-MODEL program [202] to determine secondary structure. SWISS-MODEL predicts helix, extended β-sheets and coiled structures only, but similar results were obtained.

5.2.2 SMART database

The SMART (**S**imple **M**odular **A**rchitecture **R**esearch **T**ool) was used to determine whether any protein motifs were known in the region of interest by comparing known structural domains with the RYR1 (2100-2600) amino acid sequence [203, 204]. The software identified two low compositional-biased regions between amino acids 2285-2296 and 2384-2403 in full-length human

RYR1. These regions were identified using an algorithm to identify low compositional complexity which have been linked to protein disorder, as well as having structural roles in cells [205]. In addition, they are very flexible due to a lack of well-defined folding structure and are thought to have sufficient versatility to bind several different target proteins. These disordered, flexible regions consist of repetitive short fragments that can be found in many different species. Due to their flexibility they might act as flexible linker between globular protein domains. Gene ontology analysis has suggested that these regions could be involved in specific protein binding and, when located in the central part of an amino acid sequence, could be important for transcription, transcription regulation and translation [206]. The database yielded further scores for different protein motifs but none of them had a score significantly higher (E-value<0.01) than the threshold. This threshold represents a value calculated using the SWise algorithm [207], which provides similarity scores for query sequences, when compared with the alignment database. The threshold represents the lowest score allowable for sequences to be considered as homologues. Even though the RIH domain is known [77], it was not identified by the SMART database because it is not included in the databases SMART uses for structural prediction. Therefore, no similarities were identified between known domains and RYR1 between amino acid 2100 and 2600.

5.2.3 Phyre^2

Phyre^2 **(P**rotein **H**omology/analog**Y** **R**ecognition **E**ngine V 2.0) is a program designed to predict secondary structures of proteins by using sequence alignments to proteins with known structure [208]. The RYR1 amino acid sequence 2144-2489 was analysed using the database and aligned. Thirty-eight % of this sequence (RYR1 amino acid 2144-2284) matched the IP3R type 1 binding core domain 2 structure with a confidence interval of 99.3 % (results are shown in figure 5.2). Structural predictions of amino acid sequence 2144-2489 for WT and R2452W RYR1 are shown in the appendices VIII and IX.

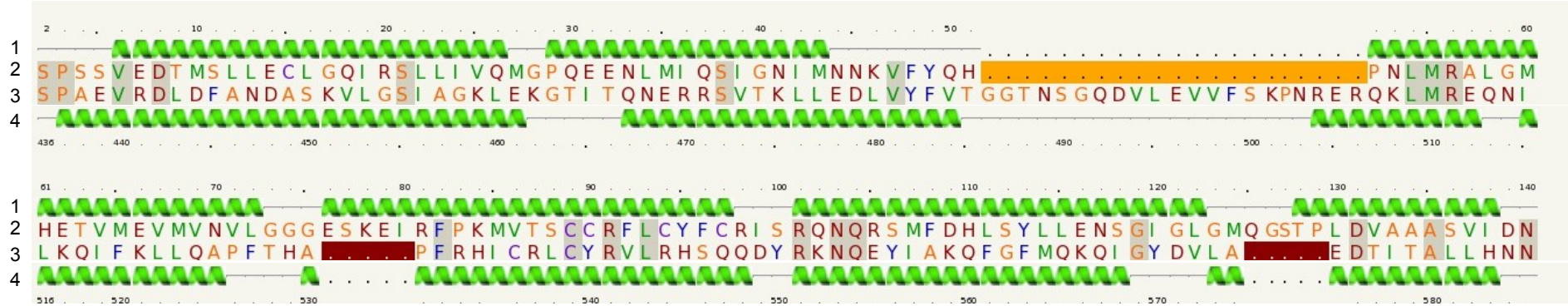

Figure 5.2 Sequence alignment of RYR1 domain (amino acid 2144-2284) and IP3R.

Lane 1 represents the predicted secondary structure of the RYR1 target sequence (amino acid sequence shown in lane 2) compared to the secondary structure of the reference protein IP3R, lane 4. For comparison the IP3R reference sequence is shown in lane 3. Green domains indicate α-helical structure and gray highlighted sequences confirm sequence identity.

5.3 Results

5.3.1 Cloning strategy

The R2452W mutation is situated in the central region of RYR1 in the DP4 domain. This region may be involved in “domain-zipping” and unzipping to control the closure and opening of the receptor, which has been shown by protein binding assays [85]. As an approach to determine the effect of the R2452W mutation on the three dimensional protein structure of RYR1, the RIH homology domain, together with the DP4 domain (figure 5.3), were cloned. The R2452W mutation is located in the central hot spot region (MH2) and was suggested to be causative of MH earlier in this study (chapter 3 and 4). No other X-ray crystallographic structural studies for MH2 have been reported to date.

The chosen sequences comprised 320 amino acids, including aa 2157-2365 of the second RIH domain and aa 2442-2477 of the DP4 domain. A crystal structure for parts of the first RIH domain in the N-terminus of RYR1 has been reported [78]. The DP4 domain itself has not yet been crystallised; however an NMR structure was published by Bannister et al., 2007 [87] showing two helices, where amino acid R2452 is located at the C-terminus within the first helix (see figure 1.10). Expressing these two domains together may result in soluble protein that could be used in crystallisation and enable the analysis of interactions between domains to test the “zipper”-model. The vectors chosen for cloning and purification of an expressed polypeptide were pProEXHtb, with a $(His)_6$tag at the C-terminus and the pET32a(+) vector with both C- and N-terminal $(His)_6$tags. Restriction endonuclease recognition sites for EcoRI and HindIII were used to clone the PCR product into the vector. The complete human *RYR1* cDNA sequence (pc*RYR1* and pc*RYR1*-R2452W, chapter 4) cloned into pcDNA3.1(+) [166], does not have any naturally occurring restriction sites suitable for cloning into pProEXHtb and pET32a(+). Restriction sites for EcoRI/HindIII and NcoI/HindIII, respectively, were introduced into the primer sequences used for PCR amplification of the target sequence.

Construct	First RYR1 amino acid	Last RYR1 amino acid
1	2157	2480
2	2151	2494
3	2144	2489
4	2129	2478

Table 5.2 Table of RYR1 inserts cloned into either the pProExHtb or pET32a(+) vector.

Four different primer sets at slightly different positions in the target sequence were designed for each expression vector to test whether different constructs yield different protein solubility when overexpressed in *E. coli*. Each construct results in a polypeptide of around 40 kD. The exact RYR1 polypeptides overexpressed in the vectors can be found in table 5.2. The same cloning strategy (shown in figure 5.3) was used for cloning into both vectors, using two different restriction sites due to different multiple cloning sites. Full vector maps are shown in the appendices VI and VII. *E. coli* DH5α competent cells were transformed with the empty vectors and isolated using the Roche High Pure Plasmid Isolation kit according to the manufacturer's instructions.

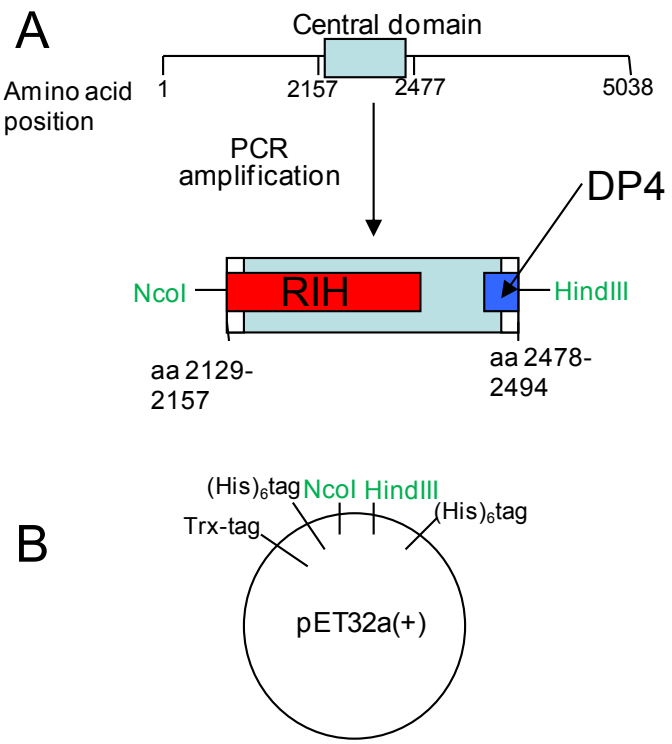

Figure 5.3 Schematic diagram showing the cloning strategy using vector pET32a(+).
A) Schematic diagram of RYR1 and the amino acid positions from 1 to 5038 with the central domain shown as a blue rectangle. The central domain was amplified with different primers introducing restriction sites for NcoI and HindIII. The amplified central domain contains the RIH (red rectangle) and DP4 (dark blue rectangle) domains. PCR products amplified with different primer pairs, resulted in amplicons representing amino acids 2131-2157 at the 5' end and aa 2477-2493 at the 3' end.
B) Scheme of the pET32a(+) vector with the restriction sites for NcoI and HindIII. The $(His)_6$tags were located next to the restriction sites at both the C- and N-terminal and the Trx-tag is 5' of RYR1. The full vector map is shown in the appendices VI and VII.

5.3.2 PCR amplification and cloning

5.3.2.1 pProEX HTb

The pProEx HTb vector was chosen as an expression vector as it has been successfully used in other protein crystallisation experiments [209, 210]. The vector contains a C-terminal $(His)_6$tag and a tobacco etch virus (TEV)-cleavage site to release the tag prior to crystallisation. The vector contains a Trc (Trp-lac) promoter that can produce high levels of recombinant protein expressed in *E. coli* and an ampicillin resistance gene, while the promoter is IPTG (Isopropyl β-D-1-thiogalactopyranoside)-inducible.

An EcoRI restriction site was chosen at the 5' end and a HindIII site at the 3' end to ensure directional cloning. Four different primer sets were designed (table 5.2) to provide a range of products that would be translated into slightly different polypeptides which may differ in protein solubility due to different N- and C-terminal amino acid residues. The full-length plasmids pc*RYR1* and pc*RYR1*-R2452W were used as templates. All primer binding sites are located within the same area so the approximately the same sized PCR products were expected (amplified products shifting +/- 50 bp for different primer pairs, figure 5.4). All PCR products yielded a single band and show no contamination in a no DNA template control (-) (figure 5.4A).

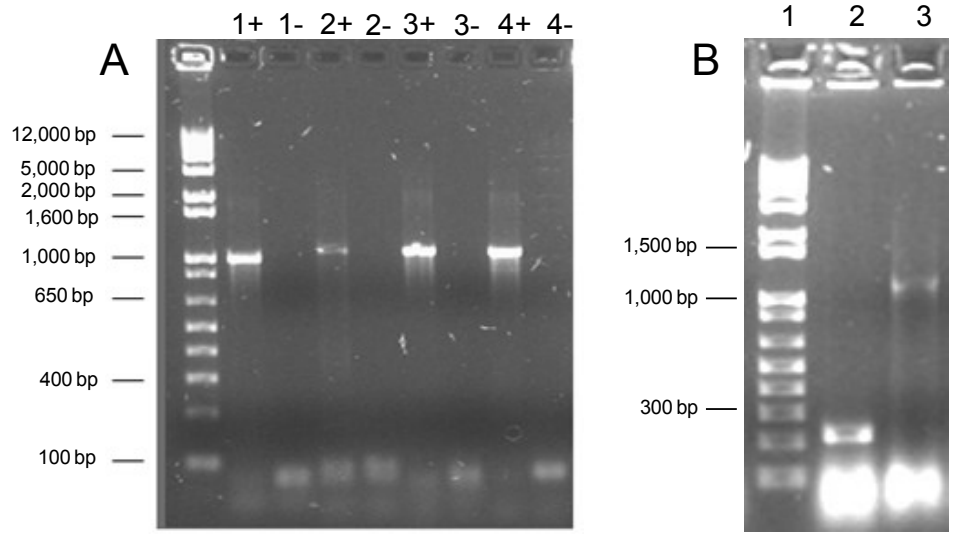

Figure 5.4 PCR amplification of pc*RYR1*-R2452W mutant plasmid and colony PCR for pProEXHtb.

PCR products (10 % of the reaction) were loaded onto a 1 % agarose gel, and separated for 1 h at 80 V and DNA bands were stained with 0.5 µg/mL ethidium bromide. A) PCR products for insert 1-4 amplified for cloning into pProEXHtb. Lanes marked with a + represents PCR reactions amplifying pc*RYR1*-R2452W while lanes marked with – were negative controls where no DNA template was added. All PCR products (1-4) were amplified with construct 2 yielding a fainter product. B) Representing colony screening of potential recombinant plasmid. Lane 1: 1 kB plus ladder, lane 2: PCR product for the non-recombinant vector (250 bp), lane 3: recombinant plasmid containing an insert (1200 bp).

Plasmids and PCR-products of *RYR1* were digested with EcoRI and HindIII and ligated as described in section 2.2.10. Colony PCR was used as a rapid screening method to check whether the colonies contained the insert using primers that annealed to the vector backbone. Colonies not containing the insert yielded a band at about 250 bp corresponding to the multiple cloning

site and tags (figure 5.4A), while plasmids containing the insert resulted in ~1200 bp PCR products (figure 5.4B).

5.3.2.2 pET 32a(+)

The pET 32a(+) vector was chosen as an alternative to pProEXHTb because Amador et al. [76] successfully used this vector in previous work for crystallisation of 210 aa of the N-terminus of the RYR1 protein. This vector contains both C- and N-terminal His_6-tags, an N-terminal S-tag (S-tagged leptin) and an N-terminal Trx-tag (thioredoxin-tag) with cleavage sites for the N-terminal tag. It has a strong T7 promoter and like pProEXHtb, the vector confers ampicillin resistance and can be induced with IPTG. Due to different reading frames in the multiple cloning site, the primers used for cloning into the pProEX HTb vector could not be used for pET 32a(+). Separate primer sets containing restriction sites for NcoI at the 5' and HindIII at the 3' end were chosen.

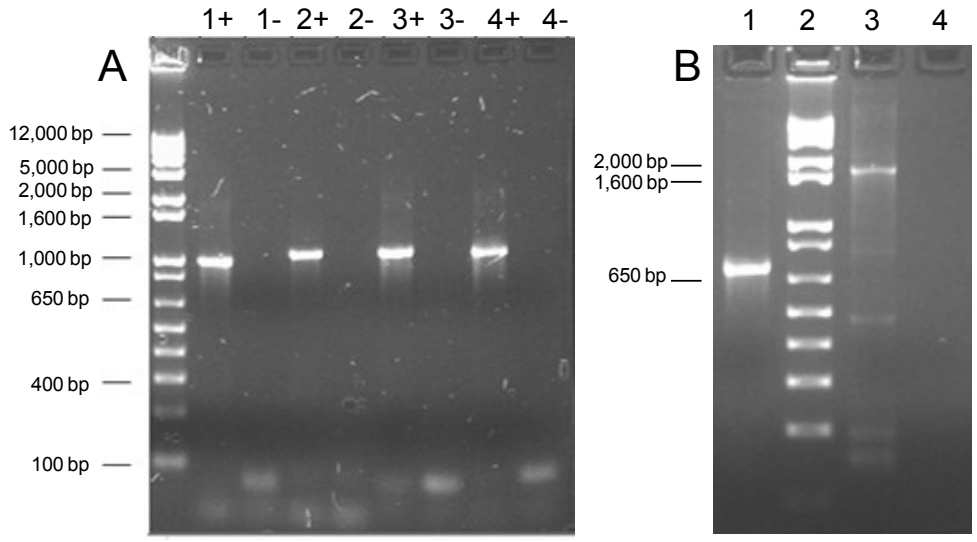

Figure 5.5 PCR amplification of pcRYR1-R2452W and colony PCR for pET32a(+).
PCR products (10 % of reaction) were loaded onto a 1 % agarose gel, separated for 1 h at 80 V and bands were stained with 0.5 µg/mL ethidium bromide. A) PCR products 1-4 ready to be cloned into pET32a(+). Lanes marked with a + represents PCR reactions amplifying pcRYR1 R2452W while lanes marked with – were negative controls when no DNA was added. All four different constructs were successfully amplified. B) Results for colony screening for the correct insert using colony PCR. Lane 1: PCR products for the non-recombinant vector (700 bp), lane 2: 1 kB plus ladder, lane 3: recombinant plasmid (1700 bp), lane 4: non-template control.

PCR products showed a single band of the correct size and showed no contamination in the non-template control (see figure 5.5A, -). Colony PCR

was carried out to verify successful cloning of inserts where primers anneal to the vector at the T7 promoter site (forward) and the T7 terminator site (reverse primer). Empty vector yielded a band of ~700 bp while recombinant plasmids showed a band at ~1700 bp. Some positive colonies (figure 5.5B) also showed a few weaker extra bands of smaller size. Five mL of LB broth was inoculated with selected colonies and and grown over night at 37 °C. Plasmid DNA was extracted the next day prior to sequencing.

5.3.3 Initial expression tests

Initial expression tests using construct 4 carrying the R2452W mutation in pProExHtb (referred to as pProEXHtb-4) as well as construct 1 expressing R2452W in pET32a(+) (referred to pET32a(+)-1) were carried out. These constructs were randomly chosen for initial testing. *E. coli* BL21(DE3) cells were transformed using either pProExHtb-4 or pET32a(+)-1 and grown to an OD_{600} of 0.4 before induction with 1 mM IPTG at 37 °C. *E. coli* cultures were harvested (0.1 mL) after 3 h and cell pellets were resuspended in 20 µL of 5x loading dye (60 mM Tris-HCl, pH 6.8, 25 % glycerol (v/v), 2 % SDS (w/v), 14.4 mM β-mercaptoethanol, 0.1 % bromphenol blue (w/v)), boiled for 5 min before being loaded onto a 12.5 % SDS gel to see whether expression was initiated. Figure 5.6 shows that pET32a(+)-1 expressed high amounts of protein (57 kDa figure 5.6, lane 3, red arrow) while pProExHtb-4 expressed protein (45 kDa figure 5.6, lane 5, blue arrow) but at much lower levels. Lane 2 and 4 in figure 5.6 show a small amount of overexpressed RYR1 protein, most likely due to leaky expression before induction.

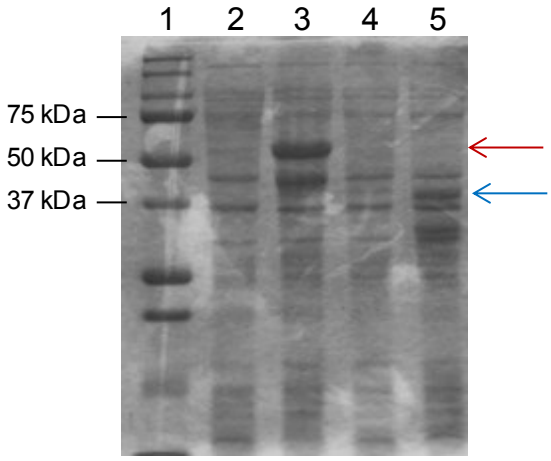

Figure 5.6 Expression tests for recombinant pET32a(+) and pProExHtb.
Cell lysates of 20 µL induced *E. coli* samples were loaded onto a 12.5 % SDS-PAGE gel and separated for 1h at 130 V before being stained with Coomassie blue. Lane 1: Precision Plus Protein Standard size marker (used in all experiments), lane 2: uninduced *E. coli* lysate pET32a(+)-1, lane 3: induced *E. coli* lysate pET32a(+)-1, lane 4: uninduced *E. coli* lysate pProExHtb-4, lane 5: induced *E. coli* lysate pProExHtb-4. The red and blue arrow indicate the overexpressed protein pET32a(+)-1 and pProExHtb-4 respectively.

5.3.4 Optimisation of expression

Induction tests at different temperatures were carried out to optimise expression levels. All colonies were initially grown at 37 °C prior to induction with 1 mM IPTG. Constructs pProEXHtb-4 and pET32a(+)-1 were induced and grown at 35°, 30°, 25°, 22° and 16°C to optimise expression temperature for either 1.5, 3, 4.5 or 20 h. Induction temperature for pET32a(+)-1 was optimised to 16 °C, as this temperature resulted in the largest amount of soluble protein and the optimal induction time was 3 h. RYR1 expressed in pProEXHtb-4 yielded no soluble protein under any condition tested. Plasmid DNA was extracted from 16 colonies for the two vectors containing an insert and sequenced to confirm the absence of nonsynonymous mutations introduced by PCR. All colonies in pProExHtb containing the correct sized insert contained at least one mutation in the reading frame and were therefore not able to be used for further studies without carrying out mutagenesis to correct the sequence. Since pProExHtb vector constructs did not yield any soluble protein (results were confirmed by western blotting), work was continued with only pET32a(+) vector constructs. Expression results are summarised in table 5.3.

Construct in **pProEXHtb**	Expression in BL21(DE3)	Soluble Protein obtained
1 R2452W	no	no
2 R2452W	no	no
3 R2452W	yes	no
4 R2452W	yes	no
1 WT	no	no
2 WT	no	no
3 WT	yes	no
4 WT	yes	no
Construct in **pET32a(+)**	Expression in BL21(DE3)	Soluble Protein obtained
1 R2452W	yes	no
2 R2452W	no	no
3 R2452W	yes	yes
4 R2452W	yes	yes
1 WT	yes	no
2 WT	no	no
3 WT	yes	yes
4 WT	yes	no

Table 5.3 Expression summary of RYR1 constructs in pProExHtb and pET32a(+).
All constructs were expressed in BL21(DE3) competent cells and induced with 1 mM IPTG. Colonies expressing pET32a(+) constructs were grown at 16 °C for 3 h while colonies expressing pProEXHtb constructs were grown at 25 °C for 4.5 h.

The eight constructs cloned into pET32a(+) were checked for their expression of soluble protein with the previously optimised conditions by centrifugation of the total cell lysate for 30 min at 16,000 x g in order to pellet insoluble protein. Only construct 3 resulted in expression of soluble protein for both WT and R2452W mutant (figure 5.7) while the other constructs either did not express RYR1 (construct 2) or only resulted in soluble protein for

either WT or R2452W mutant (table 5.3). Since the aim of this study was to compare the protein stability and structure of WT and R2452W mutant RYR1, only construct 3 was used for subsequent work.

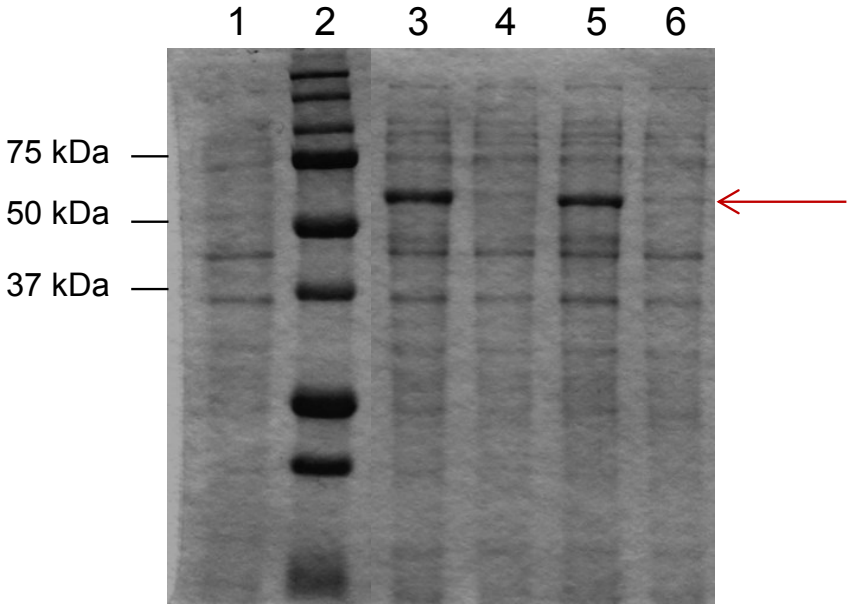

Figure 5.7 Expression of construct 3 in pET32a(+) for WT and R2452W mutant.
Total and soluble protein of 20 µL induced *E. coli* samples were separated on a 12.5 % SDS-PAGE gel for 1 h at 130 V before Coomassie blue staining. Lane 1: *E. coli* lysate from uninduced pET32a(+) construct 3, lane 2: size marker, lane 3: total overexpressed protein R2452W, lane 4: soluble overexpressed R2452W protein, lane 5: total expressed WT protein, lane 6: soluble expressed WT protein. The red arrow indicates the size of the RYR1 protein.

Since expression levels of soluble protein were low, a different approach was taken by using BL21(DE3) competent cells expressing a plasmid carrying a chloramphenicol resistance gene and the coding sequences for the chaperones GroEL and GroES. These cells reportedly increase expression of proteins by supporting the native folded state [211, 212]. Expression levels of soluble protein was optimised as described for BL21(DE3) cells and expression of soluble protein was increased. Therefore, the GroEL/ES system was used for all further studies. LB broth (5 mL) was inoculated with *E. coli* BL21(DE3) containing either R2452W mutant or WT *RYR1* construct. A reduced concentration of IPTG (0.1 mM) was used to induce expression when the culture reached an OD_{600} of 0.5, followed by incubation at 18 °C for 3 h. This protocol was used to futher enhance protein solubility.

5.3.5 Mutagenesis PCR

While designing PCR-primers for cloning into pET32a(+) the reading frame shifted at the C-terminus, due to the absence of one base, resulting in an additional 90 base pairs translated ahead of a the stop codon (vector map, appendix VI). Therefore, mutagenesis primers were designed to introduce an additional nucleotide into the sequence at the C-terminal in the multiple cloning site of the vector to restore the correct reading frame followed by a His_6tag and the stop codon. Mutagenesis PCR was carried out as described in section 2.2.11. *E. coli* DH5α were transformed for plasmid propagation and the correct sequence was verified by dideoxy chain termination sequencing. Mutated constructs were checked for expression and solubility by transformation of BL21(DE3) GroEL/ES competent cells and soluble expression was accomplished using the optimised conditions described in 5.3.4.

5.3.6 Physical properties of RYR1 central domain construct 3

The Expasy ProtParam software was used to predict physical properties of the RYR1 central domain construct 3 in pET32a(+) (table 5.3) of the fusion protein [overexpressed protein including the N-terminal tag of pET32a(+)] as well as the N-terminal vector tag by itself and the N-terminal cleaved RYR1 domain. Physical properties of all three protein constructs are listed in table 5.4.

Physical property	Fusion protein	N-terminal tag	RYR1 domain
Amino acid number	519	157	369
Size (Da)	56960.4	16947.0	40763.0
Theoretical pI	5.81	5.33	5.74
Extinction Coefficient (M^{-1} cm^{-1}) at 280 nm	29910 reduced cysteine	13980 reduced cysteine	15930 reduced cysteine
Aliphatic index	93.80	80.25	98.83

Table 5.4 Physical properties of overexpressed RYR1 fusion, cleaved and N-terminal tag proteins.

The pI of the fusion and the cleaved protein did not significantly differ so a pH range above 6 should prevent precipitation during purification.

The aliphatic index is an indicator of the hydrophobicity of a protein and it defines the volume, which is taken by aliphatic side chains in a protein. It can also be regarded as a factor for increased thermostability [213]. Aliphatic indices above 80 indicate higher hydrophobicity of the protein. The aliphatic indices of the fusion and the cleaved protein are very high with values above 93 indicating high hydrophobicity that is not present in the N-terminal tag protein.

The extinction coefficients were calculated in order to be able to determine protein concentrations using protein absorbance at 280 nm. Extinction coefficients calculated assumed all cysteines in the protein were reduced.

5.3.7 Purification of RYR1 central domain

5.3.7.1 Ni^{2+}affinity chromatography

Since the expressed RYR1 protein domain in pET32a(+) contains two His_6-tags, a Ni^{2+}-agarose resin column was used for affinity purification (section 2.3.3). After induction of transformed *E. coli,* cell pellets were harvested and resuspended in lysis buffer (50 mM Tris, pH 8.1, 500 mM NaCl, 0.5 mM DTT). Cells were processed through a French press twice at 5000 psi and insoluble proteins were sedimented by centrifugation at 16,000 x g for 30 min. Supernatant containing soluble proteins was loaded onto a His_6trap column equilibrated with lysis buffer plus 50 mM imidazole. Proteins were eluted using a gradient from 50 mM to 400 mM Imidazole. Since GroEL (60 kDa) and GroES (10 kDa) tend to bind to overexpressed protein [214], 10 mM ATP (dissolved in 0.5 mM Tris HCl buffer, pH 8.1) was added to the cell lysate and incubated for 15 min on ice to release GroEL/ES from the RYR1 protein. After loading, the column was washed with 7 column volumes of lysis buffer including 70 mM imidazole to elute non-specifically bound protein. RYR1 protein was eluted with an imidazole gradient and results are shown in figure 5.8 A and B). L represents the flow through protein not bound to the

Ni^{2+}-column. This was used as a control to ensure binding of the His_6-tagged protein. L shows a high amount of protein but no RYR1 protein can be detected. A bright band at 60 kDa most likely represents GroEL not binding to the column.

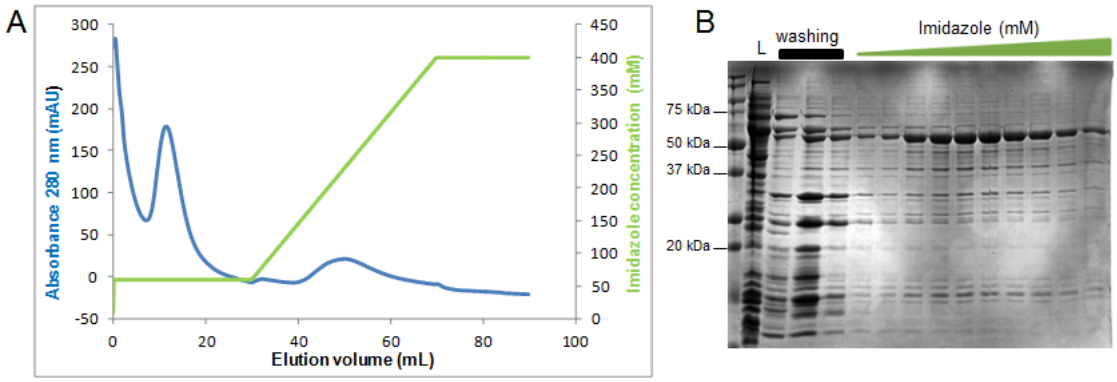

Figure 5.8 Elution chromatogram of WT RYR1 protein from Ni^{2+} NTA column.
A) Elution chromatogram of overexpressed RYR1 protein detected at 280 nm (blue trace) eluted with increasing imidazole concentrations (green line). The corresponding SDS-PAGE gel is shown in B), indicating elution of RYR1 protein (~57 kDa) with increasing imidazole concentrations. L represents the flow through. The fractions (20 µL) were loaded onto a 12.5 % SDS-PAGE gel and were separated for 1 h at 130 V before stained with Coomassie blue.

After the first Ni^{2+}-NTA purification step the eluted protein still showed major impurities represented by additional bands on an SDS gel (figure 5.8B). To reduce impurities a second Ni-NTA purification was performed. RYR1 protein containing fractions eluted in the first purification step were pooled and another 10 mM ATP was added to reduce potentially bound GroEL/ES to RYR1 protein and incubated for 20 min on ice. The protein mixture was loaded onto the His_6trap column, equilibrated with lysis buffer, and washed with 4 column volumes of lysis buffer containing 50 mM imidazole to prevent nonspecific binding. This was followed by 5 column volumes of 180 mM imidazole and protein was eluted in one step at 400 mM imidazole (figure 5.9).

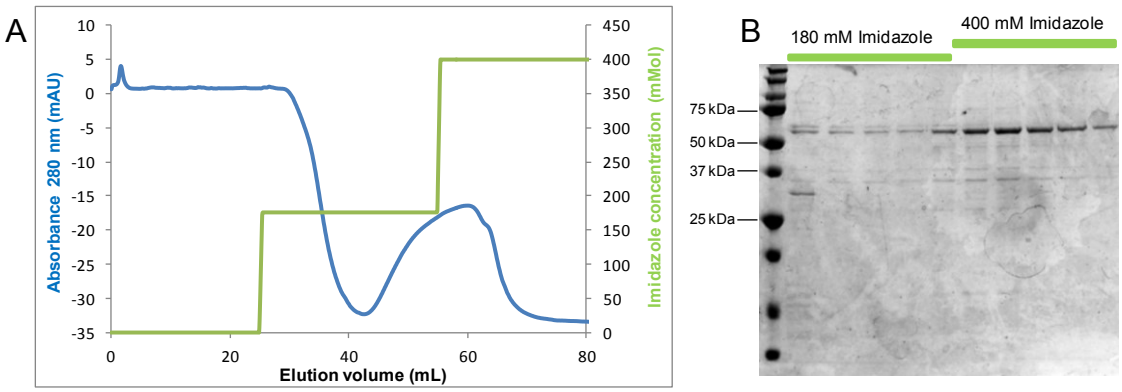

Figure 5.9 Chromatogram for the second elution from the His_6trap column using a step gradient.

A) Elution chromatogram of overexpressed RYR1 protein detected at 280 nm (blue trace) eluted with increasing imidazole concentrations (green line). The corresponding SDS-PAGE gel is shown in B), indicating elution of RYR1 protein (57 kDa) with 400 mM imidazole. The proteins loaded onto the 12.5 % SDS-PAGE gel were separated for 1 h at 130 V before staining with Coomassie blue.

Washing the column with lysis buffer and 180 mM imidazole resulted in a minor loss of RYR1 protein but also in the elution of non-specific bound protein (60 kDa), which can be seen as a faint band in figure 5.9B. Elution with 400 mM imidazole resulted in almost pure RYR1 protein with minor contamination of bands around 35 kDa (figure 5.9B).

5.3.7.2 S200 size exclusion

Size exclusion was carried out for further purification purposes. Pooled fractions from the His_6trap-purification were concentrated to 300 µL using a Vivaspin concentrator and the buffer was exchanged (10 mM Tris, pH 7.9, 10 mM NaCl and 0.1 mM DTT). The resultant protein solution was loaded onto a GE Healthcare Superdex S200 30/100 size exclusion column through a 500 µL loop using the ÄKTA FPLC system. The size exclusion column was calibrated using proteins of different sizes while the void volume was calibrated using Dextran blue (2000 kDa). A calibration curve can be found in appendix XI. Wildtype and mutant RYR1 protein were purified separately and an elution peak at 9.8 mL was detected at 214 nm for more sensitive protein visualisation (figure 5.10A, 2). SDS-PAGE shows a band of 57 kDa in size for this elution fraction with possible contamination of GroEL (60 kDa, figure

5.10B, lane 2). Pure WT RYR1 eluted at 11 mL in a broad peak and was visualised as a single band on an SDS gel (figure 5.10B, lane 3, green arrow). Using the calibration curve the RYR1 protein size is approximately 440 kDa, suggesting the RYR1 domain may oligomerise. Since RYR1 is known to form a tetramer *in vivo,* a size of 240 kDa could be expected from the central domain if the cloned region contains an oligomerisation-domain. Since size exclusion not only separates by molecular weight but also takes into account the hydrodynamic radius of proteins, this result suggests that the central domain may be a non-globular protein and may be involved in oligomerisation of RYR1 [215]. In comparison, full-length IP3R was eluted as a tetrameric protein when size exclusion studies were undertaken using a Zorbax GF-450 column and a HPLC system [75].

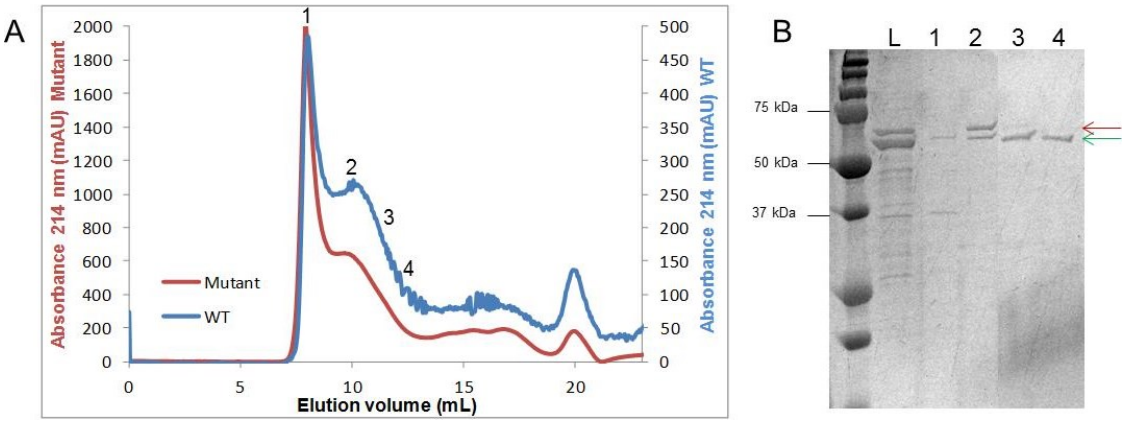

Figure 5.10 S200 size exclusion results of WT and R2452W mutant RYR1 fusion protein.
A) The trace represents the chromatogram of WT RYR1 (blue line) and R2452W mutant RYR1 (red line) detected at 214 nm. The y axis represents the absorbance in mAU (for WT and Mutant separately) while the x axis shows the elution volume. The WT and mutant proteins were run separately. The corresponding SDS-PAGE gel is shown in B), indicating elution of pure RYR1 protein at fraction 3, indicated by a green arrow. A 60 kDa contaminant is indicated by a red arrow. L represents input control. Lanes 1-4 represent eluted fractions 1-4,respectively as indicated in A. The proteins loaded onto the 12.5 % SDS-PAGE gel were separated for 1 h at 130 V before staining with Coomassie blue.

R2452W mutant protein was purified and also loaded onto the S200 size exclusion column separately (see figure 5.10A, red trace) and appears to behave in a similar manner. Overlaying the two elution profiles (see figure 5.10A) indicates that both WT and R2452W mutant RYR1 domain started eluting from the column around 9.5 mL in a broad peak suggesting a similar oligomerisation state. Therefore the R2452W mutation may not affect

quaternary structure. Elution of the potential tetrameric protein is quite close to the void volume (8 mL peak), representing elution of proteins too big to enter the column material, and both peaks overlap. Fractions loaded onto an SDS-PAGE gel showed the presence of RYR1 protein eluting at around 8.5 mL, the void volume. The eluted proteins may not be folded correctly and form aggregates and therefore have been eluted in the void volume (5.10A, lane 1). Alternatively, RYR1 protein may be visible on a gel due to the overlapping peaks (5.10B, lane 1). Since protein abundance was low the pooled fractions eluted between 8.5 and 9.5 mL could not be re-loaded on the column to verify whether they would separate into two individual protein populations. Additionally the nonrecombinant pET32a(+) vector, expressing only thioredoxin, the MCS and the N-terminal purification tags was used to express a 21 kDa protein which was subsequently purified using size exclusion. The tag, mainly consisting of thioredoxin (120 amino acids ~ 14 kDa), was eluted in two fractions. The main polypeptide was eluted at 14.6 mL representing a size of 70 kDa and may exist as a potentially non-globular protein which could be a dimer. A minor fraction was eluted at 16.3 mL (30 kDa) and thus could represent a monomer. This result agrees with results obtained in previous studies characterising the thioredoxin protein, even though the main species in other studies was the monomeric protein while only a minor fraction was present as a dimer [216]. Elution fractions were kept separate and used for further analysis.

Overexpression and purification of the RYR1 fusion protein yielded protein concentrations of ~0.2 mg/mL in 200 µL. This amount was not sufficient to do further analysis e.g. crystallisation trials which need a minimum amount of ~2 mg/mL protein. Therefore, analysis of the RYR1 secondary structure and its stability was carried out instead.

5.3.8 Circular dichroism (CD)

In order to assess protein stability of both WT and mutant RYR1 polypeptides, stability melting experiments with purified WT and R2452W mutant fusion protein were carried out using circular dichroism (CD) which provides information about the averaged secondary structure of a protein.

Figure 5.11A shows CD spectra for WT and R2452W mutant RYR1 fusion protein at RT, as well as for the N-terminal tag peptides. A minimum can be observed at 209 nm for both RYR1 fusion proteins, indicating presence of α-helix whereas no obvious minimum can be seen at 217 nm. Therefore, no conclusion about the presence of β-sheets can be drawn. A minimum at 217 nm can be clearly seen for the N-terminal tag proteins which was used as control (figure 5.11). Comparing CD profiles for RYR1 and the N-terminal tag protein, an obvious difference can be seen between the spectra at 190 and 200 nm. The tag proteins show a maxima at 198 nm followed by a signal decrease resulting in a minimum at 190 nm while RYR1 protein gives a maximum at 192 nm (figure 5.11A).

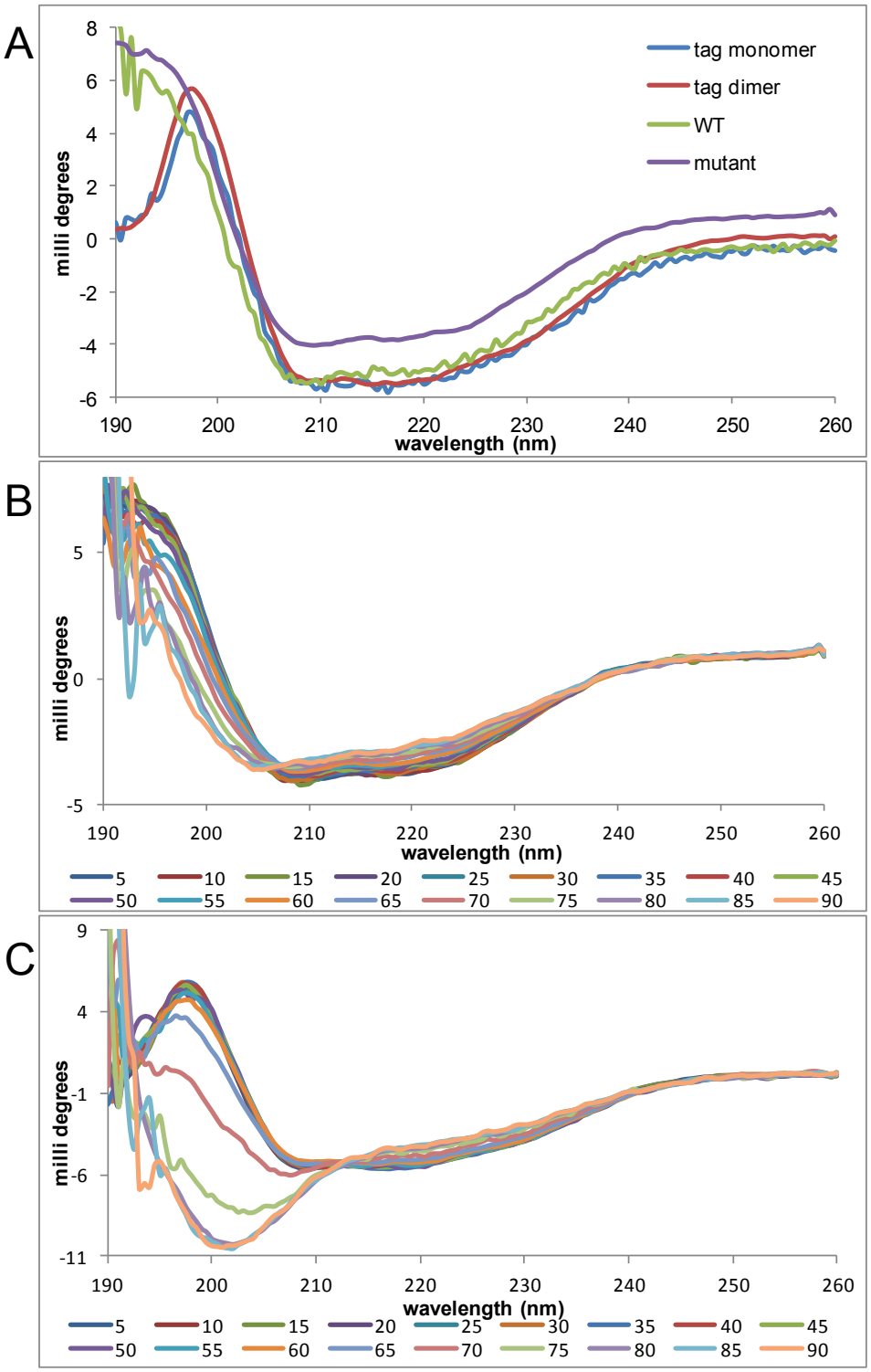

Figure 5.11 CD spectra for RYR1 fusion and N-terminal tag proteins (A) and thermal denaturation of R2452W mutant fusion (B) and N-terminal tag protein (C).

A) CD profile at room temperature for RYR1 WT and mutant fusion protein as well as for the putative monomeric and dimeric N-terminal tag protein. B) CD profile for R2452W from 190-260 nm from 5-90°C. C) CD profile for N-terminal tag from 190-260 nm from 5-90°C. The relevant temperature colour keys are provided under each profile.

The eluted monomer and dimer N-terminal protein tags were measured separately but reveal almost identical CD profiles (figure 5.11A) as well as deconvolution (see table 5.5). Deconvolution, using the CDNN software, uses a number of different algorithms to predict secondary structure. Deconvolution data of WT and R2452W mutant CD spectra, as well as for the tag proteins, from 260-195 nm are shown in table 5.5.

Secondary structure motifs	WT RYR1 fusion	R2452W mutant RYR1 fusion	N-terminal tag dimer	N-terminal tag monomer
α-helix (%)	37	40	47	54
β-sheet (%)	16	12	9	8
β-turn (%)	16	16	14	14
Random coil (%)	25	27	24	18

Table 5.5 Deconvolution results determining percentage of secondary structures.

Deconvolution showed similar results for WT and R2452W mutant proteins where the mutant protein has slightly increased α-helical and random coil content and reduced β-sheets. N-terminal tag dimer and monomer differ from each other with increased α-helical and reduced random coil structure for the monomeric protein. Since the N-terminal tag protein mainly eluted as a dimer from the S200 size exclusion column while the RYR1 fusion protein is believed to exist as oligomer, the fusion protein was compared to the N-terminal tag dimer only. The tag dimer protein differs in deconvolution results to the RYR1 proteins with increased α-helix and decreased β-sheet content in the tag protein. This suggests that the fusion protein might have a different secondary structure than the N-terminal tag protein indicating folding of RYR1.

Thermal stability of WT and R2452W mutant was assessed by measuring their secondary structure by CD while increasing the temperature from 5 °C to 90 °C (figure 5.11). The circular dichroism signal was plotted against temperature for wavelengths of 209 (α-helix minimum) and 217 nm (β-sheet minimum) in order to plot a curve with the point of inflection representing the

melting temperature (50 % of normalised CD data, figure 5.12). The normalised CD data (percent of total decrease in signal) were plotted for the N-terminal tag dimer, WT and mutant RYR1. Results in figure 5.11 showed that both WT and mutant fusion RYR1 polypeptide behaved similarly under increasing temperature.

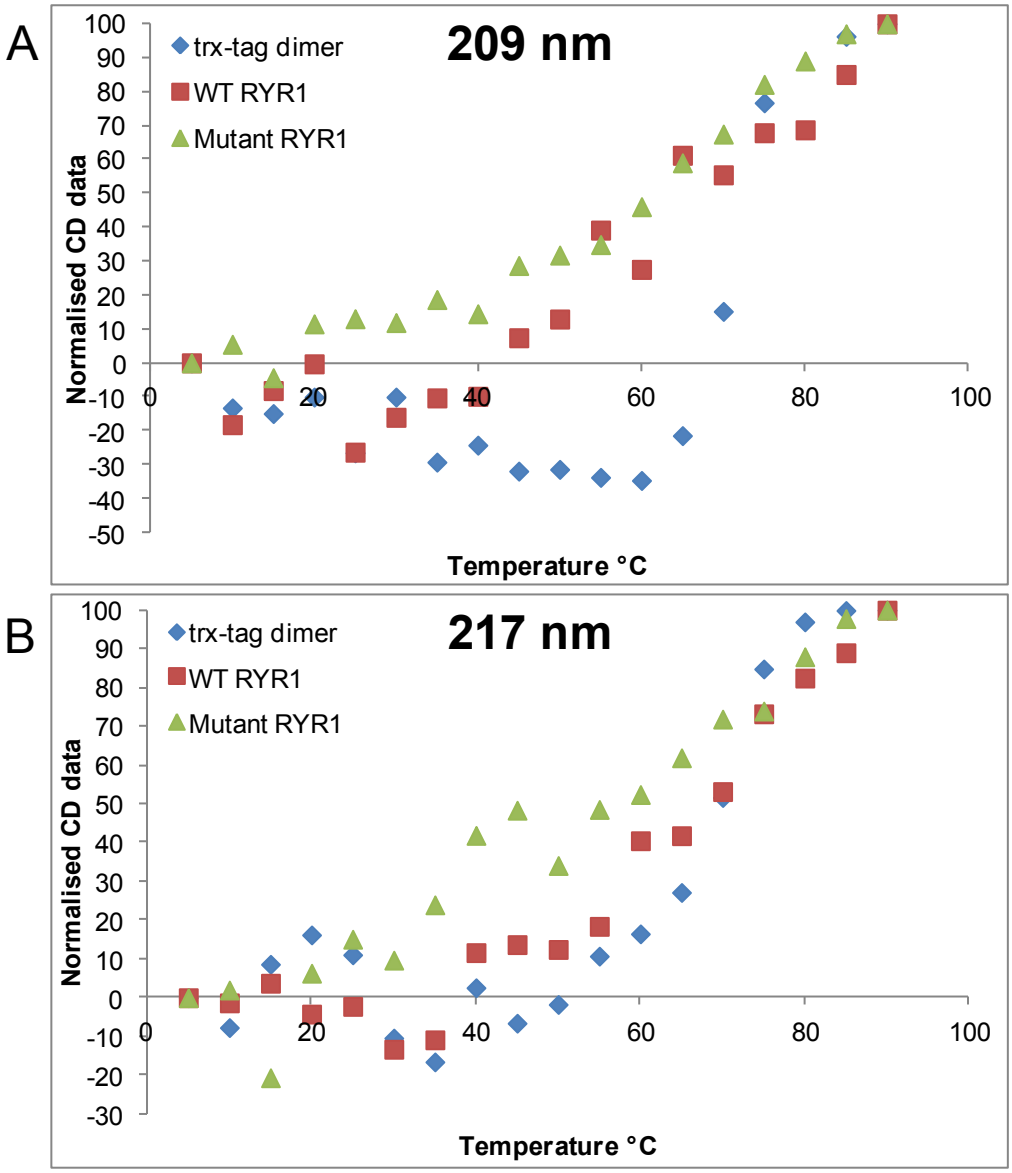

Figure 5.12 Plot of normalised CD data under thermal denaturation at 209 nm (A) and 217 nm (B).

Up to temperatures of 40 °C both RYR1 fusion proteins appear to be stable with little change in secondary structure. Small fluctuations are apparent, due to natural variation in data. Above 40 °C, the mutant RYR1 protein seems to lose secondary structure. This is indicated by a sharp decrease in intensity for the minimum at 217 nm. A plateau occurs between 40 and 60 °C,

representing loss of β-sheet structure (figure 5.12). At 209 nm however, a steady decrease in α-helical structure can be observed. Melting curves at 217 nm for WT and R2452W mutant RYR1 protein showed a point of inflection at different temperatures indicating a ~15 °C lower melting temperature for R2452W mutant protein compared to WT RYR (figure 5.12B) while no obvious difference in Tm could be observed at 209 nm.

The purified N-terminal tag proteins were also subject to stability testing using CD spectra to determine secondary structure, as well as melting temperature in order to compare data to the RYR1 fusion proteins. This approach should give an indication of whether WT and R2452W fusion proteins comprise a different secondary structure to the N-terminal tag protein, mostly consisting of thioredoxin (further referred to as trx-tag). Furthermore, the melting temperatures could be compared. At ~70°C a transition of curves could be seen at 209 and 217 nm, representing unfolding of the trx-dimer. Literature suggests 50 % unfolding of *E. coli* trx occurs at 65 °C [217] while this study showed a point of inflection at ~70 °C at both wavelengths (figure 5.12). Melting behaviour of monomeric and dimeric trx-protein tags was similar and followed a sigmoid curve. Melting temperatures may not be the same as reported in other studies since different buffer systems and methods were used but should give a melting temperature in the expected range.

Melting observed at 209 nm (figure 5.12A) showed a different pattern for trx-tag dimer compared to fusion WT RYR1, indicating higher thermal stability of trx-tag dimer. Spectra for WT and trx-dimer at 209 and 217 nm did not show a constant baseline representing 100 % folded protein. This indicates a natural fluctuation in data and since spectra were only measured once, the data do not have a high reliability and experiments need to be repeated in order to exclude measurement errors. Melting curves for both RYR1 fusion proteins do not follow a sigmoid curve since a maximum for the normalised data was not observed. Therefore, it may be possible that the fusion proteins might not be completely unfolded at 90 °C and higher temperatures need to be investigated to confirm melting behaviour above 90 °C.

Lysozyme is a stable protein where 50 % is unfolded at 70 °C [218] and was used as a positive control in this study. Melting temperature for lysozyme of ~73 °C was measured, similar to the literature melting temperature of 70 °C. Any discrepancy may be due to different buffer systems used.

While melting experiments were performed, high tension voltage (HT traces) were recorded, representing the absorbance of the sample as well as the voltage applied by the photomultipier [219]. This signal becomes saturated once it reaches a value of 1000 and secondary structure cannot be detected. The HT trace for samples at 5 °C saturated at 185 nm due to presence of Cl^- ions in the buffer used (10 mM NaCl). The HT trace of the protein reached a maximal signal at a longer wavelength with increasing temperature (see appendix X). This phenomenon occurred only with RYR1 cloned into the pET32a(+) vector as well as for the overexpressed N-terminal vector tags but was absent in stability assays carried out for the control protein lysozyme. This indicated the increase of the HT trace is a function of the pET32a(+) vector rather than the RYR1 protein.

5.3.9 Protease digestion

The pET32a(+) vector contains two protease cleavage sites: one for thrombin and one for enterokinase (see vector map in appendix VI). In an attempt to cleave the N-terminal trx-tag, as well as the His_6-tag off the expressed protein, both proteases were used initially.

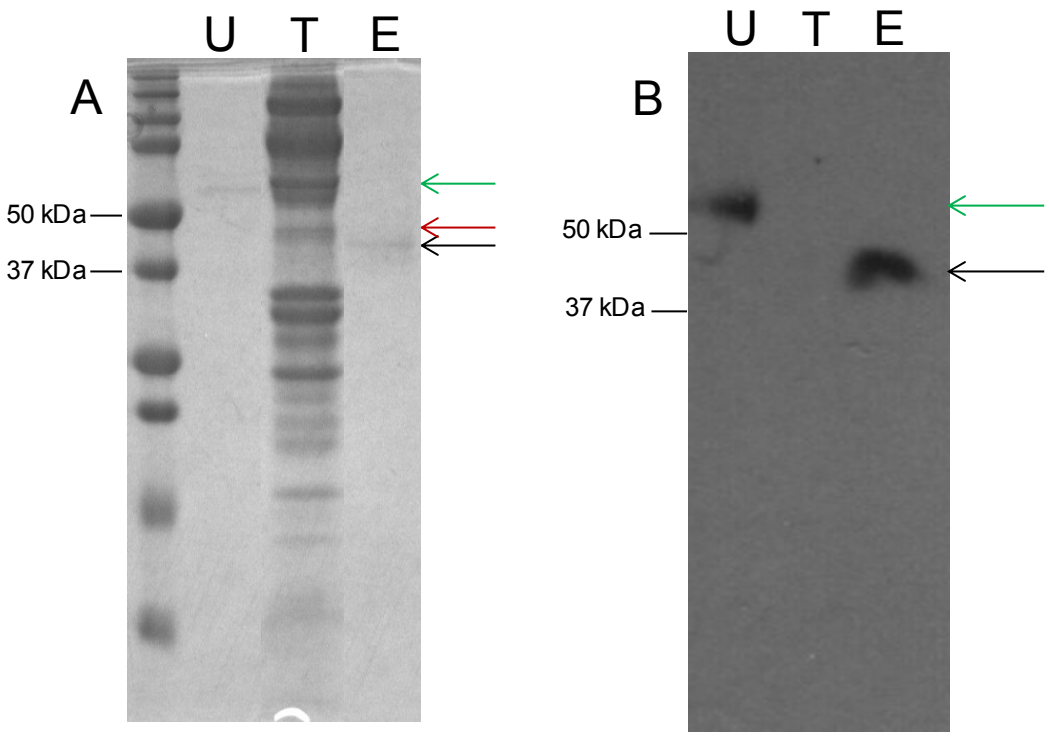

Figure 5.13 Protein cleavage experiments using enterokinase and thrombin.
A) Coomassie stained 12.5 % SDS-PAGE gel, separated for 1 h at 130 V, loaded with 0.5 µg undigested purified RYR1 protein fragment (U, green arrow), thrombin digested protein (T, red arrow) and enterokinase digested protein (E, black arrow). The cleaved N-terminal tag cannot be visualised on the gel. B) Western blot using the α-His_{6}-tag antibody. Lanes are loaded according to figure A. Only RYR1 digested with enterokinase can be seen as a single band at 40 kDa (black arrow) while the N-terminal cleaved tag was not visualised. 12.5 % SDS-PAGE gel was electrophoresed for 1 h at 130 V before being transferred for 2 h at 150 mA onto a PVDF membrane.

Figure 5.13 shows cleavage experiments using thrombin and enterokinase. Enterokinase was able to cleave the N-terminal tag from the overexpressed protein resulting in a single band at approximately 40 kDa in size (black arrow in figure 5.13 A and B), as predicted by the vector map. The cleaved tag should be represented as a band with a size of 17 kDa but cannot be visualised on the gel due to low band intensity. Figure 5.13B shows the results for western blotting of the same digest as shown in figure 5.13A. A band at approximately 40 kDa was visualised by western blotting from the enterokinase digest (figure 5.13B) confirming results of the Coomassie stained SDS-PAGE gel. Again, the cleaved tag at 17 kDa could not be visualised.

Thrombin cleavage was predicted to result in one band at 43 kDa (red arrow) as well as a band for the tag at 14 kDa. The thrombin used for this experiment was low quality and impure. Due to thrombin impurities extra bands were seen on the gel making it impossible to assess thrombin cleavage of RYR1 fusion proteins. Cleaved RYR1 protein could not be detected by western blotting using a His_6-tag antibody even though both protein fragments are His_6-tagged. Therefore enterokinase was used for all further experiments.

Enterokinase time course experiments were performed to optimise cleavage conditions. Protein (0.5 µg, in 10 mM Tris-HCl, pH 7.9, 10 mM NaCl, 1 mM DTT) was incubated for 30 min, 1 h, 2 h or 3 h at room temperature with 0.6 µg enterokinase, loaded onto a 12.5 % SDS-PAGE gel and silver stained to detect progress of cleavage. Figure 5.14 shows that after 30 min, enterokinase cleaved the N-terminal tags efficiently, resulting in two bands at 40 kDa (black arrow, RYR1 protein) and at 17 kDa (orange, N-terminal tag). In addition, a band at 37 kDa (blue arrow) was visualised by silver staining. This band was also apparent in the undigested control (line 2) and of unknown origin but is more abundant after enterokinase cleavage. After a 3 h digest, residual undigested protein (indicated by a green arrow in figure 5.14) was still apparent as well as a band at 60 kDa (red arrow), which is believed to be the protein GroEL, that has not been affected by the enterokinase digest.

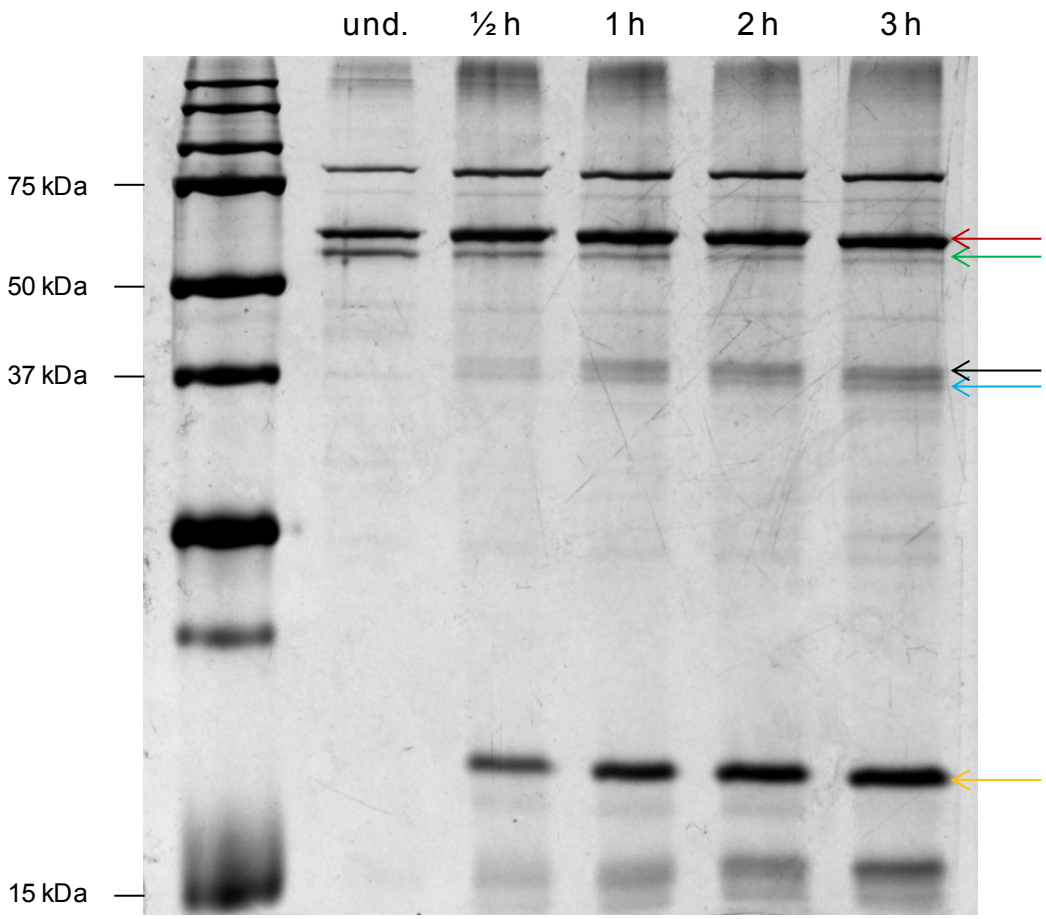

Figure 5.14 Time course experiment for enterokinase digest of RYR1 fusion protein.
Silver stained 12.5 % SDS-PAGE gel, separated for 1 h at 130 V. Undigested protein (und., 0.5 µg) was used as control, while RYR1 protein digested for ½ to 3 h was loaded from left to the right. With increasing time, enterokinase was able to cleave the 57 kDa fusion protein (green arrow) into two bands at 17 kDa (orange arrow) and 40 kDa (black arrow). The red arrow indicates the presence of GroEL unaffected by enterokinase digest. An unknown band appeared at 37 kDa (blue arrow).

Cleaved protein was obtained after digestion for 3 h and was concentrated using a Vivaspin concentrator. No concentrated cleaved RYR1 protein was obtained from the concentrator even though different approaches e.g. dialysis and different brands of concentrators, were used. Protein was concentrated first before enterokinase cleavage was attempted and loaded onto the S200 30/100 size exclusion column. No cleaved RYR1 protein was eluted from the column suggesting that it may have adhered to either the column matrix, or to plastic syringes or tubes that were used for injection into the FPLC.

Addition of detergent

In order to prevent stickiness of the enterokinase cleaved RYR1 protein, 0.1 % Triton X-100 was added to the overexpressed protein during purification. After initial His_6trap purification, eluted protein was concentrated and enterokinase digested overnight at room temperature in order to digest all RYR1 protein. Digested protein was separated using a S200 30/100 size exclusion column and a major peak was obtained at 14 mL (figure 5.15A). Fractions were analysed by a 12.5 % SDS-PAGE gel to visualise the presence of the bands (figure 5.15B).

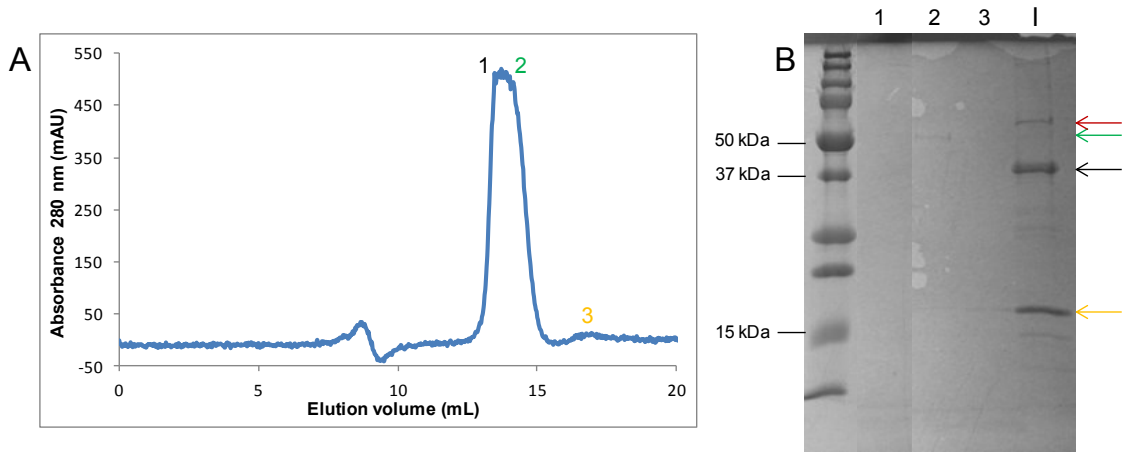

Figure 5.15 Size exclusion chromatogram using Triton X-100 in purification procedure
A) The y axis represents absorbance in mAU at 280 nm while the x axis represents elution volume in mL. RYR1 fusion protein (2) was eluted at 14 mL while the cleaved tag was eluted at 17 mL (3). B) The fractions shown in A (20 µL) were separated on an 12.5 % SDS-PAGE gel electrophoresed for 1 h at 130 V before Coomassie blue staining occured. Lane I represented the Input sample loaded onto the S200 size exclusion column while the other lanes are labelled according to figure A. Green arrow= RYR1 fusion protein, red arrow= GroEL, black arrow= cleaved RYR1 protein, yellow arrow= N-terminal vector tag.

Figure 5.15B indicated that the enterokinase digest was successful with most RYR1 protein being cleaved resulting in two main bands at 40 kDa (black arrow) and 17 kDa (orange arrow) size. Residual amounts of uncleaved protein were still present (green arrow). The elution profile of the S200 size exclusion column showed a peak at 14 mL (figure 5.15A). Fractions corresponding to the peaks were loaded onto an SDS-PAGE gel, however no protein could be visualised (figure 5.15B, 1). This could indicate the elution of Triton X-100 micelles, which have an approximate size of 66 kDa [220] and have a high UV absorbance at 280 nm. Since these micelles do not contain

peptide bonds they cannot be visualised by Coomassie blue staining. Undigested RYR1 protein (figure 5.15A, 2) was seen to elute at 14.5 mL indicated by a green arrow on the SDS gel in figure 5.15 B. The RYR1 fusion domain has been eluted with an approximate size of 85 kDa, making it a 1.4mer in the presence of detergent, indicating the presence of a non-globular monomer with the putative quaternary structure being disrupted by the addition of Triton X-100. Literature supports this suggestion [221-223], indicating that even though Triton X-100 is a non-ionic detergent it can dissociate oligomers. Figure 5.15A shows a minor peak in the size exclusion chromatogram at 17 mL which corresponds to a 17 kDa protein when analysed on a 12.5 % SDS-PAGE (Figure 5.15B). This most likely represents the N-terminal cleaved tag. The cleaved RYR1 protein (figure 5.15B, black arrow) was not eluted off the column. Since the addition of Triton X-100 was not able to purify the cleaved RYR1 by size exclusion, work was continued with the fusion protein without the addition of the detergent.

5.3.10 Mass spectrometry

Purified uncleaved R2452W mutant protein was left in the fridge for 6 weeks while additional protein was purified to obtain sufficient quantities for CD analysis. Before pooling the two samples, the previously purified protein was checked by SDS-PAGE. The concentrated protein appeared to be degraded (intact protein size: 57 kDa) showing two main bands at 37 kDa and 13 kDa in size (figure 5.16). To test whether protein is still soluble it was centrifuged for 15 min at 100,000 x g at 4 °C. Protein supernatant and pellet were analysed by 12.5 % SDS-PAGE. No protein was detected in the pellet indicating that spontaneously cleaved protein was still soluble. In order to investigate the nature, as well as the exact molecular weight of both bands found at 37 and 13 kDa, mass spectrometry experiments were performed. The degraded protein solution was purified using gel tip purification and eluted in acetonitrile (chapter 2.3.7.1). Masses were measured using an Agilent Q-TOF 6520 Instrument and the exact mass of both proteins was determined (see appendices XIII and XIV) to be 37474.67 Da and 13197.32 Da with high signal intensities.

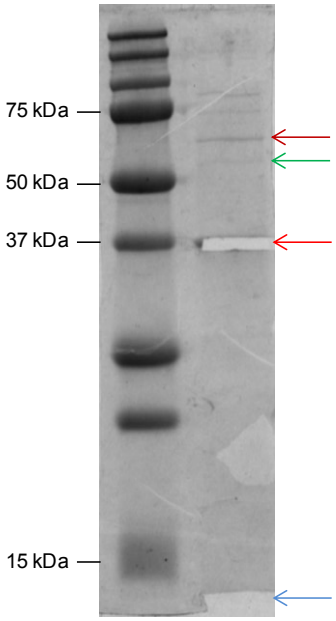

Figure 5.16 Spontaneously cleaved R2452W mutant RYR1 domain.
Samples were analysed by 12.5 % SDS-PAGE and separated for 1 h at 130 V before staining with colloidal Coomassie. Green arrow indicates residual uncleaved full-length RYR1 domain while the orange and light blue arrow indicate the position where the two cleaved fragments were excised for further analysis. The red arrow indicates the presence of GroEL, which was not affected by the spontaneous cleavage.

The exact amino acid sequence of the two fragments was determined using MS-MS. The degraded protein solution was loaded onto a 12.5 % SDS-PAGE gel and bands were stained with colloidal Coomassie blue in order to visualise and excise the two bands resulting in individual fragments (chapter 2.3.7.2). Bands excised from the SDS-PAGE gel (figure 5.16) were trypsin digested and analysed using the Agilent Q-TOF 6520 instrument. Alignment of trypsin fragments using different data bases (kindly carried out by Trevor Loo, IMBS) revealed that the 13 kDa fragment matched the thioredoxin protein sequence whereas some fragments produced by the trypsin digested of the 37 kDa band matched the RYR1 region (figure 5.17). Amino acids not highlighted in red could not be detected using MS, possibly because of their small size or the signal intensity for the fragments being too low to be above the background signal.

```
        10         20         30         40         50         60
MSDKIIHLTD DSFDTDVLKA DGAILVDFWA EWCGPCKMIA PILDEIADEY QGKLTVAKLN

        70         80         90        100        110        120
IDQNPGTAPK YGIRGIPTLL LFKNGEVAAT KVGALSKGQL KEFLDANLAG SGSGHMHHHH

       130        140        150        160        170        180
HHSSGLVPRG SGMKETAAAK FERQHMDSPD LGTDDDDKAI SPSSVEDTMS LLECLGQIRS

       190        200        210        220        230        240
LLIVQMGPQE ENLMIQSIGN IMNNKVFYQH PNLMRALGMH ETVMEVMVNV LGGGESKEIR

       250        260        270        280        290        300
FPKMVTSCCR FLCYFCRISR QNQRSMFDHL SYLLENSGIG LGMQGSTPLD VAAASVIDNN

       310        320        330        340        350        360
ELALALQEQD LEKVVSYLAG CGLQSCPMLV AKGYPDIGWN PCGGERYLDF LRFAVFVNGE

       370        380        390        400        410        420
SVEENANVVV RLLIRKPECF GPALRGEGGS GLLAAIEEAI RISEDPARDG PGIRRDRRRE

       430        440        450        460        470        480
HFGEEPPEEN RVHLGHAIMS FYAALIDLLG RCAPEMHLIQ AGKGEALRIR AILRSLVPLE

       490        500
DLVGIISLPL QIPTLGKDGA LVQPKSLRRPALQHHHHHH
```

Figure 5.17 MS-MS results for gel purified RYR1 protein sample

Results indicate a poor coverage of the RYR1 protein domain where only two fragments (highlighted red) were aligned to the RYR1 sequence. The amino acid positions in the fusion RYR1 protein are indicated above the sequence. Dark blue indicates the sequence coverage for the trx-tag protein and orange residues indicate the start and stop amino acid position of the RYR1 protein domain.

Since the coverage of the RYR1 region was rather poor, a liquid extraction of the protein bands was performed. Protein (~50 µg) was loaded onto a C18 reversed phase column using an HPLC system and the two fragments were separated according to their hydrophobicity.

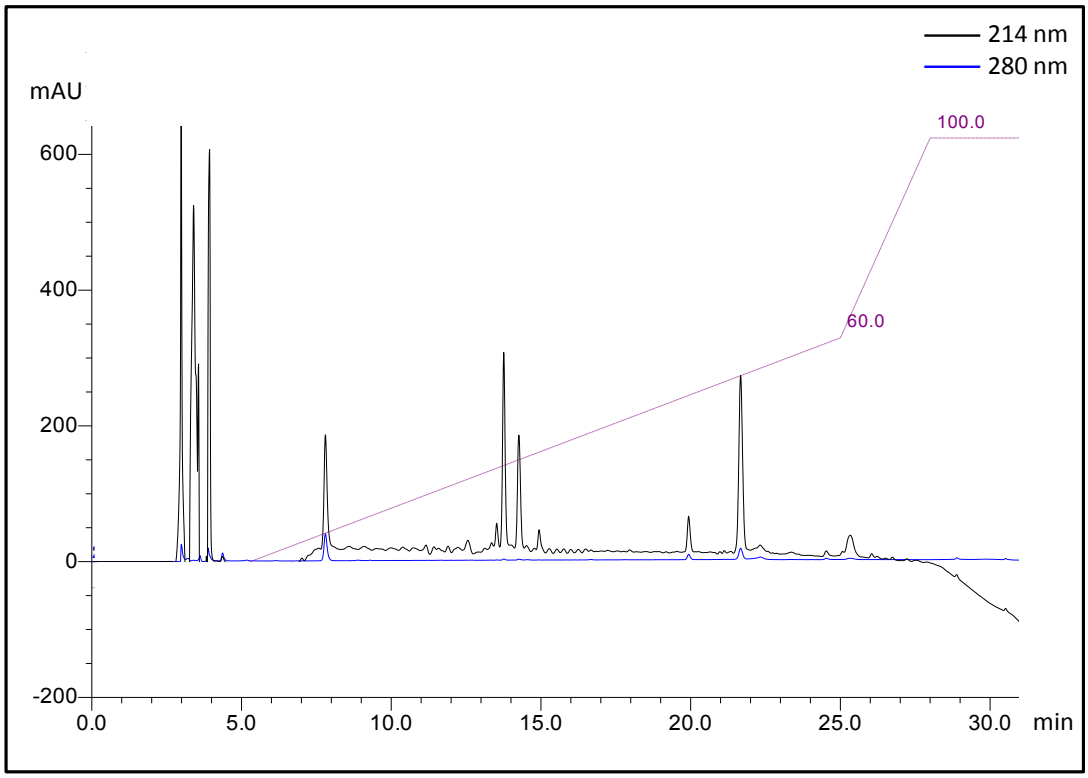

Figure 5.18 HPLC separation of spontaneously cleaved RYR1 protein

Protein absorbance (in mAU) is shown on the y-axis and represents the absorbance at 214 nm (black) while the absorbance at 280 nm is indicated as a blue curve. The dotted line represents the increasing ACN concentration used to elute the protein.

Figure 5.18 shows the absorbance spectrum for purification of the 13 and 37 kDa protein fragments using an HPLC system and monitoring the progress at 214 nm (UV1) and 280 nm (UV2). As mentioned previously, the RYR1 protein does not have a strong absorbance at 280 nm due to low percentage of aromatic amino acids (5 % of the total peptide) therefore the absorbance at 214 nm, detecting peptide bonds in proteins, was used to follow progress. One major species was eluted at 7.8 min, corresponding to 12 % acetonitrile (ACN), one small peak at 19.6 min, corresponding to 38 % ACN as well as another major peak at 21.6 min eluted at 42 % ACN. Peaks could be detected using both UV1 (214 nm) and UV2 (280 nm), whereas at 14 min two peaks showed absorbance at 214 nm but not at 280 nm and hence were discarded as noise. Fractions eluted at 19.6 and 21.6 min were kept separate in order to investigate the nature of these two different species. The absorbance ratios between 214 and 280 nm are different for the peaks eluted at 7.8 and 21.6 min, which could be due to the different protein extinction coefficients stated in table 5.4. The N-terminal tag protein absorbs more

strongly at 280 nm compared to the fusion protein, resulting in a more profound peak at 280 nm. Since it is assumed that the peaks at 19.6 and 21.6 mL peak are cleaved RYR1 protein, the extinction coefficients in table 5.4 can be used to calculate protein concentrations of 0.043 mg/mL for the peak at 7.8 min and 0.037 mg/mL for the 21.6 min peak. The peak eluted at 19.6 min was very small and assuming this protein to be RYR1, results in a concentration of 0.01 mg/mL. These calculated concentrations and the peak intensity measured at 214 nm gave an indication that the two eluted species at 7.8 and 21.6 min may have the same concentration supporting the theory that they both arise from the uncleaved RYR1 protein. Collected protein fractions at 7.8, 19.6 and 21.6 mL were trypsin-digested using a liquid digestion method (chapter 2.3.7.3) and MS-MS was carried out. Results were obtained only for the peak collected at 21.6 min. The protein concentration for the peak at 19.6 min was too low and MS-MS did not yield any results. Results for the 21.6 min peak were filtered using the Mascot program [224] and screened against the database. Results are shown in figure 5.19.

```
        10         20         30         40         50         60
MSDKIIHLTD DSFDTDVLKA DGAILVDFWA EWCGPCKMIA PILDEIADEY QGKLTVAKLN

        70         80         90        100        110        120
IDQNPGTAPK YGIRGIPTLL LFKNGEVAAT KVGALSKGQL KEFLDANLAG SGSGHMHHHH

       130        140        150        160        170        180
HHSSGLVPRG SGMKETAAAK FERQHMDSPD LGTDDDDKAI SPSSVEDTMS LLECLGQIRS

       190        200        210        220        230        240
LLIVQMGPQE ENLMIQSIGN IMNNKVFYQH PNLMRALGMH ETVMEVMVNV LGGGESKEIR

       250        260        270        280        290        300
FPKMVTSCCR FLCYFCRISR QNQRSMFDHL SYLLENSGIG LGMQGSTPLD VAAASVIDNN

       310        320        330        340        350        360
ELALALQEQD LEKVVSYLAG CGLQSCPMLV AKGYPDIGWN PCGGERYLDF LRFAVFVNGE

       370        380        390        400        410        420
SVEENANVVV RLLIRKPECF GPALRGEGGS GLLAAIEEAI RISEDPARDG PGIRRDRRRE

       430        440        450        460        470        480
HFGEEPPEEN RVHLGHAIMS FYAALIDLLG RCAPEMHLIQ AGKGEALRIR AILRSLVPLE

       490        500
DLVGIISLPL QIPTLGKDGA LVQPKSLRRPALQHHHHHH
```

Figure 5.19 Coverage obtained from liquid digestion of R2452W mutant RYR1 cleaved protein.

The blue sequence indicates the sequence for the 13 kDa fragment whereas the red sequence indicates the peptides found within the 37 kDa fragment. Orange highlighted amino acids indicate the beginning and end of the RYR1 protein domain.

Coverage of the trypsin-digested RYR1 protein band was not 100 % of the full-length protein and the exact position of autoproteolysis occuring is not clear. Results showed that the protein sequence matches the RYR1 central domain. Matched fragments showed discontinuous coverage from amino acid 164-498 of RYR1, within construct 3 in the pET32a(+) vector, which spreads across the entire cloned RYR1 region covering ~35 % of the entire RYR1 sequence (the start and finish of the RYR1 sequence is indicated by highlighting the corresponding amino acid in figure 5.19 orange). Results also revealed that this cleaved RYR1 protein still contains the region of interest, the DP4 domain including the R2452W mutation. Again, amino acids not highlighted in red could not be detected using MS-MS, maybe because of their small size or a low signal intensity to be able to be detected above the background signal.

These results give an approximate estimation of the nature of the 37 kDa band and show that the overexpressed RYR1 protein sequence is still intact and could be used for further studies. The RYR1 protein sequences for the fusion and enterokinase-cleaved protein were analysed using the computer software Expasy Peptide cutter and the ProP1.0 Server and Mobyle Portal digest program to detect different protease cleavage sites but none of the theoretically obtained protein fragments matched the 37 kDa fragment in this study. Therefore the cleavage site cannot be predicted.

Interestingly, purified pET32a(+) vector tags showed the same phenomena as the RYR1 fusion protein. The tag has been cleaved into smaller fragments within 3 days after purification. The exact mass has been determined using MS and resulted in two species with masses of 12699.79 and 12836.73 Da. The masses were similar to that detected for the N-terminal part of the spontaneously cleaved RYR1 fusion protein (13197.32 Da) and only differed by ~400 Da. This suggests similar cleavage sites for proteolysis of protein expressed from the vector backbone. In addition, cleavage of protein representing the empty vector appeared to be more rapid compared to the RYR1 fusion protein (days vs. weeks) indicating that the N-terminal cleavage site may not be easily accessible to proteases when part of the RYR1 fusion protein.

5.4 Discussion

The aim of this study was to clone and express the RYR1 central domain for structural studies and subsequently to infer potential effects of mutations that occur within this region and cause MH. The sequence of the central domain was analysed *in silico* prior to primer design and subsequent cloning. Two different vectors were used and soluble protein was obtained for purification, however insufficient quantities of pure protein were obtained for crystallisation purposes. Secondary structure and thermal stability were analysed using CD.

5.4.1 Bioinformatics

Bioinformatic analysis predicted that the cloned RYR1 central domain contained mostly α-helical structure and the introduction of the R2452W does not significantly influence its secondary structure (table 5.1). The predicted α-helical regions do not appear to be affected by the introduction of R2452W but the percentage of β-sheets is predicted to decrease by ~0.2 % while random coils are increased. Therefore, theoretically the R2452W mutation should not induce a major overall secondary structure change in this RYR1 domain.

The Phyre^2 software uses homology domains as templates and returned similar results to the Mobyle Portal for the RIH homology domain between aa 84 and 174 in RYR1 pET32a(+) construct 3. One major difference can be identified at position 2225 in the Mobyle portal prediction where this software predicts a turned motif including 30 amino acids whereas the Phyre^2 homology domain suggests another α-helical domain. Sequence alignments carried out by Pontig et al. between the two RIH domains of RYR1 and IP3R showed an α-helical domain structure with 80 % consensus [77]. It has to be kept in mind that secondary structure will always be in doubt until the actual 3D crystal structure has been solved. Since there are two RIH domains within RYR1, and with a >80 % sequence identity defined using sequence alignments by Ponting et al., it is likely that both RYR1 regions might have the same structure and folding, even though this homology domain was not identified by the Phyre^2 program [77]. Both softwares predict the location of the R2452W mutation within an α-helix motif. This prediction agrees with the NMR structure of the DP4 domain, indicating that the R2452W mutation is located within the first helix of the helix-turn-helix motif [87].

In 2010, the N-terminal RYR1 crystal structure at 2.5 Å including amino acid residues 1-559 was reported [84]. When comparing the predicted secondary structure published by CP Ponting's RIH alignment [77] and the structure published in 2010, the prediction matched the actual structure for the RYR1 N-terminus. Tung et al. [84] showed that RYR1 amino acid residues 466–532 (corresponding to RYR1 2186–2242 in the central part of RYR1) form three

major α-helices spanning most of the structure (see figure 5.20). Therefore, it is likely that the structure predicted by Ponting's RIH alignment represents the actual secondary structure.

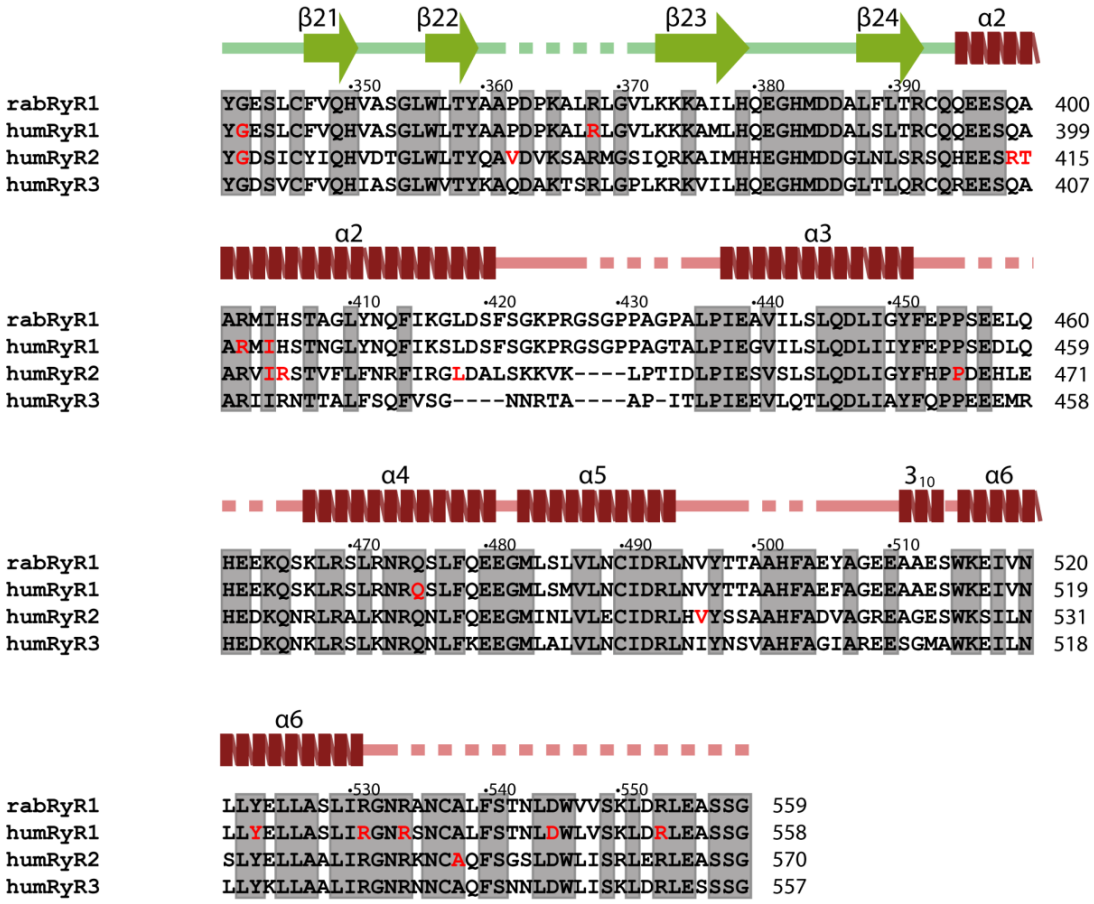

Figure 5.20 Sequence alignment of the N-terminal region of rabbit and three human RYR isoforms.

Grey shaded areas correspond to conserved residues; red residues indicate reported disease mutations. The position of the amino acid residues is shown on the right-hand side. Secondary structure elements are indicated with arrows for β-strands and coils for α-helices. Residues in loops are shown by a full line; residues not visible in the electron density map are indicated by dotted lines [84] (Permission for reproduction obtained through RightsLink).

5.4.2 Cloning and expression tests for the RYR1 central domain

pc*RYR1* and pc*RYR1*-R2452W cDNA were used as templates to amplify four central domain regions which slightly differ in their amino acid residues. Since no 3D structure for the RYR1 central domain is known, it is uncertain where protein domains are located and whether overexpression of only part of these domains might yield insoluble protein. Four different constructs for both WT and R2452W *RYR1* cDNA were PCR amplified and cloned into two

different expression vectors. Overexpression of the constructs yielded soluble protein only for constructs cloned into the pET32a(+) vector. All constructs cloned into pProExHtb yielded insoluble protein when expressed in *E. coli*. This might be due to the different tags used by each vector. pET32a(+) contains, among other purification tags, a thioredoxin-tag which enhances protein solubility, while pProExHtb expresses only a His_6-tag for protein affinity chromatography. The pET32a(+) vector has been successfully used in previous studies to purify and crystallise the N-terminal RYR1 domain [76]. Expression optimisation yielded soluble RYR1 protein when overexpressed at low temperatures (16-20 °C) for 3 h but no soluble protein was obtained when expressed at temperatures above 28 °C, suggesting misfolding. The use of an *E. coli* expression system containing the chaperones GroEL/ES was able to increase the expression of soluble protein even further, indicating GroEL/ES enhances proper folding of overexpressed RYR1.

5.4.3 Purification of overexpressed RYR1 protein

Purification and protein binding to Ni^{2+}-NTA resin of the RYR1 fusion were optimised in order to prevent unspecific binding of GroEL/ES to the RYR1 protein. The addition of 10 mM ATP to the soluble protein solution yielded relatively pure RYR1 protein while minor contamination due to residual GroEL binding still occurred.

Cleaved RYR1 protein tended to attach to size exclusion matrix or plasticware used and therefore was difficult to work with. Further work was continued with the fusion protein. The aliphatic index of RYR1 fusion and cleaved protein (table 5.4) showed similar values for the fusion and the cleaved protein. Both indices were quite high (compared to neutral proteins with an aliphatic index of 80), therefore suggesting high hydrophobicity. The tag may influence the folding of the fusion protein so that the hydrophobic regions are within the protein and are therefore not exposed to the surface, preventing it from interaction with surfaces or plasticware.

Using size exclusion, His_6trap-purified fusion protein was eluted at low elution volumes, indicating that the protein probably exists as an oligomer. Since the

RYR1 protein fusion domain eluted quite early, it is not easy to predict the exact size of this oligomer since the column has a logarithmic elution pattern meaning that even small differences in elution volume can result in a large mass difference. Using calibration standards it was concluded that the protein appears to form a tetramer of non-globular protein domains agreeing with findings that full-length RYR1 forms a homo-tetramer under native conditions [215]. Size exclusion experiments in this study were repeated several times and always showed elution of the RYR1 domain at low volumes. The empty vector tag proteins were also overexpressed and subsequently purified. They were eluted as two peaks on the S200 column where the main peak represented a dimer and the minor peak a monomer, eluting as 70 and 30 kDa proteins, respectively. Since the tag itself forms a dimer, it is possible that the tag is responsible for oligomerisation of the RYR1 domain. The RYR1 fusion protein eluted as a broad peak at 10 mL, corresponding to a theoretical size of 440 kDa. If the RYR1 fusion protein exists as a dimer, higher elution volumes would be expected due to a smaller protein mass of ~110 kDa. It has to be kept in mind however, that size exclusion also separates according to the shape of the protein and calibration curves are therefore not always accurate in predicting a protein's actual size.

Tung et al. [84] showed size exclusion results using a HiLoad 16/60 Superdex 200 prep grade (GE Healthcare) to purify the N-terminal domain (amino acids 1-559) of the full-length RYR1 and the resultant polypeptide was eluted at ~70 mL, suggesting a 1.5 mer indicating a non-globular protein running as a monomer (data from personal communication with F. Van Petegem). Since this column was not available in this study, a direct comparison cannot be made but these observations suggest that the central domain could be involved in oligomerisation while the N-terminal exists as a monomer. Comparing the data obtained in this study with studies undertaken by Tung et al. [84], it is possible that parts of the overexpressed RYR1 central domain protein are indeed responsible for RYR1 oligomerisation.

Another explanation for the low elution volume of the RYR1 domain could be that this protein is not shaped as a globular protein but has a larger effective

radius and therefore eluted early. Taking into account that the expressed protein domain should elute as a monomer of 57 kDa in size, it is unlikely that a 57 kDa monomer would run with an appearant mass above 400 kDa. Blayney et al. published antibody binding assays in 2004 showing region 2540-3207 in full-length RYR1 are likely to be involved in an RYR1-RYR1 interdomain interaction [60]. This result was further supported by Yin et al. in 2005, where cryo-EM structures revealed that the outermost region of subdomain 6 is involved in physical coupling of RYR oligomers [225]. Popova et al. were able to link specific amino acid residues to the 3D structure of RYR1 tetramers. Figure 5.21 shows that amino acid residues P1107-A1121 (2), A1368 (3) and N2756-E2803 (7) are linked to sub domain 6 (grey numbers), involved in inter RYR1 domain interaction.

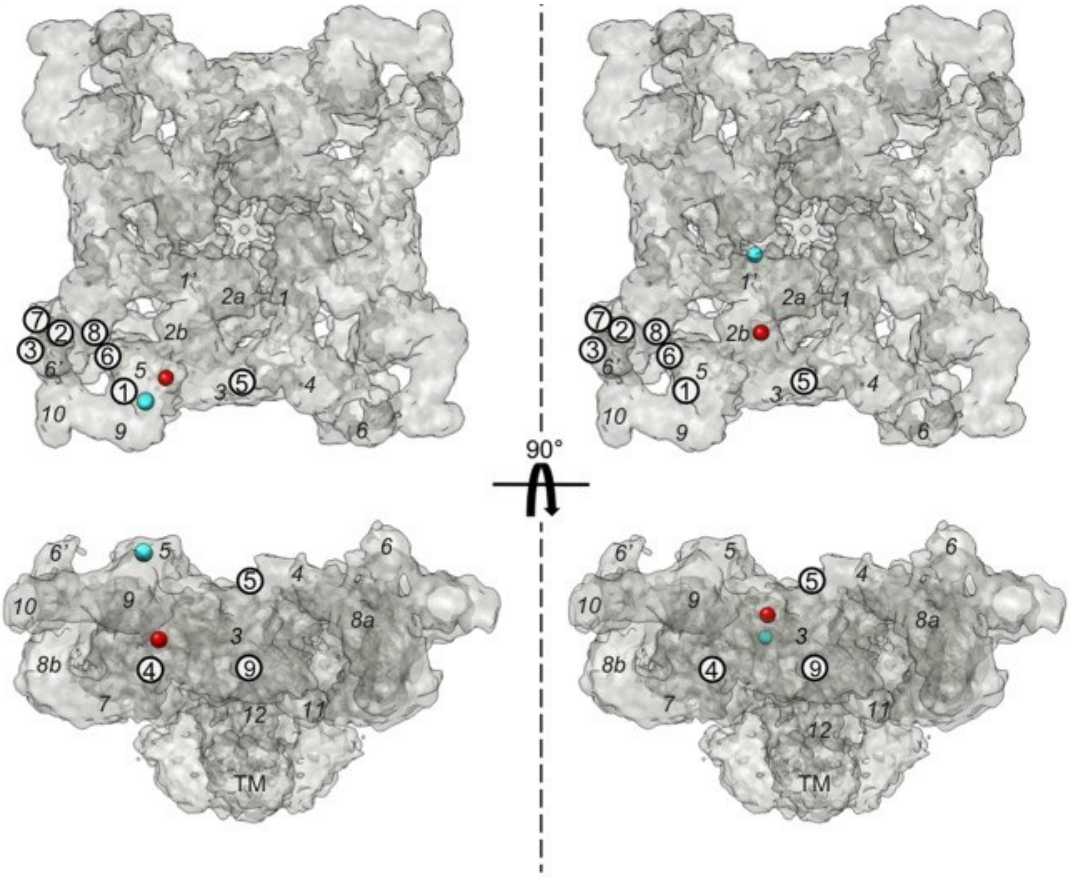

Figure 5.21 Localisation of specific residues in the 3D structure of the RYR1 oligomer.
RYR1 is shown as a 3D model and amino acid positions in the rabbit RYR1 protein are highlighted using encircled numbers: 1=S422, 2=P1107-A1121, 3=A1368, 4=E1893, 5=S2058, 6=R2399, 7=N2756-E2803, 8=K2836 9=4408. Furthermore, RYR1 domains are highlighted as grey italic numbers as well as the transmembrane domain (TM) ([83], no copyright permission needed).

Since the full crystal structure for this region has not yet been solved, it can only be speculated that the DP4 domain might be located in subdomain 6 and therefore oligomerises, since residue R2399 (6) is located between sub domain 5 and 6 (for numbering refer to figure 5.21). Residue A1368 is also aligned to subdomain 6 and might therefore be another candidate for RYR1-RYR1 interaction. RYR1 amino acid R2399 (figure 5.21, 6) is included in the protein domain overexpressed in this study and while linked to sub domain 6, it suggests involvement of the DP4 domain in oligomerisation, supporting size exclusion studies.

Yuchi et al. (2012) obtained a crystal structure for RYR1 region 2896-2915 which was mapped to RYR1 subregion 10 at close proximity to subregion 6 [195] (see figure 5.21). The supplementary material showed results for size exclusion studies and reveals that this domain exists as a monomer, suggesting those 20 amino acids are not involved in oligomerisation.

Furthermore in 2004, Blayney et al. showed that the peptides corresponding to the 34C antibody binding site (aa 2872–2893) are most likely involved in RYR-RYR oligomeric interaction. Using GST-pulldown assays they were able to demonstrate binding of these regions to full-length RYR1 protein, indicating binding of two domains [60]. These assays also support the hypothesis that the central domain might be involved in RYR1-RYR1 oligomerisation and “domain-zipping”.

The results from the current study suggest that DP4 domain is localised within domain region 6 and provides supporting evidence that the region expressed in this study could be involved in interdomain interaction.

It has been suggested that the transmembrane domains at the C-terminus were involved in oligomerisation of the IP3R [226]. This domain is homologous to the RYR1 sequence between amino acids 4938-5038 [199]. Similar studies have not been conducted for RYR1 to date, but since IP3R and RYR1 share identity, it is possible that the C-terminal domain in RYR1 is involved in tetramerisation. Only the transmembrane and the C-terminal

domains in IP3R have been investigated for their function in oligomerisation and results suggest that more than one domain is responsible for oligomerisation and stabilisation [227]. Therefore, it is possible that the central domain may play an important part in oligomerisation but further experiments need to be conducted to investigate function for this domain and what part it may play in Ca^{2+} release from the SR.

5.4.4 Stability assays using CD spectra and thermal melting

Due to the high hydrophobicity and potential non-specific adhesion of the cleaved RYR1 domain protein, it was not possible to carry out further analysis including purification. Therefore, work with the only fusion protein was continued, in order to obtain information about structure and stability of the RYR1 central domain peptide. WT and R2452W mutant constructs were purified as well as the vector tags as a control and thermal stability was measured using CD spectra with measurements at temperatures between 5 ° and 90 °C. To verify results, a positive control (lysozyme) was measured to ensure that the known melting temperature of 70 °C could be detected [218]. The melting temperature for lysozyme measured in this study as ~73 °C is similar, within experimental error, and with allowance that different buffer systems may yield slightly different results.

CD spectra of the WT and R2452W mutant RYR1 fusion protein appeared to be similar and the deconvolution reveals almost identical secondary structure. It can be concluded that the R2452W mutation does not have a major effect on the secondary structure of this domain. This result agreed with secondary structure prediction programs suggesting the the α-helix carrying the R2452 residue is not affected by the amino acid substitution. Furthermore, the deconvolution of the CD spectra using the CDNN software predicts a similar percentage of α-helix and β-sheet as predicted with the program used in section 5.2.1. Melting experiments for both constructs show that this particular fusion protein is quite stable, indicating a partially unfolded structure at 40-45 °C. Fifty percent of unfolding occurred at 65 °C for WT and 60 °C for R2452W mutant (figure 5.12). Speculatively, this could indicate that the introduction of the R2452W mutation decreases RYR1 domain stability

because the substitution of arginine (polar, hydrophilic and positively charged) to tryptophan (aromatic, hydrophobic and neutral charge) could result in an interaction between two different domains due to the hydrophobicity of the tryptophan, however data for WT were collected only once and can therefore include a high error. Comparing unfolding results at 209 and 217 nm showed different temperature values but agree with a lower melting temperature for mutant compared to WT. Two CD melting spectra were measured for the R2452W mutant from two individual protein purifications and show similar results for deconvolution. The difference in melting temperature between WT and R2452W mutant is very small and can therefore not be taken as significant. These assays need to be repeated in order to confirm these findings.

5.4.5 Spontaneously cleaved fusion protein

Another interesting factor in this study was the spontaneous cleavage of the RYR1 domain protein. The cleavage did not happen immediately, but over a time period of several weeks. It is possible that the protein might slowly unfold with longer storage, making the protein more accessible to protease activity. Interestingly, the spontaneous cleavage also seems to occur during a time course experiment involving enterokinase cleavage (figure 5.14). The fusion protein sample contains a small amount of the unknwn 37 kDa protein band but once the fusion protein is cleaved with enterokinase into a 40 kDa peptide, the additional 37 kDa fragments is apparent. The enterokinase might have exposed a cleavage site allowing a different protease to cut the 40 kDa protein. Therefore, enterokinase digestion may enhance cleavage leading to a truncated 37 kDa protein. Since the structure is not available, it is difficult to make any assumptions on folding and therefore the occurrence of this cleavage. The 37 kDa protein appears to be very stable since it can be detected even after 6 weeks in solution. It is also still soluble, demonstrated by centrifugation at 100,000 x g for 10 min.

None of the common proteases are predicted to cleave the RYR1 domain protein into an intact 37 kDa fragment. Furthermore the cleaved RYR1 amino acid sequence was analysed *in silico* to investigate whether previous

enterokinase cleavage enhances protease activity and therefore cleavage of RYR1, however no definitive results were found. Therefore, it is not clear whether the 37 kDa fragment is formed by the activity of a protease. MS-MS results revealed that most of the RYR1 protein domain is still intact and that a protease has only cut off a few amino acids at the N and the C-terminus of the RYR1 domain. None of the various *in silico* approaches were able to predict a sequence yielding a similar mass as obtained from intact mass measurements. Therefore whether this was an effect of bona fide proteolysis at a specific site or an artefact of storage remains unclear. Interestingly, the overexpressed N-terminal purification tag showed a similar spontaneous cleavage pattern resulting in a similar exact mass differing by 400 Da (3-4 amino acids), suggesting a preferred cleavage site within the vector-encoded backbone.

When separating the 13 and 37 kDa proteolysis fragments using an HPLC system, the 37 kDa fragment eluted as two species which could be separated by their different hydrophobicities (figure 5.18). When it was analysed by SDS-PAGE, the 37 kDa fragment migrated as one single band. Therefore the nature of the second peak is unclear. Looking more closely at the MS results for the intact mass detection, two peaks are observed for the 37 kDa band while the intensities, and therefore abundances, were different. The minor species had a mass of 37474.67 Da while the major peak yielded a mass of 37741.33 Da. These two peaks differ by 266.7 Da indicating a protein size difference of 2-3 amino acids. This result agrees with the HPLC finding since the major peak appeared at 21.6 min while the absorbance of a minor peak (eluted at 19.6 min) indicates a lower protein concentration. Similar abundances were obtained by analysing the mass of the proteolysed fusion protein, showing that the major peak is 4 times as high/more abundant compared to the minor peak, indicating a mass of 37741.33 Da (see appendix XIV). Therefore, it can be concluded that the 37 kDa fragment seems to contain two protein species with a much higher abundance of the 37474.67 Da fragment which might be highly hydrophobic.

5.4.6 Crystallisation

Crystallisation trials were planned for this study but because of low RYR1 protein amounts could not be undertaken. For crystallisation experiments, initial protein concentrations of ~2 mg/mL need to be obtained in order to try several different conditions. In order to yield well diffracting crystals, many different crystallisation conditions may need to be trialled, as well as different protein concentrations, since every protein behaves differently in different conditions. Since the RYR1 N-terminus [76], as well as the RYR1 phosphorylation domain [195], have been crystallised these conditions may be used as a starting point in crystallisation trials for the RYR1 central domain and may produce diffracting crystals.

In summary, results obtained in the current study suggest the RYR1 domain from amino acids 2144-2489 can be expressed as soluble protein and subsequently purified using an His_6-tag. Purification using size exclusion gives an indication that the central domain may exist as an oligomer while the elution volumes suggests that the protein might be a possible tetramer. As a control, the empty affinity tag of the expression vector was also purified using gel filtration and it suggests that this tag is involved in oligomerisation of the overexpressed RYR1 protein. Nevertheless, the elution volume of the RYR1 protein domain is quite high which indicates further oligomerisation obtained by the protein itself. This finding may be supported by data from Popova et al. [83] who mapped amino acid residues close to the central domain to the periphery of RYR1 into subunit 6, which might be involved in interdomain interactions as well as studies by Blayney et al. who showed peptides around amino acid 2880 are involved in RYR1-RYR1 interaction [60]. Further studies involving the RYR1 domain without the N-terminal tag need to be undertaken, in order to verify involvement in protein interaction and stability. Nevertheless, the limited results obtained in this part of the study are consistent with the literature and give a further indication of the importance of the RYR1 central domain in terms of protein structure.

CD spectrometry measures secondary structure and therefore folding of the overexpressed RYR1 protein. In this study a putative secondary structure

change was detected which may lead to a lower melting temperature of the R2452W mutant RYR1 construct compared to WT. These results could explain the lower 4CmC agonist threshold leading to the channel activation since the overall energy to open the channel is reduced due to amino acid changes in this region, leading to a channel with a lower energy barrier for channel opening. This study provides additional information about the significant importance of the central domain of ryanodine receptors and its involvement in oligomerisation of the channel tetramer, as well as channel opening and closing.

Chapter 6 Summary and future directions

6.1 Functional assays

Three different cell types were used to study functional effects of a single ryanodine receptor 1 mutation previously linked to MH. Functional assays were carried out using B-lymphoblastoid cells, myotubes and HEK293 cells transfected with human *RYR1* cDNA using Ca^{2+} release from the ER/SR monitored by fura 2 fluorescence emission. In all experimental systems, R2452W altered Ca^{2+} release leading to a higher amount of Ca^{2+} released from the SR/ER, making it a hypersensitive receptor in response to 4CmC, compared to cells expressing WT RYR1. Moreover, this phenotype was observed in two unrelated families indicating that under the current EMHG guidelines, the *RYR1* R2452W mutation could be classed as causative of MH.

The R2452W mutation is located in the central region of RYR1 (also known as "hot spot" region 2) which has been suggested to play a crucial role in opening and closing of the receptor [85]. Compared to WT, RYR1 carrying this mutation was activated to release Ca^{2+} at lower concentrations of the agonist 4CmC. Therefore, any of the three systems could have been used to detect altered Ca^{2+} release from the SR and thus be used to predict causation of MH. This may not necessarily apply to all *RYR1* mutations. Amino acid variants may have different functional effects depending on their localisation within RYR1. As well as being a tetramer, with a membrane-bound C-terminal region, RYR1 also interacts with several proteins in the cytosol, in the SR lumen and within the membrane itself [69].

Ca^{2+} release assays using B-lymphoblastoid cells for patients U1 and U2 gave identical results to cells isolated from MHN patients. It is currently not known if either patient U1 or U2 carries a mutation in *RYR1*, however both were diagnosed MHE_h by IVCT. Ca^{2+} release assays using myotubes showed a MHS phenotype for patient U1 while myotubes from patient U2 gave ambiguous results. Ca^{2+} release in myotubes from a MHS patient with an unknown mutation has been measured and demonstrated a positive phenotype. This result provides a positive control showing that MHS patients diagnosed by IVCT

show altered Ca^{2+} release in myotubes. Patient U1 showed altered Ca^{2+} release in myotubes which suggests that this patient may carry a mutation altering Ca^{2+} release in muscle cells. Since Ca^{2+} release results for patient U2 are equivocal, as were results for the IVCT, no further prediction can be made regarding the MH status.

In this study, 4CmC was the only agonist used to stimulate RYR1 because it is more soluble than caffeine and more specific to RYR1. Caffeine is known to non-specifically activate RYR3 in muscle cells [100] and could therefore be a confounding factor in analysis of RYR1 activated Ca^{2+} release. Halothane could also be used as an agonist but this would require a vapour delivery system and closed environment monitoring which were not available. Some mutations appear to affect RYR1 activation by disrupting depolarisation rather than altered response induced by chemical agonists. To effectively assess this type of mutation for association with MHS, excitable cells would need to be used in the presence of a depolarising agent, K^+ or an electrical impulse. The latter is preferable as response to K^+ can be non-specific and response may be very small. Electrophysiology equipment was not available in the current study but could be used in future work to investigate mutations in *RYR1* that do not appear to result in a response to chemical agonists in myotubes. It is also possible that patient U2 carries a mutation at a site that is crucial for 4CmC binding, making it insensitive to 4CmC activation but cells may still react to different agonists like caffeine or halothane. Future studies should therefore be carried out using a range of different RYR1 agonists. The relative concentrations of Ca^{2+}, K^+ and Mg^{2+} may also be important as a lower Mg^{2+} level may result in altering of the channel function [166]. The ion concentration in the SR needs to be tightly regulated in order for RYR1 to function properly. If a mutation affects the ion flow within the cell, RYR1 could become less responsive to agonist activation.

Specific *RYR1* mutations, e.g. the rabbit R4892W variant expressed in dyspedic myotubes that lack functional RYR1, have been shown to have almost no activation by 4CmC or depolarisation but the mutant receptor showed full activation with caffeine [112]. Interestingly, the corresponding mutation in

human R4893W, derived from CCD patients, showed reduced activation for K^+-induced depolarisation as well as for 4CmC, but only slightly reduced activation by caffeine compared to WT [151]. It seems plausible that a given mutation may give rise to different Ca^{2+} release behaviour, depending on the system/cell in which it is expressed. Since dyspedic myotubes are available, these could be used in further studies to determine the mechanism underlying EC coupling, as well as excitation-coupled Ca^{2+} release (ECCE). ECCE plays an important role in myotubes only and is a response to membrane depolarisation. It requires the expression of α_{1s}-DHPR and therefore transfections of HEK293 cells or Ca^{2+} release measurements using B-lymphoblastoid cells may miss abnormal reactions caused by either *RYR1* mutations or other proteins involved in EC coupling. Myotubes carrying the R163C mutation showed enhanced ECCE which may be a risk factor for MH [33]. This phenomenon can only be seen in myotubes and might therefore not be apparent when using cells other than muscle cells, making transfections using dyspedic myotubes a more relevant physiological system to study *RYR1* mutations. Abnormal Ca^{2+} induced Ca^{2+} release (CICR) has also previously been linked to MH [228]. Again, if a mutation alters CICR and leads to MHS, the use of dyspedic myotubes would be the preferred system for investigation since this effect does not occur in cells other than muscle cells.

In order to exclude mutations in *RYR1* for patients U1 and U2, their cDNA needs to be fully sequenced. If no causative mutation can be found in *RYR1* or *CACNA1S*, whole RNA or exome sequencing could be carried out to find an MH causative mutation, provided that sufficient other family members could be identified for segregation analysis purposes.

It is possible that patients U1 and U2 may carry *RYR1* variants which do not affect the receptor itself, but affect the RYR1 binding to other proteins involved in EC coupling. Therefore, the receptor may not show altered Ca^{2+} release in B-lymphoblastoid cells or in transfected HEK293 cells when activated with 4CmC, since the necessary muscle proteins are not expressed in those cells. If a mutation was identified in *RYR1*, it could be introduced into human full-length *RYR1* cDNA by mutagenesis PCR. The construct could then be used to

transfect dyspedic myotubes. If HEK293 cells transfected with a specific variant in *RYR1* show no altered Ca^{2+} release but transfected myotubes do, then the mutation could affect protein binding to RYR1 which may be important for EC coupling and therefore may disturb signal transduction in myotubes. Several amino acid substitutions not found in patients were introduced in the rabbit RYR1 central domain e.g. G2373A and S3939A (corresponding to G2373A and S3937A in human), leading to a hyposensitive RYR1 when expressed in HEK293 cells [153] similar to a MHN phenotype. Expressing these mutations in dyspedic myotubes may help to understand the effect these mutations may have upon abnormal Ca^{2+} homeostasis since RYR1 interacting skeletal muscle proteins are expressed. This may provide new knowledge about protein-protein interaction in skeletal muscle.

Furthermore, it is possible that patient U2 does not have an MH phenotype but rather has a CCD phenotype. CCD mutations can show a hyposensitive reaction to RYR1 triggering agents while releasing less Ca^{2+} from the SR/ER. Histology could have been done after the IVCT was performed in order to determine irregularities in the muscle fibers and show the presence of cores. Unfortunately, histological examination was not carried out at the time of the muscle biopsy.

Knock-in mice are a further useful system to study the effect of *RYR1* mutations *in vivo.* Mutations can be controllably expressed in homo- or heterozygous forms and potentially lethal effects of mutations can be observed. Using knock-in mice can also help to determine phenotypes other than altered Ca^{2+} release. The rabbit *RYR1*$^{I4895T/WT}$ knock-in mouse (corresponding to the human I4898T mutation) was used to show a neuronal phenotype as well as excluding this mutation as a causative factor for MH susceptibility [229, 230]. It has been speculated for quite some time that *RYR1* mutations can affect the immune system since >300 *RYR1* mutations have been reported and *RYR1* is also expressed in primary immune-cells, B-lymphocytes [180]. Knock-in mice, expressing a specific RYR1 mutation, could be a useful tool for immune studies by comparing the immune response of WT and mutant *RYR1* animals.

Mutations in *RYR1* may lead to a gain of function and enhanced immune response in carrier individuals.

6.2 Structural characterisation of the RYR1 central domain

Overexpression of the RYR1 central domain (amino acid 2144-2489) yielded sufficient soluble protein to investigate some physical properties of this domain. Size exclusion studies revealed that the protein domain possibly oligomerises, forming a tetramer. The expressed N-terminal tag protein also showed oligomerisation, however it is not clear whether the oligomerisation occurs due to the tag protein, or due to the RYR1 protein actually being involved in a RYR1-RYR1 interaction. Collectively, results suggest the N-terminal tag protein most likely forms a dimer with a size of 70 kDa whereas the RYR1 fusion protein forms a non-globular tetramer of 440 kDa. Therefore, oligomerisation due to the RYR1 protein itself is a possibility.

To further confirm these findings, enterokinase cleavage of the N-terminal tag from the overexpressed RYR1 fusion protein needs to be optimised to prevent non-specific interactions between protein and chromatography material or plasticware. This would facilitate further analysis by size exclusion and CD spectrometry, together with thermal melting experiments, to help confirm the data obtained with the fusion protein.

Results from gel filtration experiments suggest that the overexpressed RYR1 fusion protein may be a non-globular protein. To further investigate the overall shape of this domain, small angle X-ray scattering could be performed. This method can be used to investigate shape and size of a folded protein in solution as well as any oligomerisation properties. NMR has been previously used to determine the structure of the DP4 domain [87] and could be used to determine the structure of the central domain overexpressed in this study. As NMR is performed on protein in solution, it is not limited to crystallised protein although the RYR1 region may be too large for NMR studies since the upper size limit is ~20-30 kDa but in some cases has been extended to 100 kDa [231]. Nevertheless, it may be possible to gain information about structural dynamics

and flexibility of a protein and make predictions about potential protein-protein interactions.

Purification of the RYR1 fusion protein domain has been optimised and sufficient soluble protein was obtained for CD analysis. A minimum of 2 mg purified protein would be required for crystallisation trials. Using the purification method optimised in this study, a culture volume of 20 L from separate 150 mL culture volumes of induced *E. coli* would be required to yield sufficient protein, when purified in smaller batches due to insolubility at higher protein concentrations. This is certainly feasible and a crystal structure would give valuable insight into the structure of the central domain and could indicate whether or where domain interaction occurs. The 3D structure could be docked onto the cryoEM structure [53] to predict the actual position of the region in the tetrameric unit. This would also be useful in predicting any role for a RYR1-RYR1 interaction. Crystallisation experiments may be more successful using the cleaved RYR1 protein since the N-terminal tag of the RYR1 fusion protein contains 120 amino acids, which could interfere with either crystallisation or the actual 3D structure. Different detergents e.g. non-ionic (β-octylglucoside) or nondenaturing zwitterionic detergents (CHAPS) could be used to prevent non-specific adhesion of cleaved RYR1 protein during purification.

Green fluorescent protein (GFP) could be introduced behind the R2452 residue in the full-length human RYR1 protein and be used for overexpression in mammalian cells and subsequently for cryoEM studies as previously carried out by Liu et al. [81]. This would allow determination of the position of the R2452 residue in the 3D tetrameric protein. The introduction of GFP behind several different residues in pc*RYR1* may allow localisation of the residues in the 3D structure and determine whether the DP4 domain is located in subdomain 6 and therefore involved in domain interaction. Furthermore, GFP labelled residues could be mutated and be used for cryoEM structural studies to determine whether different mutations could change the 3D localisation of the residues or abolish oligomerisation.

It has been suggested that the central and N-terminal domain may interact to

form a “domain-zipper” [85]. The crystal structure of the N-terminal domain is known, as well as the purification and crystallisation conditions and the full-length human *RYR1* cDNA is available. Therefore the two domains could be expressed and purified separately and then used in binding, as well as interaction, assays and size exclusion chromatography. If the two domains interact the proteins would be eluted from the column as one peak, indicating an interaction. Due to the presumed domain interaction, the cleaved RYR1 central domain, bound to the N-terminal domain protein, may be less non-specifically adhesive to column material since hydrophobic amino acids may be involved in interdomain interactions and would not be surface exposed.

Mutagenesis can be used to introduce further MH-associated mutations into the cloned RYR1 central domain protein. CD could help to determine secondary structure changes due to the introduction of mutations while some mutations might lower the melting temperature of the RYR1 protein even further. In mutating hydrophobic amino acids, the overall hydrophobicity might be lowered, preventing the N-terminal cleaved protein from being adhesive. Mutated proteins can further be used in peptide domain binding studies, including the N-terminal RYR1 domain, to see whether one particular amino acid is important for interaction.

Co-immunoprecipitation studies using RYR1 central domain polypeptides including the 34C antibody binding site could be performed to see whether this domain can pull down other RYR1 domains including the N- or C-terminus. Co-immunoprecipitation would give valuable insights into interprotein interactions.

Förster/Fluorescence Resonance Energy transfer (FRET) studies could also be performed to investigate binding between different domains as previously described [232]. Fluorescent acceptor and donors need to be introduced into overexpressed proteins and when both proteins come in close proximity, energy between them will be transferred which can be visualised using a fluorescence microscope or spectrofluorometer. Furthermore, mutations can be introduced into the different RYR1 peptides to see whether these mutations abolish interaction. This system could also be used to determine binding of RYR1 and

other proteins involved in EC coupling. The introduction of MH causative mutations may help to determine if mutations abolish protein-protein interactions leading to a MH phenotype [233].

In summary, little is known about the structure/function relationship in RYR1 leading to the MH phenotype. It is understood that certain mutations lead to a disruption of protein-protein interactions and therefore alter Ca^{2+} release from the SR due to a loss of negative feedback regulation. *RYR1* mutations are also thought to disturb interprotein interactions leading to a leaky channel phenotype because the Ca^{2+} channel cannot close properly. Many proteins are involved in RYR1 binding and EC coupling, making it challenging to determine the cause of MH reactions. Only 50-70 % of MHS patients show mutations in RYR1, suggesting other proteins involved in EC coupling could be responsible for this phenotype. Performing functional assays to determine altered Ca^{2+} release, induced by different mutations, is important to link mutations to MH and offer DNA-based testing. It has been suggested MHS patients could be diagnosed by DNA testing instead of using the “gold standard” IVCT. At this stage this approach can only be performed for families with a known MH causative mutation. If no mutation in *RYR1* can be identified in families with a known MH background, IVCT must still be performed in order to prevent an MH episode under surgery or even under stress or physical exercise. DNA-based testing is preferable for diagnosis of MH susceptibility since IVCT is a very invasive method compared to obtaining a patient blood sample, however more research needs to be carried out to understand the function and structure of RYR1 and EC coupling in order to replace IVCT. Over 30 proteins are involved in EC coupling and any of these proteins could carry a mutation, leading to a MHS phenotype. Functional assays need to be performed for all MH-associated mutations in order to include them in the list of MH causative mutations and subsequently use DNA based testing for clinical diagnosis. This study described functional assays for the R2452W mutation which showed altered Ca^{2+} release and a more sensitive channel to 4CmC activation. Therefore, this mutation can be added to the list of MH causative mutations, making replacement of the IVCT by DNA-based diagnosis one step closer for families known to carry the R2452W mutation.

Chapter 7 References

1. Levano, S., et al., *Increasing the number of diagnostic mutations in malignant hyperthermia.* Hum Mutat, 2009. **30**(4): p. 590-8.
2. Avila, G., *Intracellular Ca^{2+} dynamics in malignant hyperthermia and central core disease: established concepts, new cellular mechanisms involved.* Cell Calcium, 2005. **37**(2): p. 121-7.
3. Britt, B.A. and W. Kalow, *Malignant hyperthermia: a statistical review.* Can Anaesth Soc J, 1970. **17**(4): p. 293-315.
4. Monnier, N., et al., *Presence of two different genetic traits in malignant hyperthermia families: implication for genetic analysis, diagnosis, and incidence of malignant hyperthermia susceptibility.* Anesthesiology, 2002. **97**(5): p. 1067-74.
5. Ibarra, M.C., et al., *Malignant hyperthermia in Japan: mutation screening of the entire ryanodine receptor type 1 gene coding region by direct sequencing.* Anesthesiology, 2006. **104**(6): p. 1146-54.
6. Brown, R.L., et al., *A novel ryanodine receptor mutation and genotype-phenotype correlation in a large malignant hyperthermia New Zealand Maori pedigree.* Hum Mol Genet, 2000. **9**(10): p. 1515-24.
7. Pollock, A.N., et al., *Suspected malignant hyperthermia reactions in New Zealand.* Anaesth Intensive Care, 2002. **30**(4): p. 453-61.
8. Anderson, A.A., et al., *Identification and biochemical characterization of a novel ryanodine receptor gene mutation associated with malignant hyperthermia.* Anesthesiology, 2008. **108**(2): p. 208-15.
9. EMHG. *List of causative MH mutations*. 2012 [cited 2012 December].
10. Jurkat-Rott, K., T. McCarthy, and F. Lehmann-Horn, *Genetics and pathogenesis of malignant hyperthermia.* Muscle Nerve, 2000. **23**(1): p. 4-17.
11. Ball, S.P. and K.J. Johnson, *The genetics of malignant hyperthermia.* J Med Genet, 1993. **30**(2): p. 89-93.
12. Balog, E.M., et al., *Divergent effects of the malignant hyperthermia-susceptible Arg(615)-->Cys mutation on the Ca^{2+} and Mg^{2+} dependence of the RyR1.* Biophys J, 2001. **81**(4): p. 2050-8.
13. Ward, A., M.O. Chaffman, and E.M. Sorkin, *Dantrolene. A review of its pharmacodynamic and pharmacokinetic properties and therapeutic use in malignant hyperthermia, the neuroleptic malignant syndrome and an update of its use in muscle spasticity.* Drugs, 1986. **32**(2): p. 130-68.
14. Denborough, M., *Malignant hyperthermia.* Lancet, 1998. **352**(9134): p. 1131-6.
15. Group, E.M.H., *A protocol for the investigation of malignant hyperpyrexia (MH) susceptibility. The European Malignant Hyperpyrexia Group.* Br J Anaesth, 1984. **56**(11): p. 1267-9.
16. Ording, H., et al., *In vitro contracture test for diagnosis of malignant hyperthermia following the protocol of the European MH Group: results of testing patients surviving fulminant MH and unrelated low-risk subjects. The European Malignant Hyperthermia Group.* Acta Anaesthesiol Scand, 1997. **41**(8): p. 955-66.
17. Ording, H., *Diagnosis of susceptibility to malignant hyperthermia in man.* Br J Anaesth, 1988. **60**(3): p. 287-302.
18. Fletcher, J.E., H. Rosenberg, and M. Aggarwal, *Comparison of European and North American malignant hyperthermia diagnostic protocol*

outcomes for use in genetic studies. Anesthesiology, 1999. **90**(3): p. 654-61.
19. Klip, A., et al., *Anaesthetic-induced increase in ionised calcium in blood mononuclear cells from malignant hyperthermia patients.* Lancet, 1987. **1**(8531): p. 463-6.
20. Klip, A., et al., *Selective increase in cytoplasmic calcium by anesthetic in lymphocytes from malignant hyperthermia-susceptible pigs.* Anesth Analg, 1987. **66**(5): p. 381-5.
21. Waldron-Mease, E., et al., *Malignant hyperthermia in a halothane-anesthetized horse.* J Am Vet Med Assoc, 1981. **179**(9): p. 896-8.
22. Roberts, M.C., et al., *Autosomal dominant canine malignant hyperthermia is caused by a mutation in the gene encoding the skeletal muscle calcium release channel (RYR1).* Anesthesiology, 2001. **95**(3): p. 716-25.
23. de Jong, R.H., J.E. Heavner, and D.W. Amory, *Malignant hyperpyrexia in the cat.* Anesthesiology, 1974. **41**(6): p. 608-9.
24. Berchtold, M.W., H. Brinkmeier, and M. Muntener, *Calcium ion in skeletal muscle: its crucial role for muscle function, plasticity, and disease.* Physiol Rev, 2000. **80**(3): p. 1215-65.
25. Fujii, J., et al., *Identification of a mutation in porcine ryanodine receptor associated with malignant hyperthermia.* Science, 1991. **253**(5018): p. 448-51.
26. Berridge, M.J., P. Lipp, and M.D. Bootman, *The versatility and universality of calcium signalling.* Nat Rev Mol Cell Biol, 2000. **1**(1): p. 11-21.
27. Meissner, G., *Ryanodine receptor/Ca^{2+} release channels and their regulation by endogenous effectors.* Annu Rev Physiol, 1994. **56**: p. 485-508.
28. Cui, Y., et al., *A dihydropyridine receptor alpha1s loop region critical for skeletal muscle contraction is intrinsically unstructured and binds to a SPRY domain of the type 1 ryanodine receptor.* Int J Biochem Cell Biol, 2009. **41**(3): p. 677-86.
29. Inesi, G., et al., *Studies of Ca^{2+} ATPase (SERCA) inhibition.* J Bioenerg Biomembr, 2005. **37**(6): p. 365-8.
30. Avila, G., et al., *FKBP12 binding to RyR1 modulates excitation-contraction coupling in mouse skeletal myotubes.* J Biol Chem, 2003. **278**(25): p. 22600-8.
31. Lamb, G.D. and D.G. Stephenson, *Effects of FK506 and rapamycin on excitation-contraction coupling in skeletal muscle fibres of the rat.* J Physiol, 1996. **494 (Pt 2)**: p. 569-76.
32. Alonso, M.T., I.M. Manjarres, and J. Garcia-Sancho, *Privileged coupling between Ca^{2+} entry through plasma membrane store-operated Ca^{2+} channels and the endoplasmic reticulum Ca^{2+} pump.* Mol Cell Endocrinol, 2012. **353**(1-2): p. 37-44.
33. Cherednichenko, G., et al., *Enhanced excitation-coupled calcium entry in myotubes expressing malignant hyperthermia mutation R163C is attenuated by dantrolene.* Mol Pharmacol, 2008. **73**(4): p. 1203-12.
34. Cherednichenko, G., et al., *Conformational activation of Ca^{2+} entry by depolarization of skeletal myotubes.* Proc Natl Acad Sci U S A, 2004. **101**(44): p. 15793-8.

35. Endo, M., *Calcium-induced calcium release in skeletal muscle.* Physiol Rev, 2009. **89**(4): p. 1153-76.
36. Weiss, R.G., et al., *Functional analysis of the R1086H malignant hyperthermia mutation in the DHPR reveals an unexpected influence of the III-IV loop on skeletal muscle EC coupling.* Am J Physiol Cell Physiol, 2004. **287**(4): p. C1094-102.
37. MacLennan, D.H., et al., *Ryanodine receptor gene is a candidate for predisposition to malignant hyperthermia.* Nature, 1990. **343**(6258): p. 559-61.
38. Phillips, M.S., et al., *The structural organization of the human skeletal muscle ryanodine receptor (RYR1) gene.* Genomics, 1996. **34**(1): p. 24-41.
39. Treves, S., et al., *Ryanodine receptor 1 mutations, dysregulation of calcium homeostasis and neuromuscular disorders.* Neuromuscul Disord, 2005. **15**(9-10): p. 577-87.
40. McCarthy, T.V., K.A. Quane, and P.J. Lynch, *Ryanodine receptor mutations in malignant hyperthermia and central core disease.* Hum Mutat, 2000. **15**(5): p. 410-7.
41. Kraeva, N., et al., *Ryanodine receptor type 1 gene mutations found in the Canadian malignant hyperthermia population.* Can J Anaesth, 2011. **58**(6): p. 504-13.
42. Monnier, N., et al., *Null mutations causing depletion of the type 1 ryanodine receptor (RYR1) are commonly associated with recessive structural congenital myopathies with cores.* Hum Mutat, 2008. **29**(5): p. 670-8.
43. Hwang, J.H., et al., *Mapping domains and mutations on the skeletal muscle ryanodine receptor channel.* Trends Mol Med, 2012. **18**(11): p. 644-57.
44. Robinson, R.L., et al., *Recent advances in the diagnosis of malignant hyperthermia susceptibility: how confident can we be of genetic testing?* Eur J Hum Genet, 2003. **11**(4): p. 342-8.
45. Hogan, K., et al., *A cysteine-for-arginine substitution (R614C) in the human skeletal muscle calcium release channel cosegregates with malignant hyperthermia.* Anesth Analg, 1992. **75**(3): p. 441-8.
46. Lanner, J.T., et al., *Ryanodine receptors: structure, expression, molecular details, and function in calcium release.* Cold Spring Harb Perspect Biol, 2010. **2**(11): p. a003996.
47. Stowell, K.M., *Malignant hyperthermia: a pharmacogenetic disorder.* Pharmacogenomics, 2008. **9**(11): p. 1657-72.
48. Takeshima, H., et al., *Primary structure and expression from complementary DNA of skeletal muscle ryanodine receptor.* Nature, 1989. **339**(6224): p. 439-45.
49. Du, G.G., et al., *Role of the sequence surrounding predicted transmembrane helix M4 in membrane association and function of the Ca^{2+} release channel of skeletal muscle sarcoplasmic reticulum (ryanodine receptor isoform 1).* J Biol Chem, 2004. **279**(36): p. 37566-74.
50. Zorzato, F., et al., *Molecular cloning of cDNA encoding human and rabbit forms of the Ca^{2+} release channel (ryanodine receptor) of skeletal muscle sarcoplasmic reticulum.* J Biol Chem, 1990. **265**(4): p. 2244-56.
51. Hamilton, S.L. and Serysheva, II, *Ryanodine receptor structure: progress and challenges.* J Biol Chem, 2009. **284**(7): p. 4047-51.

52. Serysheva, II, et al., *Structure of the skeletal muscle calcium release channel activated with Ca^{2+} and AMP-PCP.* Biophys J, 1999. **77**(4): p. 1936-44.
53. Serysheva, II, et al., *Subnanometer-resolution electron cryomicroscopy-based domain models for the cytoplasmic region of skeletal muscle RyR channel.* Proc Natl Acad Sci U S A, 2008. **105**(28): p. 9610-5.
54. Brillantes, A.B., et al., *Stabilization of calcium release channel (ryanodine receptor) function by FK506-binding protein.* Cell, 1994. **77**(4): p. 513-23.
55. Bultynck, G., et al., *Characterization and mapping of the 12 kDa FK506-binding protein (FKBP12)-binding site on different isoforms of the ryanodine receptor and of the inositol 1,4,5-trisphosphate receptor.* Biochem J, 2001. **354**(Pt 2): p. 413-22.
56. Wagenknecht, T., et al., *Locations of calmodulin and FK506-binding protein on the three-dimensional architecture of the skeletal muscle ryanodine receptor.* J Biol Chem, 1997. **272**(51): p. 32463-71.
57. Samso, M., X. Shen, and P.D. Allen, *Structural characterization of the RyR1-FKBP12 interaction.* J Mol Biol, 2006. **356**(4): p. 917-27.
58. Cheng, W., et al., *Interaction between the dihydropyridine receptor Ca^{2+} channel beta-subunit and ryanodine receptor type 1 strengthens excitation-contraction coupling.* Proc Natl Acad Sci U S A, 2005. **102**(52): p. 19225-30.
59. Rebbeck, R.T., et al., *The beta(1a) Subunit of the Skeletal DHPR Binds to Skeletal RyR1 and Activates the Channel via Its 35-Residue C-Terminal Tail.* Biophys J, 2011. **100**(4): p. 922-30.
60. Blayney, L.M., et al., *Ryanodine receptor oligomeric interaction: identification of a putative binding region.* J Biol Chem, 2004. **279**(15): p. 14639-48.
61. Marks, A.R., S. Fleischer, and P. Tempst, *Surface topography analysis of the ryanodine receptor/junctional channel complex based on proteolysis sensitivity mapping.* J Biol Chem, 1990. **265**(22): p. 13143-9.
62. Chen, S.R., J.A. Airey, and D.H. MacLennan, *Positioning of major tryptic fragments in the Ca^{2+} release channel (ryanodine receptor) resulting from partial digestion of rabbit skeletal muscle sarcoplasmic reticulum.* J Biol Chem, 1993. **268**(30): p. 22642-9.
63. Tripathy, A., et al., *Calmodulin activation and inhibition of skeletal muscle Ca^{2+} release channel (ryanodine receptor).* Biophys J, 1995. **69**(1): p. 106-19.
64. O'Connell, K.M., et al., *Calmodulin binding to the 3614-3643 region of RyR1 is not essential for excitation-contraction coupling in skeletal myotubes.* J Gen Physiol, 2002. **120**(3): p. 337-47.
65. MacLennan, D.H. and P.T. Wong, *Isolation of a calcium-sequestering protein from sarcoplasmic reticulum.* Proc Natl Acad Sci U S A, 1971. **68**(6): p. 1231-5.
66. Beard, N.A., et al., *Calsequestrin is an inhibitor of skeletal muscle ryanodine receptor calcium release channels.* Biophys J, 2002. **82**(1 Pt 1): p. 310-20.
67. Lee, J.M., et al., *Negatively charged amino acids within the intraluminal loop of ryanodine receptor are involved in the interaction with triadin.* J Biol Chem, 2004. **279**(8): p. 6994-7000.

68. Fodor, J., et al., *Altered expression of triadin 95 causes parallel changes in localized Ca^{2+} release events and global Ca^{2+} signals in skeletal muscle cells in culture.* J Physiol, 2008. **586**(Pt 23): p. 5803-18.
69. Song, D.W., et al., *Ryanodine receptor assembly: a novel systems biology approach to 3D mapping.* Prog Biophys Mol Biol, 2011. **105**(3): p. 145-61.
70. Berridge, M.J. and R.F. Irvine, *Inositol phosphates and cell signalling.* Nature, 1989. **341**(6239): p. 197-205.
71. Yoshikawa, F., et al., *Trypsinized cerebellar inositol 1,4,5-trisphosphate receptor. Structural and functional coupling of cleaved ligand binding and channel domains.* J Biol Chem, 1999. **274**(1): p. 316-27.
72. Pantazaka, E. and C.W. Taylor, *Targeting of inositol 1,4,5-trisphosphate receptor to the endoplasmic reticulum by its first transmembrane domain.* Biochem J, 2009. **425**(1): p. 61-9.
73. Bosanac, I., et al., *Crystal structure of the ligand binding suppressor domain of type 1 inositol 1,4,5-trisphosphate receptor.* Mol Cell, 2005. **17**(2): p. 193-203.
74. Ludtke, S.J., et al., *Flexible architecture of IP3R1 by Cryo-EM.* Structure, 2011. **19**(8): p. 1192-9.
75. da Fonseca, P.C., et al., *Domain organization of the type 1 inositol 1,4,5-trisphosphate receptor as revealed by single-particle analysis.* Proc Natl Acad Sci U S A, 2003. **100**(7): p. 3936-41.
76. Amador, F.J., et al., *Crystal structure of type I ryanodine receptor amino-terminal beta-trefoil domain reveals a disease-associated mutation "hot spot" loop.* Proc Natl Acad Sci U S A, 2009. **106**(27): p. 11040-4.
77. Ponting, C.P., *Novel repeats in ryanodine and IP3 receptors and protein O-mannosyltransferases.* Trends Biochem Sci, 2000. **25**(2): p. 48-50.
78. Seo, M.D., et al., *Structural and functional conservation of key domains in InsP3 and ryanodine receptors.* Nature, 2012. **483**(7387): p. 108-12.
79. Yamamoto, T., R. El-Hayek, and N. Ikemoto, *Postulated role of interdomain interaction within the ryanodine receptor in Ca^{2+} channel regulation.* J Biol Chem, 2000. **275**(16): p. 11618-25.
80. Ikemoto, N. and T. Yamamoto, *Postulated role of inter-domain interaction within the ryanodine receptor in Ca^{2+} channel regulation.* Trends Cardiovasc Med, 2000. **10**(7): p. 310-6.
81. Liu, Z., et al., *Localization of a disease-associated mutation site in the three-dimensional structure of the cardiac muscle ryanodine receptor.* J Biol Chem, 2005. **280**(45): p. 37941-7.
82. Meng, X., et al., *Three-dimensional localization of serine 2808, a phosphorylation site in cardiac ryanodine receptor.* J Biol Chem, 2007. **282**(35): p. 25929-39.
83. Popova, O.B., et al., *Identification of ATP-Binding Regions in the RyR1 Ca^{2+} Release Channel.* PLoS One, 2012. **7**(11): p. e48725.
84. Tung, C.C., et al., *The amino-terminal disease hotspot of ryanodine receptors forms a cytoplasmic vestibule.* Nature, 2010. **468**(7323): p. 585-8.
85. Kobayashi, S., et al., *Antibody probe study of Ca^{2+} channel regulation by interdomain interaction within the ryanodine receptor.* Biochem J, 2004. **380**(Pt 2): p. 561-9.

86. Paul-Pletzer, K., et al., *The skeletal muscle ryanodine receptor identified as a molecular target of [3H]azidodantrolene by photoaffinity labeling.* Biochemistry, 2001. **40**(2): p. 531-42.
87. Bannister, M.L., et al., *Malignant hyperthermia mutation sites in the Leu2442-Pro2477 (DP4) region of RyR1 (ryanodine receptor 1) are clustered in a structurally and functionally definable area.* Biochem J, 2007. **401**(1): p. 333-9.
88. Harrison, G.G., *Control of the malignant hyperpyrexic syndrome in MHS swine by dantrolene sodium.* Br J Anaesth, 1975. **47**(1): p. 62-5.
89. Snyder, H.R., Jr., et al., *1-[(5-arylfurfurylidene)amino]hydantoins. A new class of muscle relaxants.* J Med Chem, 1967. **10**(5): p. 807-10.
90. Fruen, B.R., J.R. Mickelson, and C.F. Louis, *Dantrolene inhibition of sarcoplasmic reticulum Ca^{2+} release by direct and specific action at skeletal muscle ryanodine receptors.* J Biol Chem, 1997. **272**(43): p. 26965-71.
91. Szentesi, P., et al., *Effects of dantrolene on steps of excitation-contraction coupling in mammalian skeletal muscle fibers.* J Gen Physiol, 2001. **118**(4): p. 355-75.
92. Ellis, K.O. and S.H. Bryant, *Excitation-contraction uncoupling in skeletal muscle by dantrolene sodium.* Naunyn Schmiedebergs Arch Pharmacol, 1972. **274**(1): p. 107-9.
93. Flewellen, E.H., et al., *Dantrolene dose response in awake man: implications for management of malignant hyperthermia.* Anesthesiology, 1983. **59**(4): p. 275-80.
94. Kobayashi, S., et al., *Dantrolene stabilizes domain interactions within the ryanodine receptor.* J Biol Chem, 2005. **280**(8): p. 6580-7.
95. Jiang, D., et al., *Reduced threshold for luminal Ca^{2+} activation of RyR1 underlies a causal mechanism of porcine malignant hyperthermia.* J Biol Chem, 2008. **283**(30): p. 20813-20.
96. Zucchi, R. and S. Ronca-Testoni, *The sarcoplasmic reticulum Ca^{2+} channel/ryanodine receptor: modulation by endogenous effectors, drugs and disease states.* Pharmacol Rev, 1997. **49**(1): p. 1-51.
97. Rousseau, E. and G. Meissner, *Single cardiac sarcoplasmic reticulum Ca^{2+}-release channel: activation by caffeine.* Am J Physiol, 1989. **256**(2 Pt 2): p. H328-33.
98. Dias, J.M. and P.D. Vogel, *Effects of small molecule modulators on ATP binding to skeletal ryanodine receptor.* Protein J, 2009. **28**(5): p. 240-6.
99. Lopez, J.R., et al., *Hypersensitivity of malignant hyperthermia-susceptible swine skeletal muscle to caffeine is mediated by high resting myoplasmic $[Ca^{2+}]$.* Anesthesiology, 2000. **92**(6): p. 1799-806.
100. Liu, Z., et al., *Three-dimensional reconstruction of the recombinant type 3 ryanodine receptor and localization of its amino terminus.* Proc Natl Acad Sci U S A, 2001. **98**(11): p. 6104-9.
101. Takeshima, H., et al., *Ca^{2+}-induced Ca^{2+} release in myocytes from dyspedic mice lacking the type-1 ryanodine receptor.* Embo J, 1995. **14**(13): p. 2999-3006.
102. Nelson, T.E., D.M. Bedell, and E.W. Jones, *Porcine malignant hyperthermia: effects of temperature and extracellular calcium concentration on halothane-induced contracture of susceptible skeletal muscle.* Anesthesiology, 1975. **42**(3): p. 301-6.

103. Harrison, S.M., et al., *Mechanisms underlying the inotropic action of halothane on intact rat ventricular myocytes.* Br J Anaesth, 1999. **82**(4): p. 609-21.
104. Sauviat, M.P., et al., *Effects of halothane on the membrane potential in skeletal muscle of the frog.* Br J Pharmacol, 2000. **130**(3): p. 619-24.
105. Zorzato, F., et al., *Chlorocresol: an activator of ryanodine receptor-mediated Ca^{2+} release.* Mol Pharmacol, 1993. **44**(6): p. 1192-201.
106. Tegazzin, V., et al., *Chlorocresol, an additive to commercial succinylcholine, induces contracture of human malignant hyperthermia-susceptible muscles via activation of the ryanodine receptor Ca^{2+} channel.* Anesthesiology, 1996. **84**(6): p. 1380-5.
107. Herrmann-Frank, A., et al., *4-Chloro-m-cresol, a potent and specific activator of the skeletal muscle ryanodine receptor.* Biochim Biophys Acta, 1996. **1289**(1): p. 31-40.
108. Al-Mousa, F. and F. Michelangeli, *Commonly used ryanodine receptor activator, 4-chloro-m-cresol (4CmC), is also an inhibitor of SERCA Ca^{2+} pumps.* Pharmacol Rep, 2009. **61**(5): p. 838-42.
109. Vukcevic, M., et al., *Functional Properties of RYR1 Mutations Identified in Swedish Patients with Malignant Hyperthermia and Central Core Disease.* Anesth Analg, 2010: p. 185-190.
110. Wehner, M., et al., *The Ile2453Thr mutation in the ryanodine receptor gene 1 is associated with facilitated calcium release from sarcoplasmic reticulum by 4-chloro-m-cresol in human myotubes.* Cell Calcium, 2003. **34**(2): p. 163-8.
111. Herrmann-Frank, A., M. Richter, and F. Lehmann-Horn, *4-Chloro-m-cresol: a specific tool to distinguish between malignant hyperthermia-susceptible and normal muscle.* Biochem Pharmacol, 1996. **52**(1): p. 149-55.
112. Avila, G., K.M. O'Connell, and R.T. Dirksen, *The pore region of the skeletal muscle ryanodine receptor is a primary locus for excitation-contraction uncoupling in central core disease.* J Gen Physiol, 2003. **121**(4): p. 277-86.
113. Fessenden, J.D., et al., *Identification of a key determinant of ryanodine receptor type 1 required for activation by 4-chloro-m-cresol.* J Biol Chem, 2003. **278**(31): p. 28727-35.
114. Copello, J.A., et al., *Heterogeneity of Ca^{2+} gating of skeletal muscle and cardiac ryanodine receptors.* Biophys J, 1997. **73**(1): p. 141-56.
115. Perez, C.F., J.R. Lopez, and P.D. Allen, *Expression levels of RyR1 and RyR3 control resting free Ca^{2+} in skeletal muscle.* Am J Physiol Cell Physiol, 2005. **288**(3): p. C640-9.
116. Laver, D.R. and B.N. Honen, *Luminal Mg^{2+}, a key factor controlling RYR2-mediated Ca^{2+} release: cytoplasmic and luminal regulation modeled in a tetrameric channel.* J Gen Physiol, 2008. **132**(4): p. 429-46.
117. Gillespie, D., H. Chen, and M. Fill, *Is ryanodine receptor a calcium or magnesium channel? Roles of K^{+} and Mg^{2+} during Ca^{2+} release.* Cell Calcium, 2012. **51**(6): p. 427-33.
118. Laver, D.R., *Ca^{2+} stores regulate ryanodine receptor Ca^{2+} release channels via luminal and cytosolic Ca^{2+} sites.* Biophys J, 2007. **92**(10): p. 3541-55.

119. Shtifman, A., et al., *Interdomain interactions within ryanodine receptors regulate Ca^{2+} spark frequency in skeletal muscle.* J Gen Physiol, 2002. **119**(1): p. 15-32.
120. Laver, D.R., *Regulation of ryanodine receptors from skeletal and cardiac muscle during rest and excitation.* Clin Exp Pharmacol Physiol, 2006. **33**(11): p. 1107-13.
121. Gillespie, D. and M. Fill, *Intracellular calcium release channels mediate their own countercurrent: the ryanodine receptor case study.* Biophys J, 2008. **95**(8): p. 3706-14.
122. Steele, D.S. and A.M. Duke, *Defective Mg^{2+} regulation of RyR1 as a causal factor in malignant hyperthermia.* Arch Biochem Biophys, 2007. **458**(1): p. 57-64.
123. Duke, A.M., P.M. Hopkins, and D.S. Steele, *Mg^{2+} dependence of halothane-induced Ca^{2+} release from the sarcoplasmic reticulum in rat skeletal muscle.* J Physiol, 2003. **551**(Pt 2): p. 447-54.
124. Meissner, G., E. Darling, and J. Eveleth, *Kinetics of rapid Ca^{2+} release by sarcoplasmic reticulum. Effects of Ca^{2+}, Mg^{2+}, and adenine nucleotides.* Biochemistry, 1986. **25**(1): p. 236-44.
125. Magee, K.R. and G.M. Shy, *A new congenital non-progressive myopathy.* Brain, 1956. **79**(4): p. 610-21.
126. Romero, N.B., et al., *Dominant and recessive central core disease associated with RYR1 mutations and fetal akinesia.* Brain, 2003. **126**(Pt 11): p. 2341-9.
127. Haan, E.A., et al., *Assignment of the gene for central core disease to chromosome 19.* Hum Genet, 1990. **86**(2): p. 187-90.
128. Tilgen, N., et al., *Identification of four novel mutations in the C-terminal membrane spanning domain of the ryanodine receptor 1: association with central core disease and alteration of calcium homeostasis.* Hum Mol Genet, 2001. **10**(25): p. 2879-87.
129. Jungbluth, H., *Central core disease.* Orphanet J Rare Dis, 2007. **2**: p. 25.
130. Colleoni, L., et al., *Central core disease and susceptibility to malignant hyperthermia in a single family.* J Neurol, 2009. **256**(7): p. 1161-3.
131. Kossugue, P.M., et al., *Central core disease due to recessive mutations in RYR1 gene: is it more common than described?* Muscle Nerve, 2007. **35**(5): p. 670-4.
132. Broman, M., et al., *Mutation screening of the RYR1-cDNA from peripheral B-lymphocytes in 15 Swedish malignant hyperthermia index cases.* Br J Anaesth, 2009. **102**(5): p. 642-9.
133. Sei, Y., K.L. Gallagher, and A.S. Basile, *Skeletal muscle type ryanodine receptor is involved in calcium signaling in human B lymphocytes.* J Biol Chem, 1999. **274**(9): p. 5995-6002.
134. Hogan, P.G., R.S. Lewis, and A. Rao, *Molecular basis of calcium signaling in lymphocytes: STIM and ORAI.* Annu Rev Immunol, 2010. **28**: p. 491-533.
135. Migita, T., et al., *Functional analysis of ryanodine receptor type 1 p.R2508C mutation in exon 47.* J Anesth, 2009. **23**(3): p. 341-6.
136. Luo, D., et al., *Signaling pathways underlying muscarinic receptor-induced $[Ca^{2+}]i$ oscillations in HEK293 cells.* J Biol Chem, 2001. **276**(8): p. 5613-21.
137. Bennett, D.L., et al., *Expression and function of ryanodine receptors in nonexcitable cells.* J Biol Chem, 1996. **271**(11): p. 6356-62.

138. Bugaj, V., et al., *Functional properties of endogenous receptor- and store-operated calcium influx channels in HEK293 cells.* J Biol Chem, 2005. **280**(17): p. 16790-7.
139. Moore, R.A., et al., *A transgenic myogenic cell line lacking ryanodine receptor protein for homologous expression studies: reconstitution of Ry1R protein and function.* J Cell Biol, 1998. **140**(4): p. 843-51.
140. Zvaritch, E., et al., *An Ryr1I4895T mutation abolishes Ca^{2+} release channel function and delays development in homozygous offspring of a mutant mouse line.* Proc Natl Acad Sci U S A, 2007. **104**(47): p. 18537-42.
141. Yang, T., et al., *Functional defects in six ryanodine receptor isoform-1 (RyR1) mutations associated with malignant hyperthermia and their impact on skeletal excitation-contraction coupling.* J Biol Chem, 2003. **278**(28): p. 25722-30.
142. Sei, Y., et al., *Patients with malignant hyperthermia demonstrate an altered calcium control mechanism in B lymphocytes.* Anesthesiology, 2002. **97**(5): p. 1052-8.
143. Wehner, M., et al., *Increased sensitivity to 4-chloro-m-cresol and caffeine in primary myotubes from malignant hyperthermia susceptible individuals carrying the ryanodine receptor 1 Thr2206Met (C6617T) mutation.* Clin Genet, 2002. **62**(2): p. 135-46.
144. Censier, K., et al., *Intracellular calcium homeostasis in human primary muscle cells from malignant hyperthermia-susceptible and normal individuals. Effect Of overexpression of recombinant wild-type and Arg163Cys mutated ryanodine receptors.* J Clin Invest, 1998. **101**(6): p. 1233-42.
145. Lynch, P.J., et al., *A mutation in the transmembrane/luminal domain of the ryanodine receptor is associated with abnormal Ca^{2+} release channel function and severe central core disease.* Proc Natl Acad Sci U S A, 1999. **96**(7): p. 4164-9.
146. Tong, J., T.V. McCarthy, and D.H. MacLennan, *Measurement of resting cytosolic Ca^{2+} concentrations and Ca^{2+} store size in HEK-293 cells transfected with malignant hyperthermia or central core disease mutant Ca^{2+} release channels.* J Biol Chem, 1999. **274**(2): p. 693-702.
147. MacLennan, D.H. and M.S. Phillips, *Malignant hyperthermia.* Science, 1992. **256**(5058): p. 789-94.
148. MacLennan, D.H. and M.S. Phillips, *The role of the skeletal muscle ryanodine receptor (RYR1) gene in malignant hyperthermia and central core disease.* Soc Gen Physiol Ser, 1995. **50**: p. 89-100.
149. Brini, M., et al., *Ca^{2+} signaling in HEK-293 and skeletal muscle cells expressing recombinant ryanodine receptors harboring malignant hyperthermia and central core disease mutations.* J Biol Chem, 2005. **280**(15): p. 15380-9.
150. Avila, G., J.J. O'Brien, and R.T. Dirksen, *Excitation--contraction uncoupling by a human central core disease mutation in the ryanodine receptor.* Proc Natl Acad Sci U S A, 2001. **98**(7): p. 4215-20.
151. Ducreux, S., et al., *Effect of ryanodine receptor mutations on interleukin-6 release and intracellular calcium homeostasis in human myotubes from malignant hyperthermia-susceptible individuals and patients affected by central core disease.* J Biol Chem, 2004. **279**(42): p. 43838-46.

152. Robinson, R., et al., *Mutations in RYR1 in malignant hyperthermia and central core disease.* Hum Mutat, 2006. **27**(10): p. 977-89.
153. Du, G.G., et al., *Mutations to Gly2370, Gly2373 or Gly2375 in malignant hyperthermia domain 2 decrease caffeine and cresol sensitivity of the rabbit skeletal-muscle Ca^{2+}-release channel (ryanodine receptor isoform 1).* Biochem J, 2001. **360**(Pt 1): p. 97-105.
154. Brini, M., *Ryanodine receptor defects in muscle genetic diseases.* Biochem Biophys Res Commun, 2004. **322**(4): p. 1245-55.
155. Zhou, H., et al., *Molecular mechanisms and phenotypic variation in RYR1-related congenital myopathies.* Brain, 2007. **130**(Pt 8): p. 2024-36.
156. Monnier, N., et al., *Malignant-hyperthermia susceptibility is associated with a mutation of the alpha 1-subunit of the human dihydropyridine-sensitive L-type voltage-dependent calcium-channel receptor in skeletal muscle.* Am J Hum Genet, 1997. **60**(6): p. 1316-25.
157. Toppin, P.J., et al., *A report of fulminant malignant hyperthermia in a patient with a novel mutation of the CACNA1S gene.* Can J Anaesth, 2010.
158. Carpenter, D., et al., *The role of CACNA1S in predisposition to malignant hyperthermia.* BMC Med Genet, 2009. **10**: p. 104.
159. Levitt, R.C., et al., *Evidence for the localization of a malignant hyperthermia susceptibility locus (MHS2) to human chromosome 17q.* Genomics, 1992. **14**(3): p. 562-6.
160. Robinson, R.L., et al., *A genome wide search for susceptibility loci in three European malignant hyperthermia pedigrees.* Hum Mol Genet, 1997. **6**(6): p. 953-61.
161. Sudbrak, R., et al., *Mapping of a further malignant hyperthermia susceptibility locus to chromosome 3q13.1.* Am J Hum Genet, 1995. **56**(3): p. 684-91.
162. Iles, D.E., et al., *Localization of the gene encoding the alpha 2/delta-subunits of the L-type voltage-dependent calcium channel to chromosome 7q and analysis of the segregation of flanking markers in malignant hyperthermia susceptible families.* Hum Mol Genet, 1994. **3**(6): p. 969-75.
163. Liu, N., et al., *Ryanodine receptor and calsequestrin in arrhythmogenesis: what we have learnt from genetic diseases and transgenic mice.* J Mol Cell Cardiol, 2009. **46**(2): p. 149-59.
164. Protasi, F., C. Paolini, and M. Dainese, *Calsequestrin-1: a new candidate gene for malignant hyperthermia and exertional/environmental heat stroke.* J Physiol, 2009. **587**(Pt 13): p. 3095-100.
165. Chamley, D., et al., *Malignant hyperthermia in infancy and identification of novel RYR1 mutation.* Br J Anaesth, 2000. **84**(4): p. 500-4.
166. Sato, K., N. Pollock, and K.M. Stowell, *Functional Studies of RYR1 Mutations in the Skeletal Muscle Ryanodine Receptor Using Human RYR1 Complementary DNA.* Anesthesiology, 2010: p. 1350-1354.
167. Neitzel, H., *A routine method for the establishment of permanent growing lymphoblastoid cell lines.* Hum Genet, 1986. **73**(4): p. 320-6.
168. Bers, D.M., C.W. Patton, and R. Nuccitelli, *A practical guide to the preparation of Ca^{2+} buffers.* Methods Cell Biol, 2010. **99**: p. 1-26.
169. Grynkiewicz, G., M. Poenie, and R.Y. Tsien, *A new generation of Ca^{2+} indicators with greatly improved fluorescence properties.* J Biol Chem, 1985. **260**(6): p. 3440-50.

170. Mauro, A., *Satellite cell of skeletal muscle fibers.* J Biophys Biochem Cytol, 1961. **9**: p. 493-5.
171. Velleman, S.G. and D.C. McFarland, *Myotube morphology, and expression and distribution of collagen type I during normal and low score normal avian satellite cell myogenesis.* Dev Growth Differ, 1999. **41**(2): p. 153-61.
172. Eberli, D., et al., *Optimization of human skeletal muscle precursor cell culture and myofiber formation in vitro.* Methods, 2009. **47**(2): p. 98-103.
173. Kuhl, U., et al., *Role of laminin and fibronectin in selecting myogenic versus fibrogenic cells from skeletal muscle cells in vitro.* Dev Biol, 1986. **117**(2): p. 628-35.
174. Damsky, C.H., et al., *Distribution of the cell substratum attachment (CSAT) antigen on myogenic and fibroblastic cells in culture.* J Cell Biol, 1985. **100**(5): p. 1528-39.
175. Springer, M.L., T.A. Rando, and H.M. Blau, *Gene delivery to muscle.* Curr Protoc Hum Genet, 2002. **Chapter 13**: p. Unit13 4.
176. Knudsen, K.A., *The calcium-dependent myoblast adhesion that precedes cell fusion is mediated by glycoproteins.* J Cell Biol, 1985. **101**(3): p. 891-7.
177. Okazaki, Y., et al., *Cell surface expression of calnexin, a molecular chaperone in the endoplasmic reticulum.* J Biol Chem, 2000. **275**(46): p. 35751-8.
178. McKinney, L.C., et al., *Characterization of ryanodine receptor-mediated calcium release in human B cells: relevance to diagnostic testing for malignant hyperthermia.* Anesthesiology, 2006. **104**(6): p. 1191-201.
179. Sei, Y., K.L. Gallagher, and J.W. Daly, *Multiple effects of caffeine on Ca^{2+} release and influx in human B lymphocytes.* Cell Calcium, 2001. **29**(3): p. 149-60.
180. Girard, T., et al., *B-lymphocytes from malignant hyperthermia-susceptible patients have an increased sensitivity to skeletal muscle ryanodine receptor activators.* J Biol Chem, 2001. **276**(51): p. 48077-82.
181. Liu, Q.C., et al., *Comparative expression profiling identifies differential roles for Myogenin and p38alpha MAPK signaling in myogenesis.* J Mol Cell Biol, 2012: p. 386-397.
182. Mailloux, R.J. and M.E. Harper, *Glucose regulates enzymatic sources of mitochondrial NADPH in skeletal muscle cells; a novel role for glucose-6-phosphate dehydrogenase.* Faseb J, 2010. **24**(7): p. 2495-506.
183. Wehner, M., et al., *Functional characterization of malignant hyperthermia-associated RyR1 mutations in exon 44, using the human myotube model.* Neuromuscul Disord, 2004. **14**(7): p. 429-37.
184. Kaufmann, A., et al., *Novel double and single ryanodine receptor 1 variants in two Austrian malignant hyperthermia families.* Anesth Analg, 2012. **114**(5): p. 1017-25.
185. Kaufmann, A., et al., *Novel ryanodine receptor mutation that may cause malignant hyperthermia.* Anesthesiology, 2008. **109**(3): p. 457-64.
186. Weigl, L.G., C. Ludwig-Papst, and H.G. Kress, *4-chloro-m-cresol cannot detect malignant hyperthermia equivocal cells in an alternative minimally invasive diagnostic test of malignant hyperthermia susceptibility.* Anesth Analg, 2004. **99**(1): p. 103-7.
187. NCBI. *SNP database*. 2012 [cited 2012 December]; Available from: http://www.ncbi.nlm.nih.gov/snp.

188. Steen, A.M., et al., *Levels of hypoxanthine phosphoribosyltransferase RNA in human cells.* Exp Cell Res, 1990. **186**(2): p. 236-44.
189. Grievink, H., *Malignant Hyperthermia- Allele specific expression and mutation screening of the ryanodine receptor 1*, in *IMBS*. 2009, Massey University: Palmerston North.
190. Pfaffl, M.W., *A new mathematical model for relative quantification in real-time RT-PCR.* Nucleic Acids Res, 2001. **29**(9): p. 2002-2007.
191. Pfaffl, M.W., G.W. Horgan, and L. Dempfle, *Relative expression software tool (REST) for group-wise comparison and statistical analysis of relative expression results in real-time PCR.* Nucleic Acids Res, 2002. **30**(9): p. e36.
192. Vergara, J., R.Y. Tsien, and M. Delay, *Inositol 1,4,5-trisphosphate: a possible chemical link in excitation-contraction coupling in muscle.* Proc Natl Acad Sci U S A, 1985. **82**(18): p. 6352-6.
193. Lee, E.H. and P.D. Allen, *Homo-dimerization of RyR1 C-terminus via charged residues in random coils or in an alpha-helix.* Exp Mol Med, 2007. **39**(5): p. 594-602.
194. Takekura, H., et al., *Abnormal junctions between surface membrane and sarcoplasmic reticulum in skeletal muscle with a mutation targeted to the ryanodine receptor.* Proc Natl Acad Sci U S A, 1995. **92**(8): p. 3381-5.
195. Yuchi, Z., K. Lau, and F. Van Petegem, *Disease mutations in the ryanodine receptor central region: crystal structures of a phosphorylation hot spot domain.* Structure, 2012. **20**(7): p. 1201-11.
196. Gaburjakova, M., et al., *FKBP12 binding modulates ryanodine receptor channel gating.* J Biol Chem, 2001. **276**(20): p. 16931-5.
197. Wen, H., et al., *Characterization of the binding sites for the interactions between FKBP12 and intracellular calcium release channels.* Arch Biochem Biophys, 2011. **517**(1): p. 37-42.
198. Bosanac, I., et al., *Structural insights into the regulatory mechanism of IP3 receptor.* Biochim Biophys Acta, 2004. **1742**(1-3): p. 89-102.
199. Taylor, C.W., P.C. da Fonseca, and E.P. Morris, *IP(3) receptors: the search for structure.* Trends Biochem Sci, 2004. **29**(4): p. 210-9.
200. Mignery, G.A. and T.C. Sudhof, *The ligand binding site and transduction mechanism in the inositol-1,4,5-triphosphate receptor.* Embo J, 1990. **9**(12): p. 3893-8.
201. Neron, B., et al., *Mobyle: a new full web bioinformatics framework.* Bioinformatics, 2009. **25**(22): p. 3005-11.
202. Arnold, K., et al., *The SWISS-MODEL workspace: a web-based environment for protein structure homology modelling.* Bioinformatics, 2006. **22**(2): p. 195-201.
203. Schultz, J., et al., *SMART, a simple modular architecture research tool: identification of signaling domains.* Proc Natl Acad Sci U S A, 1998. **95**(11): p. 5857-64.
204. Letunic, I., T. Doerks, and P. Bork, *SMART 7: recent updates to the protein domain annotation resource.* Nucleic Acids Res, 2011. **40**(Database issue): p. D302-5.
205. Wootton, J.C. and S. Federhen, *Analysis of compositionally biased regions in sequence databases.* Methods Enzymol, 1996. **266**: p. 554-71.
206. Coletta, A., et al., *Low-complexity regions within protein sequences have position-dependent roles.* BMC Syst Biol, 2010. **4**: p. 43.

207. Birney, E., J.D. Thompson, and T.J. Gibson, *PairWise and SearchWise: finding the optimal alignment in a simultaneous comparison of a protein profile against all DNA translation frames.* Nucleic Acids Res, 1996. **24**(14): p. 2730-9.
208. Kelley, L.A. and M.J. Sternberg, *Protein structure prediction on the Web: a case study using the Phyre server.* Nat Protoc, 2009. **4**(3): p. 363-71.
209. Clark, A.R., et al., *Skeletal dysplasias due to filamin A mutations result from a gain-of-function mechanism distinct from allelic neurological disorders.* Hum Mol Genet, 2009. **18**(24): p. 4791-800.
210. Sawyer, G.M., et al., *Disease-associated substitutions in the filamin B actin binding domain confer enhanced actin binding affinity in the absence of major structural disturbance: Insights from the crystal structures of filamin B actin binding domains.* J Mol Biol, 2009. **390**(5): p. 1030-47.
211. Goenka, S. and C.M. Rao, *Expression of recombinant zeta-crystallin in Escherichia coli with the help of GroEL/ES and its purification.* Protein Expr Purif, 2001. **21**(2): p. 260-7.
212. Fenton, W.A. and A.L. Horwich, *GroEL-mediated protein folding.* Protein Sci, 1997. **6**(4): p. 743-60.
213. Ikai, A., *Thermostability and aliphatic index of globular proteins.* J Biochem, 1980. **88**(6): p. 1895-8.
214. Rohman, M. and K.J. Harrison-Lavoie, *Separation of copurifying GroEL from glutathione-S-transferase fusion proteins.* Protein Expr Purif, 2000. **20**(1): p. 45-7.
215. Saito, A., et al., *Ultrastructure of the calcium release channel of sarcoplasmic reticulum.* J Cell Biol, 1988. **107**(1): p. 211-9.
216. Andersen, J.F., et al., *Human thioredoxin homodimers: regulation by pH, role of aspartate 60, and crystal structure of the aspartate 60 --> asparagine mutant.* Biochemistry, 1997. **36**(46): p. 13979-88.
217. Oblong, J.E., et al., *Purification of human thioredoxin reductase: properties and characterization by absorption and circular dichroism spectroscopy.* Biochemistry, 1993. **32**(28): p. 7271-7.
218. Booth, D.R., et al., *Instability, unfolding and aggregation of human lysozyme variants underlying amyloid fibrillogenesis.* Nature, 1997. **385**(6619): p. 787-93.
219. Kelly, S.M., T.J. Jess, and N.C. Price, *How to study proteins by circular dichroism.* Biochim Biophys Acta, 2005. **1751**(2): p. 119-39.
220. Molina-Bolı´var J.A., A.J.a.C.R.C., *Growth and Hydration Of Triton X-100 Micelles In Monovalent Alkali Salts: A Light*
Scattering Study. J. Phys. Chem. B 2002. **106**(4): p. 870-877.
221. Shaw, A., et al., *Crystal structure and subunit dynamics of the abalone sperm lysin dimer: egg envelopes dissociate dimers, the monomer is the active species.* J Cell Biol, 1995. **130**(5): p. 1117-25.
222. Kunimoto, M., K. Shibata, and T. Miura, *Comparison of the cytoskeleton fractions of rat red blood cells prepared with non-ionic detergents.* J Biochem, 1989. **105**(2): p. 190-5.
223. Liu, W. and R. Guo, *Effects of Triton X-100 nanoaggregates on dimerization and antioxidant activity of morin.* Mol Pharm, 2008. **5**(4): p. 588-97.

224. Perkins, D.N., et al., *Probability-based protein identification by searching sequence databases using mass spectrometry data.* Electrophoresis, 1999. **20**(18): p. 3551-67.
225. Yin, C.C., L.M. Blayney, and F.A. Lai, *Physical coupling between ryanodine receptor-calcium release channels.* J Mol Biol, 2005. **349**(3): p. 538-46.
226. Joseph, S.K., et al., *Membrane insertion, glycosylation, and oligomerization of inositol trisphosphate receptors in a cell-free translation system.* J Biol Chem, 1997. **272**(3): p. 1579-88.
227. Galvan, D.L. and G.A. Mignery, *Carboxyl-terminal sequences critical for inositol 1,4,5-trisphosphate receptor subunit assembly.* J Biol Chem, 2002. **277**(50): p. 48248-60.
228. Maehara, Y., et al., *Genetic analysis with calcium-induced calcium release test in Japanese malignant hyperthermia susceptible (MHS) families.* Hiroshima J Med Sci, 1999. **48**(1): p. 9-15.
229. De Crescenzo, V., et al., *Type 1 ryanodine receptor knock-in mutation causing central core disease of skeletal muscle also displays a neuronal phenotype.* Proc Natl Acad Sci U S A, 2012. **109**(2): p. 610-5.
230. Loy, R.E., et al., *Muscle weakness in Ryr1I4895T/WT knock-in mice as a result of reduced ryanodine receptor Ca^{2+} ion permeation and release from the sarcoplasmic reticulum.* J Gen Physiol, 2010. **137**(1): p. 43-57.
231. Fiaux, J., et al., *NMR analysis of a 900K GroEL GroES complex.* Nature, 2002. **418**(6894): p. 207-11.
232. Fessenden, J.D., *Forster resonance energy transfer measurements of ryanodine receptor type 1 structure using a novel site-specific labeling method.* PLoS One, 2009. **4**(10): p. e7338.
233. Cornea, R.L., et al., *Mapping the ryanodine receptor (RyR) FK506-binding protein (FKBP) subunit using fluorescence resonance energy transfer(FRET).* J Biol Chem, 2010.

Chapter 8 Appendices

Appendix I. Example for lymphocytes Ca^{2+} release raw data for patient C1

4CmC concentration (μM)	delta	SEM
100	0.046	0.006
200	0.086	0.009
400	0.198	0.01
600	0.33	0.014
800	0.50	0.024
1000	0.76	0.027

Appendix II. Histogram plots for immuno co-localisation studies

A: Histogram for transiently transfected HEK293 cells with WT RYR1 cDNA

B: Histogram for transiently transfected HEK293 cells with mutant RYR1 cDNA

C: Histogram for stably transfected HEK293 cells with WT RYR1 cDNA

D: Histogram for stably transfected HEK293 cells with mutant RYR1 cDNA

E: Histogram for untransfected HEK293 cells

The insert shows which cell has been measured to create the histogram

Blue trace: DAPI

Green trace: RYR1

Red trace: PDI

The x-axis represents the size of the cell in μm while the y-axis represents the signal intensity.

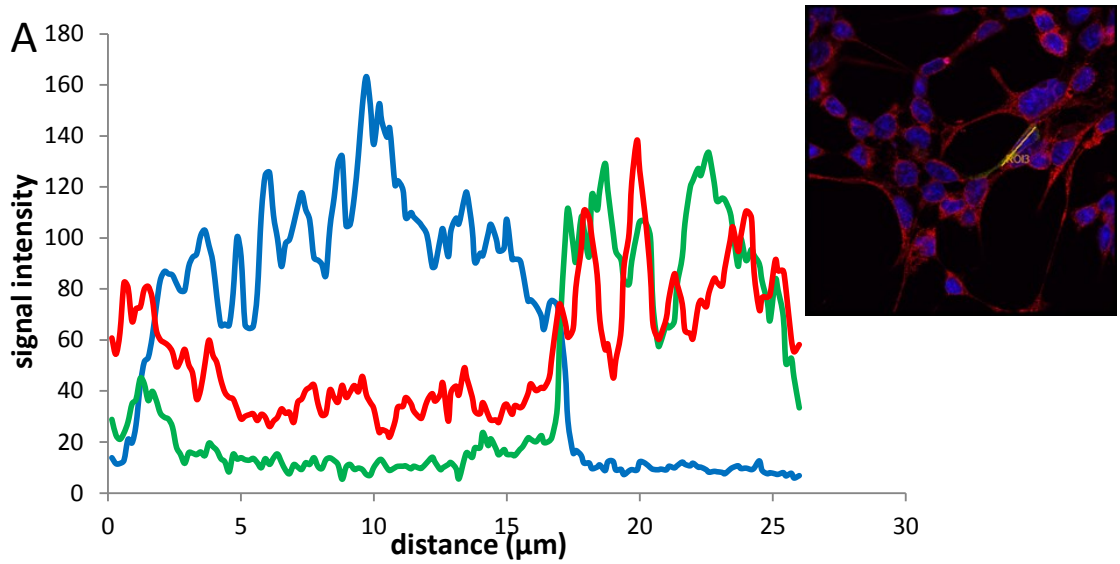
A
signal intensity
distance (µm)

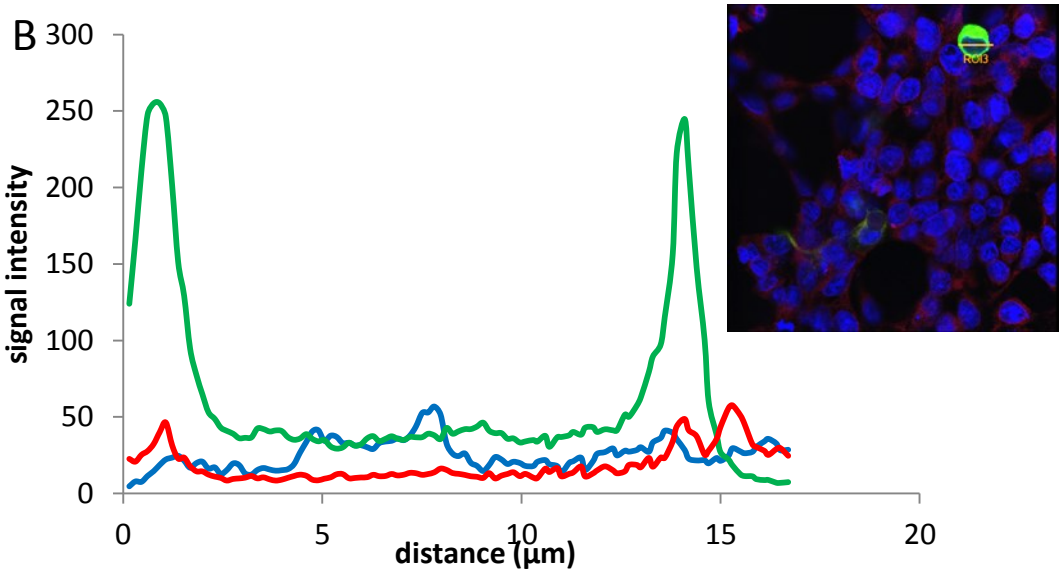
B
signal intensity
distance (µm)

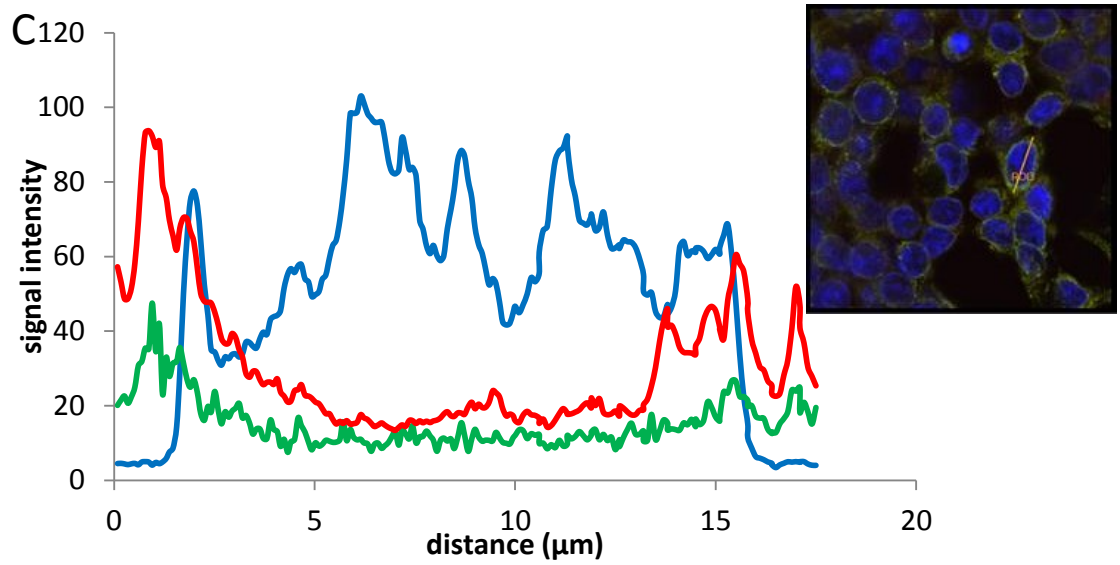
C
signal intensity
distance (µm)

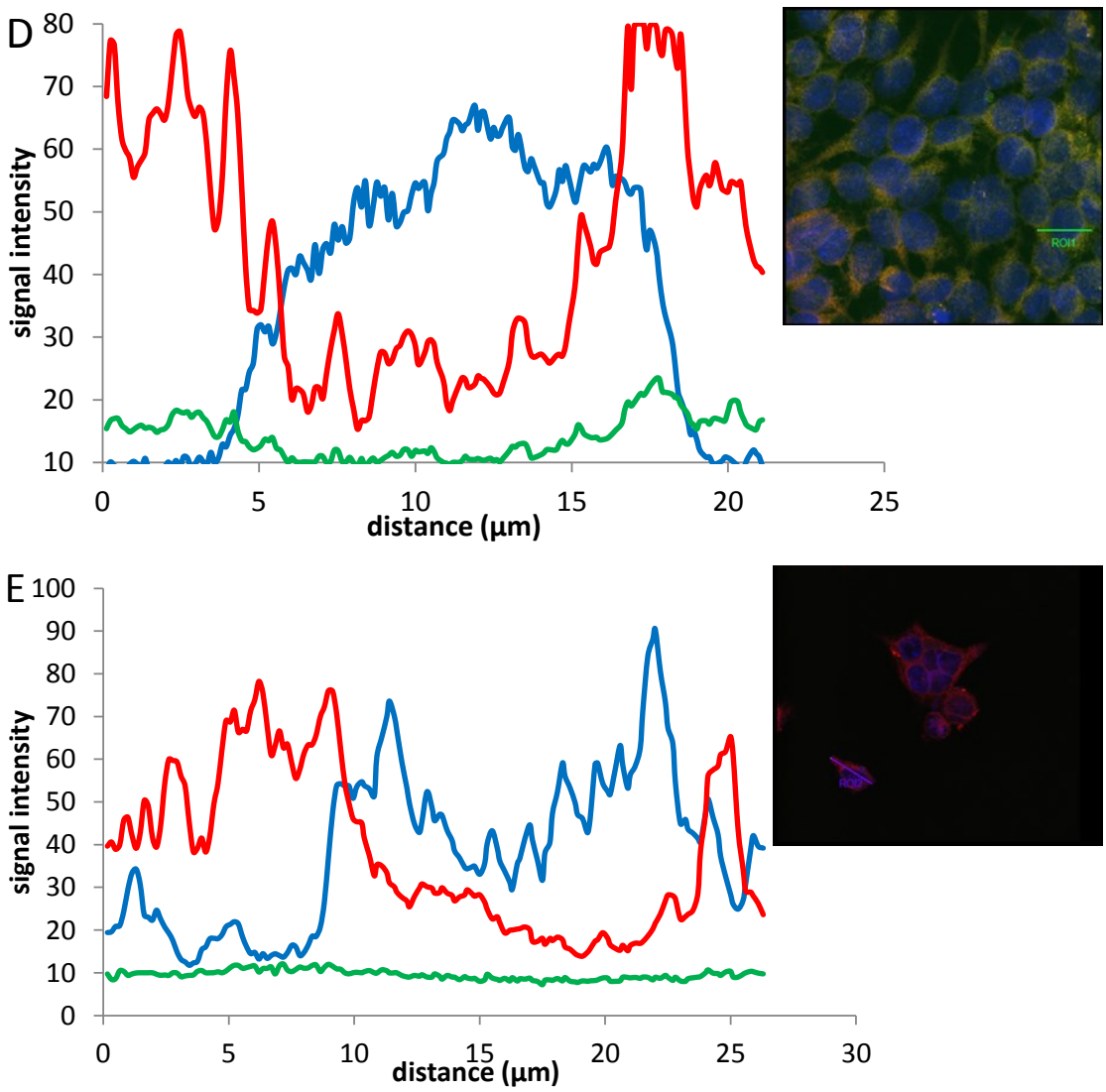

Appendix III. Delta ratio for different cell lines at stimulation with 1 mM 4CmC

patients	R2452W	Lymphoblastoid cells	Myotubes	HEK293		
A	pos	0.6	0.08	plasmid	stable	transients
BI	pos	0.6	na	Wildtype	0.08	0.08
BII:1	neg	0.8	na	Mutant	0.07	0.1
BII:2	pos	0.55	na			
BII:3	pos	0.7	na			
C1	neg	0.8	0.06			
C2	neg	0.8	0.07			
U1	unkn	0.8	0.06			
U2	unkn	0.7	0.07			

Appendix IV. Delta Ca^{2+} release raw data for RYR1 transiently transfected HEK293 cells (n=9)

4CmC concentration (μM)	Delta WT	SEM	Delta Mutant	SEM
100	0.0017	0.001	0.006	0.0016
200	0.008	0.001	0.029	0.0024
400	0.024	0.002	0.047	0.005
600	0.035	0.005	0.066	0.005
800	0.040	0.005	0.081	0.007
1000	0.067	0.004	0.092	0.007

Appendix V. Primer sequences

Primer	Sequence 5'-3'	T_m °C
Mutagenesis construct 3 F	GCTTGCGGCCCGCACTCGAGC	80.1
Mutagenesis construct 3 R	GCTCGAGTGCGGGCCGCAAGC	80.6
pET32a(+) NcoI 1f	CGGCCCATGGTCGAGTGCCTCGGCCAGATC	87.8
pET32a(+) HindIII 1r	CGCGAAGCTTCCCAGGGTGGGAATCTGCAG	83.9
pET32a(+) NcoI 2f	CGGCGCCATGGACACCATGAGCCTGCTGAG	86.8
pET32a(+)HindIII 2r	CGGGAAGCTTAAGGATGCTGACATCTTTGG	76.1
pET32a(+) NcoI 3f	CGCGCATGGCCATCTCACCGTCCTCCGTG	89.0
pET32a(+)HindIII 3r	CGCGAAGCTTTTTGGCTGCACCAGAGC	80.2
pET32a(+) NcoI 4f	CGGCGCCATGGGGTGGGTGAGCTGCTGCG	92.2
pET32a(+)HindIII 4r	CGCGAAGCTTGTGGGAATCTGCAGTGGGAG	82.4
pProExHtb EcoRI 1f	CGGCGAATTCCGAGTGCCTCGGCCAGATC	84.9
pProExHtb HindIII 1r	CGGGAAGCTTCAGGGTGGGAATCTGCAGTG	81.6
pProExHtb EcoRI 2f	CGGCGAATTCACACCATGAGCCTGCTGAG	81.6
pProExHtb HindIII 2r	CGGGAAGCTTGGATGCTGACATCTTTGGC	79.6
pProExHtb EcoRI 3f	CGGCGAATTCCCATGTCACCGTCCTCCGTG	85.4
pProExHtb HindIII 3r87.6	CGCGAAGCTTCTTTGGCTGCACCAGAGCC	82.5
pProExHtb EcoRI 4f	CGGCGAATTCGGCTGGGTGAGCTGCTGCG	87.6
pProExHtb HindIII 4r	CGCGAAGCTTGGGAATCTGCAGTGGGAGG	82.5
LC Primer pair 1F (2434F)	CTTTGGTGAGGAACCGCCTGAAG	71.6

LC Primer pair 1R (RYR1 47ex R)	GGATGCTGACATCTTTGGCT	64.1
LC Primer pair 1F (4833 F)	CCATCCTGTCCTCTGTCAGCC	68.3
LC Primer pair 1R (4833 R)	TGGCGGTGGTCGTCTACC	67.3
HRM R2452W F	AGCCAAAGATGTCAGCATCC	54.3
HRM R2452W R	AGGGTTGCTCACCGTGTC	54.3
HPRT F	TCCAAAGATGGTCAAGGTCGC	68.6
HPRT R	TTCAAATCCAACAAAGTCTGGCT	65.6
pProExHtb M13 F	AGCGGATAACAATTTCACACAGG	65.8
pProExHtb M rvs	TTCTCTCATCCGCCAAAACAGC	69.4
pET_Upstream F	ATGCGTCCGGCGTAGA	53.5
T7_Terminator R	TGCTAGTTATTGCTCAGCGGT	63.0
H4833Y Primer Probe F	CACAGTCCTTCCTGTACC	59.1
H4833Y Primer Probe R	GCCCTTATCCCTTCACC	59.0
H4833Y Hybrid Probe F	GCGCACCATCCTGCCTC	61.0
H4833Y Hybrid Probe R	CACCCACAATGGGAAACAGC	59.4

Appendix VI. pET32a(+) vector map (Novagen)

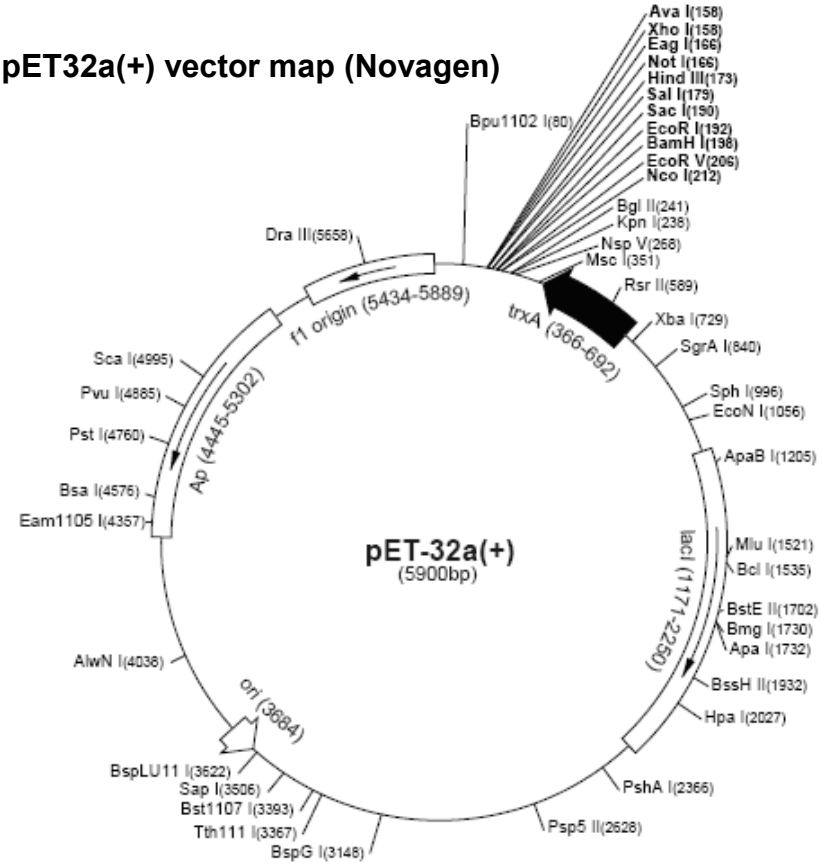

pET-32a-c(+) cloning/expression region

RYR1 central domain was cloned using the NcoI and HindIII restriction sites.

Appendix VII. pProExHtb vector map (Invitrogen)

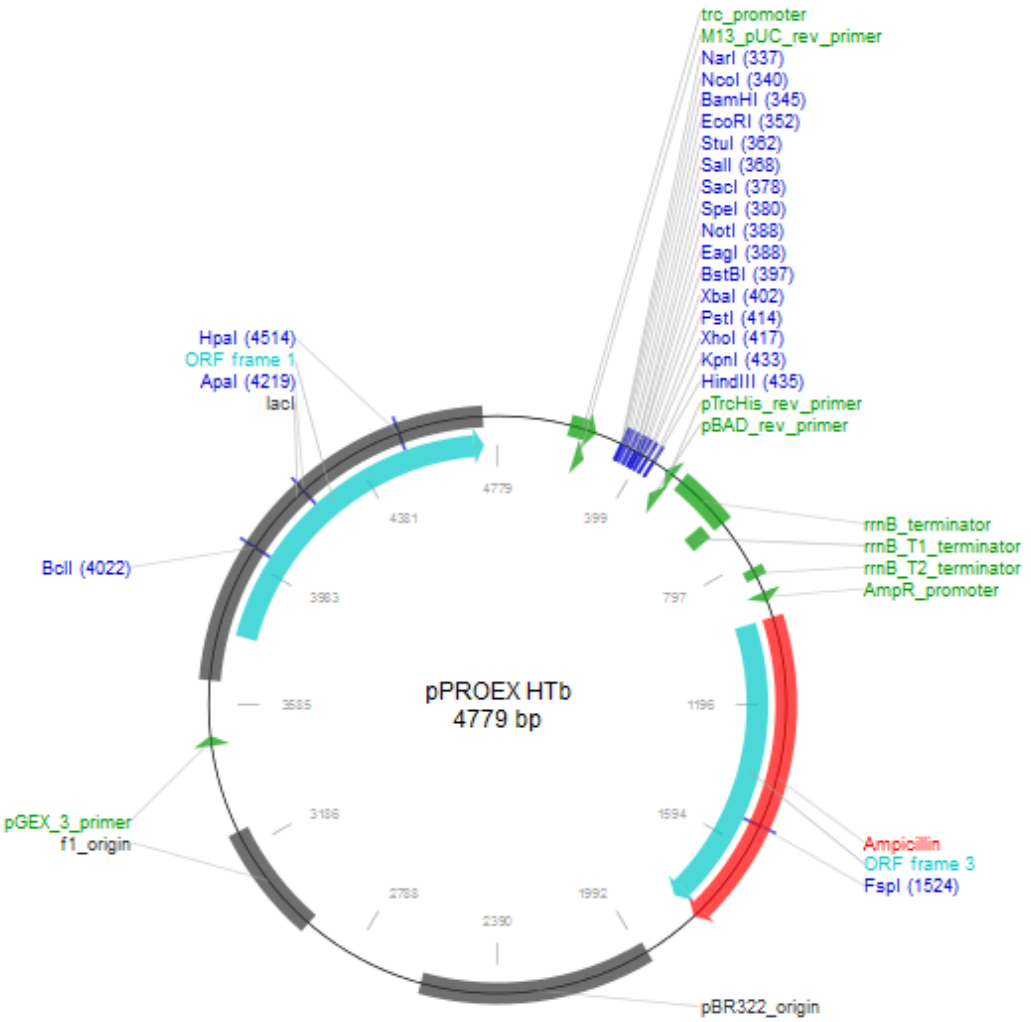

EcoRI and HindIII restriction sites were used to clone the RYR1 central domain into this vector.

Appendix VIII. Phyre^2 results for the R2452W RYR1 amino acids 2144-2489

Appendix IX. Phyre^2 results for WT RYR1 amino acids 2144-2489

Appendix X. HT trace for CD melting spectra of WT RYR1

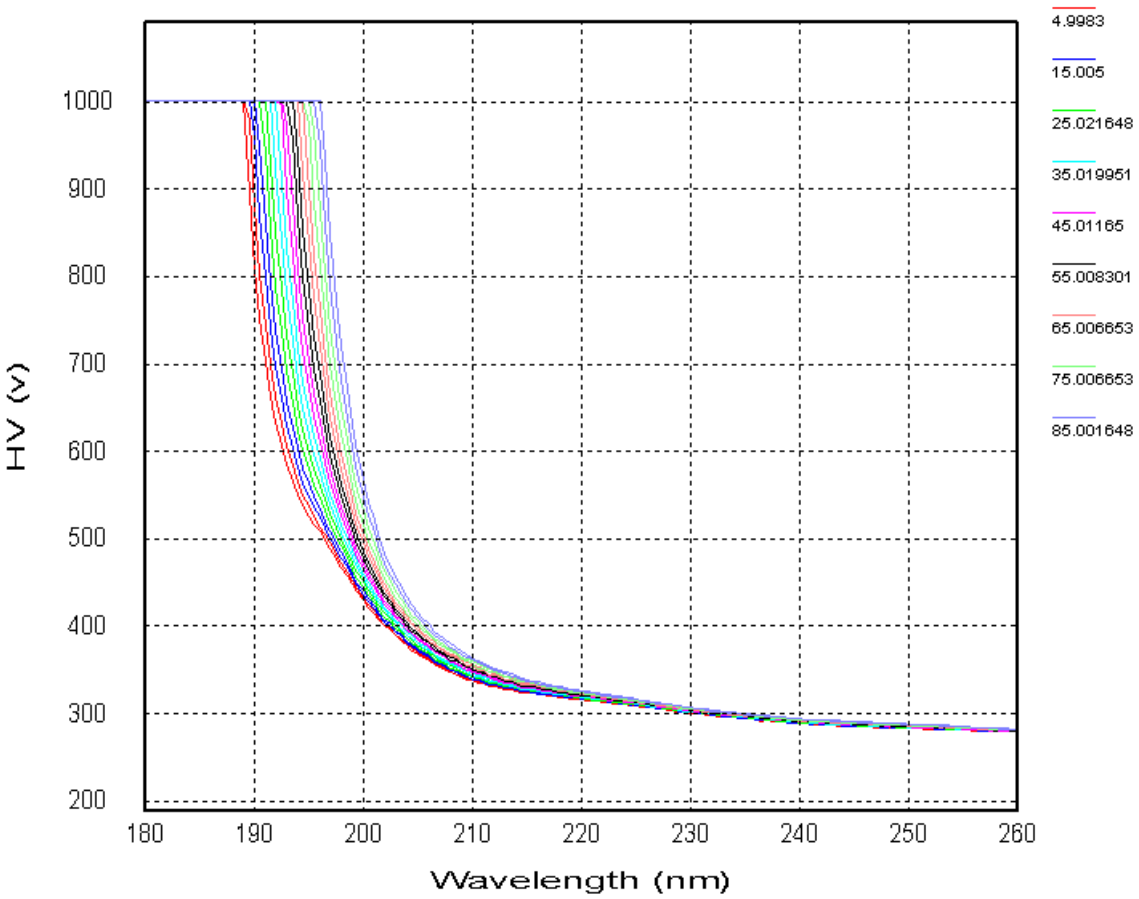

Temperatures are indicated on the right hand side. CD spectra show shifted HT traces to higher wavelengths with higher temperatures.

Appendix XI. Calibration curves Superdex S200 30/100

Void volume (V_o) = 7.8 mL

Column volume (V_c) = 24 mL

Elution volume (V_e)

$$K_{av} = \frac{V_e - V_o}{V_c - V_o}$$

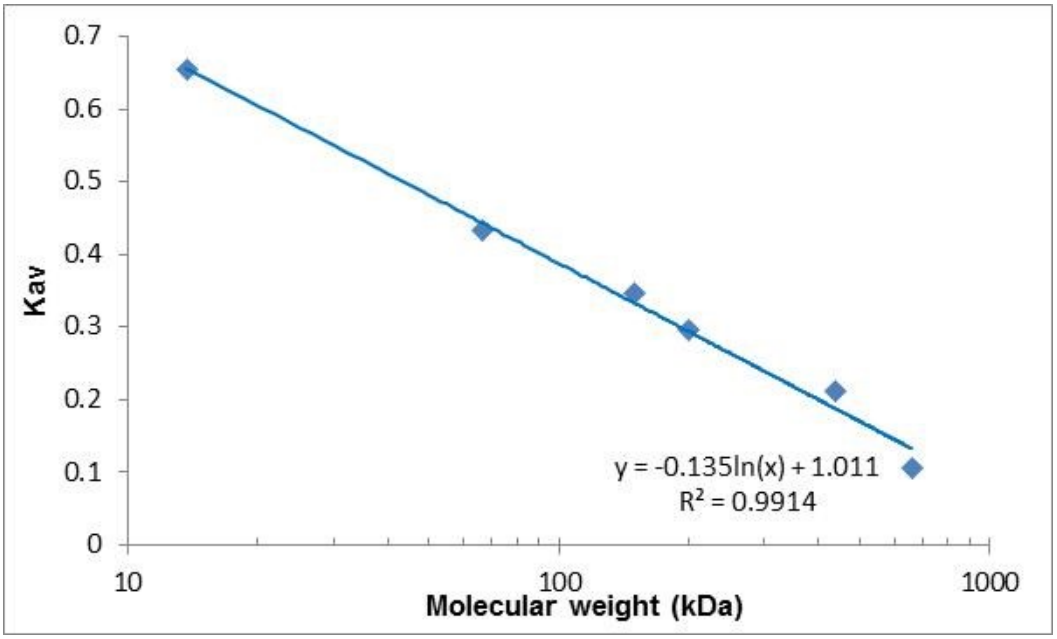

Buffer conditions: 10 mM Tris-HCl, pH 7.9, 10 mM NaCl, 1 mM DTT

Appendix XII. LightCycler standard curves

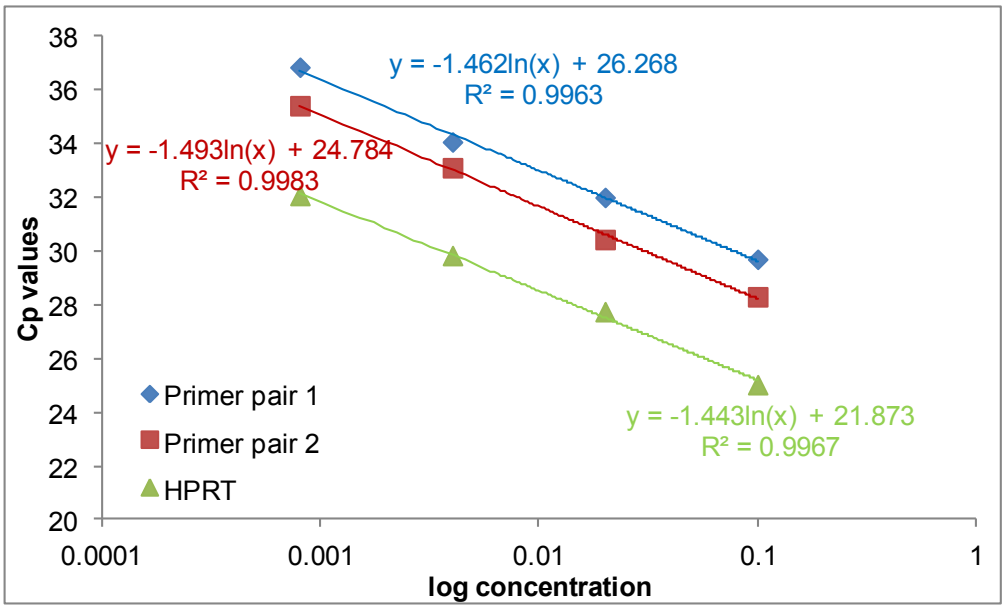

RT-pPCR standard curves using B-lymphoblastoid cell cDNA for primer pair 1 and 2 and HPRT primers.

Appendix XIII. Mass spec results 13 kDa fragment

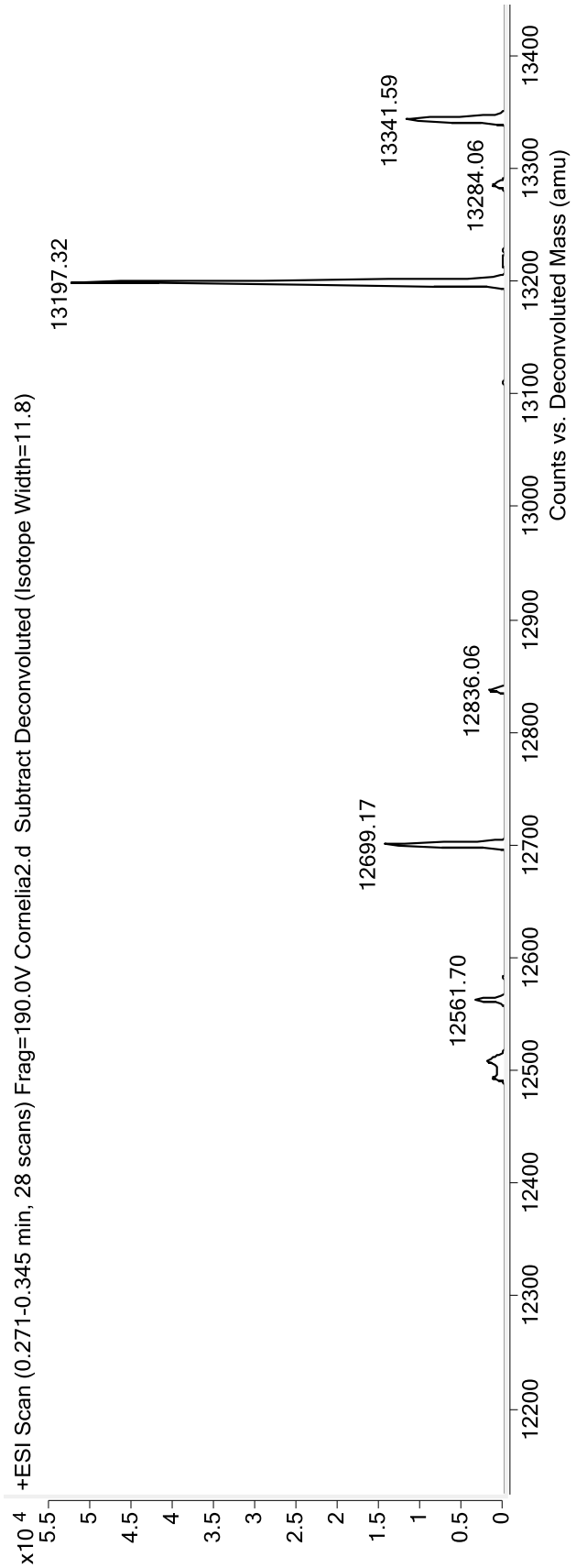

Appendix XIV. Mass spec results 37 kDa fragment

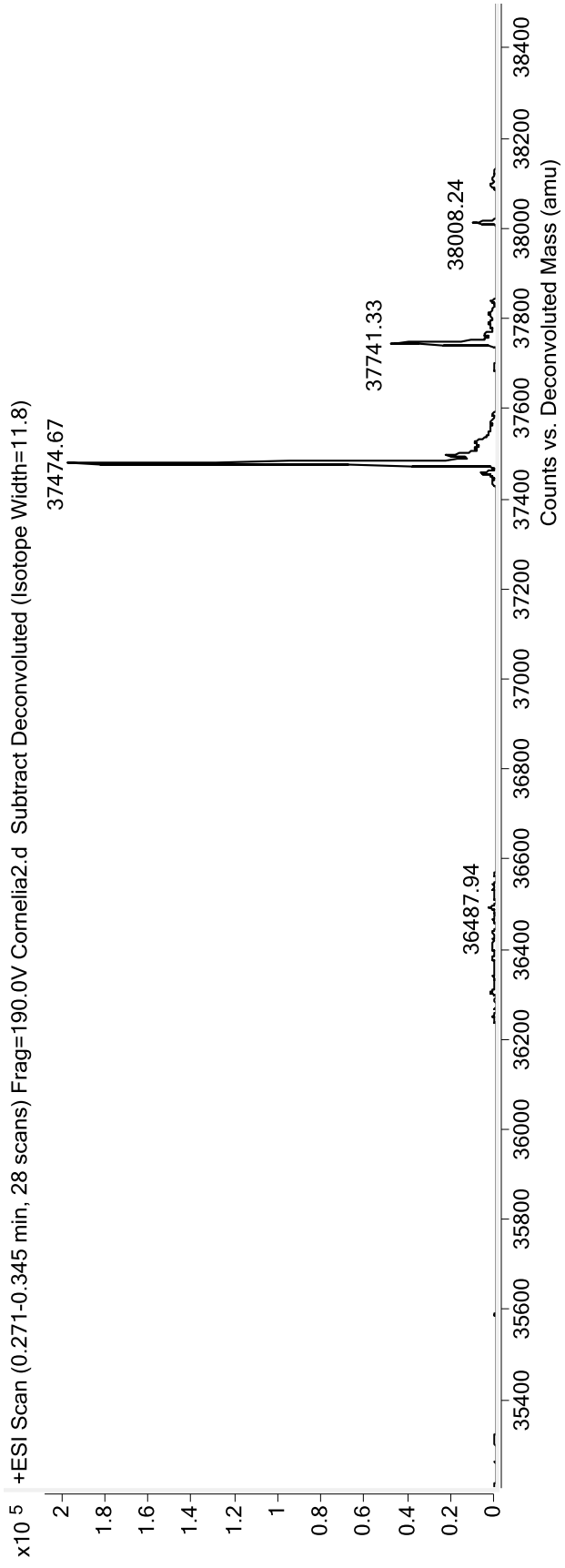

Appendix XV. Full-length pc-R2452W sequence

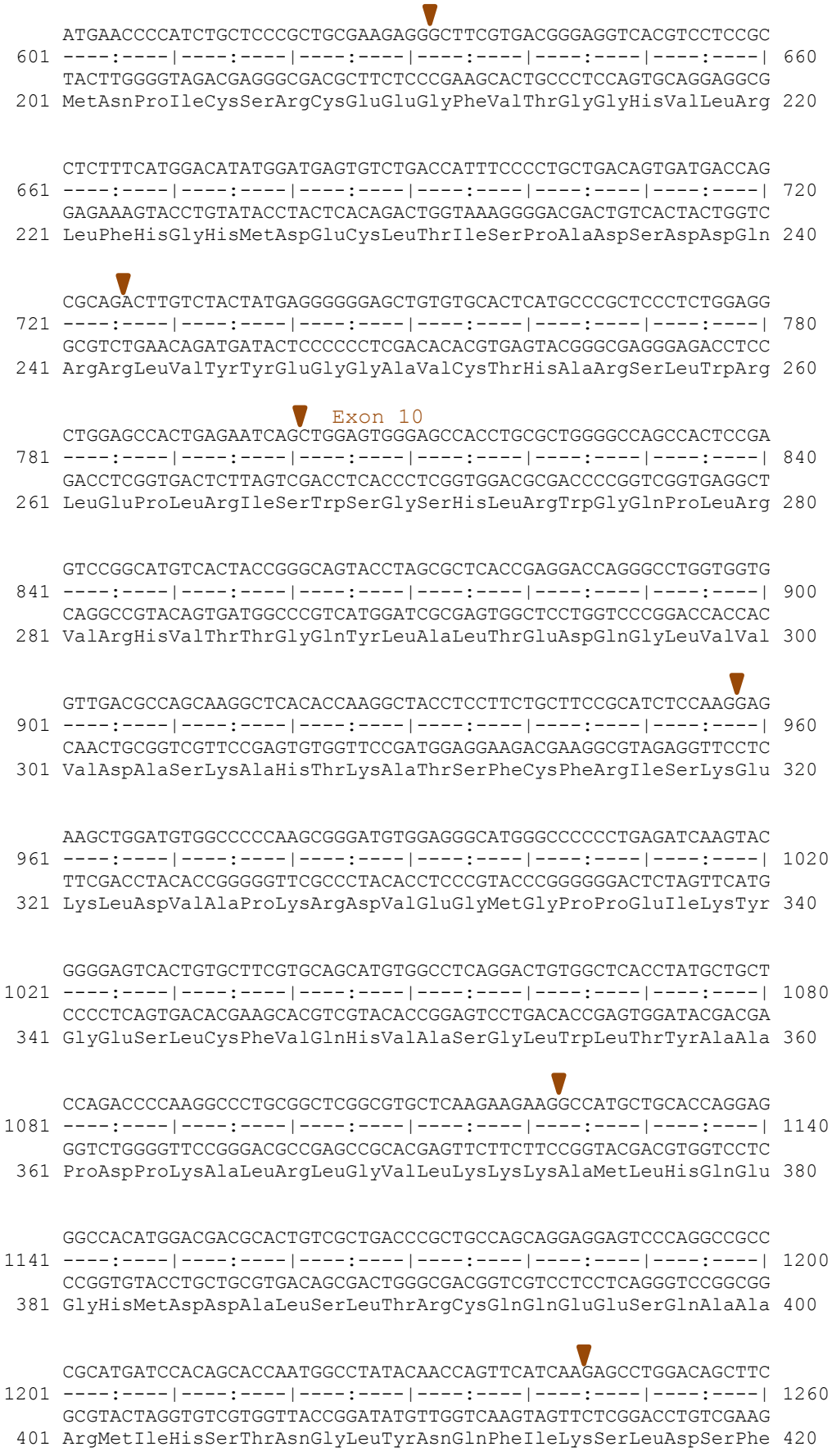
ATGAACCCCATCTGCTCCCGCTGCGAAGAGGGCTTCGTGACGGGAGGTCACGTCCTCCGC
601 ----:----|----:----|----:----|----:----|----:----|----:----| 660
TACTTGGGGTAGACGAGGGCGACGCTTCTCCCGAAGCACTGCCCTCCAGTGCAGGAGGCG
201 MetAsnProIleCysSerArgCysGluGluGlyPheValThrGlyGlyHisValLeuArg 220
CTCTTTCATGGACATATGGATGAGTGTCTGACCATTTCCCCTGCTGACAGTGATGACCAG
661 ----:----|----:----|----:----|----:----|----:----|----:----| 720
GAGAAAGTACCTGTATACCTACTCACAGACTGGTAAAGGGGACGACTGTCACTACTGGTC
221 LeuPheHisGlyHisMetAspGluCysLeuThrIleSerProAlaAspSerAspAspGln 240
CGCAGACTTGTCTACTATGAGGGGGGAGCTGTGTGCACTCATGCCCGCTCCCTCTGGAGG
721 ----:----|----:----|----:----|----:----|----:----|----:----| 780
GCGTCTGAACAGATGATACTCCCCCCTCGACACACGTGAGTACGGGCGAGGGAGACCTCC
241 ArgArgLeuValTyrTyrGluGlyGlyAlaValCysThrHisAlaArgSerLeuTrpArg 260
Exon 10
CTGGAGCCACTGAGAATCAGCTGGAGTGGGAGCCACCTGCGCTGGGGCCAGCCACTCCGA
781 ----:----|----:----|----:----|----:----|----:----|----:----| 840
GACCTCGGTGACTCTTAGTCGACCTCACCCTCGGTGGACGCGACCCCGGTCGGTGAGGCT
261 LeuGluProLeuArgIleSerTrpSerGlySerHisLeuArgTrpGlyGlnProLeuArg 280
GTCCGGCATGTCACTACCGGGCAGTACCTAGCGCTCACCGAGGACCAGGGCCTGGTGGTG
841 ----:----|----:----|----:----|----:----|----:----|----:----| 900
CAGGCCGTACAGTGATGGCCCGTCATGGATCGCGAGTGGCTCCTGGTCCCGGACCACCAC
281 ValArgHisValThrThrGlyGlnTyrLeuAlaLeuThrGluAspGlnGlyLeuValVal 300
GTTGACGCCAGCAAGGCTCACACCAAGGCTACCTCCTTCTGCTTCCGCATCTCCAAGGAG
901 ----:----|----:----|----:----|----:----|----:----|----:----| 960
CAACTGCGGTCGTTCCGAGTGTGGTTCCGATGGAGGAAGACGAAGGCGTAGAGGTTCCTC
301 ValAspAlaSerLysAlaHisThrLysAlaThrSerPheCysPheArgIleSerLysGlu 320
AAGCTGGATGTGGCCCCCAAGCGGGATGTGGAGGGCATGGGCCCCCCCTGAGATCAAGTAC
961 ----:----|----:----|----:----|----:----|----:----|----:----| 1020
TTCGACCTACACCGGGGGTTCGCCCTACACCTCCCGTACCCGGGGGGACTCTAGTTCATG
321 LysLeuAspValAlaProLysArgAspValGluGlyMetGlyProProGluIleLysTyr 340
GGGGAGTCACTGTGCTTCGTGCAGCATGTGGCCTCAGGACTGTGGCTCACCTATGCTGCT
1021 ----:----|----:----|----:----|----:----|----:----|----:----| 1080
CCCCTCAGTGACACGAAGCACGTCGTACACCGGAGTCCTGACACCGAGTGGATACGACGA
341 GlyGluSerLeuCysPheValGlnHisValAlaSerGlyLeuTrpLeuThrTyrAlaAla 360
CCAGACCCCAAGGCCCTGCGGCTCGGCGTGCTCAAGAAGAAGGCCATGCTGCACCAGGAG
1081 ----:----|----:----|----:----|----:----|----:----|----:----| 1140
GGTCTGGGGTTCCGGGACGCCGAGCCGCACGAGTTCTTCTTCCGGTACGACGTGGTCCTC
361 ProAspProLysAlaLeuArgLeuGlyValLeuLysLysLysAlaMetLeuHisGlnGlu 380
GGCCACATGGACGACGCACTGTCGCTGACCCGCTGCCAGCAGGAGGAGTCCCAGGCCGCC
1141 ----:----|----:----|----:----|----:----|----:----|----:----| 1200
CCGGTGTACCTGCTGCGTGACAGCGACTGGGCGACGGTCGTCCTCCTCAGGGTCCGGCGG
381 GlyHisMetAspAspAlaLeuSerLeuThrArgCysGlnGlnGluGluSerGlnAlaAla 400
CGCATGATCCACAGCACCAATGGCCTATACAACCAGTTCATCAAGAGCCTGGACAGCTTC
1201 ----:----|----:----|----:----|----:----|----:----|----:----| 1260
GCGTACTAGGTGTCGTGGTTACCGGATATGTTGGTCAAGTAGTTCTCGGACCTGTCGAAG
401 ArgMetIleHisSerThrAsnGlyLeuTyrAsnGlnPheIleLysSerLeuAspSerPhe 420


AGCGGGAAGCCACGGGGCTCGGGGCCACCCGCTGGCACGGCGCTGCCCATCGAGGGCGTT
1261 ----:----|----:----|----:----|----:----|----:----|----:----|----:----| 1320
TCGCCCTTCGGTGCCCCGAGCCCCGGTGGGCGACCGTGCCGCGACGGGTAGCTCCCGCAA
421 SerGlyLysProArgGlySerGlyProProAlaGlyThrAlaLeuProIleGluGlyVal 440
ATCCTGAGCCTGCAGGACCTCATCATCTACTTCGAGCCTCCCTCCGAGGACTTGCAGCAC
1321 ----:----|----:----|----:----|----:----|----:----|----:----|----:----| 1380
TAGGACTCGGACGTCCTGGAGTAGTAGATGAAGCTCGGAGGGAGGCTCCTGAACGTCGTG
441 IleLeuSerLeuGlnAspLeuIleIleTyrPheGluProProSerGluAspLeuGlnHis 460
GAGGAGAAGCAGAGCAAGCTGCGAAGCCTGCGCAACCGCCAGAGCCTCTTCCAGGAGGAG
1381 ----:----|----:----|----:----|----:----|----:----|----:----|----:----| 1440
CTCCTCTTCGTCTCGTTCGACGCTTCGGACGCGTTGGCGGTCTCGGAGAAGGTCCTCCTC
461 GluGluLysGlnSerLysLeuArgSerLeuArgAsnArgGlnSerLeuPheGlnGluGlu 480
GGGATGCTCTCCATGGTCCTGAATTGCATAGACCGCCTAAATGTCTACACCACTGCTGCC
1441 ----:----|----:----|----:----|----:----|----:----|----:----|----:----| 1500
CCCTACGAGAGGTACCAGGACTTAACGTATCTGGCGGATTTACAGATGTGGTGACGACGG
481 GlyMetLeuSerMetValLeuAsnCysIleAspArgLeuAsnValTyrThrThrAlaAla 500
CACTTTGCTGAGTTTGCAGGGGAGGAGGCAGCCGAGTCCTGGAAAGAGATTGTGAATCTT
1501 ----:----|----:----|----:----|----:----|----:----|----:----|----:----| 1560
GTGAAACGACTCAAACGTCCCCTCCTCCGTCGGCTCAGGACCTTTCTCTAACACTTAGAA
501 HisPheAlaGluPheAlaGlyGluGluAlaAlaGluSerTrpLysGluIleValAsnLeu 520
CTCTATGAACTCCTAGCTTCTCTAATCCGTGGCAATCGTAGCAACTGTGCCCTCTTCTCC
1561 ----:----|----:----|----:----|----:----|----:----|----:----|----:----| 1620
GAGATACTTGAGGATCGAAGAGATTAGGCACCGTTAGCATCGTTGACACGGGAGAAGAGG
521 LeuTyrGluLeuLeuAlaSerLeuIleArgGlyAsnArgSerAsnCysAlaLeuPheSer 540
Exon 15
ACAAACTTGGACTGGCTGGTCAGCAAGCTGGATCGGCTGGAGGCCTCGTCTGGCATCCTG
1621 ----:----|----:----|----:----|----:----|----:----|----:----|----:----| 1680
TGTTTGAACCTGACCGACCAGTCGTTCGACCTAGCCGACCTCCGGAGCAGACCGTAGGAC
541 ThrAsnLeuAspTrpLeuValSerLysLeuAspArgLeuGluAlaSerSerGlyIleLeu 560
GAGGTCCTGTACTGTGTCCTCATTGAGAGTCCAGAGGTTCTGAACATCATCCAGGAGAAT
1681 ----:----|----:----|----:----|----:----|----:----|----:----|----:----| 1740
CTCCAGGACATGACACAGGAGTAACTCTCAGGTCTCCAAGACTTGTAGTAGGTCCTCTTA
561 GluValLeuTyrCysValLeuIleGluSerProGluValLeuAsnIleIleGlnGluAsn 580
CACATCAAGTCCATCATCTCCCTCCTGGACAAGCATGGGAGGAACCACAAGGTCCTGGAC
1741 ----:----|----:----|----:----|----:----|----:----|----:----|----:----| 1800
GTGTAGTTCAGGTAGTAGAGGGAGGACCTGTTCGTACCCTCCTTGGTGTTCCAGGACCTG
581 HisIleLysSerIleIleSerLeuLeuAspLysHisGlyArgAsnHisLysValLeuAsp 600
GTGCTATGCTCCCTGTGTGTGTGTAATGGTGTGGCTGTACGCTCCAACCAAGATCTTATT
1801 ----:----|----:----|----:----|----:----|----:----|----:----|----:----| 1860
CACGATACGAGGGACACACACACATTACCACACCGACATGCGAGGTTGGTTCTAGAATAA
601 ValLeuCysSerLeuCysValCysAsnGlyValAlaValArgSerAsnGlnAspLeuIle 620
ACTGAGAACTTGCTGCCTGGCCGTGAGCTTCTGCTGCAGACAAACCTCATCAACTATGTC
1861 ----:----|----:----|----:----|----:----|----:----|----:----|----:----| 1920
TGACTCTTGAACGACGGACCGGCACTCGAAGACGACGTCTGTTTGGAGTAGTTGATACAG
621 ThrGluAsnLeuLeuProGlyArgGluLeuLeuLeuGlnThrAsnLeuIleAsnTyrVal 640
ACCAGCATCCGCCCCAACATCTTTGTGGGCCGAGCGGAAGGCACCACGCAGTACAGCAAA
1921 ----:----|----:----|----:----|----:----|----:----|----:----|----:----| 1980
TGGTCGTAGGCGGGGTTGTAGAAACACCCGGCTCGCCTTCCGTGGTGCGTCATGTCGTTT
641 ThrSerIleArgProAsnIlePheValGlyArgAlaGluGlyThrThrGlnTyrSerLys 660

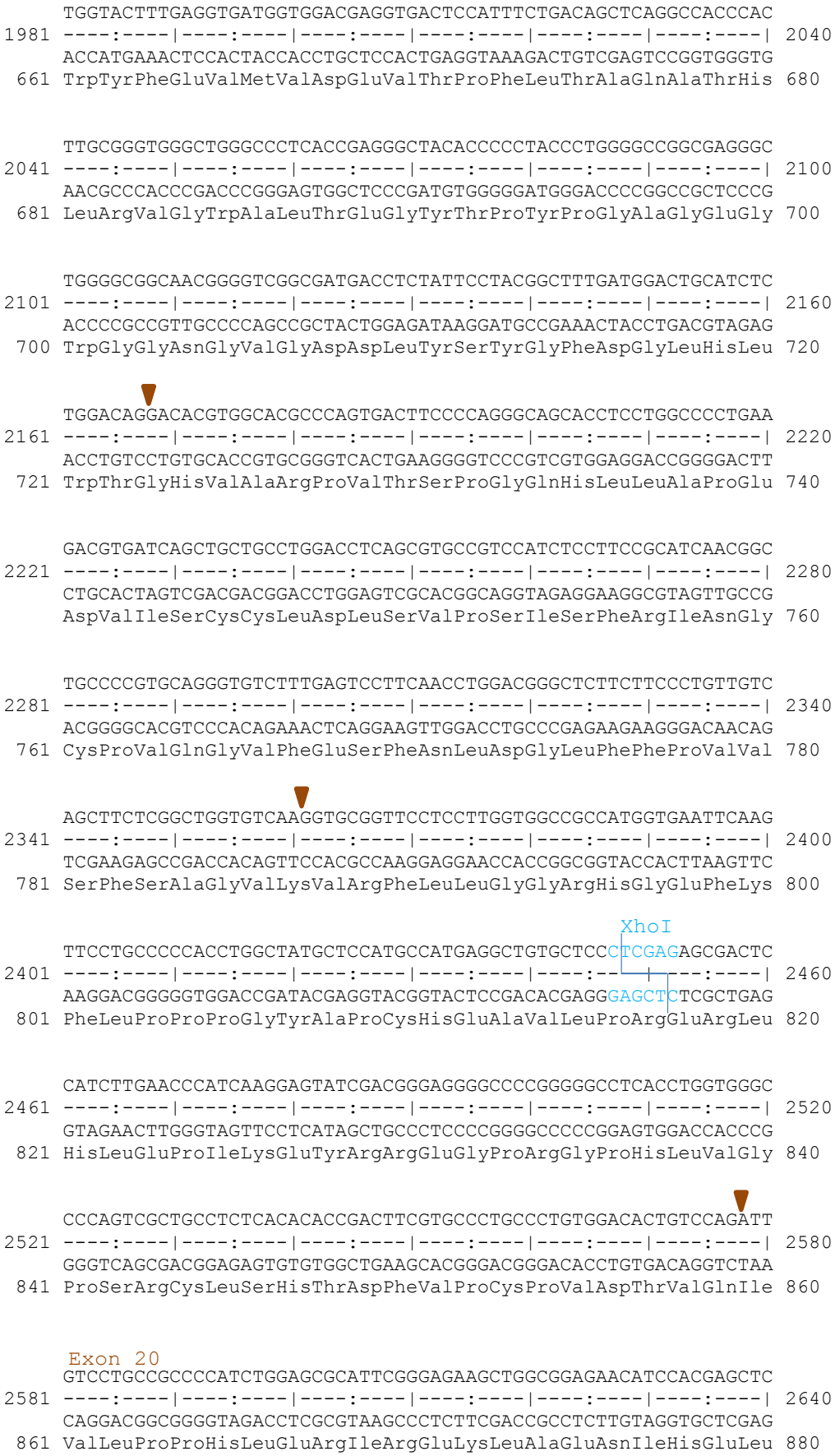
TGGTACTTTGAGGTGATGGTGGACGAGGTGACTCCATTTCTGACAGCTCAGGCCACCCAC
1981 ----:----|----:----|----:----|----:----|----:----|----:----|----:----| 2040
ACCATGAAACTCCACTACCACCTGCTCCACTGAGGTAAAGACTGTCGAGTCCGGTGGGTG
661 TrpTyrPheGluValMetValAspGluValThrProPheLeuThrAlaGlnAlaThrHis 680
TTGCGGGTGGGCTGGGCCCTCACCGAGGGCTACACCCCCTACCCTGGGGCCGGCGAGGGC
2041 ----:----|----:----|----:----|----:----|----:----|----:----|----:----| 2100
AACGCCCACCCGACCCGGGAGTGGCTCCCGATGTGGGGGATGGGACCCCGGCCGCTCCCG
681 LeuArgValGlyTrpAlaLeuThrGluGlyTyrThrProTyrProGlyAlaGlyGluGly 700
TGGGGCGGCAACGGGGTCGGCGATGACCTCTATTCCTACGGCTTTGATGGACTGCATCTC
2101 ----:----|----:----|----:----|----:----|----:----|----:----|----:----| 2160
ACCCCGCCGTTGCCCCAGCCGCTACTGGAGATAAGGATGCCGAAACTACCTGACGTAGAG
700 TrpGlyGlyAsnGlyValGlyAspAspLeuTyrSerTyrGlyPheAspGlyLeuHisLeu 720
TGGACAGGACACGTGGCACGCCCAGTGACTTCCCCAGGGCAGCACCTCCTGGCCCCTGAA
2161 ----:----|----:----|----:----|----:----|----:----|----:----|----:----| 2220
ACCTGTCCTGTGCACCGTGCGGGTCACTGAAGGGGTCCCGTCGTGGAGGACCGGGGACTT
721 TrpThrGlyHisValAlaArgProValThrSerProGlyGlnHisLeuLeuAlaProGlu 740
GACGTGATCAGCTGCTGCCTGGACCTCAGCGTGCCGTCCATCTCCTTCCGCATCAACGGC
2221 ----:----|----:----|----:----|----:----|----:----|----:----|----:----| 2280
CTGCACTAGTCGACGACGGACCTGGAGTCGCACGGCAGGTAGAGGAAGGCGTAGTTGCCG
AspValIleSerCysCysLeuAspLeuSerValProSerIleSerPheArgIleAsnGly 760
TGCCCCGTGCAGGGTGTCTTTGAGTCCTTCAACCTGGACGGGCTCTTCTTCCCTGTTGTC
2281 ----:----|----:----|----:----|----:----|----:----|----:----|----:----| 2340
ACGGGGCACGTCCCACAGAAACTCAGGAAGTTGGACCTGCCCGAGAAGAAGGGACAACAG
761 CysProValGlnGlyValPheGluSerPheAsnLeuAspGlyLeuPhePheProValVal 780
AGCTTCTCGGCTGGTGTCAAGGTGCGGTTCCTCCTTGGTGGCCGCCATGGTGAATTCAAG
2341 ----:----|----:----|----:----|----:----|----:----|----:----|----:----| 2400
TCGAAGAGCCGACCACAGTTCCACGCCAAGGAGGAACCACCGGCGGTACCACTTAAGTTC
781 SerPheSerAlaGlyValLysValArgPheLeuLeuGlyGlyArgHisGlyGluPheLys 800
XhoI
TTCCTGCCCCCACCTGGCTATGCTCCATGCCATGAGGCTGTGCTCCCTCGAGAGCGACTC
2401 ----:----|----:----|----:----|----:----|----:----|----:----|----:----| 2460
AAGGACGGGGGTGGACCGATACGAGGTACGGTACTCCGACACGAGGGAGCTCTCGCTGAG
801 PheLeuProProProGlyTyrAlaProCysHisGluAlaValLeuProArgGluArgLeu 820
CATCTTGAACCCATCAAGGAGTATCGACGGGAGGGGCCCCGGGGGCCTCACCTGGTGGGC
2461 ----:----|----:----|----:----|----:----|----:----|----:----|----:----| 2520
GTAGAACTTGGGTAGTTCCTCATAGCTGCCCTCCCCGGGGCCCCCGGAGTGGACCACCCG
821 HisLeuGluProIleLysGluTyrArgArgGluGlyProArgGlyProHisLeuValGly 840
CCCAGTCGCTGCCTCTCACACACCGACTTCGTGCCCTGCCCTGTGGACACTGTCCAGATT
2521 ----:----|----:----|----:----|----:----|----:----|----:----|----:----| 2580
GGGTCAGCGACGGAGAGTGTGTGGCTGAAGCACGGGACGGGACACCTGTGACAGGTCTAA
841 ProSerArgCysLeuSerHisThrAspPheValProCysProValAspThrValGlnIle 860
Exon 20
GTCCTGCCGCCCCATCTGGAGCGCATTCGGGAGAAGCTGGCGGAGAACATCCACGAGCTC
2581 ----:----|----:----|----:----|----:----|----:----|----:----|----:----| 2640
CAGGACGGCGGGGTAGACCTCGCGTAAGCCCTCTTCGACCGCCTCTTGTAGGTGCTCGAG
861 ValLeuProProHisLeuGluArgIleArgGluLysLeuAlaGluAsnIleHisGluLeu 880

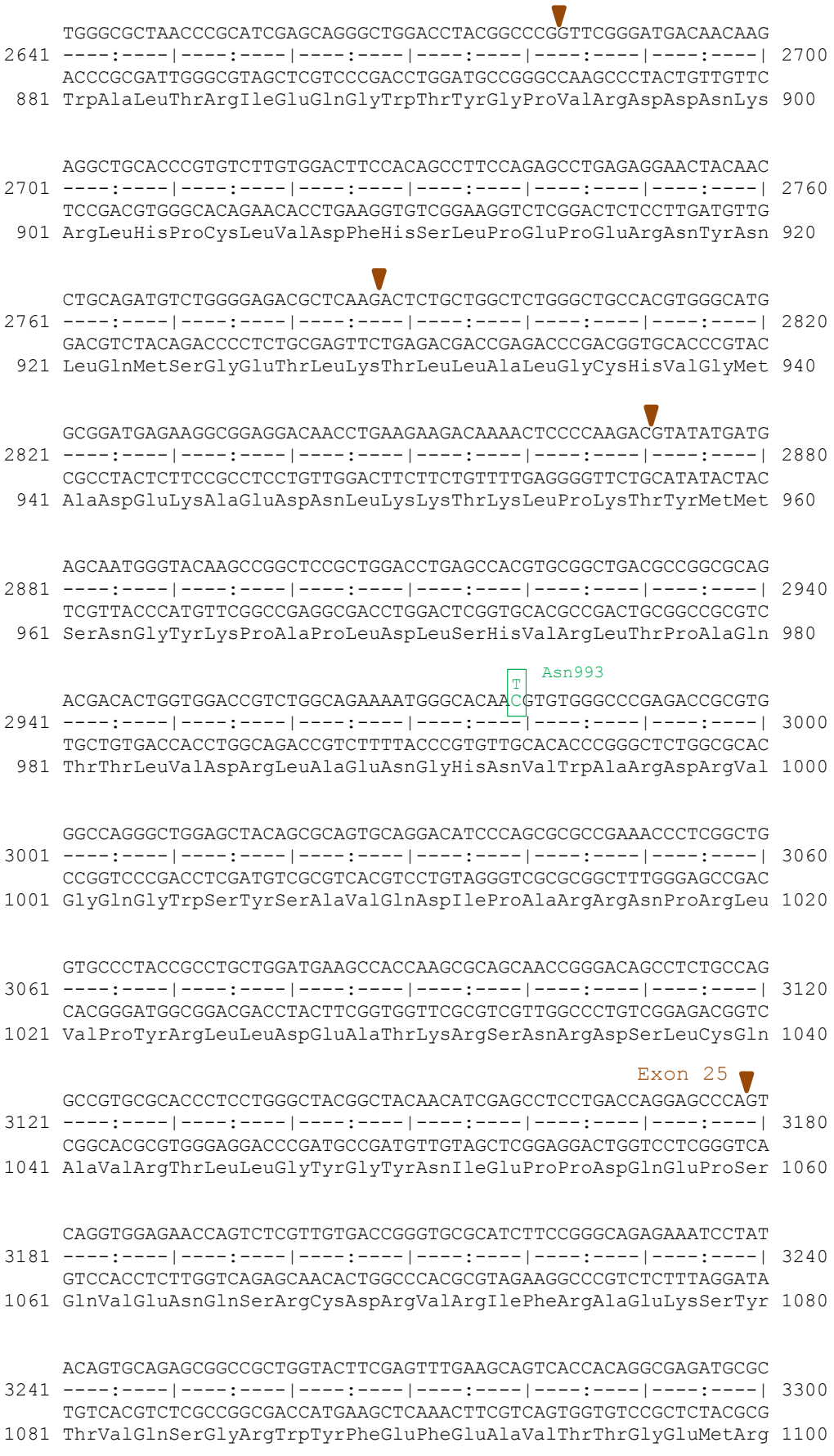
TGGGCGCTAACCCGCATCGAGCAGGGCTGGACCTACGGCCCGGTTCGGGATGACAACAAG
2641 ----:----|----:----|----:----|----:----|----:----|----:----|----:----| 2700
ACCCGCGATTGGGCGTAGCTCGTCCCGACCTGGATGCCGGGCCAAGCCCTACTGTTGTTC
881 TrpAlaLeuThrArgIleGluGlnGlyTrpThrTyrGlyProValArgAspAspAsnLys 900
AGGCTGCACCCGTGTCTTGTGGACTTCCACAGCCTTCCAGAGCCTGAGAGGAACTACAAC
2701 ----:----|----:----|----:----|----:----|----:----|----:----|----:----| 2760
TCCGACGTGGGCACAGAACACCTGAAGGTGTCGGAAGGTCTCGGACTCTCCTTGATGTTG
901 ArgLeuHisProCysLeuValAspPheHisSerLeuProGluProGluArgAsnTyrAsn 920
CTGCAGATGTCTGGGGAGACGCTCAAGACTCTGCTGGCTCTGGGCTGCCACGTGGGCATG
2761 ----:----|----:----|----:----|----:----|----:----|----:----|----:----| 2820
GACGTCTACAGACCCCTCTGCGAGTTCTGAGACGACCGAGACCCGACGGTGCACCCGTAC
921 LeuGlnMetSerGlyGluThrLeuLysThrLeuLeuAlaLeuGlyCysHisValGlyMet 940
GCGGATGAGAAGGCGGAGGACAACCTGAAGAAGACAAAACTCCCCAAGACGTATATGATG
2821 ----:----|----:----|----:----|----:----|----:----|----:----|----:----| 2880
CGCCTACTCTTCCGCCTCCTGTTGGACTTCTTCTGTTTTGAGGGGTTCTGCATATACTAC
941 AlaAspGluLysAlaGluAspAsnLeuLysLysThrLysLeuProLysThrTyrMetMet 960
AGCAATGGGTACAAGCCGGCTCCGCTGGACCTGAGCCACGTGCGGCTGACGCCGGCGCAG
2881 ----:----|----:----|----:----|----:----|----:----|----:----|----:----| 2940
TCGTTACCCATGTTCGGCCGAGGCGACCTGGACTCGGTGCACGCCGACTGCGGCCGCGTC
961 SerAsnGlyTyrLysProAlaProLeuAspLeuSerHisValArgLeuThrProAlaGln 980
Asn993
T
ACGACACTGGTGGACCGTCTGGCAGAAAATGGGCACAACGTGTGGGCCCGAGACCGCGTG
2941 ----:----|----:----|----:----|----:----|----:----|----:----|----:----| 3000
TGCTGTGACCACCTGGCAGACCGTCTTTTACCCGTGTTGCACACCCGGGCTCTGGCGCAC
981 ThrThrLeuValAspArgLeuAlaGluAsnGlyHisAsnValTrpAlaArgAspArgVal 1000
GGCCAGGGCTGGAGCTACAGCGCAGTGCAGGACATCCCAGCGCGCCGAAACCCTCGGCTG
3001 ----:----|----:----|----:----|----:----|----:----|----:----|----:----| 3060
CCGGTCCCGACCTCGATGTCGCGTCACGTCCTGTAGGGTCGCGCGGCTTTGGGAGCCGAC
1001 GlyGlnGlyTrpSerTyrSerAlaValGlnAspIleProAlaArgArgAsnProArgLeu 1020
GTGCCCTACCGCCTGCTGGATGAAGCCACCAAGCGCAGCAACCGGGACAGCCTCTGCCAG
3061 ----:----|----:----|----:----|----:----|----:----|----:----|----:----| 3120
CACGGGATGGCGGACGACCTACTTCGGTGGTTCGCGTCGTTGGCCCTGTCGGAGACGGTC
1021 ValProTyrArgLeuLeuAspGluAlaThrLysArgSerAsnArgAspSerLeuCysGln 1040
Exon 25
GCCGTGCGCACCCTCCTGGGCTACGGCTACAACATCGAGCCTCCTGACCAGGAGCCCAGT
3121 ----:----|----:----|----:----|----:----|----:----|----:----|----:----| 3180
CGGCACGCGTGGGAGGACCCGATGCCGATGTTGTAGCTCGGAGGACTGGTCCTCGGGTCA
1041 AlaValArgThrLeuLeuGlyTyrGlyTyrAsnIleGluProProAspGlnGluProSer 1060
CAGGTGGAGAACCAGTCTCGTTGTGACCGGGTGCGCATCTTCCGGGCAGAGAAATCCTAT
3181 ----:----|----:----|----:----|----:----|----:----|----:----|----:----| 3240
GTCCACCTCTTGGTCAGAGCAACACTGGCCCACGCGTAGAAGGCCCGTCTCTTTAGGATA
1061 GlnValGluAsnGlnSerArgCysAspArgValArgIlePheArgAlaGluLysSerTyr 1080
ACAGTGCAGAGCGGCCGCTGGTACTTCGAGTTTGAAGCAGTCACCACAGGCGAGATGCGC
3241 ----:----|----:----|----:----|----:----|----:----|----:----|----:----| 3300
TGTCACGTCTCGCCGGCGACCATGAAGCTCAAACTTCGTCAGTGGTGTCCGCTCTACGCG
1081 ThrValGlnSerGlyArgTrpTyrPheGluPheGluAlaValThrThrGlyGluMetArg 1100

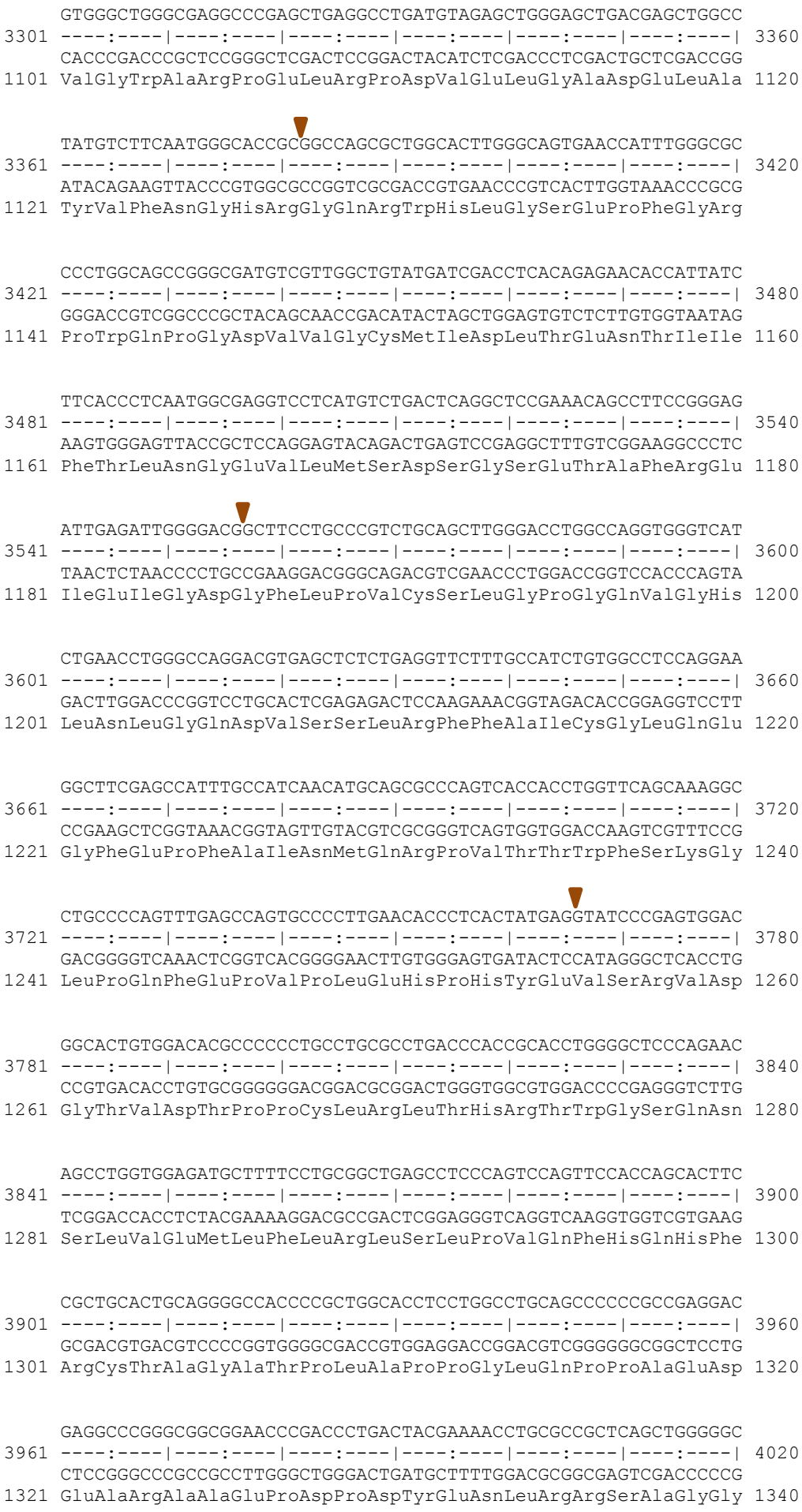
GTGGGCTGGGCGAGGCCCGAGCTGAGGCCTGATGTAGAGCTGGGAGCTGACGAGCTGGCC
3301 ----:----|----:----|----:----|----:----|----:----|----:----|----:----| 3360
CACCCGACCCGCTCCGGGCTCGACTCCGGACTACATCTCGACCCTCGACTGCTCGACCGG
1101 ValGlyTrpAlaArgProGluLeuArgProAspValGluLeuGlyAlaAspGluLeuAla 1120
TATGTCTTCAATGGGCACCGCGGCCAGCGCTGGCACTTGGGCAGTGAACCATTTGGGCGC
3361 ----:----|----:----|----:----|----:----|----:----|----:----|----:----| 3420
ATACAGAAGTTACCCGTGGCGCCGGTCGCGACCGTGAACCCGTCACTTGGTAAACCCGCG
1121 TyrValPheAsnGlyHisArgGlyGlnArgTrpHisLeuGlySerGluProPheGlyArg
CCCTGGCAGCCGGGCGATGTCGTTGGCTGTATGATCGACCTCACAGAGAACACCATTATC
3421 ----:----|----:----|----:----|----:----|----:----|----:----|----:----| 3480
GGGACCGTCGGCCCGCTACAGCAACCGACATACTAGCTGGAGTGTCTCTTGTGGTAATAG
1141 ProTrpGlnProGlyAspValValGlyCysMetIleAspLeuThrGluAsnThrIleIle 1160
TTCACCCTCAATGGCGAGGTCCTCATGTCTGACTCAGGCTCCGAAACAGCCTTCCGGGAG
3481 ----:----|----:----|----:----|----:----|----:----|----:----|----:----| 3540
AAGTGGGAGTTACCGCTCCAGGAGTACAGACTGAGTCCGAGGCTTTGTCGGAAGGCCCTC
1161 PheThrLeuAsnGlyGluValLeuMetSerAspSerGlySerGluThrAlaPheArgGlu 1180
ATTGAGATTGGGGACGGCTTCCTGCCCGTCTGCAGCTTGGGACCTGGCCAGGTGGGTCAT
3541 ----:----|----:----|----:----|----:----|----:----|----:----|----:----| 3600
TAACTCTAACCCCTGCCGAAGGACGGGCAGACGTCGAACCCTGGACCGGTCCACCCAGTA
1181 IleGluIleGlyAspGlyPheLeuProValCysSerLeuGlyProGlyGlnValGlyHis 1200
CTGAACCTGGGCCAGGACGTGAGCTCTCTGAGGTTCTTTGCCATCTGTGGCCTCCAGGAA
3601 ----:----|----:----|----:----|----:----|----:----|----:----|----:----| 3660
GACTTGGACCCGGTCCTGCACTCGAGAGACTCCAAGAAACGGTAGACACCGGAGGTCCTT
1201 LeuAsnLeuGlyGlnAspValSerSerLeuArgPhePheAlaIleCysGlyLeuGlnGlu 1220
GGCTTCGAGCCATTTGCCATCAACATGCAGCGCCCAGTCACCACCTGGTTCAGCAAAGGC
3661 ----:----|----:----|----:----|----:----|----:----|----:----|----:----| 3720
CCGAAGCTCGGTAAACGGTAGTTGTACGTCGCGGGTCAGTGGTGGACCAAGTCGTTTCCG
1221 GlyPheGluProPheAlaIleAsnMetGlnArgProValThrThrTrpPheSerLysGly 1240
CTGCCCCAGTTTGAGCCAGTGCCCCTTGAACACCCTCACTATGAGGTATCCCGAGTGGAC
3721 ----:----|----:----|----:----|----:----|----:----|----:----|----:----| 3780
GACGGGGTCAAACTCGGTCACGGGGAACTTGTGGGAGTGATACTCCATAGGGCTCACCTG
1241 LeuProGlnPheGluProValProLeuGluHisProHisTyrGluValSerArgValAsp 1260
GGCACTGTGGACACGCCCCCCTGCCTGCGCCTGACCCACCGCACCTGGGGCTCCCAGAAC
3781 ----:----|----:----|----:----|----:----|----:----|----:----|----:----| 3840
CCGTGACACCTGTGCGGGGGGACGGACGCGGACTGGGTGGCGTGGACCCCGAGGGTCTTG
1261 GlyThrValAspThrProProCysLeuArgLeuThrHisArgThrTrpGlySerGlnAsn 1280
AGCCTGGTGGAGATGCTTTTCCTGCGGCTGAGCCTCCCAGTCCAGTTCCACCAGCACTTC
3841 ----:----|----:----|----:----|----:----|----:----|----:----|----:----| 3900
TCGGACCACCTCTACGAAAAGGACGCCGACTCGGAGGGTCAGGTCAAGGTGGTCGTGAAG
1281 SerLeuValGluMetLeuPheLeuArgLeuSerLeuProValGlnPheHisGlnHisPhe 1300
CGCTGCACTGCAGGGGCCACCCCGCTGGCACCTCCTGGCCTGCAGCCCCCCGCCGAGGAC
3901 ----:----|----:----|----:----|----:----|----:----|----:----|----:----| 3960
GCGACGTGACGTCCCCGGTGGGGCGACCGTGGAGGACCGGACGTCGGGGGGCGGCTCCTG
1301 ArgCysThrAlaGlyAlaThrProLeuAlaProProGlyLeuGlnProProAlaGluAsp 1320
GAGGCCCGGGCGGCGGAACCCGACCCTGACTACGAAAACCTGCGCCGCTCAGCTGGGGGC
3961 ----:----|----:----|----:----|----:----|----:----|----:----|----:----| 4020
CTCCGGGCCCGCCGCCTTGGGCTGGGACTGATGCTTTTGGACGCGGCGAGTCGACCCCCG
1321 GluAlaArgAlaAlaGluProAspProAspTyrGluAsnLeuArgArgSerAlaGlyGly 1340

```
     TGGAGCGAGGCAGAGAACGGCAAAGAAGGGACTGCGAAGGAGGGCGCCCCCGGGGGCACC
4021 ----:----|----:----|----:----|----:----|----:----|----:----|----:----| 4080
     ACCTCGCTCCGTCTCTTGCCGTTTCTTCCCTGACGCTTCCTCCCGCGGGGGCCCCCGTGG
1341 TrpSerGluAlaGluAsnGlyLysGluGlyThrAlaLysGluGlyAlaProGlyGlyThr

     CCGCAGGCGGGGGGAGAGGCGCAGCCCGCCAGGGCGGAGAATGAGAAGGATGCCACCACC
4081 ----:----|----:----|----:----|----:----|----:----|----:----|----:----| 4140
     GGCGTCCGCCCCCCTCTCCGCGTCGGGCGGTCCCGCCTCTTACTCTTCCTACGGTGGTGG
1361 ProGlnAlaGlyGlyGluAlaGlnProAlaArgAlaGluAsnGluLysAspAlaThrThr 1380

     GAGAAGAACAAGAAGAGAGGCTTCTTATTCAAGGCCAAGAAGGTCGCCATGATGACCCAG
4141 ----:----|----:----|----:----|----:----|----:----|----:----|----:----| 4200
     CTCTTCTTGTTCTTCTCTCCGAAGAATAAGTTCCGGTTCTTCCAGCGGTACTACTGGGTC
1381 GluLysAsnLysLysArgGlyPheLeuPheLysAlaLysLysValAlaMetMetThrGln 1400

     CCACCGGCCACCCCCACGCTGCCCCGACTCCCTCACGACGTGGTGCCTGCAGACAACCGC
4201 ----:----|----:----|----:----|----:----|----:----|----:----|----:----| 4260
     GGTGGCCGGTGGGGGTGCGACGGGGCTGAGGGAGTGCTGCACCACGGACGTCTGTTGGCG
1401 ProProAlaThrProThrLeuProArgLeuProHisAspValValProAlaAspAsnArg 1420

                                                Exon 30
     GATGACCCCGAGATCATCCTCAACACCACCACGTACTATTACTCCGTGAGGGTCTTTGCT
4261 ----:----|----:----|----:----|----:----|----:----|----:----|----:----| 4320
     CTACTGGGGCTCTAGTAGGAGTTGTGGTGGTGCATGATAATGAGGCACTCCCAGAAACGA
1421 AspAspProGluIleIleLeuAsnThrThrThrTyrTyrTyrSerValArgValPheAla 1440

     GGACAGGAGCCCAGCTGCGTGTGGGCGGGCTGGGTCACCCCTGACTACCATCAGCACGAC
4321 ----:----|----:----|----:----|----:----|----:----|----:----|----:----| 4380
     CCTGTCCTCGGGTCGACGCACACCCGCCCGACCCAGTGGGGACTGATGGTAGTCGTGCTG
1441 GlyGlnGluProSerCysValTrpAlaGlyTrpValThrProAspTyrHisGlnHisAsp 1460

     ATGAGCTTCGACCTCAGCAAGGTCCGGGTCGTGACGGTGACCATGGGGGATGAACAAGGC
4381 ----:----|----:----|----:----|----:----|----:----|----:----|----:----| 4440
     TACTCGAAGCTGGAGTCGTTCCAGGCCCAGCACTGCCACTGGTACCCCCTACTTGTTCCG
1461 MetSerPheAspLeuSerLysValArgValValThrValThrMetGlyAspGluGlnGly 1480

     AACGTCCACAGCAGCCTCAAGTGTAGCAACTGCTACATGGTGTGGGGCGGAGACTTTGTG
4441 ----:----|----:----|----:----|----:----|----:----|----:----|----:----| 4500
     TTGCAGGTGTCGTCGGAGTTCACATCGTTGACGATGTACCACACCCCGCCTCTGAAACAC
1481 AsnValHisSerSerLeuLysCysSerAsnCysTyrMetValTrpGlyGlyAspPheVal 1500

     AGTCCCGGGCAGCAGGGCCGGATCAGCCACACGGACCTTGTCATTGGGTGCCTGGTGGAC
4501 ----:----|----:----|----:----|----:----|----:----|----:----|----:----| 4560
     TCAGGGCCCGTCGTCCCGGCCTAGTCGGTGTGCCTGGAACAGTAACCCACGGACCACCTG
1501 SerProGlyGlnGlnGlyArgIleSerHisThrAspLeuValIleGlyCysLeuValAsp 1520

     TTGGCCACTGGCTTAATGACCTTTACAGCCAATGGCAAAGAGAGCAACACCTTTTTCCAG
4561 ----:----|----:----|----:----|----:----|----:----|----:----|----:----| 4620
     AACCGGTGACCGAATTACTGGAAATGTCGGTTACCGTTTCTCTCGTTGTGGAAAAAGGTC
1521 LeuAlaThrGlyLeuMetThrPheThrAlaAsnGlyLysGluSerAsnThrPhePheGln 1540

     GTGGAACCCAACACTAAGCTATTTCCTGCCGTCTTCGTCCTGCCCACCCACCAGAACGTC
4620 ----:----|----:----|----:----|----:----|----:----|----:----|----:----| 4680
     CACCTTGGGTTGTGATTCGATAAAGGACGGCAGAAGCAGGACGGGTGGGTGGTCTTGCAG
1541 ValGluProAsnThrLysLeuPheProAlaValPheValLeuProThrHisGlnAsnVal 1560

     ATCCAGTTTGAGCTGGGGAAGCAGAAGAACATCATGCCGTTGTCAGCCGCCATGTTCCAA
4681 ----:----|----:----|----:----|----:----|----:----|----:----|----:----| 4740
     TAGGTCAAACTCGACCCCTTCGTCTTCTTGTAGTACGGCAACAGTCGGCGGTACAAGGTT
1561 IleGlnPheGluLeuGlyLysGlnLysAsnIleMetProLeuSerAlaAlaMetPheGln 1580
```

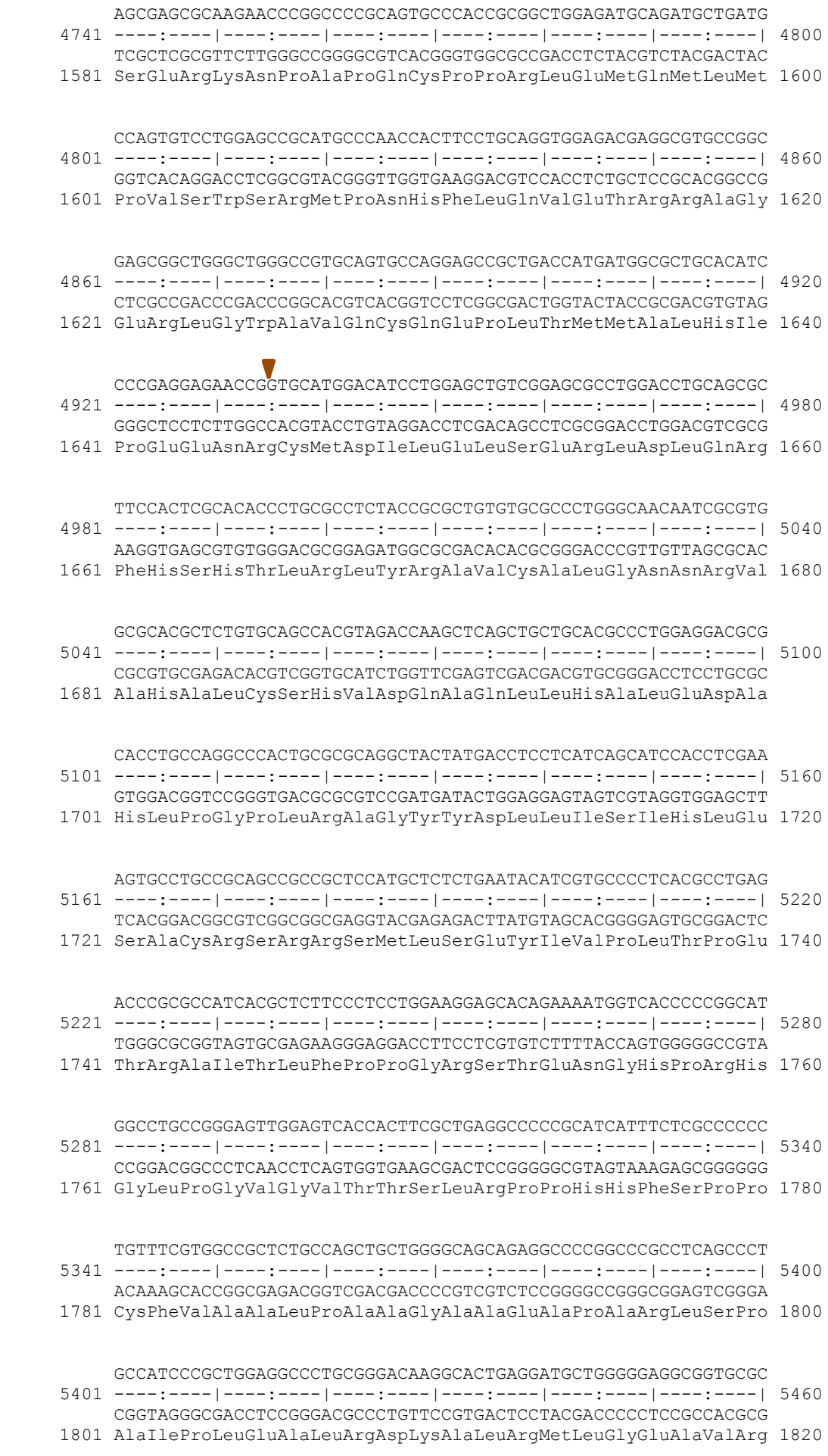
AGCGAGCGCAAGAACCCGGCCCCGCAGTGCCCACCGCGGCTGGAGATGCAGATGCTGATG
4741 ----:----|----:----|----:----|----:----|----:----|----:----| 4800
TCGCTCGCGTTCTTGGGCCGGGGCGTCACGGGTGGCGCCGACCTCTACGTCTACGACTAC
1581 SerGluArgLysAsnProAlaProGlnCysProProArgLeuGluMetGlnMetLeuMet 1600
CCAGTGTCCTGGAGCCGCATGCCCAACCACTTCCTGCAGGTGGAGACGAGGCGTGCCGGC
4801 ----:----|----:----|----:----|----:----|----:----|----:----| 4860
GGTCACAGGACCTCGGCGTACGGGTTGGTGAAGGACGTCCACCTCTGCTCCGCACGGCCG
1601 ProValSerTrpSerArgMetProAsnHisPheLeuGlnValGluThrArgArgAlaGly 1620
GAGCGGCTGGGCTGGGCCGTGCAGTGCCAGGAGCCGCTGACCATGATGGCGCTGCACATC
4861 ----:----|----:----|----:----|----:----|----:----|----:----| 4920
CTCGCCGACCCGACCCGGCACGTCACGGTCCTCGGCGACTGGTACTACCGCGACGTGTAG
1621 GluArgLeuGlyTrpAlaValGlnCysGlnGluProLeuThrMetMetAlaLeuHisIle 1640
CCCGAGGAGAACCGGTGCATGGACATCCTGGAGCTGTCGGAGCGCCTGGACCTGCAGCGC
4921 ----:----|----:----|----:----|----:----|----:----|----:----| 4980
GGGCTCCTCTTGGCCACGTACCTGTAGGACCTCGACAGCCTCGCGGACCTGGACGTCGCG
1641 ProGluGluAsnArgCysMetAspIleLeuGluLeuSerGluArgLeuAspLeuGlnArg 1660
TTCCACTCGCACACCCTGCGCCTCTACCGCGCTGTGTGCGCCCTGGGCAACAATCGCGTG
4981 ----:----|----:----|----:----|----:----|----:----|----:----| 5040
AAGGTGAGCGTGTGGGACGCGGAGATGGCGCGACACACGCGGGACCCGTTGTTAGCGCAC
1661 PheHisSerHisThrLeuArgLeuTyrArgAlaValCysAlaLeuGlyAsnAsnArgVal 1680
GCGCACGCTCTGTGCAGCCACGTAGACCAAGCTCAGCTGCTGCACGCCCTGGAGGACGCG
5041 ----:----|----:----|----:----|----:----|----:----|----:----| 5100
CGCGTGCGAGACACGTCGGTGCATCTGGTTCGAGTCGACGACGTGCGGGACCTCCTGCGC
1681 AlaHisAlaLeuCysSerHisValAspGlnAlaGlnLeuLeuHisAlaLeuGluAspAla
CACCTGCCAGGCCCACTGCGCGCAGGCTACTATGACCTCCTCATCAGCATCCACCTCGAA
5101 ----:----|----:----|----:----|----:----|----:----|----:----| 5160
GTGGACGGTCCGGGTGACGCGCGTCCGATGATACTGGAGGAGTAGTCGTAGGTGGAGCTT
1701 HisLeuProGlyProLeuArgAlaGlyTyrTyrAspLeuLeuIleSerIleHisLeuGlu 1720
AGTGCCTGCCGCAGCCGCCGCTCCATGCTCTCTGAATACATCGTGCCCCTCACGCCTGAG
5161 ----:----|----:----|----:----|----:----|----:----|----:----| 5220
TCACGGACGGCGTCGGCGGCGAGGTACGAGAGACTTATGTAGCACGGGGAGTGCGGACTC
1721 SerAlaCysArgSerArgArgSerMetLeuSerGluTyrIleValProLeuThrProGlu 1740
ACCCGCGCCATCACGCTCTTCCCTCCTGGAAGGAGCACAGAAAATGGTCACCCCCGGCAT
5221 ----:----|----:----|----:----|----:----|----:----|----:----| 5280
TGGGCGCGGTAGTGCGAGAAGGGAGGACCTTCCTCGTGTCTTTTACCAGTGGGGGCCGTA
1741 ThrArgAlaIleThrLeuPheProProGlyArgSerThrGluAsnGlyHisProArgHis 1760
GGCCTGCCGGGAGTTGGAGTCACCACTTCGCTGAGGCCCCCGCATCATTTCTCGCCCCCC
5281 ----:----|----:----|----:----|----:----|----:----|----:----| 5340
CCGGACGGCCCTCAACCTCAGTGGTGAAGCGACTCCGGGGGCGTAGTAAAGAGCGGGGGG
1761 GlyLeuProGlyValGlyValThrThrSerLeuArgProProHisHisPheSerProPro 1780
TGTTTCGTGGCCGCTCTGCCAGCTGCTGGGGCAGCAGAGGCCCCGGCCCGCCTCAGCCCT
5341 ----:----|----:----|----:----|----:----|----:----|----:----| 5400
ACAAAGCACCGGCGAGACGGTCGACGACCCCGTCGTCTCCGGGGCCGGGCGGAGTCGGGA
1781 CysPheValAlaAlaLeuProAlaAlaGlyAlaAlaGluAlaProAlaArgLeuSerPro 1800
GCCATCCCGCTGGAGGCCCTGCGGGACAAGGCACTGAGGATGCTGGGGGAGGCGGTGCGC
5401 ----:----|----:----|----:----|----:----|----:----|----:----| 5460
CGGTAGGGCGACCTCCGGGACGCCCTGTTCCGTGACTCCTACGACCCCCTCCGCCACGCG
1801 AlaIleProLeuGluAlaLeuArgAspLysAlaLeuArgMetLeuGlyGluAlaValArg 1820


GACGGTGGGCAGCACGCTCGCGACCCCGTCGGGGGCTCCGTGGAGTTCCAGTTTGTGCCT
5461 ----:----|----:----|----:----|----:----|----:----|----:----|----:----| 5520
CTGCCACCCGTCGTGCGAGCGCTGGGGCAGCCCCCGAGGCACCTCAAGGTCAAACACGGA
1821 AspGlyGlyGlnHisAlaArgAspProValGlyGlySerValGluPheGlnPheValPro 1840
Exon 35
GTGCTCAAGCTCGTGTCCACCCTGCTGGTGATGGGCATCTTTGGCGATGAGGATGTGAAA
5521 ----:----|----:----|----:----|----:----|----:----|----:----|----:----| 5580
CACGAGTTCGAGCACAGGTGGGACGACCACTACCCGTAGAAACCGCTACTCCTACACTTT
1841 ValLeuLysLeuValSerThrLeuLeuValMetGlyIlePheGlyAspGluAspValLys 1860
CAGATCTTGAAGATGATTGAGCCTGAGGTCTTCACTGAGGAAGAAGAGGAGGAGGACGAG
5581 ----:----|----:----|----:----|----:----|----:----|----:----|----:----| 5640
GTCTAGAACTTCTACTAACTCGGACTCCAGAAGTGACTCCTTCTTCTCCTCCTCCTGCTC
1861 GlnIleLeuLysMetIleGluProGluValPheThrGluGluGluGluGluAspGlu 1880
GAGGAAGAGGGTGAAGAGGAAGATGAGGAGGAGAAGGAGGAGGATGAGGAGGAAACAGCA
5641 ----:----|----:----|----:----|----:----|----:----|----:----|----:----| 5700
CTCCTTCTCCCACTTCTCCTTCTACTCCTCCTCTTCCTCCTCCTACTCCTCCTTTGTCGT
1881 GluGluGluGlyGluGluGluAspGluGluGluLysGluGluAspGluGluGluThrAla 1900
CAGGAAAAGGAAGATGAGGAAAAAGAGGAAGAGGAGGCAGCAGAAGGGGAGAAAGAAGAA
5701 ----:----|----:----|----:----|----:----|----:----|----:----|----:----| 5760
GTCCTTTTCCTTCTACTCCTTTTTCTCCTTCTCCTCCGTCGTCTTCCCCTCTTTCTTCTT
1901 GlnGluLysGluAspGluGluLysGluGluGluGluAlaAlaGluGlyGluLysGluGlu 1920
GGCTTGGAGGAAGGGCTGCTCCAGATGAAGTTGCCAGAGTCTGTGAAGTTACAGATGTGC
5761 ----:----|----:----|----:----|----:----|----:----|----:----|----:----| 5820
CCGAACCTCCTTCCCGACGAGGTCTACTTCAACGGTCTCAGACACTTCAATGTCTACACG
1921 GlyLeuGluGluGlyLeuLeuGlnMetLysLeuProGluSerValLysLeuGlnMetCys 1940
CACCTGCTGGAGTATTTCTGTGACCAAGAGCTGCAGCACCGTGTGGAGTCCCTGGCAGCC
5821 ----:----|----:----|----:----|----:----|----:----|----:----|----:----| 5880
GTGGACGACCTCATAAAGACACTGGTTCTCGACGTCGTGGCACACCTCAGGGACCGTCGG
1941 HisLeuLeuGluTyrPheCysAspGlnGluLeuGlnHisArgValGluSerLeuAlaAla 1960
TTTGCGGAGCGCTATGTGGACAAGCTCCAGGCCAACCAGCGGAGCCGCTATGGCCTCCTC
5881 ----:----|----:----|----:----|----:----|----:----|----:----|----:----| 5940
AAACGCCTCGCGATACACCTGTTCGAGGTCCGGTTGGTCGCCTCGGCGATACCGGAGGAG
1961 PheAlaGluArgTyrValAspLysLeuGlnAlaAsnGlnArgSerArgTyrGlyLeuLeu 1980
ATAAAAGCCTTCAGCATGACCGCAGCAGAGACTGCAAGACGTACCCGCGAGTTCCGCTCC
5941 ----:----|----:----|----:----|----:----|----:----|----:----|----:----| 6000
TATTTTCGGAAGTCGTACTGGCGTCGTCTCTGACGTTCTGCATGGGCGCTCAAGGCGAGG
1981 IleLysAlaPheSerMetThrAlaAlaGluThrAlaArgArgThrArgGluPheArgSer 2000
CCACCCCAGGAACAGATCAATATGCTATTGCAATTCAAAGATGGTACAGATGAGGAAGAC
6001 ----:----|----:----|----:----|----:----|----:----|----:----|----:----| 6060
GGTGGGGTCCTTGTCTAGTTATACGATAACGTTAAGTTTCTACCATGTCTACTCCTTCTG
2001 ProProGlnGluGlnIleAsnMetLeuLeuGlnPheLysAspGlyThrAspGluGluAsp 2020
TGTCCTCTCCCTGAAGAGATTCGACAGGATTTGCTTGACTTTCATCAAGACCTGCTGGCA
6061 ----:----|----:----|----:----|----:----|----:----|----:----|----:----| 6120
ACAGGAGAGGGACTTCTCTAAGCTGTCCTAAACGAACTGAAAGTAGTTCTGGACGACCGT
2021 CysProLeuProGluGluIleArgGlnAspLeuLeuAspPheHisGlnAspLeuLeuAla 2040
CACTGTGGAATTCAGCTAGATGGAGAGGAGGAGGAACCAGAGGAAGAGACCACCCTGGGC
6121 ----:----|----:----|----:----|----:----|----:----|----:----|----:----| 6180
GTGACACCTTAAGTCGATCTACCTCTCCTCCTCCTTGGTCTCCTTCTCTGGTGGGACCCG
2041 HisCysGlyIleGlnLeuAspGlyGluGluGluGluProGluGluGluThrThrLeuGly 2060

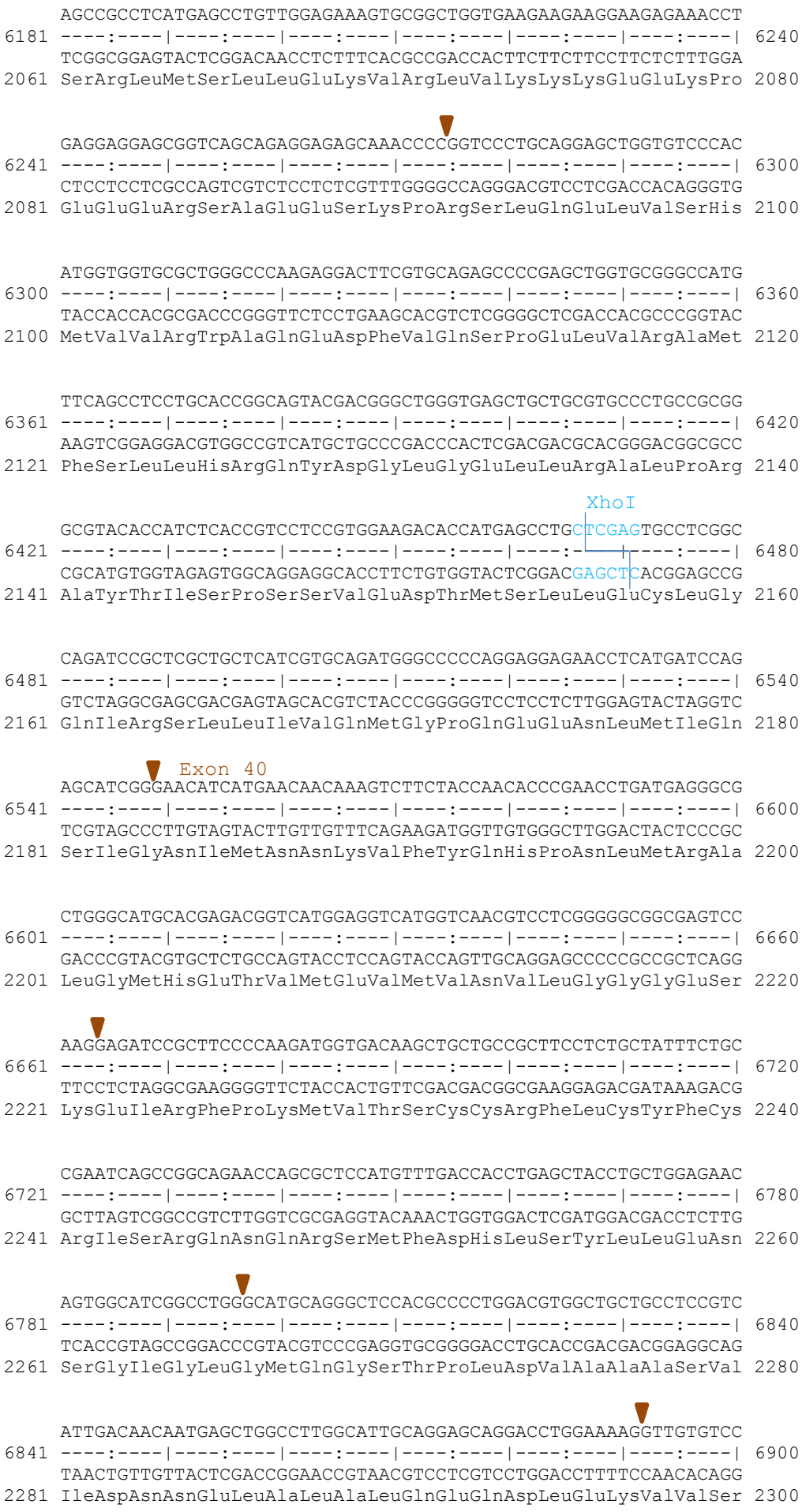
XhoI
Exon 40


Exon 45
LC Primer pair 2F
C7354T
R2452W
LC Primer pair 2R

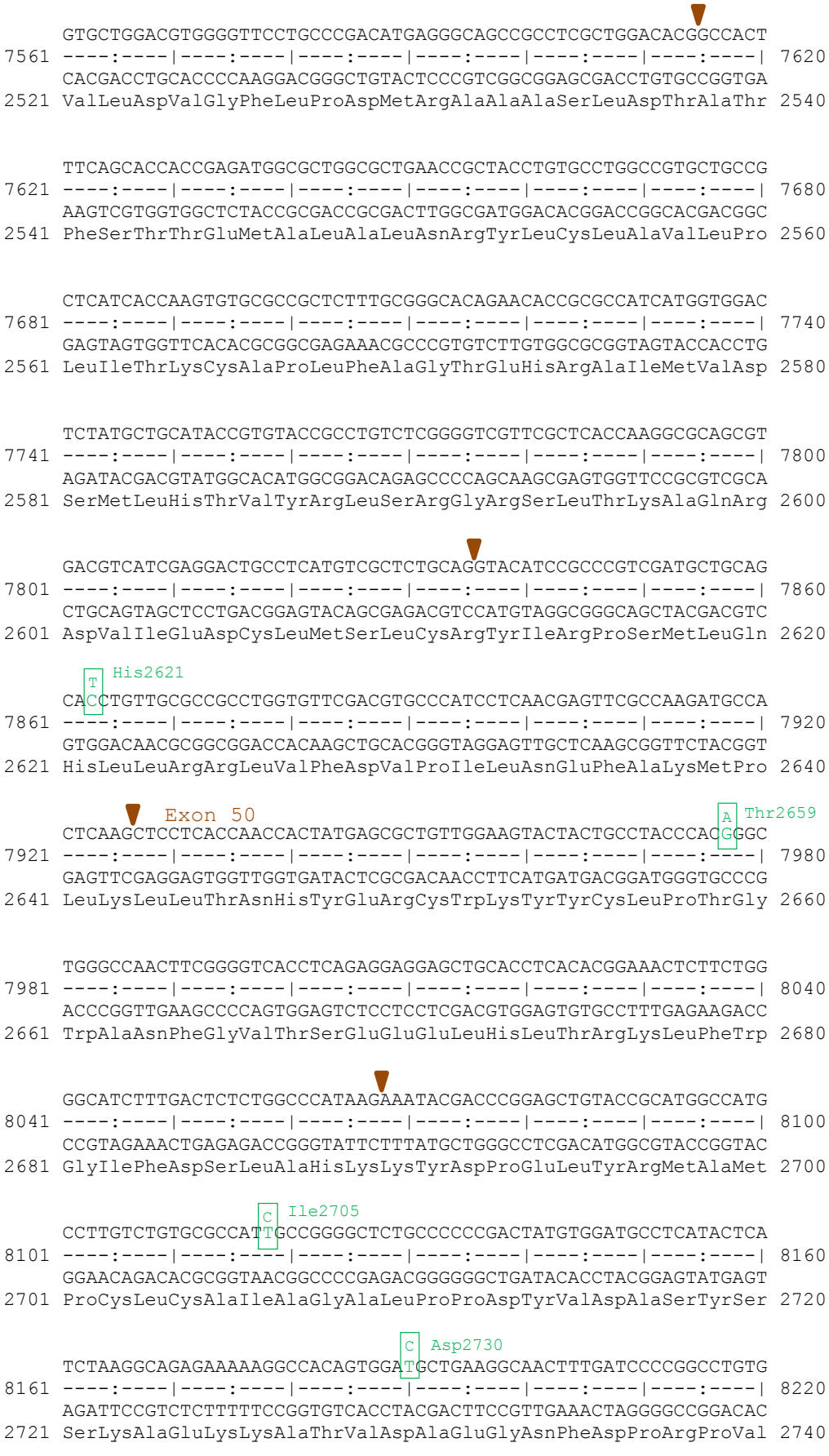
GTGCTGGACGTGGGGTTCCTGCCCGACATGAGGGCAGCCGCCTCGCTGGACACGGCCACT
7561 ----:----|----:----|----:----|----:----|----:----|----:----|----:----| 7620
CACGACCTGCACCCCAAGGACGGGCTGTACTCCCGTCGGCGGAGCGACCTGTGCCGGTGA
2521 ValLeuAspValGlyPheLeuProAspMetArgAlaAlaAlaSerLeuAspThrAlaThr 2540
TTCAGCACCACCGAGATGGCGCTGGCGCTGAACCGCTACCTGTGCCTGGCCGTGCTGCCG
7621 ----:----|----:----|----:----|----:----|----:----|----:----|----:----| 7680
AAGTCGTGGTGGCTCTACCGCGACCGCGACTTGGCGATGGACACGGACCGGCACGACGGC
2541 PheSerThrThrGluMetAlaLeuAlaLeuAsnArgTyrLeuCysLeuAlaValLeuPro 2560
CTCATCACCAAGTGTGCGCCGCTCTTTGCGGGCACAGAACACCGCGCCATCATGGTGGAC
7681 ----:----|----:----|----:----|----:----|----:----|----:----|----:----| 7740
GAGTAGTGGTTCACACGCGGCGAGAAACGCCCGTGTCTTGTGGCGCGGTAGTACCACCTG
2561 LeuIleThrLysCysAlaProLeuPheAlaGlyThrGluHisArgAlaIleMetValAsp 2580
TCTATGCTGCATACCGTGTACCGCCTGTCTCGGGGTCGTTCGCTCACCAAGGCGCAGCGT
7741 ----:----|----:----|----:----|----:----|----:----|----:----|----:----| 7800
AGATACGACGTATGGCACATGGCGGACAGAGCCCCAGCAAGCGAGTGGTTCCGCGTCGCA
2581 SerMetLeuHisThrValTyrArgLeuSerArgGlyArgSerLeuThrLysAlaGlnArg 2600
GACGTCATCGAGGACTGCCTCATGTCGCTCTGCAGGTACATCCGCCCGTCGATGCTGCAG
7801 ----:----|----:----|----:----|----:----|----:----|----:----|----:----| 7860
CTGCAGTAGCTCCTGACGGAGTACAGCGAGACGTCCATGTAGGCGGGCAGCTACGACGTC
2601 AspValIleGluAspCysLeuMetSerLeuCysArgTyrIleArgProSerMetLeuGln 2620
T
His2621
CACCTGTTGCGCCGCCTGGTGTTCGACGTGCCCATCCTCAACGAGTTCGCCAAGATGCCA
7861 ----:----|----:----|----:----|----:----|----:----|----:----|----:----| 7920
GTGGACAACGCGGCGGACCACAAGCTGCACGGGTAGGAGTTGCTCAAGCGGTTCTACGGT
2621 HisLeuLeuArgArgLeuValPheAspValProIleLeuAsnGluPheAlaLysMetPro 2640
Exon 50
A
Thr2659
CTCAAGCTCCTCACCAACCACTATGAGCGCTGTTGGAAGTACTACTGCCTACCCACGGGC
7921 ----:----|----:----|----:----|----:----|----:----|----:----|----:----| 7980
GAGTTCGAGGAGTGGTTGGTGATACTCGCGACAACCTTCATGATGACGGATGGGTGCCCG
2641 LeuLysLeuLeuThrAsnHisTyrGluArgCysTrpLysTyrTyrCysLeuProThrGly 2660
TGGGCCAACTTCGGGGTCACCTCAGAGGAGGAGCTGCACCTCACACGGAAACTCTTCTGG
7981 ----:----|----:----|----:----|----:----|----:----|----:----|----:----| 8040
ACCCGGTTGAAGCCCCAGTGGAGTCTCCTCCTCGACGTGGAGTGTGCCTTTGAGAAGACC
2661 TrpAlaAsnPheGlyValThrSerGluGluGluLeuHisLeuThrArgLysLeuPheTrp 2680
GGCATCTTTGACTCTCTGGCCCATAAGAAATACGACCCGGAGCTGTACCGCATGGCCATG
8041 ----:----|----:----|----:----|----:----|----:----|----:----|----:----| 8100
CCGTAGAAACTGAGAGACCGGGTATTCTTTATGCTGGGCCTCGACATGGCGTACCGGTAC
2681 GlyIlePheAspSerLeuAlaHisLysLysTyrAspProGluLeuTyrArgMetAlaMet 2700
C
Ile2705
CCTTGTCTGTGCGCCATTGCCGGGGCTCTGCCCCCCGACTATGTGGATGCCTCATACTCA
8101 ----:----|----:----|----:----|----:----|----:----|----:----|----:----| 8160
GGAACAGACACGCGGTAACGGCCCCGAGACGGGGGGCTGATACACCTACGGAGTATGAGT
2701 ProCysLeuCysAlaIleAlaGlyAlaLeuProProAspTyrValAspAlaSerTyrSer 2720
C
Asp2730
TCTAAGGCAGAGAAAAAGGCCACAGTGGATGCTGAAGGCAACTTTGATCCCCGGCCTGTG
8161 ----:----|----:----|----:----|----:----|----:----|----:----|----:----| 8220
AGATTCCGTCTCTTTTTCCGGTGTCACCTACGACTTCCGTTGAAACTAGGGGCCGGACAC
2721 SerLysAlaGluLysLysAlaThrValAspAlaGluGlyAsnPheAspProArgProVal 2740


GAGACCCTCAATGTGATCATCCCGGAGAAGCTGGACTCCTTCATTAACAAGTTTGCGGAG
8221 ----:----|----:----|----:----|----:----|----:----|----:----|----:----| 8280
CTCTGGGAGTTACACTAGTAGGGCCTCTTCGACCTGAGGAAGTAATTGTTCAAACGCCTC
2741 GluThrLeuAsnValIleIleProGluLysLeuAspSerPheIleAsnLysPheAlaGlu 2761
C Glu2779
TACACACACGAGAAGTGGGCCTTCGACAAGATCCAGAACAACTGGTCCTATGGAGAGAAC
8281 ----:----|----:----|----:----|----:----|----:----|----:----|----:----| 8340
ATGTGTGTGCTCTTCACCCGGAAGCTGTTCTAGGTCTTGTTGACCAGGATACCTCTCTTG
2761 TyrThrHisGluLysTrpAlaPheAspLysIleGlnAsnAsnTrpSerTyrGlyGluAsn 2780
ATAGACGAGGAGCTGAAGACCCACCCCATGCTGAGGCCCTACAAGACCTTTTCAGAGAAG
8341 ----:----|----:----|----:----|----:----|----:----|----:----|----:----| 8400
TATCTGCTCCTCGACTTCTGGGTGGGGTACGACTCCGGGATGTTCTGGAAAAGTCTCTTC
2781 IleAspGluGluLeuLysThrHisProMetLeuArgProTyrLysThrPheSerGluLys 2800
GACAAAGAGATTTACCGCTGGCCCATCAAGGAGTCCCTGAAGGCCATGATTGCCTGGGAA
8401 ----:----|----:----|----:----|----:----|----:----|----:----|----:----| 8460
CTGTTTCTCTAAATGGCGACCGGGTAGTTCCTCAGGGACTTCCGGTACTAACGGACCCTT
2801 AspLysGluIleTyrArgTrpProIleLysGluSerLeuLysAlaMetIleAlaTrpGlu 2820
TGGACGATAGAGAAGGCCAGGGAGGGTGAGGAGGAGAAGACGGAAAAGAAAAAAACGCGG
8461 ----:----|----:----|----:----|----:----|----:----|----:----|----:----| 8520
ACCTGCTATCTCTTCCGGTCCCTCCCACTCCTCCTCTTCTGCCTTTTCTTTTTTTGCGCC
2821 TrpThrIleGluLysAlaArgGluGlyGluGluLysThrGluLysLysLysThrArg 2840
Exon 55
XhoI
AAGATATCACAAAGTGCCCAGACCTATGATCCTCGAGAAGGCTACAACCCTCAGCCCCCC
8521 ----:----|----:----|----:----|----:----|----:----|----:----|----:----| 8580
TTCTATAGTGTTTCACGGGTCTGGATACTAGGAGCTCTTCCGATGTTGGGAGTCGGGGGG
2841 LysIleSerGlnSerAlaGlnThrTyrAspProArgGluGlyTyrAsnProGlnProPro 2860
GACCTTAGTGCTGTTACCCTGTCCCGGGAGCTGCAGGCCATGGCAGAACAACTGGCAGAA
8581 ----:----|----:----|----:----|----:----|----:----|----:----|----:----| 8640
CTGGAATCACGACAATGGGACAGGGCCCTCGACGTCCGGTACCGTCTTGTTGACCGTCTT
2861 AspLeuSerAlaValThrLeuSerArgGluLeuGlnAlaMetAlaGluGlnLeuAlaGlu 2880
AATTACCACAACACGTGGGGACGGAAGAAGAAGCAGGAGCTGGAAGCCAAAGGCGGTGGG
8641 ----:----|----:----|----:----|----:----|----:----|----:----|----:----| 8700
TTAATGGTGTTGTGCACCCCTGCCTTCTTCTTCGTCCTCGACCTTCGGTTTCCGCCACCC
2881 AsnTyrHisAsnThrTrpGlyArgLysLysLysGlnGluLeuGluAlaLysGlyGlyGly 2900
ACCCACCCCCTGCTGGTCCCCTACGACACGCTCACGGCCAAGGAGAAGGCACGAGATCGA
8701 ----:----|----:----|----:----|----:----|----:----|----:----|----:----| 8760
TGGGTGGGGGACGACCAGGGGATGCTGTGCGAGTGCCGGTTCCTCTTCCGTGCTCTAGCT
2901 ThrHisProLeuLeuValProTyrAspThrLeuThrAlaLysGluLysAlaArgAspArg 2920
GAGAAGGCCCAGGAGCTACTGAAATTCCTGCAGATGAATGGCTACGCGGTTACAAGAGGC
8761 ----:----|----:----|----:----|----:----|----:----|----:----|----:----| 8820
CTCTTCCGGGTCCTCGATGACTTTAAGGACGTCTACTTACCGATGCGCCAATGTTCTCCG
2921 GluLysAlaGlnGluLeuLeuLysPheLeuGlnMetAsnGlyTyrAlaValThrArgGly 2940
CTTAAGGACATGGAACTGGACTCGTCTTCCATTGAAAAGCGGTTTGCCTTTGGCTTCCTG
8821 ----:----|----:----|----:----|----:----|----:----|----:----|----:----| 8880
GAATTCCTGTACCTTGACCTGAGCAGAAGGTAACTTTTCGCCAAACGGAAACCGAAGGAC
2941 LeuLysAspMetGluLeuAspSerSerSerIleGluLysArgPheAlaPheGlyPheLeu 2960

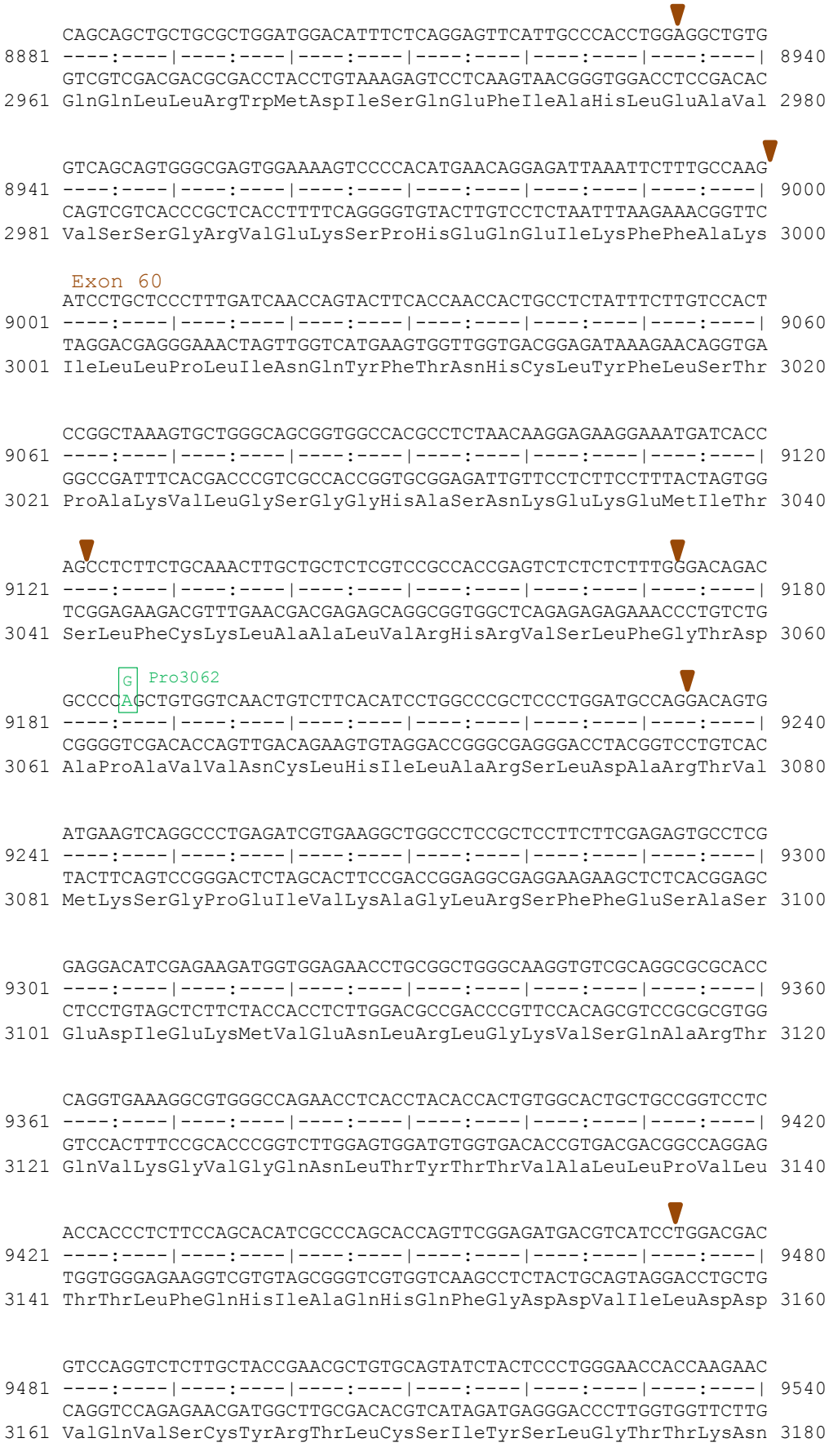
CAGCAGCTGCTGCGCTGGATGGACATTTCTCAGGAGTTCATTGCCCACCTGGAGGCTGTG
8881 ----:----|----:----|----:----|----:----|----:----|----:----|----:----| 8940
GTCGTCGACGACGCGACCTACCTGTAAAGAGTCCTCAAGTAACGGGTGGACCTCCGACAC
2961 GlnGlnLeuLeuArgTrpMetAspIleSerGlnGluPheIleAlaHisLeuGluAlaVal 2980
GTCAGCAGTGGGCGAGTGGAAAAGTCCCCACATGAACAGGAGATTAAATTCTTTGCCAAG
8941 ----:----|----:----|----:----|----:----|----:----|----:----|----:----| 9000
CAGTCGTCACCCGCTCACCTTTTCAGGGGTGTACTTGTCCTCTAATTTAAGAAACGGTTC
2981 ValSerSerGlyArgValGluLysSerProHisGluGlnGluIleLysPhePheAlaLys 3000
Exon 60
ATCCTGCTCCCTTTGATCAACCAGTACTTCACCAACCACTGCCTCTATTTCTTGTCCACT
9001 ----:----|----:----|----:----|----:----|----:----|----:----|----:----| 9060
TAGGACGAGGGAAACTAGTTGGTCATGAAGTGGTTGGTGACGGAGATAAAGAACAGGTGA
3001 IleLeuLeuProLeuIleAsnGlnTyrPheThrAsnHisCysLeuTyrPheLeuSerThr 3020
CCGGCTAAAGTGCTGGGCAGCGGTGGCCACGCCTCTAACAAGGAGAAGGAAATGATCACC
9061 ----:----|----:----|----:----|----:----|----:----|----:----|----:----| 9120
GGCCGATTTCACGACCCGTCGCCACCGGTGCGGAGATTGTTCCTCTTCCTTTACTAGTGG
3021 ProAlaLysValLeuGlySerGlyGlyHisAlaSerAsnLysGluLysGluMetIleThr 3040
AGCCTCTTCTGCAAACTTGCTGCTCTCGTCCGCCACCGAGTCTCTCTCTTTGGGACAGAC
9121 ----:----|----:----|----:----|----:----|----:----|----:----|----:----| 9180
TCGGAGAAGACGTTTGAACGACGAGAGCAGGCGGTGGCTCAGAGAGAGAAACCCTGTCTG
3041 SerLeuPheCysLysLeuAlaAlaLeuValArgHisArgValSerLeuPheGlyThrAsp 3060
G Pro3062
GCCCCAGCTGTGGTCAACTGTCTTCACATCCTGGCCCGCTCCCTGGATGCCAGGACAGTG
9181 ----:----|----:----|----:----|----:----|----:----|----:----|----:----| 9240
CGGGGTCGACACCAGTTGACAGAAGTGTAGGACCGGGCGAGGGACCTACGGTCCTGTCAC
3061 AlaProAlaValValAsnCysLeuHisIleLeuAlaArgSerLeuAspAlaArgThrVal 3080
ATGAAGTCAGGCCCTGAGATCGTGAAGGCTGGCCTCCGCTCCTTCTTCGAGAGTGCCTCG
9241 ----:----|----:----|----:----|----:----|----:----|----:----|----:----| 9300
TACTTCAGTCCGGGACTCTAGCACTTCCGACCGGAGGCGAGGAAGAAGCTCTCACGGAGC
3081 MetLysSerGlyProGluIleValLysAlaGlyLeuArgSerPhePheGluSerAlaSer 3100
GAGGACATCGAGAAGATGGTGGAGAACCTGCGGCTGGGCAAGGTGTCGCAGGCGCGCACC
9301 ----:----|----:----|----:----|----:----|----:----|----:----|----:----| 9360
CTCCTGTAGCTCTTCTACCACCTCTTGGACGCCGACCCGTTCCACAGCGTCCGCGCGTGG
3101 GluAspIleGluLysMetValGluAsnLeuArgLeuGlyLysValSerGlnAlaArgThr 3120
CAGGTGAAAGGCGTGGGCCAGAACCTCACCTACACCACTGTGGCACTGCTGCCGGTCCTC
9361 ----:----|----:----|----:----|----:----|----:----|----:----|----:----| 9420
GTCCACTTTCCGCACCCGGTCTTGGAGTGGATGTGGTGACACCGTGACGACGGCCAGGAG
3121 GlnValLysGlyValGlyGlnAsnLeuThrTyrThrThrValAlaLeuLeuProValLeu 3140
ACCACCCTCTTCCAGCACATCGCCCAGCACCAGTTCGGAGATGACGTCATCCTGGACGAC
9421 ----:----|----:----|----:----|----:----|----:----|----:----|----:----| 9480
TGGTGGGAGAAGGTCGTGTAGCGGGTCGTGGTCAAGCCTCTACTGCAGTAGGACCTGCTG
3141 ThrThrLeuPheGlnHisIleAlaGlnHisGlnPheGlyAspAspValIleLeuAspAsp 3160
GTCCAGGTCTCTTGCTACCGAACGCTGTGCAGTATCTACTCCCTGGGAACCACCAAGAAC
9481 ----:----|----:----|----:----|----:----|----:----|----:----|----:----| 9540
CAGGTCCAGAGAACGATGGCTTGCGACACGTCATAGATGAGGGACCCTTGGTGGTTCTTG
3161 ValGlnValSerCysTyrArgThrLeuCysSerIleTyrSerLeuGlyThrThrLysAsn 3180

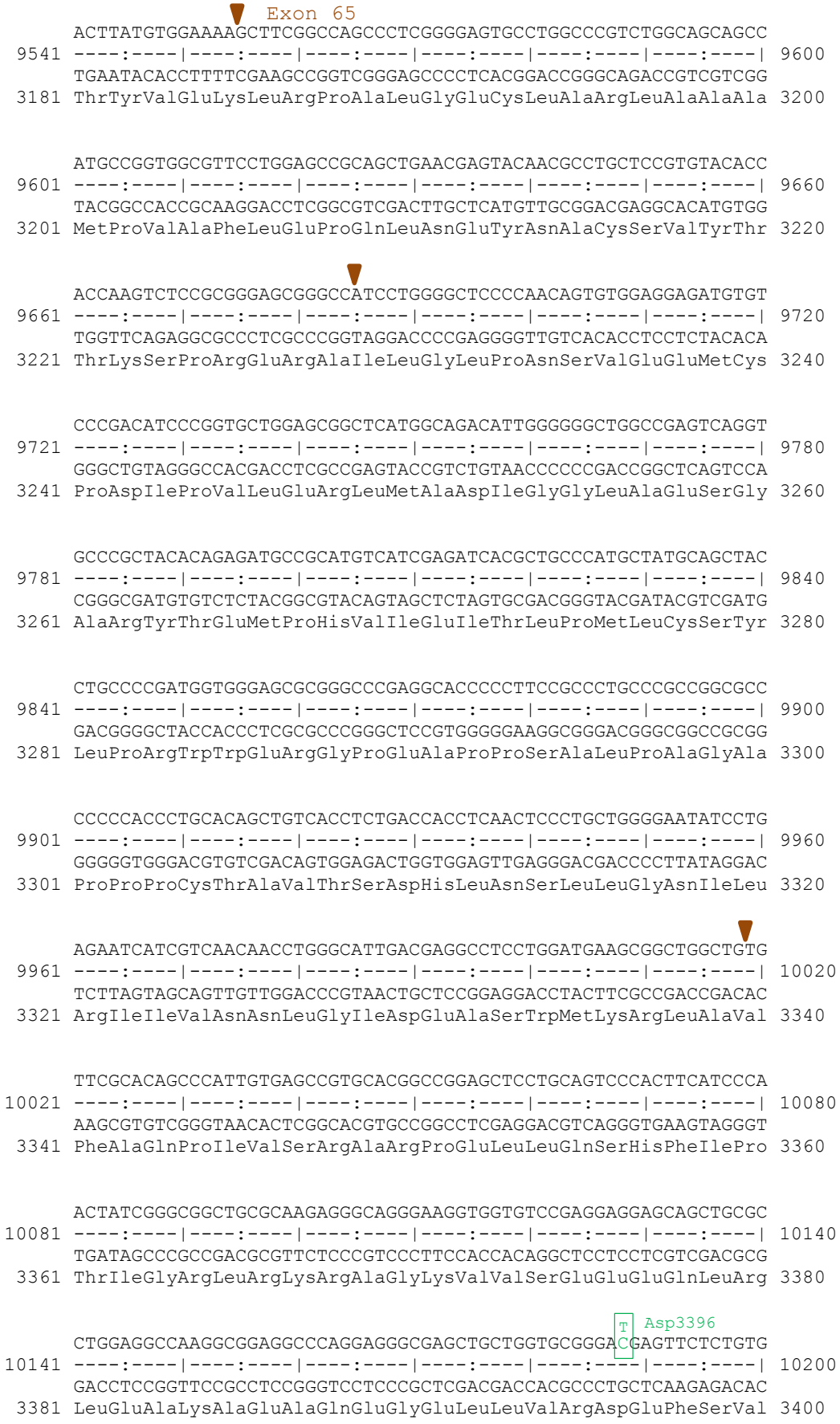
Exon 65
ACTTATGTGGAAAAGCTTCGGCCAGCCCTCGGGGAGTGCCTGGCCCGTCTGGCAGCAGCC
9541 ----:----|----:----|----:----|----:----|----:----|----:----| 9600
TGAATACACCTTTTCGAAGCCGGTCGGGAGCCCCTCACGGACCGGGCAGACCGTCGTCGG
3181 ThrTyrValGluLysLeuArgProAlaLeuGlyGluCysLeuAlaArgLeuAlaAlaAla 3200
ATGCCGGTGGCGTTCCTGGAGCCGCAGCTGAACGAGTACAACGCCTGCTCCGTGTACACC
9601 ----:----|----:----|----:----|----:----|----:----|----:----| 9660
TACGGCCACCGCAAGGACCTCGGCGTCGACTTGCTCATGTTGCGGACGAGGCACATGTGG
3201 MetProValAlaPheLeuGluProGlnLeuAsnGluTyrAsnAlaCysSerValTyrThr 3220
ACCAAGTCTCCGCGGGAGCGGGCCATCCTGGGGCTCCCCAACAGTGTGGAGGAGATGTGT
9661 ----:----|----:----|----:----|----:----|----:----|----:----| 9720
TGGTTCAGAGGCGCCCTCGCCCGGTAGGACCCCGAGGGGTTGTCACACCTCCTCTACACA
3221 ThrLysSerProArgGluArgAlaIleLeuGlyLeuProAsnSerValGluGluMetCys 3240
CCCGACATCCCGGTGCTGGAGCGGCTCATGGCAGACATTGGGGGGCTGGCCGAGTCAGGT
9721 ----:----|----:----|----:----|----:----|----:----|----:----| 9780
GGGCTGTAGGGCCACGACCTCGCCGAGTACCGTCTGTAACCCCCCGACCGGCTCAGTCCA
3241 ProAspIleProValLeuGluArgLeuMetAlaAspIleGlyGlyLeuAlaGluSerGly 3260
GCCCGCTACACAGAGATGCCGCATGTCATCGAGATCACGCTGCCCATGCTATGCAGCTAC
9781 ----:----|----:----|----:----|----:----|----:----|----:----| 9840
CGGGCGATGTGTCTCTACGGCGTACAGTAGCTCTAGTGCGACGGGTACGATACGTCGATG
3261 AlaArgTyrThrGluMetProHisValIleGluIleThrLeuProMetLeuCysSerTyr 3280
CTGCCCCGATGGTGGGAGCGCGGGCCCGAGGCACCCCCTTCCGCCCTGCCCGCCGGCGCC
9841 ----:----|----:----|----:----|----:----|----:----|----:----| 9900
GACGGGGCTACCACCCTCGCGCCCGGGCTCCGTGGGGGAAGGCGGGACGGGCGGCCGCGG
3281 LeuProArgTrpTrpGluArgGlyProGluAlaProProSerAlaLeuProAlaGlyAla 3300
CCCCCACCCTGCACAGCTGTCACCTCTGACCACCTCAACTCCCTGCTGGGGAATATCCTG
9901 ----:----|----:----|----:----|----:----|----:----|----:----| 9960
GGGGGTGGGACGTGTCGACAGTGGAGACTGGTGGAGTTGAGGGACGACCCCTTATAGGAC
3301 ProProProCysThrAlaValThrSerAspHisLeuAsnSerLeuLeuGlyAsnIleLeu 3320
AGAATCATCGTCAACAACCTGGGCATTGACGAGGCCTCCTGGATGAAGCGGCTGGCTGTG
9961 ----:----|----:----|----:----|----:----|----:----|----:----| 10020
TCTTAGTAGCAGTTGTTGGACCCGTAACTGCTCCGGAGGACCTACTTCGCCGACCGACAC
3321 ArgIleIleValAsnAsnLeuGlyIleAspGluAlaSerTrpMetLysArgLeuAlaVal 3340
TTCGCACAGCCCATTGTGAGCCGTGCACGGCCGGAGCTCCTGCAGTCCCACTTCATCCCA
10021 ----:----|----:----|----:----|----:----|----:----|----:----| 10080
AAGCGTGTCGGGTAACACTCGGCACGTGCCGGCCTCGAGGACGTCAGGGTGAAGTAGGGT
3341 PheAlaGlnProIleValSerArgAlaArgProGluLeuLeuGlnSerHisPheIlePro 3360
ACTATCGGGCGGCTGCGCAAGAGGGCAGGGAAGGTGGTGTCCGAGGAGGAGCAGCTGCGC
10081 ----:----|----:----|----:----|----:----|----:----|----:----| 10140
TGATAGCCCGCCGACGCGTTCTCCCGTCCCTTCCACCACAGGCTCCTCCTCGTCGACGCG
3361 ThrIleGlyArgLeuArgLysArgAlaGlyLysValValSerGluGluGluGlnLeuArg 3380
T Asp3396
CTGGAGGCCAAGGCGGAGGCCCAGGAGGGCGAGCTGCTGGTGCGGGACGAGTTCTCTGTG
10141 ----:----|----:----|----:----|----:----|----:----|----:----| 10200
GACCTCCGGTTCCGCCTCCGGGTCCTCCCGCTCGACGACCACGCCCTGCTCAAGAGACAC
3381 LeuGluAlaLysAlaGluAlaGlnGluGlyGluLeuLeuValArgAspGluPheSerVal 3400

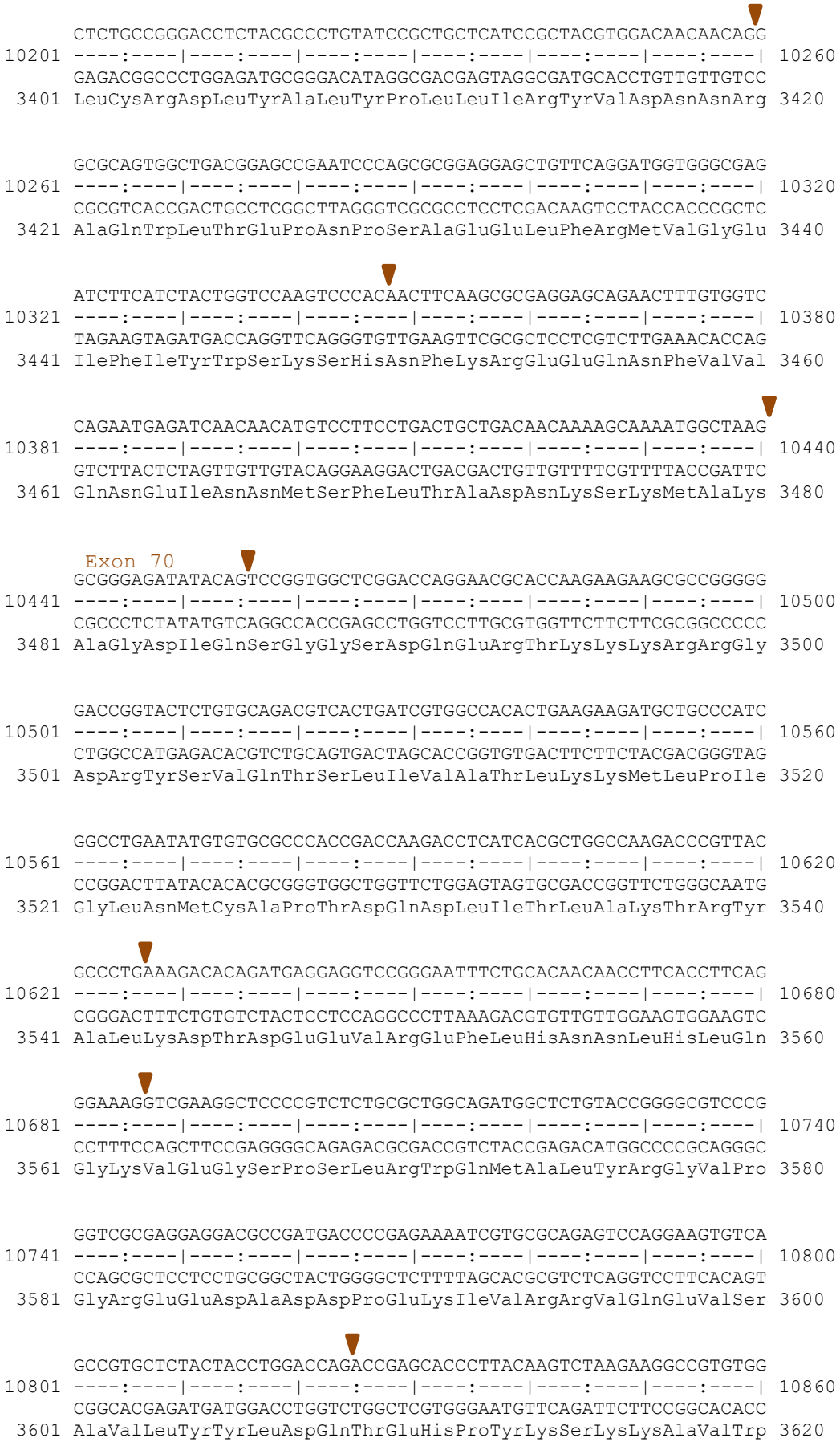
CTCTGCCGGGACCTCTACGCCCTGTATCCGCTGCTCATCCGCTACGTGGACAACAACAGG
10201 ----:----|----:----|----:----|----:----|----:----|----:----| 10260
GAGACGGCCCTGGAGATGCGGGACATAGGCGACGAGTAGGCGATGCACCTGTTGTTGTCC
3401 LeuCysArgAspLeuTyrAlaLeuTyrProLeuLeuIleArgTyrValAspAsnAsnArg 3420
GCGCAGTGGCTGACGGAGCCGAATCCCAGCGCGGAGGAGCTGTTCAGGATGGTGGGCGAG
10261 ----:----|----:----|----:----|----:----|----:----|----:----| 10320
CGCGTCACCGACTGCCTCGGCTTAGGGTCGCGCCTCCTCGACAAGTCCTACCACCCGCTC
3421 AlaGlnTrpLeuThrGluProAsnProSerAlaGluGluLeuPheArgMetValGlyGlu 3440
ATCTTCATCTACTGGTCCAAGTCCCACAACTTCAAGCGCGAGGAGCAGAACTTTGTGGTC
10321 ----:----|----:----|----:----|----:----|----:----|----:----| 10380
TAGAAGTAGATGACCAGGTTCAGGGTGTTGAAGTTCGCGCTCCTCGTCTTGAAACACCAG
3441 IlePheIleTyrTrpSerLysSerHisAsnPheLysArgGluGluGlnAsnPheValVal 3460
CAGAATGAGATCAACAACATGTCCTTCCTGACTGCTGACAACAAAAGCAAAATGGCTAAG
10381 ----:----|----:----|----:----|----:----|----:----|----:----| 10440
GTCTTACTCTAGTTGTTGTACAGGAAGGACTGACGACTGTTGTTTTCGTTTTACCGATTC
3461 GlnAsnGluIleAsnAsnMetSerPheLeuThrAlaAspAsnLysSerLysMetAlaLys 3480
Exon 70
GCGGGAGATATACAGTCCGGTGGCTCGGACCAGGAACGCACCAAGAAGAAGCGCCGGGGG
10441 ----:----|----:----|----:----|----:----|----:----|----:----| 10500
CGCCCTCTATATGTCAGGCCACCGAGCCTGGTCCTTGCGTGGTTCTTCTTCGCGGCCCCC
3481 AlaGlyAspIleGlnSerGlyGlySerAspGlnGluArgThrLysLysLysArgArgGly 3500
GACCGGTACTCTGTGCAGACGTCACTGATCGTGGCCACACTGAAGAAGATGCTGCCCATC
10501 ----:----|----:----|----:----|----:----|----:----|----:----| 10560
CTGGCCATGAGACACGTCTGCAGTGACTAGCACCGGTGTGACTTCTTCTACGACGGGTAG
3501 AspArgTyrSerValGlnThrSerLeuIleValAlaThrLeuLysLysMetLeuProIle 3520
GGCCTGAATATGTGTGCGCCCACCGACCAAGACCTCATCACGCTGGCCAAGACCCGTTAC
10561 ----:----|----:----|----:----|----:----|----:----|----:----| 10620
CCGGACTTATACACACGCGGGTGGCTGGTTCTGGAGTAGTGCGACCGGTTCTGGGCAATG
3521 GlyLeuAsnMetCysAlaProThrAspGlnAspLeuIleThrLeuAlaLysThrArgTyr 3540
GCCCTGAAAGACACAGATGAGGAGGTCCGGGAATTTCTGCACAACAACCTTCACCTTCAG
10621 ----:----|----:----|----:----|----:----|----:----|----:----| 10680
CGGGACTTTCTGTGTCTACTCCTCCAGGCCCTTAAAGACGTGTTGTTGGAAGTGGAAGTC
3541 AlaLeuLysAspThrAspGluGluValArgGluPheLeuHisAsnAsnLeuHisLeuGln 3560
GGAAAGGTCGAAGGCTCCCCGTCTCTGCGCTGGCAGATGGCTCTGTACCGGGGCGTCCCG
10681 ----:----|----:----|----:----|----:----|----:----|----:----| 10740
CCTTTCCAGCTTCCGAGGGGCAGAGACGCGACCGTCTACCGAGACATGGCCCCGCAGGGC
3561 GlyLysValGluGlySerProSerLeuArgTrpGlnMetAlaLeuTyrArgGlyValPro 3580
GGTCGCGAGGAGGACGCCGATGACCCCGAGAAAATCGTGCGCAGAGTCCAGGAAGTGTCA
10741 ----:----|----:----|----:----|----:----|----:----|----:----| 10800
CCAGCGCTCCTCCTGCGGCTACTGGGGCTCTTTTAGCACGCGTCTCAGGTCCTTCACAGT
3581 GlyArgGluGluAspAlaAspAspProGluLysIleValArgArgValGlnGluValSer 3600
GCCGTGCTCTACTACCTGGACCAGACCGAGCACCCTTACAAGTCTAAGAAGGCCGTGTGG
10801 ----:----|----:----|----:----|----:----|----:----|----:----| 10860
CGGCACGAGATGATGGACCTGGTCTGGCTCGTGGGAATGTTCAGATTCTTCCGGCACACC
3601 AlaValLeuTyrTyrLeuAspGlnThrGluHisProTyrLysSerLysLysAlaValTrp 3620

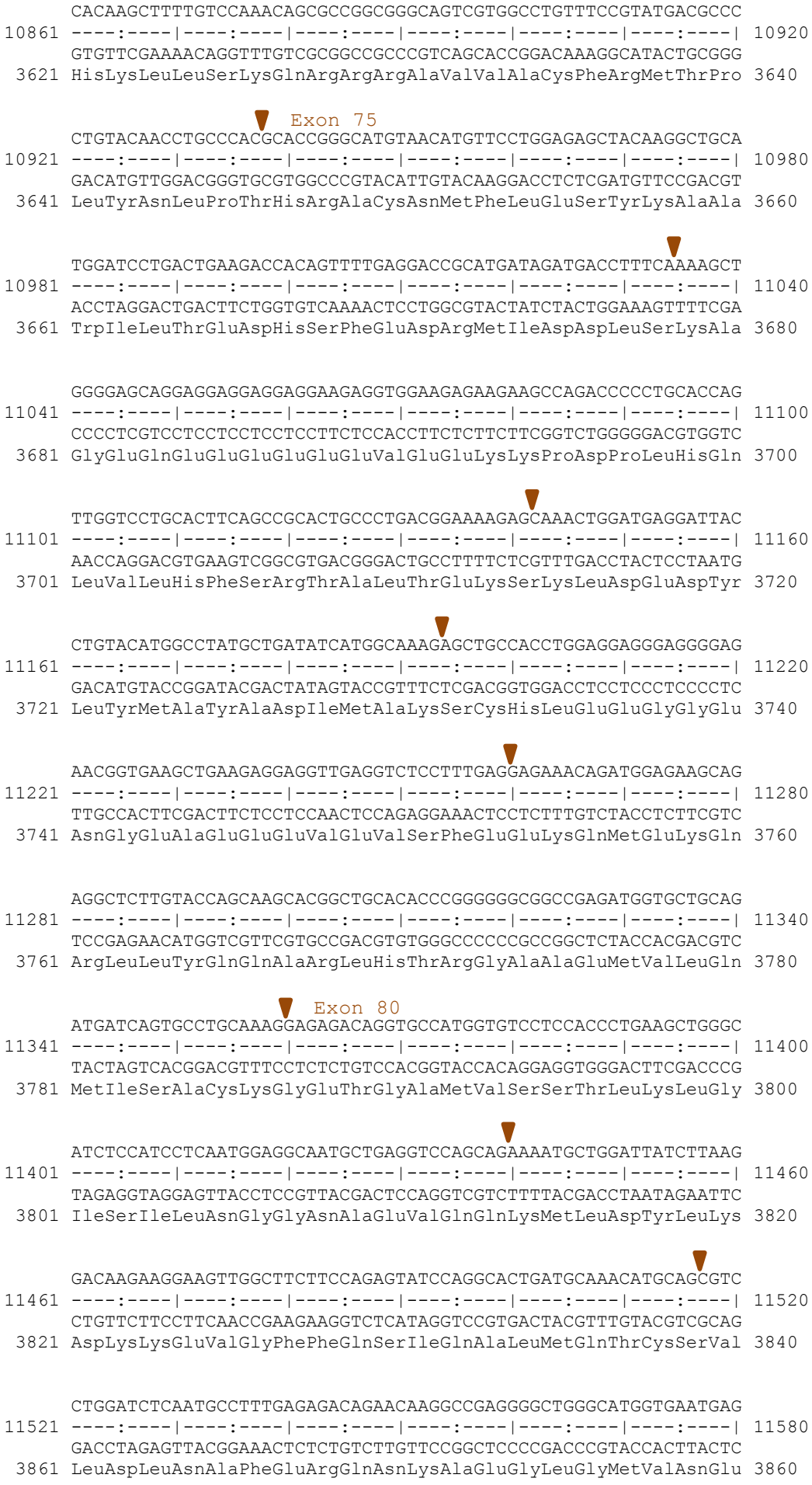
CACAAGCTTTTGTCCAAACAGCGCCGGCGGGCAGTCGTGGCCTGTTTCCGTATGACGCCC
10861 ----:----|----:----|----:----|----:----|----:----|----:----| 10920
GTGTTCGAAAACAGGTTTGTCGCGGCCGCCCGTCAGCACCGGACAAAGGCATACTGCGGG
3621 HisLysLeuLeuSerLysGlnArgArgArgAlaValValAlaCysPheArgMetThrPro 3640
Exon 75
CTGTACAACCTGCCCACGCACCGGGCATGTAACATGTTCCTGGAGAGCTACAAGGCTGCA
10921 ----:----|----:----|----:----|----:----|----:----|----:----| 10980
GACATGTTGGACGGGTGCGTGGCCCGTACATTGTACAAGGACCTCTCGATGTTCCGACGT
3641 LeuTyrAsnLeuProThrHisArgAlaCysAsnMetPheLeuGluSerTyrLysAlaAla 3660
TGGATCCTGACTGAAGACCACAGTTTTGAGGACCGCATGATAGATGACCTTTCAAAAGCT
10981 ----:----|----:----|----:----|----:----|----:----|----:----| 11040
ACCTAGGACTGACTTCTGGTGTCAAAACTCCTGGCGTACTATCTACTGGAAAGTTTTCGA
3661 TrpIleLeuThrGluAspHisSerPheGluAspArgMetIleAspAspLeuSerLysAla 3680
GGGGAGCAGGAGGAGGAGGAGGAAGAGGTGGAAGAGAAGAAGCCAGACCCCCTGCACCAG
11041 ----:----|----:----|----:----|----:----|----:----|----:----| 11100
CCCCTCGTCCTCCTCCTCCTCCTTCTCCACCTTCTCTTCTTCGGTCTGGGGGACGTGGTC
3681 GlyGluGlnGluGluGluGluGluValGluGluLysLysProAspProLeuHisGln 3700
TTGGTCCTGCACTTCAGCCGCACTGCCCTGACGGAAAAGAGCAAACTGGATGAGGATTAC
11101 ----:----|----:----|----:----|----:----|----:----|----:----| 11160
AACCAGGACGTGAAGTCGGCGTGACGGGACTGCCTTTTCTCGTTTGACCTACTCCTAATG
3701 LeuValLeuHisPheSerArgThrAlaLeuThrGluLysSerLysLeuAspGluAspTyr 3720
CTGTACATGGCCTATGCTGATATCATGGCAAAGAGCTGCCACCTGGAGGAGGGAGGGGAG
11161 ----:----|----:----|----:----|----:----|----:----|----:----| 11220
GACATGTACCGGATACGACTATAGTACCGTTTCTCGACGGTGGACCTCCTCCCTCCCCTC
3721 LeuTyrMetAlaTyrAlaAspIleMetAlaLysSerCysHisLeuGluGluGlyGlyGlu 3740
AACGGTGAAGCTGAAGAGGAGGTTGAGGTCTCCTTTGAGGAGAAACAGATGGAGAAGCAG
11221 ----:----|----:----|----:----|----:----|----:----|----:----| 11280
TTGCCACTTCGACTTCTCCTCCAACTCCAGAGGAAACTCCTCTTTGTCTACCTCTTCGTC
3741 AsnGlyGluAlaGluGluGluValGluValSerPheGluGluLysGlnMetGluLysGln 3760
AGGCTCTTGTACCAGCAAGCACGGCTGCACACCCGGGGGGCGGCCGAGATGGTGCTGCAG
11281 ----:----|----:----|----:----|----:----|----:----|----:----| 11340
TCCGAGAACATGGTCGTTCGTGCCGACGTGTGGGCCCCCCGCCGGCTCTACCACGACGTC
3761 ArgLeuLeuTyrGlnGlnAlaArgLeuHisThrArgGlyAlaAlaGluMetValLeuGln 3780
Exon 80
ATGATCAGTGCCTGCAAAGGAGAGACAGGTGCCATGGTGTCCTCCACCCTGAAGCTGGGC
11341 ----:----|----:----|----:----|----:----|----:----|----:----| 11400
TACTAGTCACGGACGTTTCCTCTCTGTCCACGGTACCACAGGAGGTGGGACTTCGACCCG
3781 MetIleSerAlaCysLysGlyGluThrGlyAlaMetValSerSerThrLeuLysLeuGly 3800
ATCTCCATCCTCAATGGAGGCAATGCTGAGGTCCAGCAGAAAATGCTGGATTATCTTAAG
11401 ----:----|----:----|----:----|----:----|----:----|----:----| 11460
TAGAGGTAGGAGTTACCTCCGTTACGACTCCAGGTCGTCTTTTACGACCTAATAGAATTC
3801 IleSerIleLeuAsnGlyGlyAsnAlaGluValGlnGlnLysMetLeuAspTyrLeuLys 3820
GACAAGAAGGAAGTTGGCTTCTTCCAGAGTATCCAGGCACTGATGCAAACATGCAGCGTC
11461 ----:----|----:----|----:----|----:----|----:----|----:----| 11520
CTGTTCTTCCTTCAACCGAAGAAGGTCTCATAGGTCCGTGACTACGTTTGTACGTCGCAG
3821 AspLysLysGluValGlyPhePheGlnSerIleGlnAlaLeuMetGlnThrCysSerVal 3840
CTGGATCTCAATGCCTTTGAGAGACAGAACAAGGCCGAGGGGCTGGGCATGGTGAATGAG
11521 ----:----|----:----|----:----|----:----|----:----|----:----| 11580
GACCTAGAGTTACGGAAACTCTCTGTCTTGTTCCGGCTCCCCGACCCGTACCACTTACTC
3861 LeuAspLeuAsnAlaPheGluArgGlnAsnLysAlaGluGlyLeuGlyMetValAsnGlu 3860

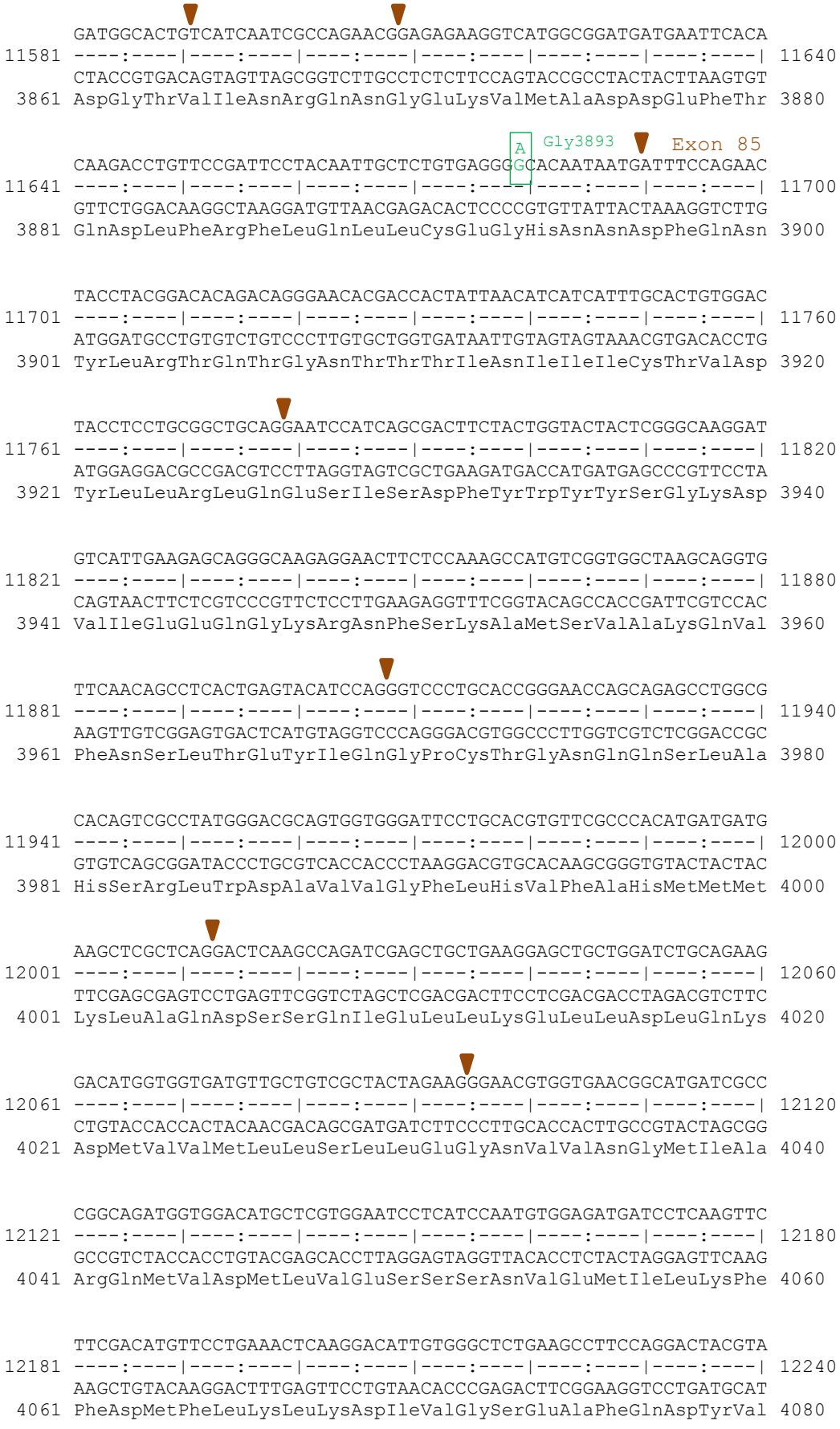
GATGGCACTGTCATCAATCGCCAGAACGGAGAGAAGGTCATGGCGGATGATGAATTCACA
11581 ----:----|----:----|----:----|----:----|----:----|----:----|----:----| 11640
CTACCGTGACAGTAGTTAGCGGTCTTGCCTCTCTTCCAGTACCGCCTACTACTTAAGTGT
3861 AspGlyThrValIleAsnArgGlnAsnGlyGluLysValMetAlaAspAspGluPheThr 3880
A
Gly3893
Exon 85
CAAGACCTGTTCCGATTCCTACAATTGCTCTGTGAGGGGCACAATAATGATTTCCAGAAC
11641 ----:----|----:----|----:----|----:----|----:----|----:----|----:----| 11700
GTTCTGGACAAGGCTAAGGATGTTAACGAGACACTCCCCGTGTTATTACTAAAGGTCTTG
3881 GlnAspLeuPheArgPheLeuGlnLeuLeuCysGluGlyHisAsnAsnAspPheGlnAsn 3900
TACCTACGGACACAGACAGGGAACACGACCACTATTAACATCATCATTTGCACTGTGGAC
11701 ----:----|----:----|----:----|----:----|----:----|----:----|----:----| 11760
ATGGATGCCTGTGTCTGTCCCTTGTGCTGGTGATAATTGTAGTAGTAAACGTGACACCTG
3901 TyrLeuArgThrGlnThrGlyAsnThrThrThrIleAsnIleIleIleCysThrValAsp 3920
TACCTCCTGCGGCTGCAGGAATCCATCAGCGACTTCTACTGGTACTACTCGGGCAAGGAT
11761 ----:----|----:----|----:----|----:----|----:----|----:----|----:----| 11820
ATGGAGGACGCCGACGTCCTTAGGTAGTCGCTGAAGATGACCATGATGAGCCCGTTCCTA
3921 TyrLeuLeuArgLeuGlnGluSerIleSerAspPheTyrTrpTyrTyrSerGlyLysAsp 3940
GTCATTGAAGAGCAGGGCAAGAGGAACTTCTCCAAAGCCATGTCGGTGGCTAAGCAGGTG
11821 ----:----|----:----|----:----|----:----|----:----|----:----|----:----| 11880
CAGTAACTTCTCGTCCCGTTCTCCTTGAAGAGGTTTCGGTACAGCCACCGATTCGTCCAC
3941 ValIleGluGluGlnGlyLysArgAsnPheSerLysAlaMetSerValAlaLysGlnVal 3960
TTCAACAGCCTCACTGAGTACATCCAGGGTCCCTGCACCGGGAACCAGCAGAGCCTGGCG
11881 ----:----|----:----|----:----|----:----|----:----|----:----|----:----| 11940
AAGTTGTCGGAGTGACTCATGTAGGTCCCAGGGACGTGGCCCTTGGTCGTCTCGGACCGC
3961 PheAsnSerLeuThrGluTyrIleGlnGlyProCysThrGlyAsnGlnGlnSerLeuAla 3980
CACAGTCGCCTATGGGACGCAGTGGTGGGATTCCTGCACGTGTTCGCCCACATGATGATG
11941 ----:----|----:----|----:----|----:----|----:----|----:----|----:----| 12000
GTGTCAGCGGATACCCTGCGTCACCACCCTAAGGACGTGCACAAGCGGGTGTACTACTAC
3981 HisSerArgLeuTrpAspAlaValValGlyPheLeuHisValPheAlaHisMetMetMet 4000
AAGCTCGCTCAGGACTCAAGCCAGATCGAGCTGCTGAAGGAGCTGCTGGATCTGCAGAAG
12001 ----:----|----:----|----:----|----:----|----:----|----:----|----:----| 12060
TTCGAGCGAGTCCTGAGTTCGGTCTAGCTCGACGACTTCCTCGACGACCTAGACGTCTTC
4001 LysLeuAlaGlnAspSerSerGlnIleGluLeuLeuLysGluLeuLeuAspLeuGlnLys 4020
GACATGGTGGTGATGTTGCTGTCGCTACTAGAAGGGAACGTGGTGAACGGCATGATCGCC
12061 ----:----|----:----|----:----|----:----|----:----|----:----|----:----| 12120
CTGTACCACCACTACAACGACAGCGATGATCTTCCCTTGCACCACTTGCCGTACTAGCGG
4021 AspMetValValMetLeuLeuSerLeuLeuGluGlyAsnValValAsnGlyMetIleAla 4040
CGGCAGATGGTGGACATGCTCGTGGAATCCTCATCCAATGTGGAGATGATCCTCAAGTTC
12121 ----:----|----:----|----:----|----:----|----:----|----:----|----:----| 12180
GCCGTCTACCACCTGTACGAGCACCTTAGGAGTAGGTTACACCTCTACTAGGAGTTCAAG
4041 ArgGlnMetValAspMetLeuValGluSerSerSerAsnValGluMetIleLeuLysPhe 4060
TTCGACATGTTCCTGAAACTCAAGGACATTGTGGGCTCTGAAGCCTTCCAGGACTACGTA
12181 ----:----|----:----|----:----|----:----|----:----|----:----|----:----| 12240
AAGCTGTACAAGGACTTTGAGTTCCTGTAACACCCGAGACTTCGGAAGGTCCTGATGCAT
4061 PheAspMetPheLeuLysLeuLysAspIleValGlySerGluAlaPheGlnAspTyrVal 4080

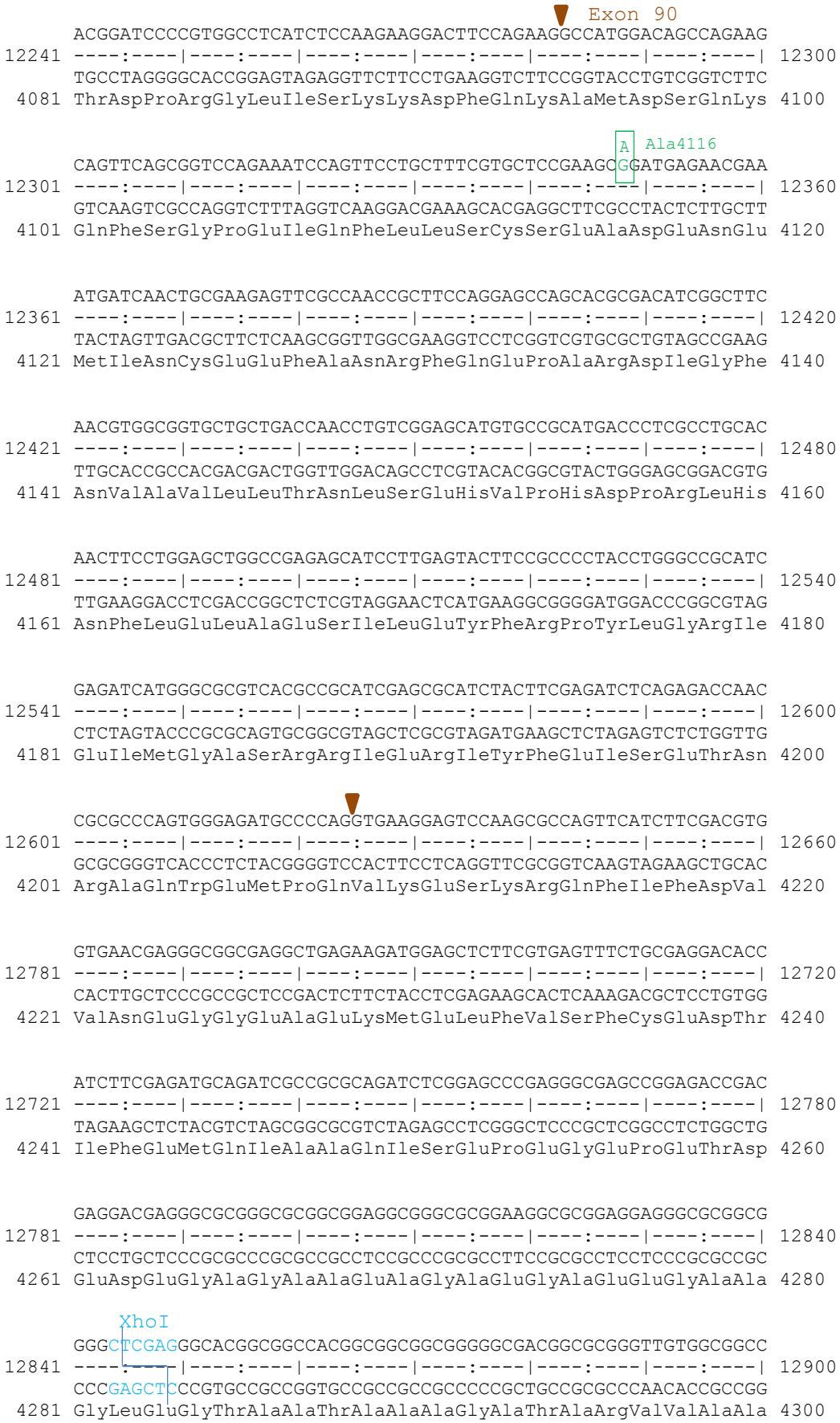
Exon 90
ACGGATCCCCGTGGCCTCATCTCCAAGAAGGACTTCCAGAAGGCCATGGACAGCCAGAAG
12241 ----:----|----:----|----:----|----:----|----:----|----:----| 12300
TGCCTAGGGGCACCGGAGTAGAGGTTCTTCCTGAAGGTCTTCCGGTACCTGTCGGTCTTC
4081 ThrAspProArgGlyLeuIleSerLysLysAspPheGlnLysAlaMetAspSerGlnLys 4100
A Ala4116
CAGTTCAGCGGTCCAGAAATCCAGTTCCTGCTTTCGTGCTCCGAAGCGGATGAGAACGAA
12301 ----:----|----:----|----:----|----:----|----:----|----:----| 12360
GTCAAGTCGCCAGGTCTTTAGGTCAAGGACGAAAGCACGAGGCTTCGCCTACTCTTGCTT
4101 GlnPheSerGlyProGluIleGlnPheLeuLeuSerCysSerGluAlaAspGluAsnGlu 4120
ATGATCAACTGCGAAGAGTTCGCCAACCGCTTCCAGGAGCCAGCACGCGACATCGGCTTC
12361 ----:----|----:----|----:----|----:----|----:----|----:----| 12420
TACTAGTTGACGCTTCTCAAGCGGTTGGCGAAGGTCCTCGGTCGTGCGCTGTAGCCGAAG
4121 MetIleAsnCysGluGluPheAlaAsnArgPheGlnGluProAlaArgAspIleGlyPhe 4140
AACGTGGCGGTGCTGCTGACCAACCTGTCGGAGCATGTGCCGCATGACCCTCGCCTGCAC
12421 ----:----|----:----|----:----|----:----|----:----|----:----| 12480
TTGCACCGCCACGACGACTGGTTGGACAGCCTCGTACACGGCGTACTGGGAGCGGACGTG
4141 AsnValAlaValLeuLeuThrAsnLeuSerGluHisValProHisAspProArgLeuHis 4160
AACTTCCTGGAGCTGGCCGAGAGCATCCTTGAGTACTTCCGCCCCTACCTGGGCCGCATC
12481 ----:----|----:----|----:----|----:----|----:----|----:----| 12540
TTGAAGGACCTCGACCGGCTCTCGTAGGAACTCATGAAGGCGGGGATGGACCCGGCGTAG
4161 AsnPheLeuGluLeuAlaGluSerIleLeuGluTyrPheArgProTyrLeuGlyArgIle 4180
GAGATCATGGGCGCGTCACGCCGCATCGAGCGCATCTACTTCGAGATCTCAGAGACCAAC
12541 ----:----|----:----|----:----|----:----|----:----|----:----| 12600
CTCTAGTACCCGCGCAGTGCGGCGTAGCTCGCGTAGATGAAGCTCTAGAGTCTCTGGTTG
4181 GluIleMetGlyAlaSerArgArgIleGluArgIleTyrPheGluIleSerGluThrAsn 4200
CGCGCCCAGTGGGAGATGCCCCAGGTGAAGGAGTCCAAGCGCCAGTTCATCTTCGACGTG
12601 ----:----|----:----|----:----|----:----|----:----|----:----| 12660
GCGCGGGTCACCCTCTACGGGGTCCACTTCCTCAGGTTCGCGGTCAAGTAGAAGCTGCAC
4201 ArgAlaGlnTrpGluMetProGlnValLysGluSerLysArgGlnPheIlePheAspVal 4220
GTGAACGAGGGCGGCGAGGCTGAGAAGATGGAGCTCTTCGTGAGTTTCTGCGAGGACACC
12781 ----:----|----:----|----:----|----:----|----:----|----:----| 12720
CACTTGCTCCCGCCGCTCCGACTCTTCTACCTCGAGAAGCACTCAAAGACGCTCCTGTGG
4221 ValAsnGluGlyGlyGluAlaGluLysMetGluLeuPheValSerPheCysGluAspThr 4240
ATCTTCGAGATGCAGATCGCCGCGCAGATCTCGGAGCCCGAGGGCGAGCCGGAGACCGAC
12721 ----:----|----:----|----:----|----:----|----:----|----:----| 12780
TAGAAGCTCTACGTCTAGCGGCGCGTCTAGAGCCTCGGGCTCCCGCTCGGCCTCTGGCTG
4241 IlePheGluMetGlnIleAlaAlaGlnIleSerGluProGluGlyGluProGluThrAsp 4260
GAGGACGAGGGCGCGGGCGCGGCGGAGGCGGGCGCGGAAGGCGCGGAGGAGGGCGCGGCG
12781 ----:----|----:----|----:----|----:----|----:----|----:----| 12840
CTCCTGCTCCCGCGCCCGCGCCGCCTCCGCCCGCGCCTTCCGCGCCTCCTCCCGCGCCGC
4261 GluAspGluGlyAlaGlyAlaAlaGluAlaGlyAlaGluGlyAlaGluGluGlyAlaAla 4280
XhoI
GGGCTCGAGGGCACGGCGGCCACGGCGGCGGCGGGGGCGACGGCGCGGGTTGTGGCGGCC
12841 ----:----|----:----|----:----|----:----|----:----|----:----| 12900
CCCGAGCTCCCGTGCCGCCGGTGCCGCCGCCGCCCCCGCTGCCGCGCCCAACACCGCCGG
4281 GlyLeuGluGlyThrAlaAlaThrAlaAlaAlaGlyAlaThrAlaArgValValAlaAla 4300

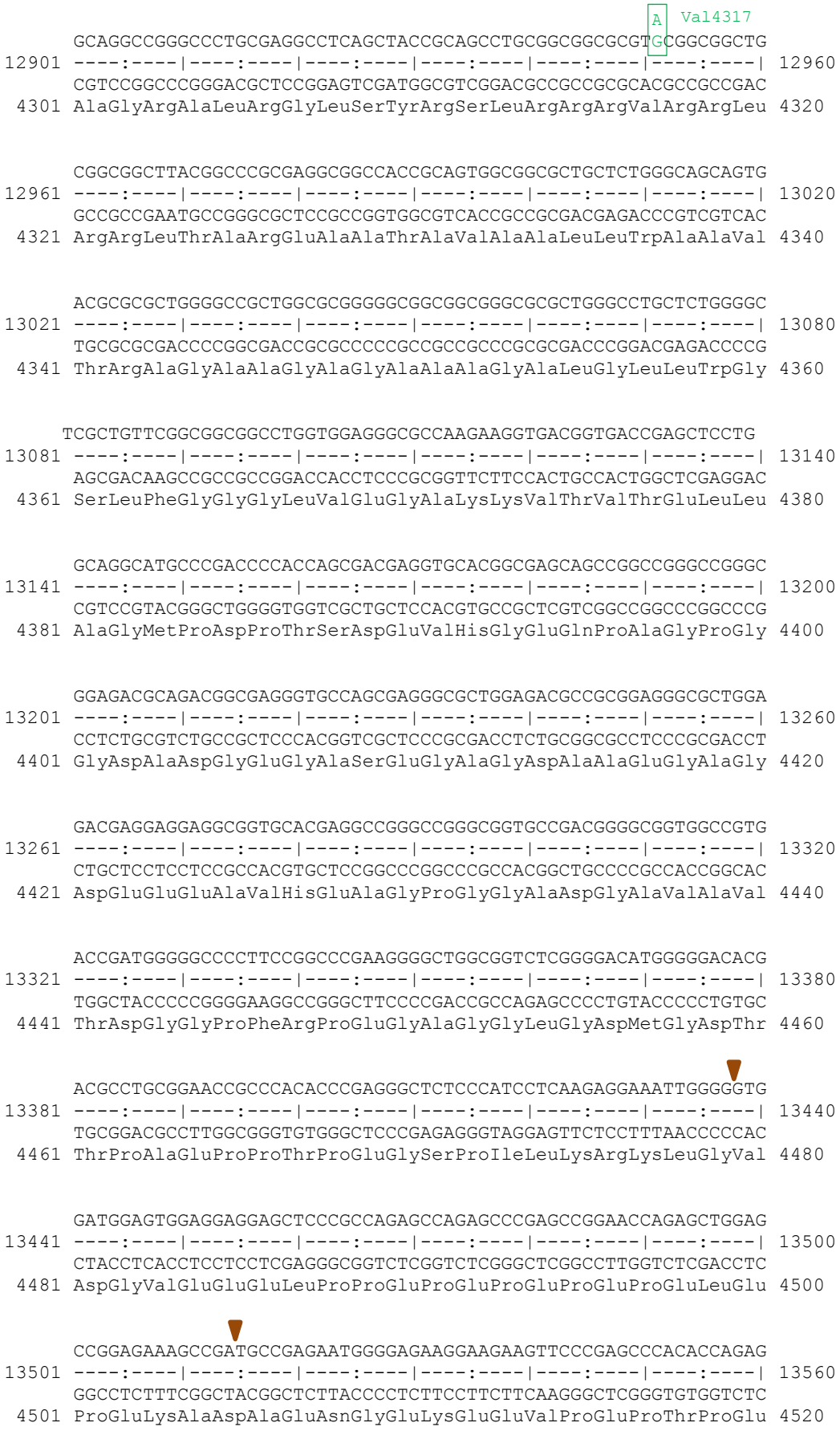
A Val4317
GCAGGCCGGGCCCTGCGAGGCCTCAGCTACCGCAGCCTGCGGCGGCGCGTGCCGGCGGCTG
12901 ----:----|----:----|----:----|----:----|----:----|----:----| 12960
CGTCCGGCCCGGGACGCTCCGGAGTCGATGGCGTCGGACGCCGCCGCGCACGCCGCCGAC
4301 AlaGlyArgAlaLeuArgGlyLeuSerTyrArgSerLeuArgArgArgValArgArgLeu 4320
CGGCGGCTTACGGCCCGCGAGGCGGCCACCGCAGTGGCGGCGCTGCTCTGGGCAGCAGTG
12961 ----:----|----:----|----:----|----:----|----:----|----:----| 13020
GCCGCCGAATGCCGGGCGCTCCGCCGGTGGCGTCACCGCCGCGACGAGACCCGTCGTCAC
4321 ArgArgLeuThrAlaArgGluAlaAlaThrAlaValAlaAlaLeuLeuTrpAlaAlaVal 4340
ACGCGCGCTGGGGCCGCTGGCGCGGGGGCGGCGGCGGGCGCGCTGGGCCTGCTCTGGGGC
13021 ----:----|----:----|----:----|----:----|----:----|----:----| 13080
TGCGCGCGACCCCGGCGACCGCGCCCCCGCCGCCGCCCGCGCGACCCGGACGAGACCCCG
4341 ThrArgAlaGlyAlaAlaGlyAlaGlyAlaAlaAlaGlyAlaLeuGlyLeuLeuTrpGly 4360
TCGCTGTTCGGCGGCGGCCTGGTGGAGGGCGCCAAGAAGGTGACGGTGACCGAGCTCCTG
13081 ----:----|----:----|----:----|----:----|----:----|----:----| 13140
AGCGACAAGCCGCCGCCGGACCACCTCCCGCGGTTCTTCCACTGCCACTGGCTCGAGGAC
4361 SerLeuPheGlyGlyGlyLeuValGluGlyAlaLysLysValThrValThrGluLeuLeu 4380
GCAGGCATGCCCGACCCCACCAGCGACGAGGTGCACGGCGAGCAGCCGGCCGGGCCGGGC
13141 ----:----|----:----|----:----|----:----|----:----|----:----| 13200
CGTCCGTACGGGCTGGGGTGGTCGCTGCTCCACGTGCCGCTCGTCGGCCGGCCCGGCCCG
4381 AlaGlyMetProAspProThrSerAspGluValHisGlyGluGlnProAlaGlyProGly 4400
GGAGACGCAGACGGCGAGGGTGCCAGCGAGGGCGCTGGAGACGCCGCGGAGGGCGCTGGA
13201 ----:----|----:----|----:----|----:----|----:----|----:----| 13260
CCTCTGCGTCTGCCGCTCCCACGGTCGCTCCCGCGACCTCTGCGGCGCCTCCCGCGACCT
4401 GlyAspAlaAspGlyGluGlyAlaSerGluGlyAlaGlyAspAlaAlaGluGlyAlaGly 4420
GACGAGGAGGAGGCGGTGCACGAGGCCGGGCCGGGCGGTGCCGACGGGGCGGTGGCCGTG
13261 ----:----|----:----|----:----|----:----|----:----|----:----| 13320
CTGCTCCTCCTCCGCCACGTGCTCCGGCCCGGCCCGCCACGGCTGCCCCGCCACCGGCAC
4421 AspGluGluGluAlaValHisGluAlaGlyProGlyGlyAlaAspGlyAlaValAlaVal 4440
ACCGATGGGGGCCCCTTCCGGCCCGAAGGGGCTGGCGGTCTCGGGGACATGGGGGACACG
13321 ----:----|----:----|----:----|----:----|----:----|----:----| 13380
TGGCTACCCCCGGGGAAGGCCGGGCTTCCCCGACCGCCAGAGCCCCTGTACCCCCTGTGC
4441 ThrAspGlyGlyProPheArgProGluGlyAlaGlyGlyLeuGlyAspMetGlyAspThr 4460
ACGCCTGCGGAACCGCCCACACCCGAGGGCTCTCCCATCCTCAAGAGGAAATTGGGGGTG
13381 ----:----|----:----|----:----|----:----|----:----|----:----| 13440
TGCGGACGCCTTGGCGGGTGTGGGCTCCCGAGAGGGTAGGAGTTCTCCTTTAACCCCCAC
4461 ThrProAlaGluProProThrProGluGlySerProIleLeuLysArgLysLeuGlyVal 4480
GATGGAGTGGAGGAGGAGCTCCCGCCAGAGCCAGAGCCCGAGCCGGAACCAGAGCTGGAG
13441 ----:----|----:----|----:----|----:----|----:----|----:----| 13500
CTACCTCACCTCCTCCTCGAGGGCGGTCTCGGTCTCGGGCTCGGCCTTGGTCTCGACCTC
4481 AspGlyValGluGluGluLeuProProGluProGluProGluProGluProGluLeuGlu 4500
CCGGAGAAAGCCGATGCCGAGAATGGGGAGAAGGAAGAAGTTCCCGAGCCCACACCAGAG
13501 ----:----|----:----|----:----|----:----|----:----|----:----| 13560
GGCCTCTTTCGGCTACGGCTCTTACCCCTCTTCCTTCTTCAAGGGCTCGGGTGTGGTCTC
4501 ProGluLysAlaAspAlaGluAsnGlyGluLysGluGluValProGluProThrProGlu 4520


CCCCCCAAGAAGCAAGCACCTCCCTCACCCCCTCCAAAGAAGGAGGAAGCTGGAGGCGAA
13561 ----:----|----:----|----:----|----:----|----:----|----:----|----:----| 13620
GGGGGGTTCTTCGTTCGTGGAGGGAGTGGGGGAGGTTTCTTCCTCCTTCGACCTCCGCTT
4521 ProProLysLysGlnAlaProProSerProProProLysLysGluGluAlaGlyGlyGlu 4540
TTCTGGGGAGAACTGGAGGTGCAGAGGGTGAAGTTCCTGAACTACCTGTCCCGGAACTTT
13621 ----:----|----:----|----:----|----:----|----:----|----:----|----:----| 13680
AAGACCCCTCTTGACCTCCACGTCTCCCACTTCAAGGACTTGATGGACAGGGCCTTGAAA
4541 PheTrpGlyGluLeuGluValGlnArgValLysPheLeuAsnTyrLeuSerArgAsnPhe 4560
TACACCCTGCGGTTCCTTGCCCTCTTCTTGGCATTTGCCATCAACTTCATCTTGCTGTTT
13681 ----:----|----:----|----:----|----:----|----:----|----:----|----:----| 13740
ATGTGGGACGCCAAGGAACGGGAGAAGAACCGTAAACGGTAGTTGAAGTAGAACGACAAA
4561 TyrThrLeuArgPheLeuAlaLeuPheLeuAlaPheAlaIleAsnPheIleLeuLeuPhe 4580
Exon 95
G Ser4584
TATAAGGTCTCAGACTCTCCACCAGGGGAGGACGACATGGAAGGCTCAGCTGCTGGGGAT
13741 ----:----|----:----|----:----|----:----|----:----|----:----|----:----| 13800
ATATTCCAGAGTCTGAGAGGTGGTCCCCTCCTGCTGTACCTTCCGAGTCGACGACCCCTA
4581 TyrLysValSerAspSerProProGlyGluAspAspMetGluGlySerAlaAlaGlyAsp 4600
GTGTCAGGTGCAGGCTCTGGTGGCAGCTCTGGCTGGGGCTTGGGGGCCGGAGAGGAGGCA
13801 ----:----|----:----|----:----|----:----|----:----|----:----|----:----| 13860
CACAGTCCACGTCCGAGACCACCGTCGAGACCGACCCCGAACCCCCGGCCTCTCCTCCGT
4601 ValSerGlyAlaGlySerGlyGlySerSerGlyTrpGlyLeuGlyAlaGlyGluGluAla 4620
GAGGGCGATGAGGATGAGAACATGGTGTACTACTTCCTGGAGGAAAGCACAGGCTACATG
13861 ----:----|----:----|----:----|----:----|----:----|----:----|----:----| 13920
CTCCCGCTACTCCTACTCTTGTACCACATGATGAAGGACCTCCTTTCGTGTCCGATGTAC
4621 GluGlyAspGluAspGluAsnMetValTyrTyrPheLeuGluGluSerThrGlyTyrMet 4640
GAACCCGCCCTGCGGTGTCTGAGCCTCCTGCATACACTGGTGGCCTTTCTCTGCATCATT
13921 ----:----|----:----|----:----|----:----|----:----|----:----|----:----| 13980
CTTGGGCGGGACGCCACAGACTCGGAGGACGTATGTGACCACCGGAAAGAGACGTAGTAA
4641 GluProAlaLeuArgCysLeuSerLeuLeuHisThrLeuValAlaPheLeuCysIleIle 4660
Leu4687 A
GGCTATAATTGTCTCAAGGTGCCCCTGGTAATCTTTAAGCGGGAGAAGGAGCTGGCCCGG
13981 ----:----|----:----|----:----|----:----|----:----|----:----|----:----| 14040
CCGATATTAACAGAGTTCCACGGGGACCATTAGAAATTCGCCCTCTTCCTCGACCGGGCC
4661 GlyTyrAsnCysLeuLysValProLeuValIlePheLysArgGluLysGluLeuAlaArg 4680
AAGCTGGAGTTTGATGGCCTGTACATCACGGAGCAGCCTGAGGACGATGACGTGAAGGGG
14041 ----:----|----:----|----:----|----:----|----:----|----:----|----:----| 14100
TTCGACCTCAAACTACCGGACATGTAGTGCCTCGTCGGACTCCTGCTACTGCACTTCCCC
4681 LysLeuGluPheAspGlyLeuTyrIleThrGluGlnProGluAspAspAspValLysGly 4700
CAGTGGGACCGACTGGTGCTCAACACGCCGTCTTTCCCTAGCAACTACTGGGACAAGTTT
14101 ----:----|----:----|----:----|----:----|----:----|----:----|----:----| 14160
GTCACCCTGGCTGACCACGAGTTGTGCGGCAGAAAGGGATCGTTGATGACCCTGTTCAAA
4701 GlnTrpAspArgLeuValLeuAsnThrProSerPheProSerAsnTyrTrpAspLysPhe 4720
GTCAAGCGCAAGGTCCTGGACAAACATGGGGACATCTACGGGCGGGAGCGGATTGCTGAG
14161 ----:----|----:----|----:----|----:----|----:----|----:----|----:----| 14220
CAGTTCGCGTTCCAGGACCTGTTTGTACCCCTGTAGATGCCCGCCCTCGCCTAACGACTC
4721 ValLysArgLysValLeuAspLysHisGlyAspIleTyrGlyArgGluArgIleAlaGlu 4740

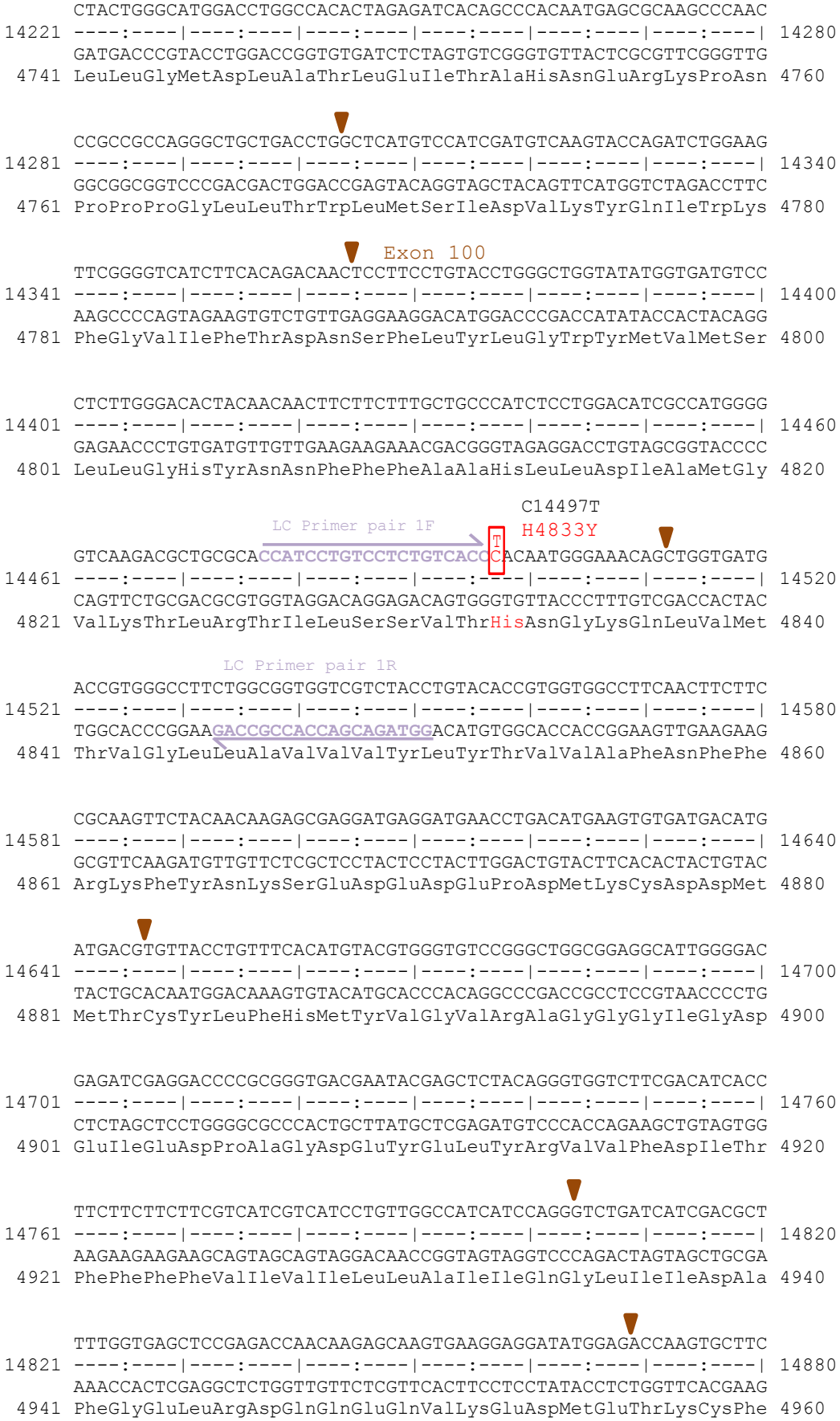
Exon 100
C14497T
H4833Y
LC Primer pair 1F
LC Primer pair 1R

Primers are shown as purple arrows with highlighted sequence. Mutations are shown in red while XhoI restriction sides are shown in light blue. Polymorphisms are shown in green and exon-exon boundaries are indicated by brown arrows. Start and stop codons are highlighted in orange. The sequence was taken from ensemble (Transcript ID: ENST00000359596).